PhD Thesis

Accelerated Discovery in Organic Photocatalysis using High-Throughput Robotic Platforms

Sriram Vijayakrishnan

Primary Supervisor: Prof. Andrew Cooper

Secondary Supervisor: Dr. John Ward

2022

Table of Contents:

Abstract

The resurgence of photocatalysis has propelled the development of a variety of novel synthetic reactions powered by visible light. However, the majority of photocatalysts typically used in these reactions are homogenous dyes or expensive organometallic complexes, which have issues with cost, and recyclability which hinders large-scale applications. The following work first summarizes the recent developments in modern photoredox catalysis, along with some advances in high throughput experiments. This thesis then describes the use of a high-throughput screening strategy to discover a covalent triazine framework, CTF-2, as heterogeneous organic photocatalyst for a variety of reactions, including conjugate addition, metallaphotoredox arylation, metallaphotoredox alkylation, dehydrogenative arylation, and fluorination. Finally, progress towards a fully-autonomous workflow for photochemical reaction optimization using mobile robots is highlighted.

Chapter Summaries:

Chapter 1 overviews homogeneous photocatalysis using transition metal complexes, organic dyes, heterogeneous photocatalysis, and summarizes some recent advances in high throughput experimentation (HTE) and applications of robotic platforms for discovery and optimization.

Chapter 2 describes a discovery workflow for the discovery of novel heterogeneous organic photoredox catalysis for synthetic chemistry. Using a combination of pre-selected photoactive cores, we created polymeric analogues of these cores, and benchmarked them using robotic platforms against a variety of reactions with synthetic utility. While many reactions were unsuccessfully catalysed by any of the polymers we synthesized, we were able to discover active photocatalysts a variety of reactions including C-H trifluoromethylation, beta ketone functionalization, decarboxylative metallaphotoredox arylation, and decarboxylative conjugate addition. We found that CTF-2, a stable covalent triazine framework (CTF) material, was able to catalyse 3 different reactions performed by the iridium catalyst $Ir[(dFCF_3ppy)_2(dtbbpy)][PF_6]$.

Chapter 3 explores the substrate and reaction scope of CTF-2 for a variety of reactions. In total, we demonstrated 24 examples of decarboxylative conjugate addition, and successfully applied CTF-2 for a decarboxylative alkylation, arylation, fluorination, and further applied it to a dehydrogenative arylation reaction. We then used CTF-2 for a transition-metal-free synthesis of the antidepressant Rolipram. Recycling experiments showed that CTF-2 was photostable and catalysed decarboxylative conjugate addition in 3 recycling experiments, showing no appreciable loss in catalytic performance.

Chapter 4 expands upon our use of robotic platforms and describes the progress towards an autonomous platform for closed loop optimization in photocatalytic reactions using a KUKA mobile robot. Using ISynth platforms, several photoreactors, and LC-MS, we integrate these in our optimization workflow, and demonstrate a full loop of vial transfer, photoreactor vial placement, and LC-MS analysis. We also screen materials for catalysing dehydrogenative arylation, and find that dibenzo[b,d]thiophene 5,5-dioxide containing polymers are active photocatalysts for this reaction, and provided higher yields than CTF-2.

Chapter 5 presents the overall conclusions of the thesis and presents suggestions and directions for future work.

Acknowledgements

I would first like to thank Andy for providing me the opportunity to do this research, and for providing all the tools and resources I could possibly ask for.

A big thank you to John for all his advice, and support throughout the years, and for all his patience with my endless questions.

Thank you to Rob and Nicola, without whom many of these projects would have never gotten off the ground. Tianwei for all the discussions about the reaction optimization workflow, and with all the work developing the reaction optimization project.

Thank you to all the other people in the Cooper group, past and present, who've made the last 4 years amazing. Wei, Xue, Yongjie – thanks for being there to encourage me and to provide me with all the advice I needed for materials chemistry. Ian, Rich, Mike – thanks for being there to listen to me when things went wrong, and to provide fresh ideas on how to overcome them. Veronica, thank you for all your help with the electrochemistry experiments, and Tom for looking at all my awful 'crystals'.

I would like to especially thank the Leverhulme Centre for their generous funding that allowed for these projects to happen.

Finally, I would like to thank my family for their support over the past few years.

List of Abbreviations

- **4CzIPN** - 1,2,3,5-Tetrakis(carbazol-9-yl)-4,6-dicyanobenzene, 2,4,5,6-Tetrakis(9*H*-carbazol-9-yl) isophthalonitrile
- **Ac** - Acetyl
- **API** – Active Pharmaceutical Ingredient
- **BET** – Brunauer-Emmet-Teller
- **Boc** – tertbutoxylcarbonyl
- **BODIPY** - 4,4-difluoro-4-bora-3a,4a-diaza-s-indacene
- **BTTP -** tert-Butylimino-tri(pyrrolidino)phosphorane
- **Cbz** – benzyloxycarbonyl
- **CFL** – Compact fluorescent lamp
- **CN-K** – Potassium doped carbon nitride
- **COF** – Covalent Organic Framework
- **CTF** – Covalent Triazine Framework
- **DABCO** - 1,4-Diazabicyclo[2.2.2]octane
- **DBU** - 1,8-Diazabicyclo[5.4.0]undec-7-ene
- **DCE** – 1,2-dichloroethane
- **DCM** – Dichloromethane
- **DFT** – Density Functional Theory
- **DIPEA** – N,N-Diisopropylethylamine
- **DMA** – Dimethylacetamide
- **DMF** – Dimethylformamide
- **dmgH** – Dimethylglyoxime
- **DMPU** - 1,3-Dimethyl-3,4,5,6-tetrahydro-2(1*H*)-pyrimidinone
- **DMSO** – Dimethylsulfoxide
- **dppf –** 1,1′-Bis(diphenylphosphino)ferrocene
- **dtbbpy** – Ditertbutyl bipyridine
- **EA** – Electron Affinity
- **ESI** – Electrospray ionization
- **eV** – Electron Volts
- **FT-IR** – Fourier Transform-Infrared
- **GC-MS** – Gas Chromatography – Mass Spectroscopy
- **glyme** – Dimethoxyethane
- **GPC** – Gel Permeation Chromatography
- **HAT** – Hydrogen Atom Transfer

- **HATU** - [Bis(dimethylamino)methylene]-1H-1,2,3-triazolo[4,5-b]pyridinium 3-oxide hexafluorophosphate)
- **HCP** – Hyper-Crosslinked Polymer
- **HPLC** – High Performance Liquid Chromatography
- **HTE** – High-Throughput Experimentation
- **ICP-OES** - Inductively Coupled Plasma Optical Emission Spectroscopy
- **IP** – Ionization Potential
- **iPr** – Isopropyl
- **LC-MS** – Liquid Chromatography – Mass Spectrometry
- **LED** – Light Emitting Diode
- **Mes-Acr-Ph** - 9-Mesityl-10-phenylacridinium tetrafluoroborate
- **mpg-CN** – Mesoporous graphitic carbon nitride
- **NBS** – N-Bromo Succinimide
- **Ni-mpg-CN** – Nickel doped mesoporous graphitic carbon nitride
- **NMP** – 1-methyl-2-pyrrolidinone
- **pin** – 2,3-dimethylbutane-2,3-diol
- **ppy** - 2-phenylpyridinato
- **QD** – Quantum Dot
- **SCE** – Saturated Calomel Electrode
- **SET** – Single Electron Transfer
- **SHE** – Standard Hydrogen Electrode
- **TBADT** – Tetrabutylammonium decatungstate
- **TCSPC** – Time Correlated Single Photon Counting
- **TEMPO** - 2,2,6,6-Tetramethylpiperidine 1-oxyl
- **TEOA** – Triethanolamine
- **TFA** – Trifluoroacetic Acid
- **TFE** – Trifluoroethanol
- **TMG** – Tetramethylguanidine
- **TMS** – Trimethylsilyl
- **TRIP** - 3,3′-Bis(2,4,6-triisopropylphenyl)-1,1′-binaphthyl-2,2′-diyl hydrogenphosphate
- **UV-Vis** – UV-Visible
- **XML** – Extensible Markup Language

Chapter 1

Introduction

Transition Metal Photoredox Catalysis

The pressing drive for sustainable chemical synthesis has driven the development of multiple methods for green and efficient synthesis. Among those that have generated significant interest is photoredox catalysis,[1] which has seen a resurgence over the past decade. Historically, photochemical reactions have tended to rely on the use of ultraviolet (UV) light involving specialized photoreactors, which come with significant associated challenges[2]. The safety concerns associated with using UV light, along with its general lack of selectivity has hindered the widespread use of the technique.

In recent years, significant progress has been made to address these challenges. Rather than relying exclusively on UV irradiation, seminal work by Macmillan,[3] Yoon,[4] Stephenson,[5] showed that the use of photosensitizing transition metal complexes containing precious metal cores could drive reactions using visible light using house-hold light bulbs or cheap light-emitting diode (LED) arrays. These transition metal complexes have long lived excited states that can engage in single electron transfer (SET) and can be used highly efficiently with low catalyst loadings.

Removing the barriers of potentially hazardous and expensive UV photoreactors has significantly contributed to the accessibility of synthetic photochemistry, demonstrating a wide variety of chemical reactions using mild conditions.[6] The availability of standardized and commercial photoreactors has,[7] in addition, made great strides towards improving the reproducibility of the technique, and allowed for standardized protocols.

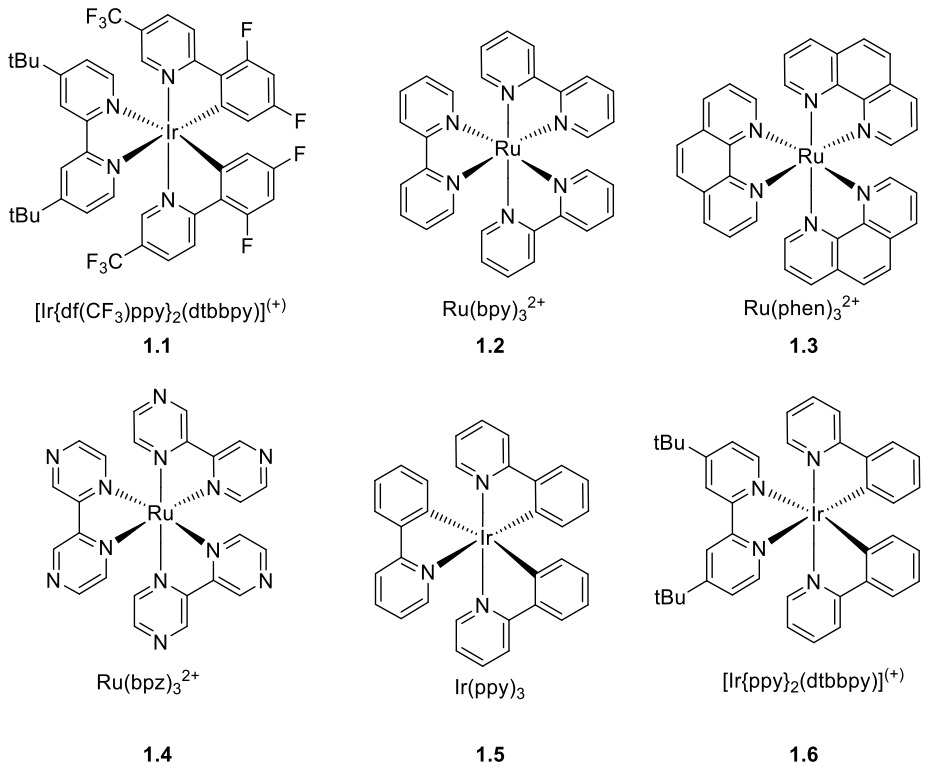

Figure 1-1: Commonly used precious metal photoredox catalysts

A recently reported procedure using transition metal photoredox catalysts was the coupling of dicyanobenzene with tertiary amines developed by Macmillan and co-workers (Scheme **1-1**).[8] In this reaction, the photoredox catalyst $Ir(ppy)_3$ **1.7** is excited to $*Ir(ppy)_3$ **1.8** following irradiation. **1.8** subsequently reduces dicyanobenzene (**1.9**) and yields oxidized $Ir^{IV}(ppy)_3$ (**1.11**) as a result. Intermediate **1.11** is then reduced by the tertiary amine **1.12**. Oxidized **1.13** couples with intermediate **1.10** and is followed by cyanide elimination – forming the final product **1.16**. The reaction, however, was largely limited to N-aryl amines, but was very efficient, requiring < 1 mol % catalyst in many cases, and was powered by a standard CFL bulb – obviating the need for costly UV-photoreactors.

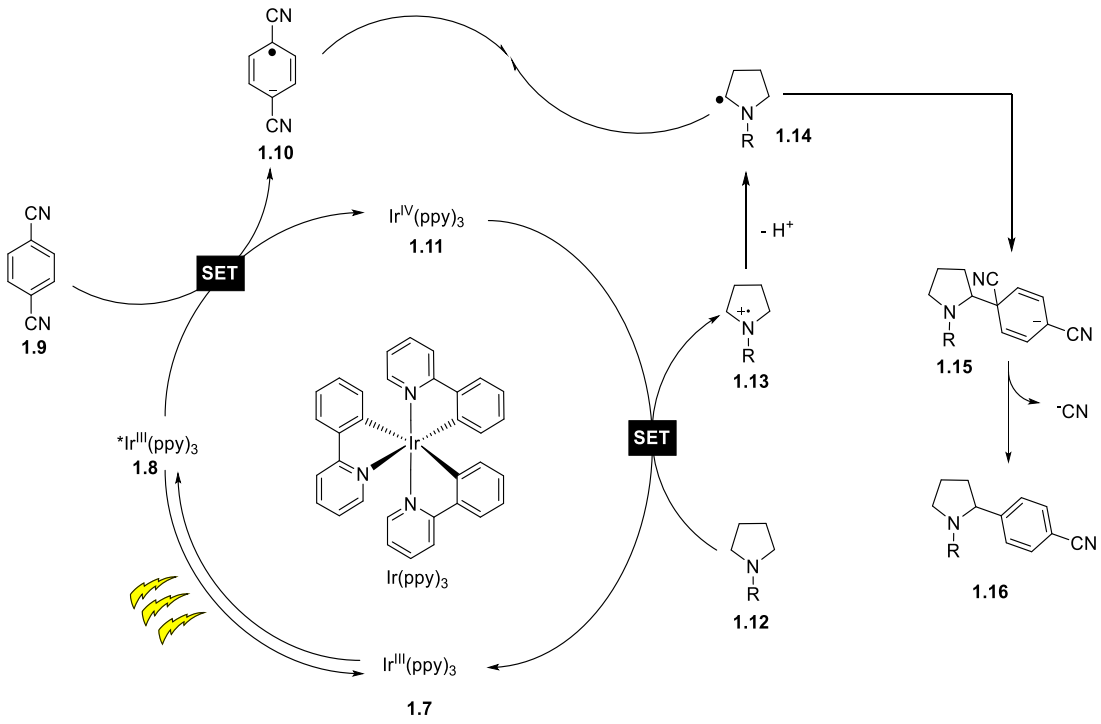

Scheme 1-1: Mechanism of photocatalytic C-H arylation of tertiary arylamines.

Another significant advantage of photoredox catalysis has been its ability to catalyse reactions in tandem with other modes of catalysis, such as organic catalysts, enzymes,[9] and other transition metals for metallaphotoredox catalysis, allowing for broad reactivity.

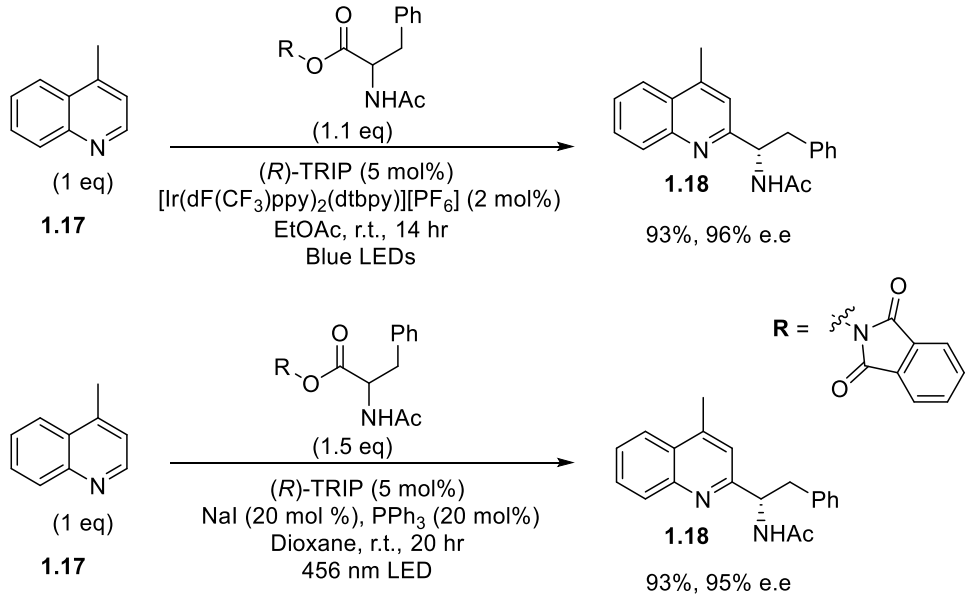

Scheme 1-2: Enantioselective Minisci addition with iridium and charge-transfer complexes

Phipps and co-workers have adapted chiral phosphoric acids as a co-catalyst with an iridium catalyst for enantioselective Minisci addition. The TRIP co-catalyst both serves as an acid for activating the heteroarene for addition, as well as controlling the stereochemistry of the addition products (Scheme **1-2**).[10] This reaction has also recently been catalysed by a combination of NaI/PPh_3 as a photoactive charge transfer complex, in place of the iridium catalyst.[11]

Macmillan recently developed a platform for the beta functionalization of ketones and aldehydes (Scheme **1-3**). Selective beta reactivity of a ketone or aldehyde is challenging due to the inert nature of the C-H bond, and typical approaches often rely on the use of directing groups[12]. Using simple cyclic amines as co-catalysts, Macmillan was able to selectively generate radicals on this beta position and leverage it for a variety of reactions, [13–17] including arylation, ketone addition, and Michael addition.

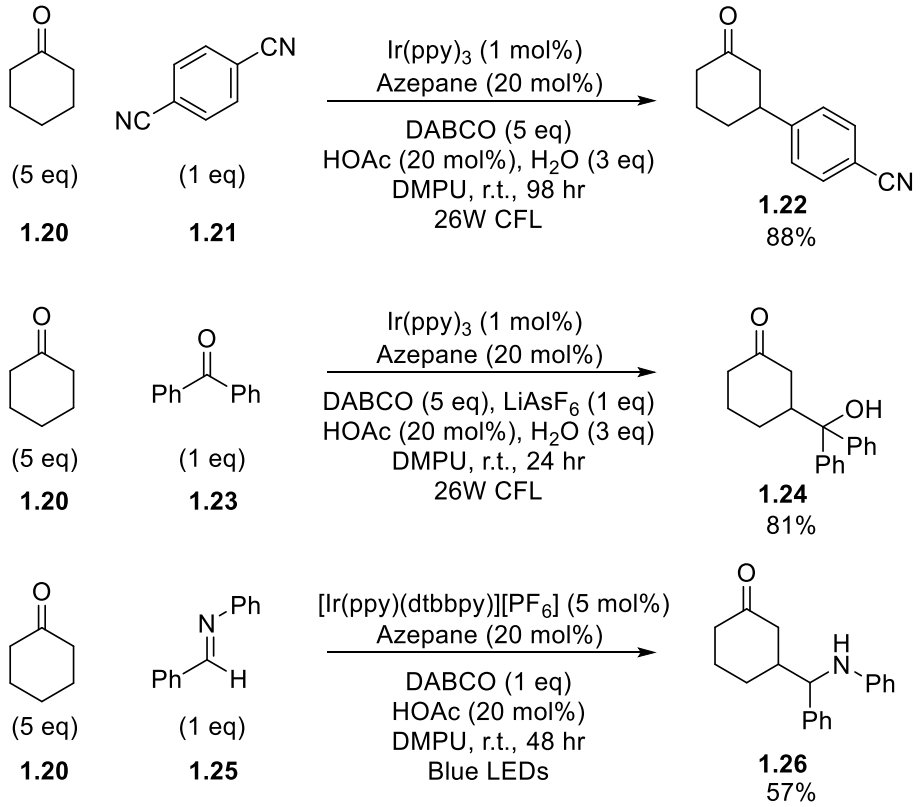

Scheme 1-3: Direct beta-functionalization of ketones with various acceptors.

Merging cross-coupling and photocatalysts has demonstrated promise, particularly in C-C bond forming reactions.[18] In one of the first such examples, Macmillan used a combination of an iridium photocatalyst, and a nickel co-catalyst to develop a decarboxylative cross -coupling reactions of carboxylic acids and aryl halides (Scheme **1-4**).[19] In the proposed mechanism, the excited iridium photocatalyst (**1.28**) oxidizes the carboxylic acid substrate (**1.29**). Alkyl radical **1.30** is then captured by nickel species **1.33** to form **1.34**, which then undergoes reductive elimination to yield the decarboxylative C-C coupling product **1.35**.

This dual decarboxylative/metal cross coupling approach has been further extended to C-C alkylation.[20] Nickel cross-coupling methods are attractive, due to their low cost and high abundance of the metal, in comparison to metals such as palladium.

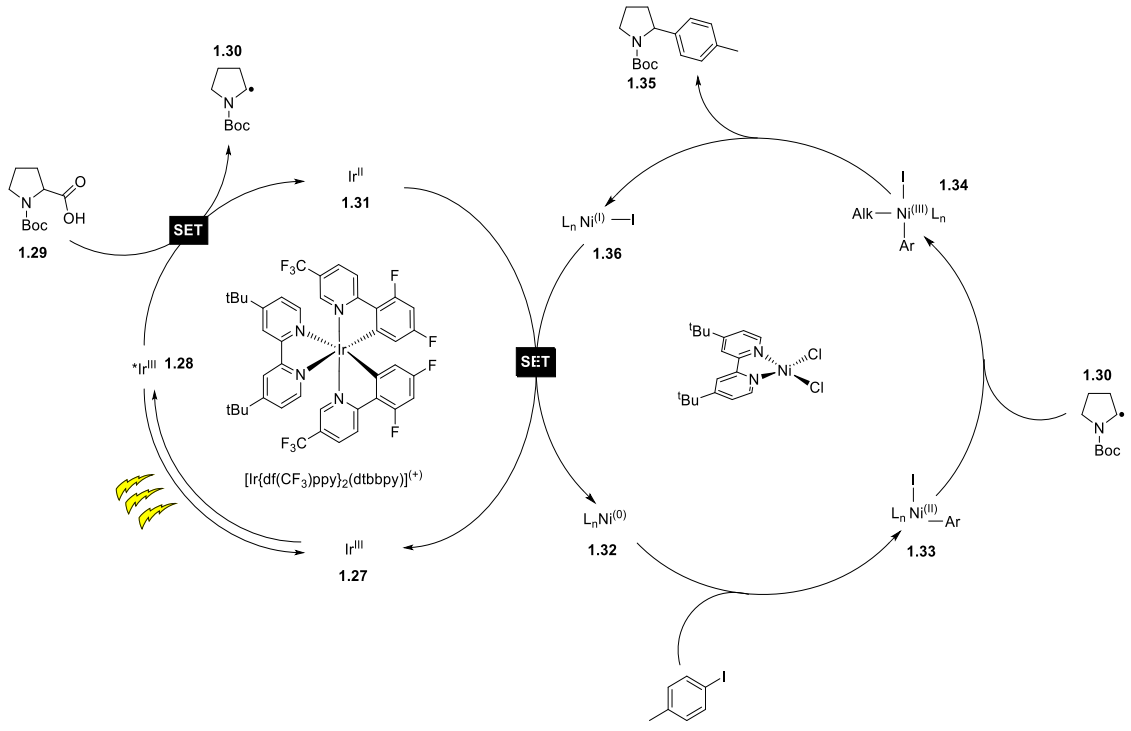

Scheme 1-4: Decarboxylative metallaphotoredox arylation using iridium and nickel cocatalysts.

While iridium and ruthenium complexes have undoubtedly been the most prominent transition metal photocatalysts, other metals have been applied. Macmillan reported on the use of a tetrabutylammonium decatungstate (TBADT) photocatalyst and nickel catalyst combination for direct C-H arylation of aliphatic compounds such as cyclohexane (Scheme **1-5**).[21] Decatungstate has also been used by the Noel group[22,23] for direct functionalization of hydrocarbons, such as methane, and propane in conjugate addition reactions. Decatungstate is reported to work through hydrogen atom transfer (HAT), directly activating the strong C-H bond, and forming the alkyl radical.

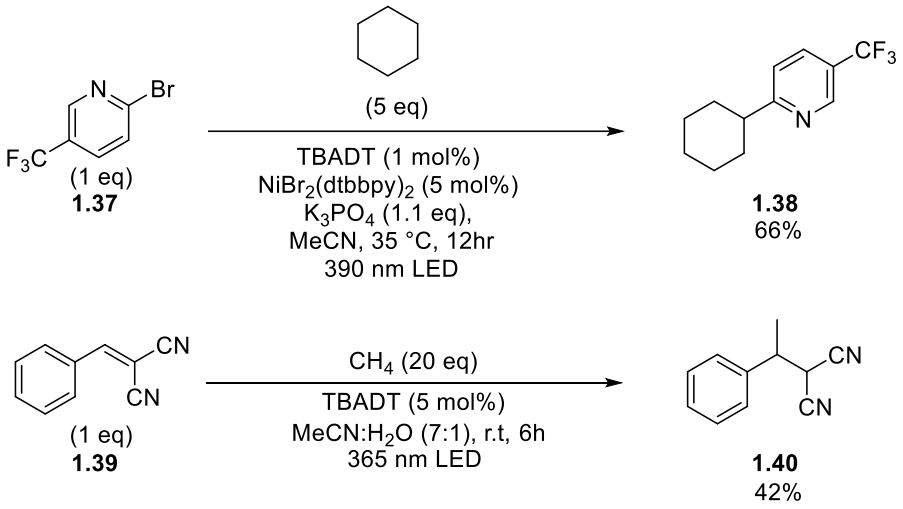

Scheme 1-5: Direct C-H Functionalization of aliphatic substrates using tungsten polyoxometalate photocatalysts.

The scope of transition metal catalysed photoredox catalysts has seen enormous advances in recent years, but there are significant drawbacks. First, the cost of these catalysts is often prohibitively high due to their precious metal core. This has no doubt hindered large scale industrial applications in synthetic photochemistry, and the first commercial application of these catalysts has only very recently been reported.[24] In addition, iridium and ruthenium are among the rarest naturally occurring elements and are finite resources that are also in demand in various other industries,[25] raising questions about long-term sustainability. Lastly, many of these catalysts have little practical recyclability, and concerns regarding the environmental and social impact of metal mining have been well documented.[26]

Homogeneous Organic Photoredox Catalysis

Several organic molecules have also been applied as photocatalysts as alternatives to iridium and ruthenium.[27–30] Developed by Nicewicz and co-workers, acridinium photocatalysts [31] have catalysed a host of arene oxidizing reactions (Scheme **1-6**), including cyanation, amination, and substitution.[32–34] Remarkably, while acridiniums were originally developed as oxidizing catalysts, Nicewicz and co-workers recently discovered that Mes-Acr-Ph could also act as a potent reductant,[35] with potentials comparable to elemental lithium. While acridiniums are no doubt far more sustainable than using complexes such as $Ir(ppy)_3$, the purchase cost of photocatalysts such as Mes-Acr-Ph are also high, comparable to the cost of iridium-based catalysts. In addition, these dyes are synthetically elaborate, requiring non-trivial synthesis, and sensitive organometallic reagents in some cases, which could limit large scale applications.

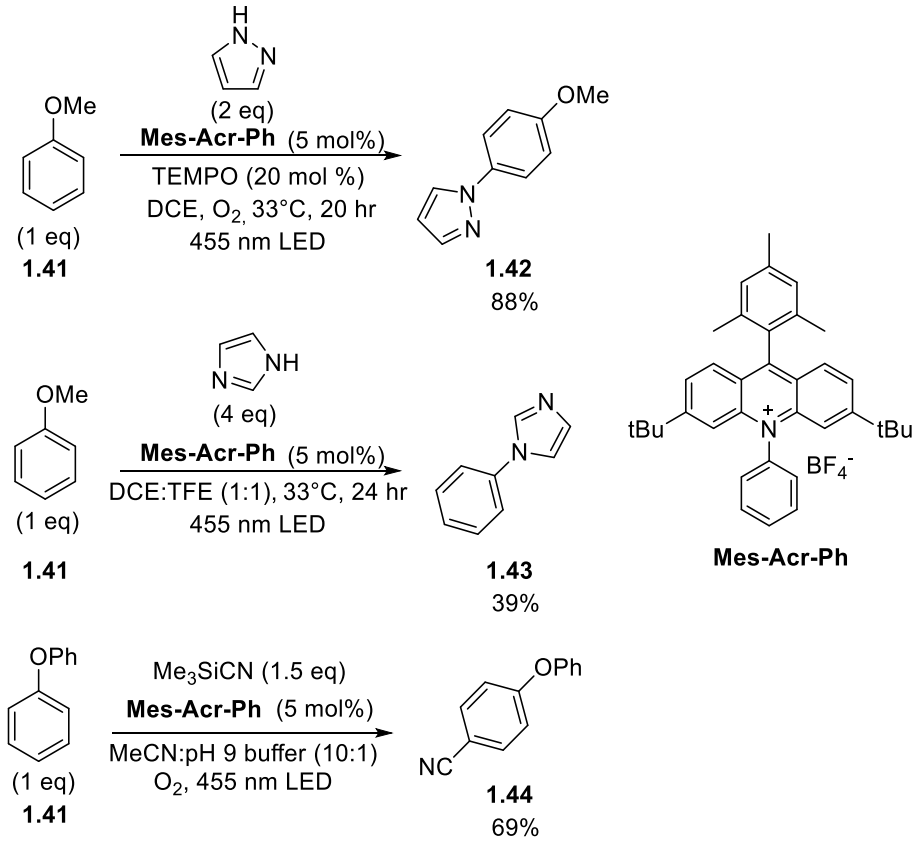

Scheme 1-6: Functionalization of arenes using acridinium photocatalysts.

Commercially available dyes such as Eosin Y have been successfully used for a variety of reactions (Scheme **1-7**).[36–39] König and co-workers utilized Eosin Y for arylation of diazonium salts,[40] along with alkyl halide reduction, and enantioselective aldehyde alkylation, demonstrating that they could be combined with complementary modes of catalysis – similar to ruthenium photocatalysts.[41]

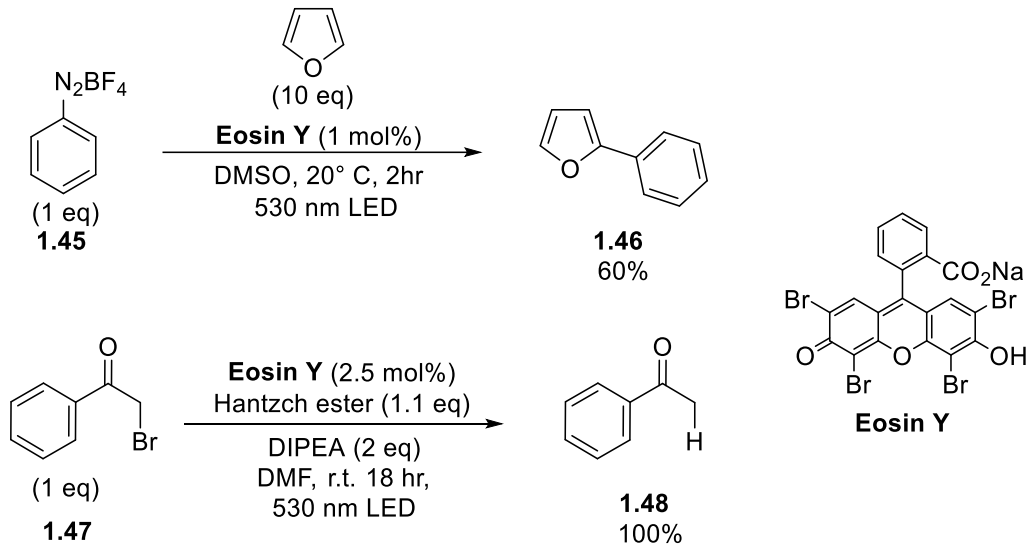

Scheme 1-7: Arylation and dehalogenation reactions catalysed by Eosin Y

Miyake and co-workers have reported on using several[42–47] phenoxazine and phenazine based photocatalysts as exceptionally reductive photocatalysts (Figure **1-2**). Initially developed as replacements for iridium photocatalysts in atom transfer radical addition polymerizations,[44,45] they have been used for various transformations in synthetic photochemistry.

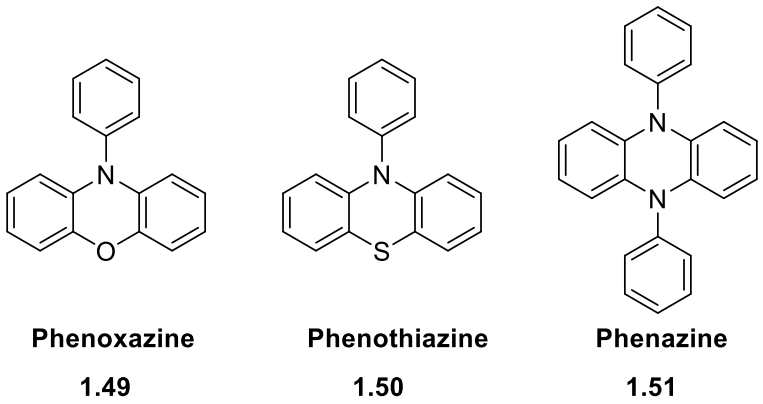

Figure 1-2: Phenoxazine, phenothiazine, and phenazine photocatalyst cores.

Glorious and co-workers used a reductive phenazine photocatalyst to convert feedstock carboxylic acid derivatives for decarboxylative olefination in alkene synthesis.[48] Phenazine, and phenoxazine catalysts are far more sustainable than precious metal counterparts – and could present cost effective alternatives, although their applications have still been limited.

Another widely used dye is a carbazole based catalyst 4CzIPN. Zhang and co-workers used 4CzIPN for decarboxylative arylation, using the organic photocatalyst as a direct replacement for $Ir[(dFCF_3ppy)_2(dtbbpy)][PF_6]$[49]. Other known applications of 4CzIPN include Minisci reactions,[50] decarboxylative cyclopropane synthesis,[51] and desilylative reactions (Scheme **1-8**).[52] The broad scope of reactions possible from this one catalyst highlights its promise as an inexpensive transition metal catalyst replacement.

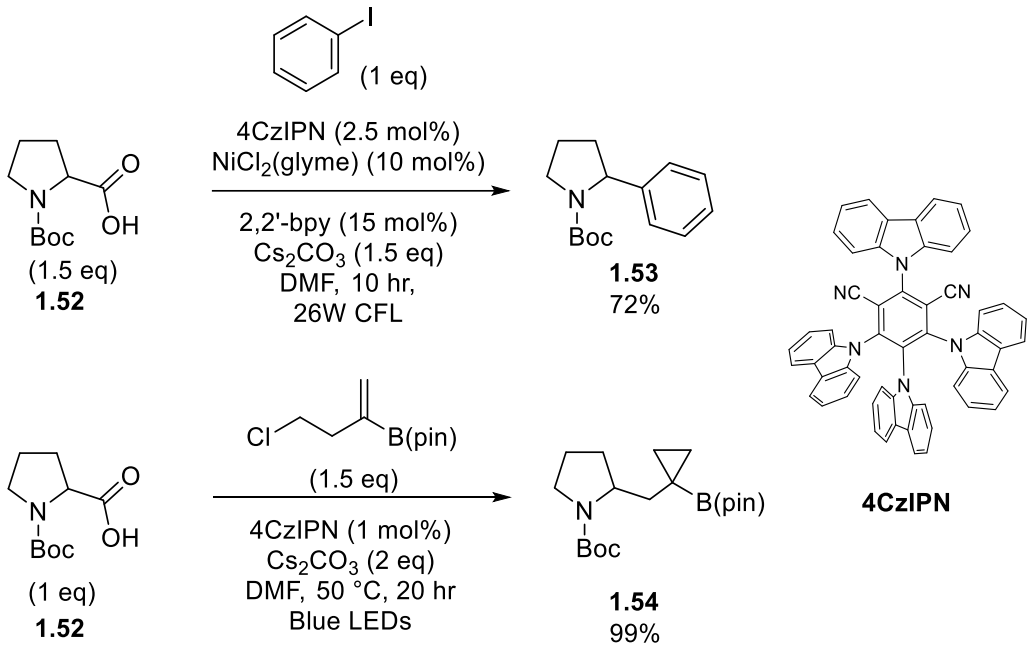

Scheme 1-8: Decarboxylative reactions catalysed by 4CzIPN.

Heterogeneous Photoredox Catalysis for Organic Synthesis

While remarkable progress has been made in the development of organic dyes as replacements for transition metal photocatalysts, there are still outstanding challenges associated with them. Many of these dyes are synthetically elaborate, requiring lengthy synthesis, and often approach the cost of transition metal complexes. In addition, like their transition metal counterparts, organic dyes are difficult to practically recycle and typically require higher catalyst loadings. A solution to some of these issues would be with heterogeneous photoredox catalysts. Heterogeneous photocatalysts are easily separated from reaction mixtures, and could also be more chemically resistant, allowing for catalyst recycling.

Heterogeneous photocatalysts have been widely explored for applications such as hydrogen evolution,[53–62] and CO_2 reduction,[63–66] but their use in synthetic organic photochemistry has been limited and is still in its infancy. While many reactions that have been performed using transition metal complexes have been substituted using organic dyes, many reactions have never been performed using a heterogeneous photocatalyst before.[67–74]

Carbon Nitrides

Many successful applications utilizing visible light have centred around carbon nitride[75–79] a cheap and scalable organic polymer that has seen successful applications in a variety of reactions. König and co-workers successfully used mesoporous carbon nitride (mpg-CN) in a host of reactions (Scheme **1-9**),[80] including arene trifluoromethylation, metallaphotoredox amination, and arene halogenation. The polymer was successfully recovered from reaction mixtures and recycled 4 times in different reactions and maintained comparable yields to unused carbon nitride in each of different reactions.

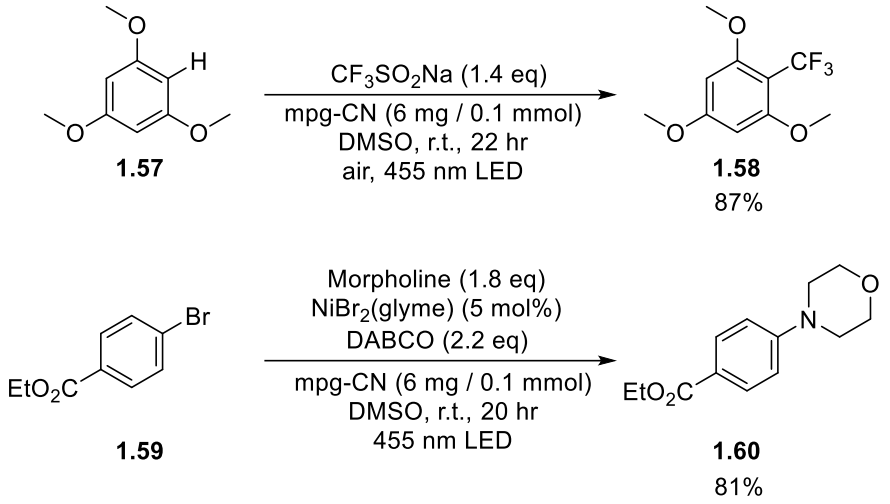

Scheme 1-9: Functionalization of arenes using mesoporous carbon nitride

Likewise, Seeberger and co-workers used a modified carbon nitride (CN-OA-m) for the esterification of aryl halides (Scheme **1-10**),[77] in combination with a homogeneous nickel cocatalyst, whilst also demonstrating that the polymer could be recycled multiple times. While the ester products were formed in good yields, no formation of the decarboxylative C-C coupling product was observed.

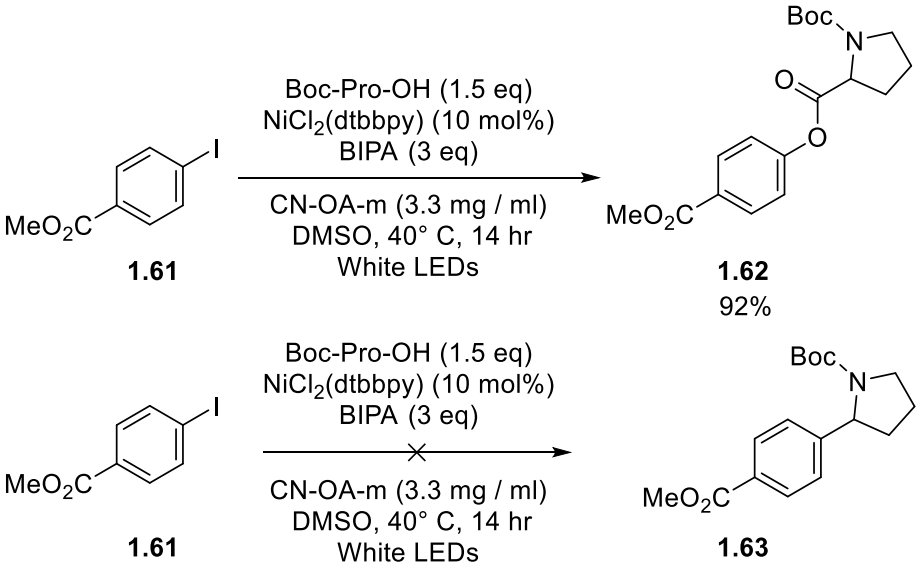

Scheme 1-10: Metallaphotoredox esterification of aryl halides using modified carbon nitride.

Recently, Reisner and co-workers demonstrated the metallaphotoredox etherification of aryl halides using carbon nitride (Scheme **1-11**).[81] Notably, Reisner and co-workers showed that the nickel co-catalyst (Ni-mpg-CN) can be integrated with carbon nitride for a unified catalyst for aryl halide esterification, obviating the need for a homogeneous nickel catalyst, or the requirement of a ligand for the nickel cocatalyst. Reisner and co-workers have further applied this integrated photocatalyst for the amination of aryl halides using sodium azide[82] and showed that the Ni/CN catalyst was easily recycled and retained catalytic activity.

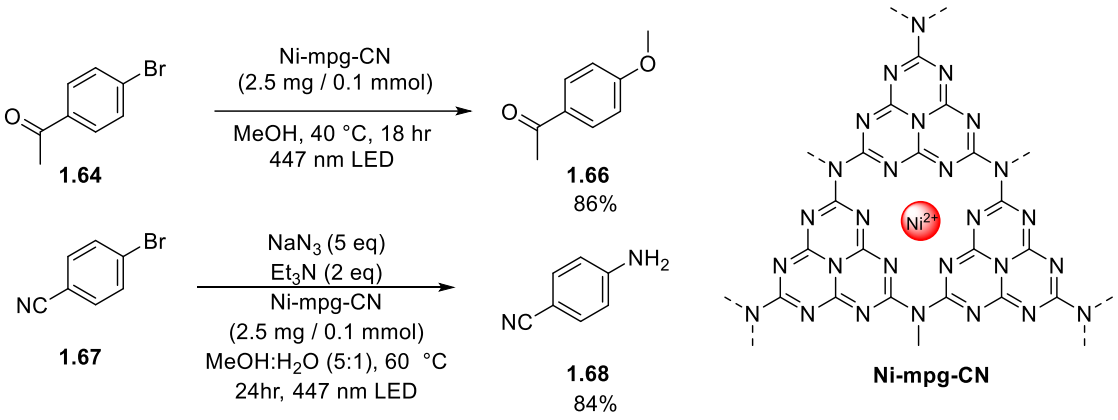

Scheme 1-11: Metallaphotoredox amination and etherification of aryl halides using an integrated nickel-carbon nitride photocatalyst.

Carbon nitride has been used for decarboxylative reactions by a number of groups. Rueping and co-workers used graphitic carbon nitride for Michael addition reactions of N-aryl glycines under visible light (Scheme **1-12**).[83] They also applied g-C_3N_4 for desilylative conjugate addition and arylation. Recycling the catalyst 7 times, the polymer maintained good catalytic activity, and was also applied for a gram scale synthesis in flow. Seeberger and co-workers reported on the decarboxylative fluorination of phenoxyacetic carboxylic acids using a modified carbon nitride.[84] This reaction was also performed in flow, with the modified carbon nitride forming a stable suspension.

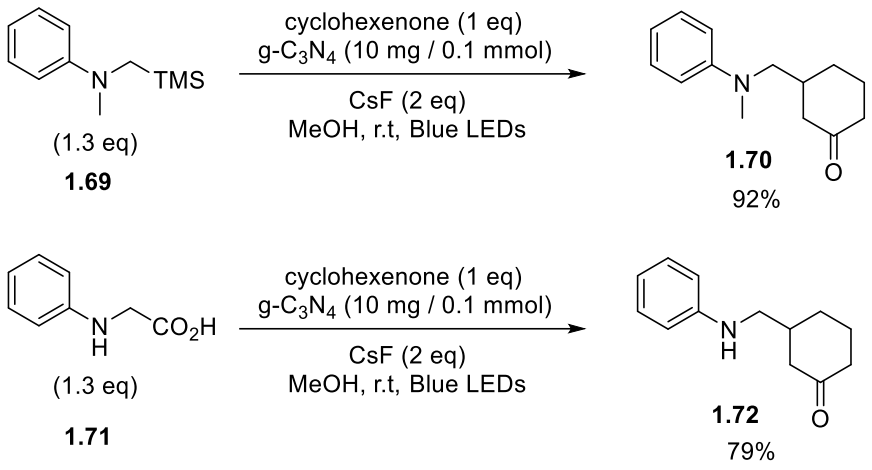

Scheme 1-12: Desilylative and decarboxylative conjugate addition of N-Aryl amines using graphitic carbon nitride.

Cai and co-workers recently used a potassium doped carbon nitride (CN-K) for decarboxylative addition of several carboxylic acids (Scheme **1-13**),[85] and Wang and co-workers have used boron carbon nitride (BCN) for decarboxylative arylation and amination of aryl several acetic acids. In both reports, the modified carbon nitride polymer catalyst was easily recovered and recycled.[86]

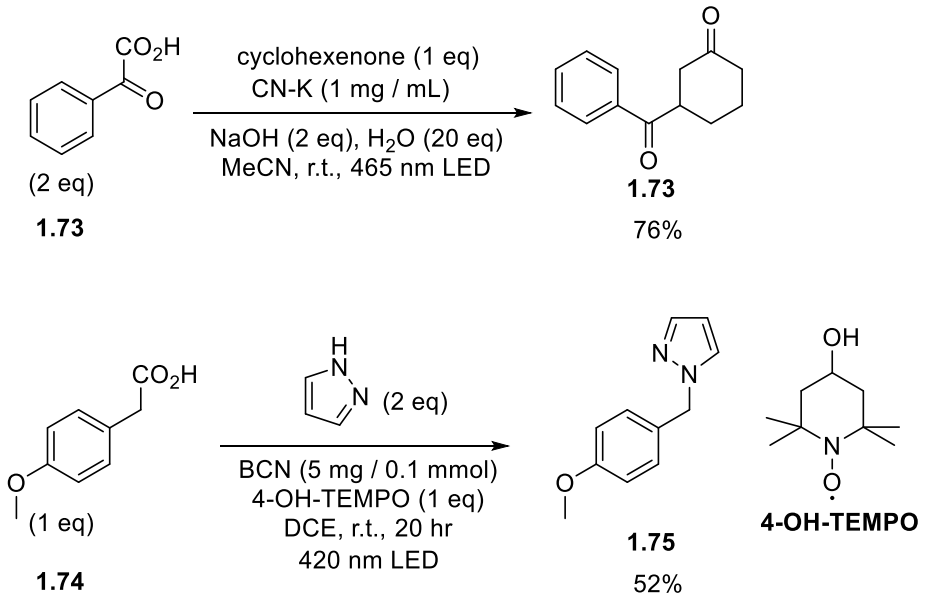

Scheme 1-13: Decarboxylative functionalization using potassium doped carbon nitride and boron carbon nitride.

Benzothiadiazole Polymers

Distinct from carbon nitrides, other conjugated polymers have been applied for photoredox catalysis. Various groups used benzothiadiazole containing polymers for a host of different reactions.[87] Using a carbazole-benzothiadiazole polymer under air, Zhang and co-workers were able to selectively oxidize aryl sulfides to sulfoxides (Scheme **1-14**),[88] without the use of external oxidant such as hydrogen peroxide. Notably, they also immobilized the benzothiadiazole polymer onto a column and performed the photocatalysis in flow. Benzothiadiazole polymers have also been used for conversion of arylboronic esters into phenols,[89] and halogenation of arenes.[90] The ability of benzothiadiazole based polymers to catalyse several of these reactions demonstrates the potential of organic polymers to enable a broad range of synthetic chemistry.

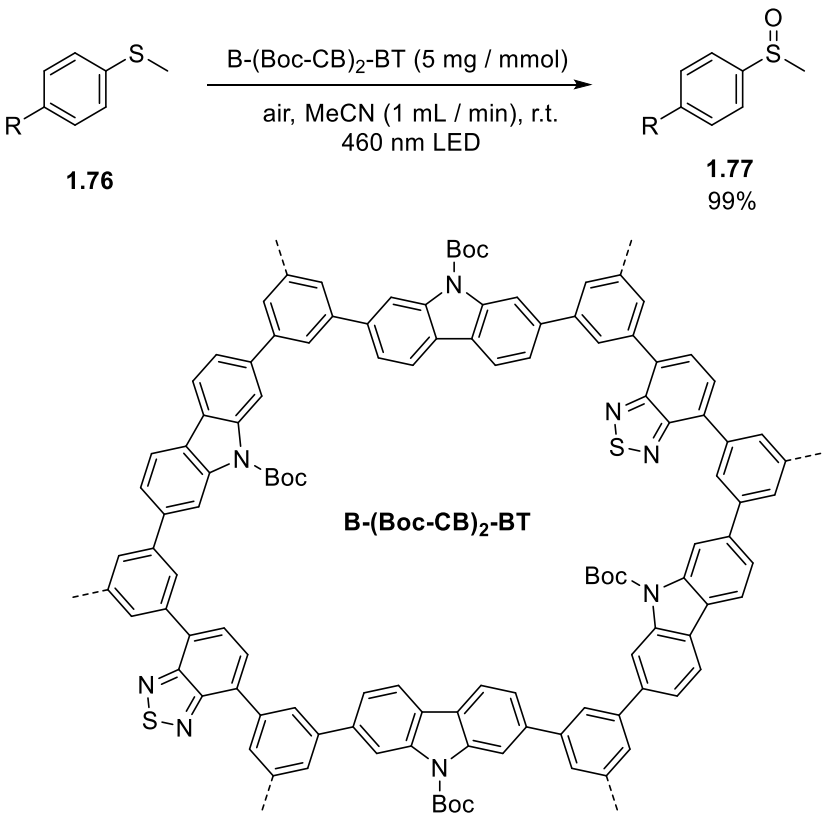

Scheme 1-14: Selective oxidation of aryl sulfides using a benzothiadiazole-carbazole polymer.

Similarly, the Zhang group has also used a triethynylbenzene-benzothiadiazole polymer for highly enantioselective alkylation of aldehydes, and alkyl halide reduction (Scheme **1-15**).[91] The B-Bt polymer was also successfully immobilized on a column and used under flow conditions. Recycling experiments showed that the polymer retained its photocatalytic activity over 5 cycles, and enantioselectivity of the products were retained. This also demonstrates that organic polymer photocatalysts can work in tandem with other catalysts, chiral amines in this case. Stereoselective synthesis of molecules with recyclable polymers is a promising approach for sustainable synthesis.

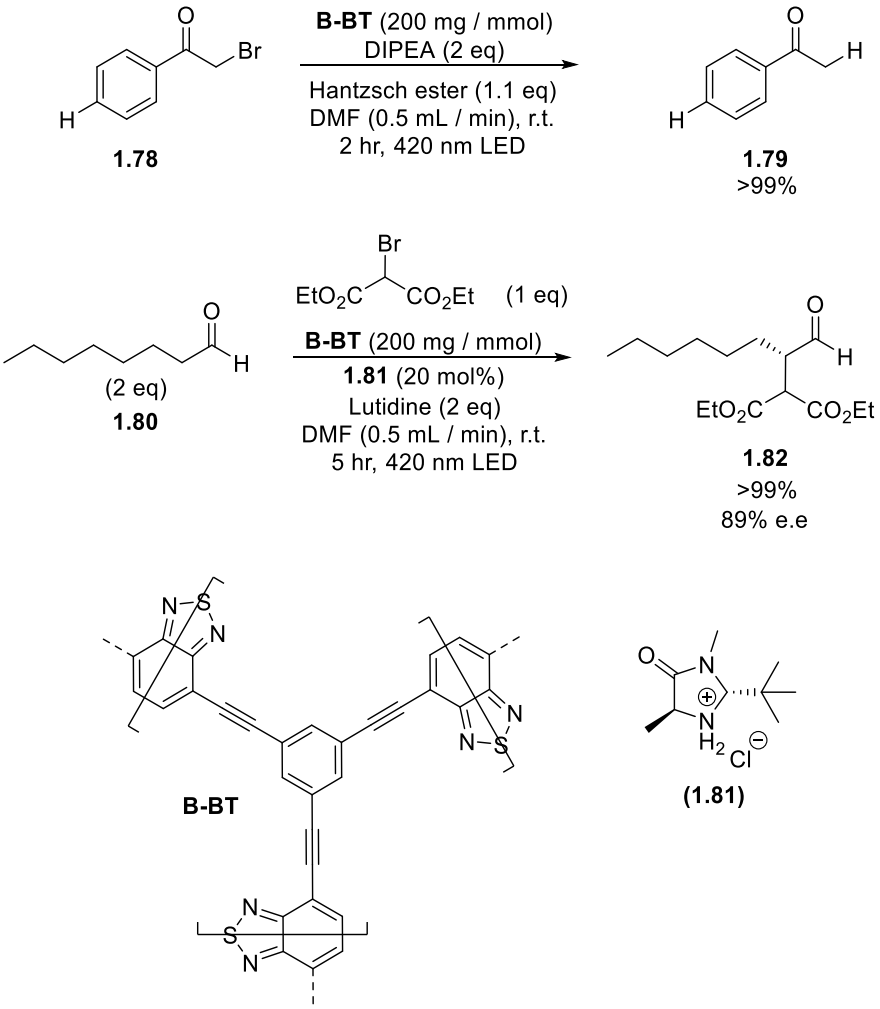

Scheme 1-15: Alkyl dehalogenation, and enantioselective alkylation of aldehydes using benzothiadiazole / triethynylbenzene photocatalysts.

Covalent Triazine Frameworks

Covalent Triazine Frameworks (CTFs), a specific class of conjugated polymer, have been leveraged for metal-free organic photosynthesis in multiple reports. Zhang and co-workers have used CTFs for production benzophosphole oxide (Scheme **1-16**),[92] using an asymmetric CTF, which showed superior performance over its symmetric counterparts, demonstrating the benefits of being able to tune the properties of the materials at the molecular level. The polymerization of the asymmetric monomer, led to the presence of a non-uniform covalent triazine framework with 4 possible triazine units (**M1** – **M4**) that could be formed from the polymerization.

Savateev and co-workers have reported on the applications of CTFs for metallaphotoredox amination (Scheme **1-17**),[93] and arene halogenation. However, the substrates successful for bromination were limited to electron rich arenes, and electron deficient arenes for metallaphotoredox amination. CTF materials have also been used as highly photostable catalysts for hydrogen evolution,[94–98] and hydrogen peroxide production. CTFs can also be prepared without palladium cross coupling, unlike other polymer photocatalysts, though polycondensation,[99] or ionothermal synthesis,[100] and can be a large advantage in sensitive applications such as pharmaceutical synthesis, where metal leaching is a concern.

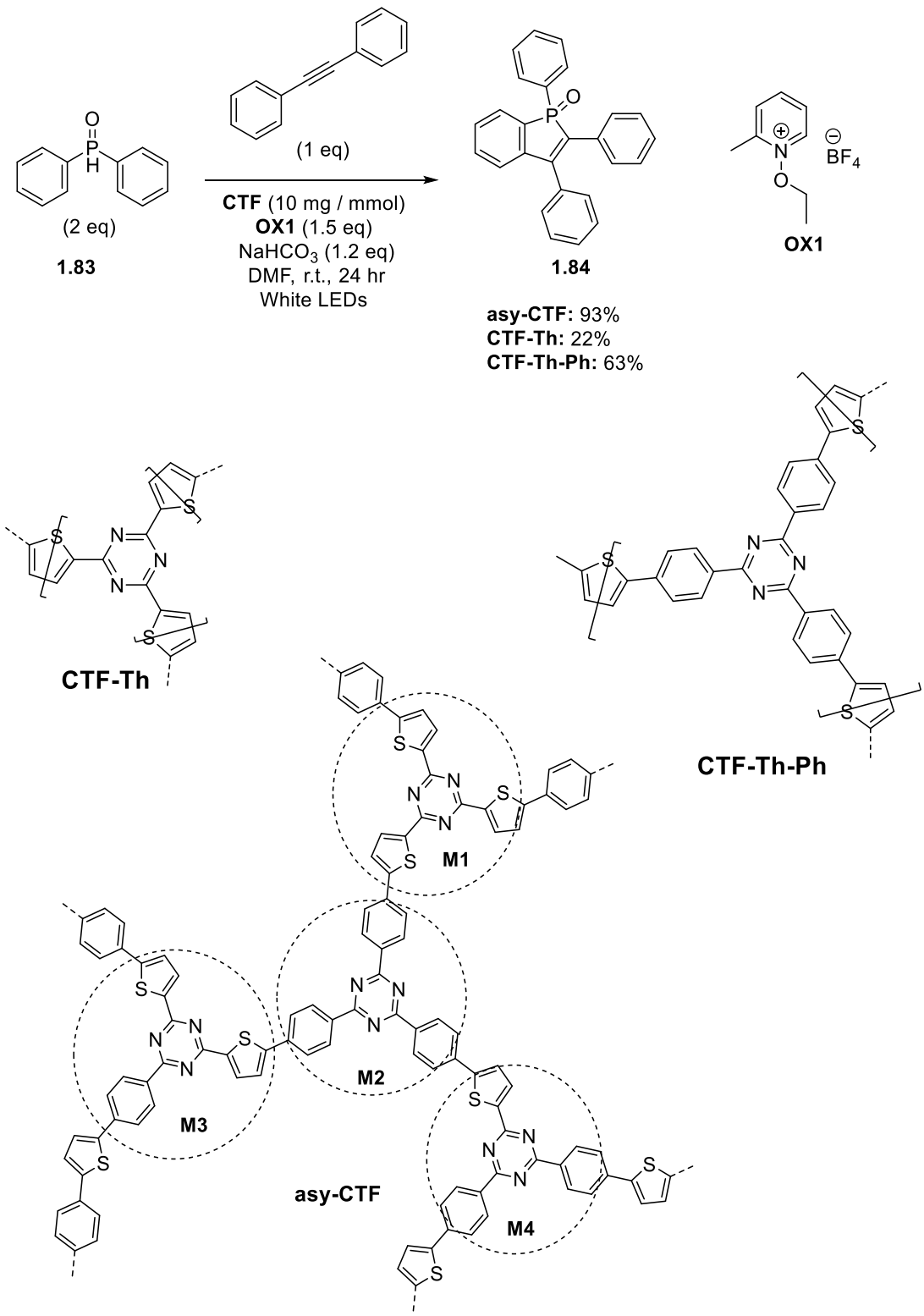

Scheme 1-16: Benzophosphole oxide synthesis using symmetric and asymmetric CTFs.

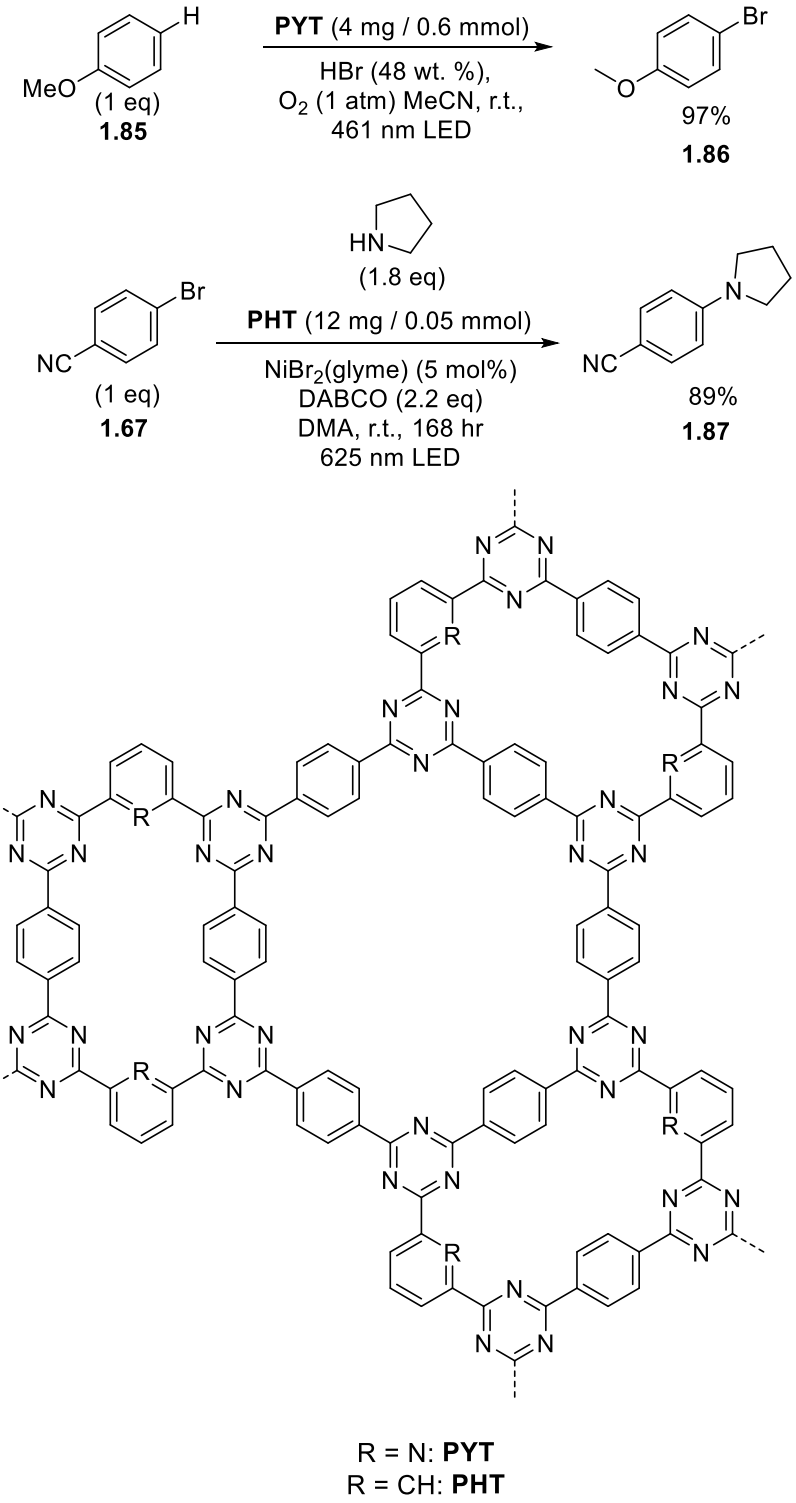

Scheme 1-17: Arene halogenation and metallaphotoredox amination using CTF polymers.

Dye Integration

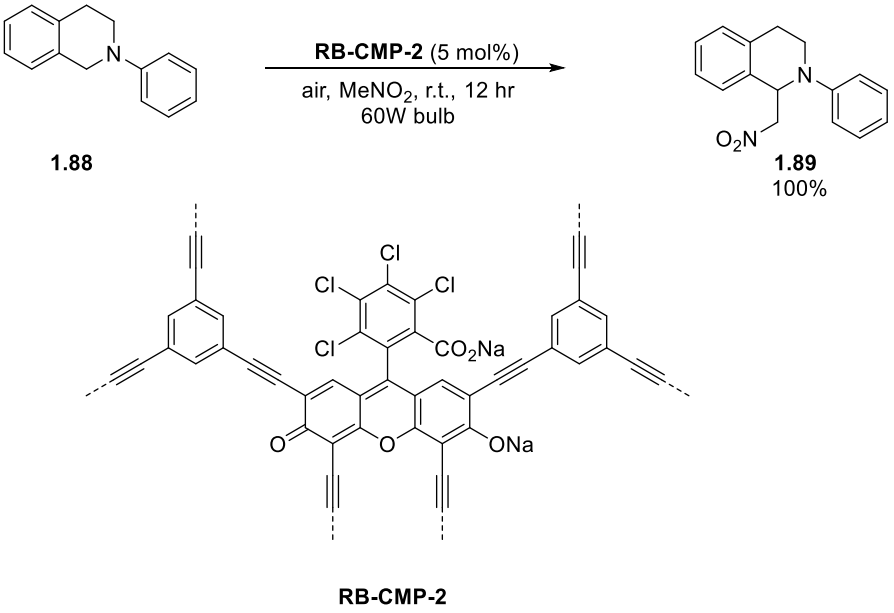

Scheme 1-18: Synthesis of Rose Bengal conjugated polymer and application towards photocatalytic Aza-Henry reaction.

Integration of dyes into polymer backbones, or the creation of heterogeneous analogues of molecular dyes has been explored by several groups. The Cooper group reported the synthesis of Rose Bengal based polymers (Scheme **1-18**),[101] through the reaction with triethynyl benzene, producing conjugated microporous polymers that were active for the Aza-Henry reaction of tetrahydroisoquinolines. This was also similarly applied for construction of Eosin Y based polymers,[102] for the same reaction. This Eosin based polymer has also been successfully utilized for photocatalytic CO_2 reduction.[103]

Vilela and co-workers have also used this approach by incorporating 4,4-difluoro-4-bora-3a,4a-diaza-s-indacene (BODIPY) into polymers (Scheme **1-19**),[104] for oxidation of terpinene to ascaridole. BODIPY has been reported as a photosensitizing catalyst for several reactions.[105] Using a post-synthetic modification strategy, Vilela and co-workers installed a BODIPY moiety onto a resin. The functionalized polymers then underwent a second modification, through chlorination, and the resultant polymers showed greater performance compared to the to the non-chlorinated polymers. The resultant polymers were stable after 96 hours of irradiation.

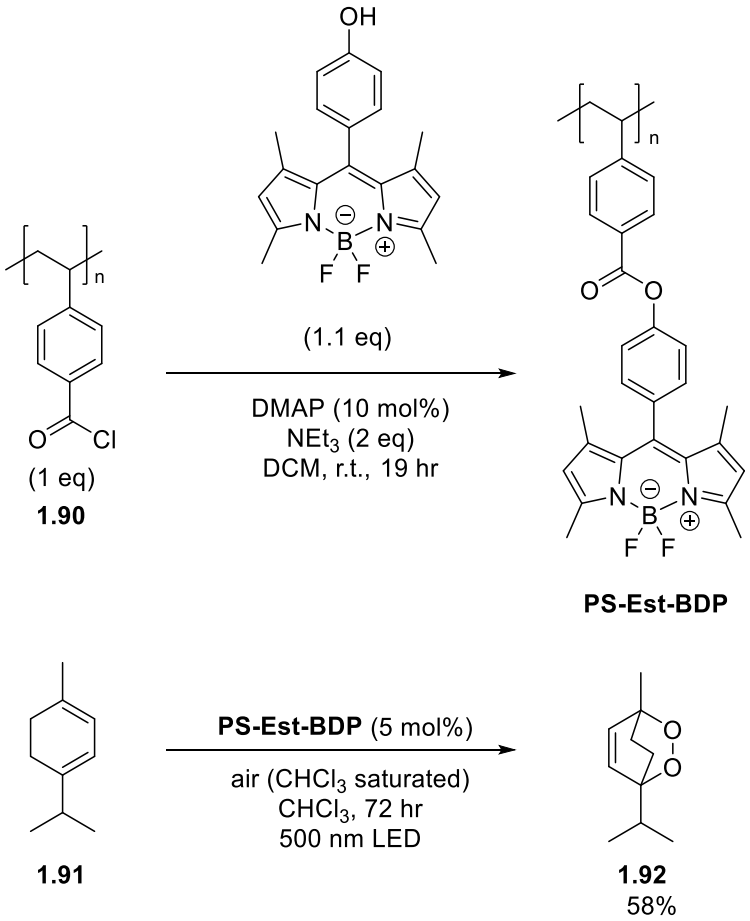

Scheme 1-19: Post-synthetic modification and installation of a BODIPY polymer photocatalyst, and application in ascaridole synthesis.

In a similar approach, Vilela and co-workers co-polymerized a photoactive benzothiadiazole unit with styrene,[106] creating a polymer photosensitizer for oxidation of terpinene. Notably, they found that efficiencies were comparable between irradiation with direct sunlight and 420 nm LED irradiation. Undoubtedly, using natural sunlight would be a major advantage compared to having to construct or purchase photoreactor setups.

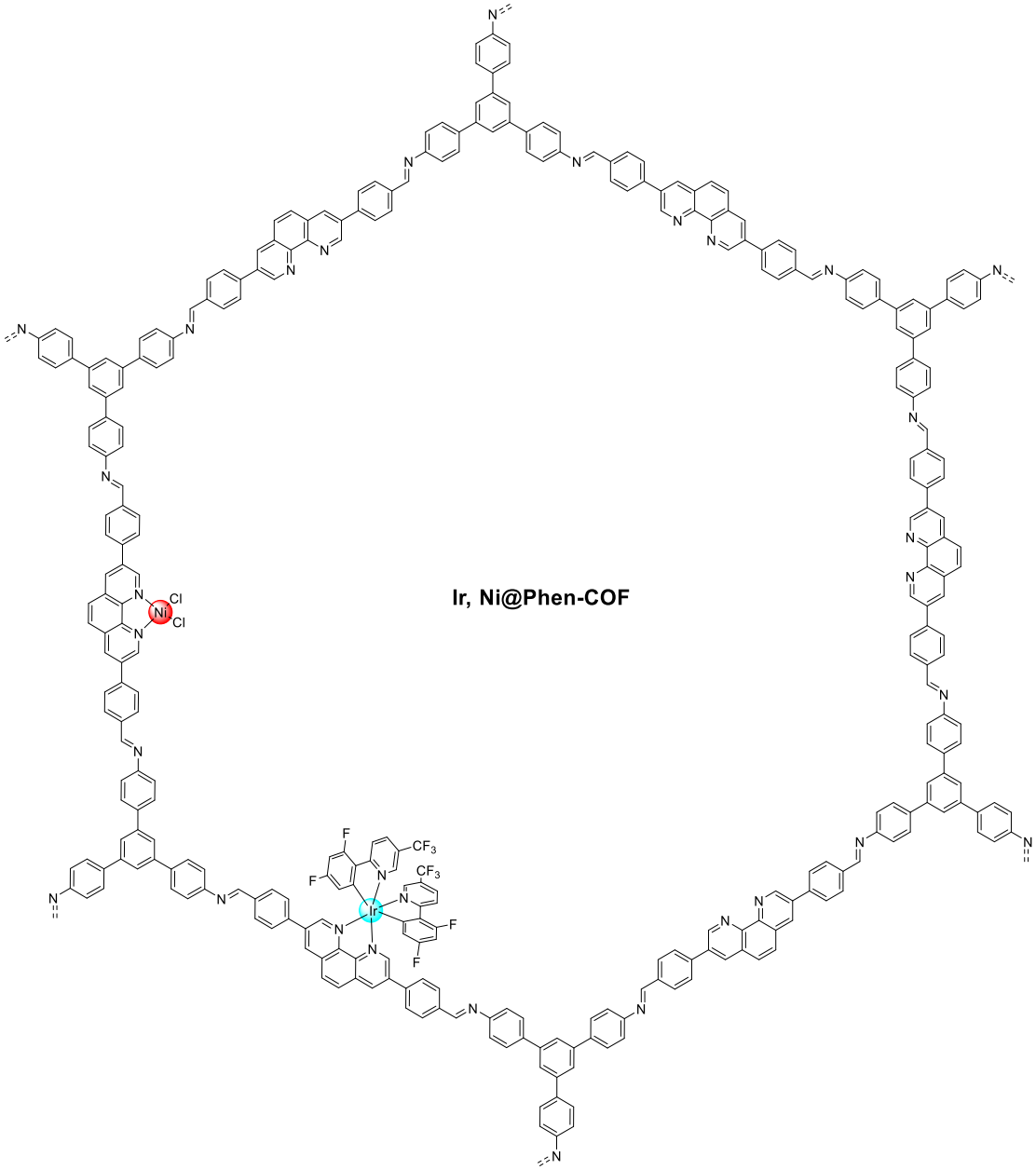

Figure 1-3: Dual iridium and nickel COF as a unified material for heterogeneous metallaphotoredox catalysis.

Porous, crystalline covalent organic frameworks (COFs) have also been applied for a variety of photocatalytic applications. Aleman and co-workers have very recently reported on the synthesis of a porous, crystalline, dual-metal COF (Figure **1-3**),[107] containing both nickel and iridium centres. This bimetallic COF resulted in a singular, recyclable, material that could be applied for metallaphotoredox reactions, without the addition of external ligands. Ir,Ni@Phen-COF was successful in catalysing several reactions including decarboxylative arylation, and arylation of trifluoroborates. The material was recycled 8 times, and showed consistent catalytic properties, and retained its

crystallinity and porosity. A very similar approach was also recently used by Banerjee and co-workers,[108] who also used an iridium and nickel loaded COF for metallaphotoredox amination of aryl halides, and again showed catalytic retention over 10 cycles. Likewise, Pieber and co-workers have constructed acridine based COF materials for metallaphotoredox amination.[109]

While these successful reports of organic heterogeneous photoredox catalysts have successfully demonstrated the promise of robust materials as replacements for transition metals, there are several challenges that these materials themselves face in aiding the wider adoption of photochemistry. Materials should be readily scalable to use in practical applications. Any potential applications of polymers as photocatalysts on industrial scale, for example, would require reproducible, sustainable, cost-effective synthesis methods. COF materials, for example, are infrequently synthesized on gram scale.

Aside from organic materials, transition metal semiconductor materials have also been explored. TiO_2, which has been studied for decades as a catalyst for photochemical hydrogen production,[110] has been applied to a variety of reactions. Pt/TiO_2 catalysts have been used for hydrodecarboxylation by Wang [111] and co-workers, functionalizing fatty acids into alkanes. Nocera and co-workers have recently demonstrated decarboxylative conjugate addition of carboxylic acids using TiO_2 to electron deficient Michael acceptors.[112] Remarkably, TiO_2 was also able to catalyse photodecarboxylation of acetic acid, enabling direct methyl group installation (Scheme **1-20**), without the use of Grignard or other organometallic reagents. Nocera also demonstrated direct functionalization of the pharmaceutical Gemfibrozil. A significant drawback in using TiO_2, however, is that it has poor absorbance in visible light, requiring UV irradiation, which adds additional complexity and cost, although strategies such as dye sensitization could potentially mitigate this issue.[113]

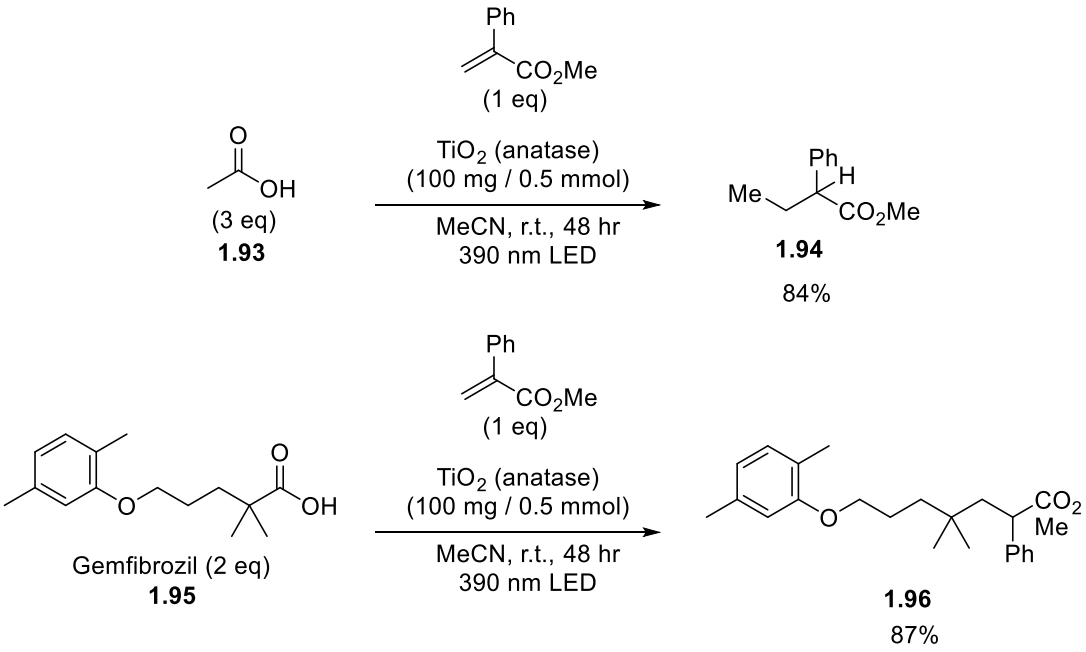

Scheme 1-20: Decarboxylative conjugate addition of carboxylic acids using TiO2 in near-visible light.

Xiao and co-workers meanwhile have successfully applied CdS for photocatalytic amination and etherification, in combination with a homogeneous nickel catalyst.[114] Similarly, Weix and co-workers utilized CdSe quantum dots (QDs) for direct beta alkylation of aldehydes (Scheme **1-21**),[115] beta amino-alkylation of cyclic ketones, and aryl dehalogenation mimicking the performance of the iridium catalysts used by Macmillan.

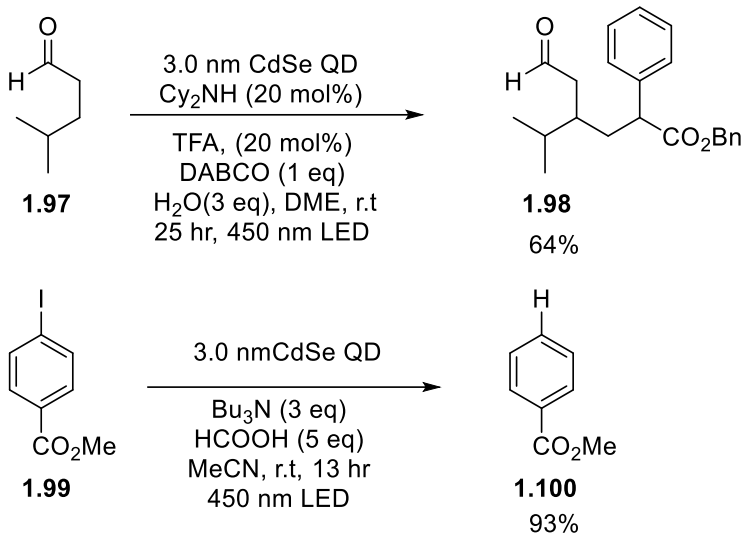

Scheme 1-21: Beta alkylation and reductive dehalogenation of aryl halides using CdSe quantum dots.

High Throughput Experimentation and Discovery

The demand, and necessity, for faster and more efficient discovery processes has driven the rise of high throughput experimentation (HTE) in various sectors. In the pharmaceutical industry, this has become standard procedure, where large number of trial molecules and analogues are tested in parallel, and synthetic routes are optimized.[116–118] The emergence of new technologies, and standardization of lab equipment has helped accelerate discovery. For example, 96 well plates, autosamplers, and standardized vial sizes have all aided researchers in easily translating samples to different equipment and analytical techniques. Stevens and co-workers recently used an impressive high throughput approach to optimize the synthesis of the API branebrutinib (Figure **1-4**),[119] which was initially produced in discovery stage using an 8-step synthesis, and was a major limitation for production in clinical trials.

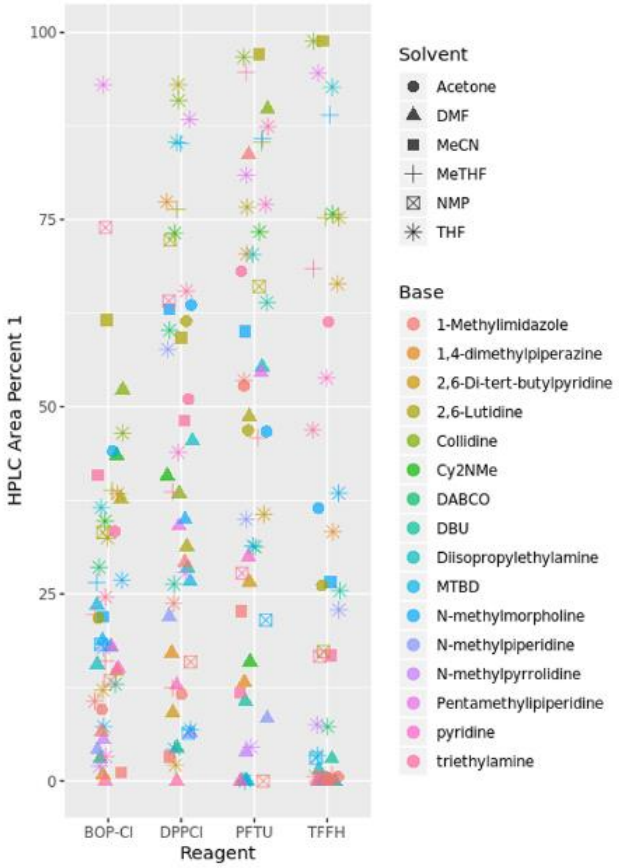

Figure 1-4: HTE for parallel solvent/base screening for amide bond formation. Figure reproduced from literature. [119]

Using high throughput experimentation, they optimized the various steps in the production of the API, in parallel, running thousands of reactions, and shortened the synthetic route to 4 steps. The optimized synthetic route was then successfully scaled up to a kilogram scale.

High-throughput experimentation has also been leveraged for additive discovery in organic synthesis. Macmillan and co-workers recently used a phenotypic approach to improve their reported photocatalytic decarboxylative arylation reaction,[120] which has been limited, particularly, by slow decarboxylation in substrates without an adjacent heteroatom, and was unamenable to further improvement using traditional optimization. Using HTE, Macmillan and co-workers investigated additives for the cross coupling of non-activated carboxylic acids with aryl halide partners for a total of 3840 reactions (Figure **1-5**). While most additives resulted in no improvement or poisoned the reaction, phthalimide was unexpectedly found to be highly beneficial.

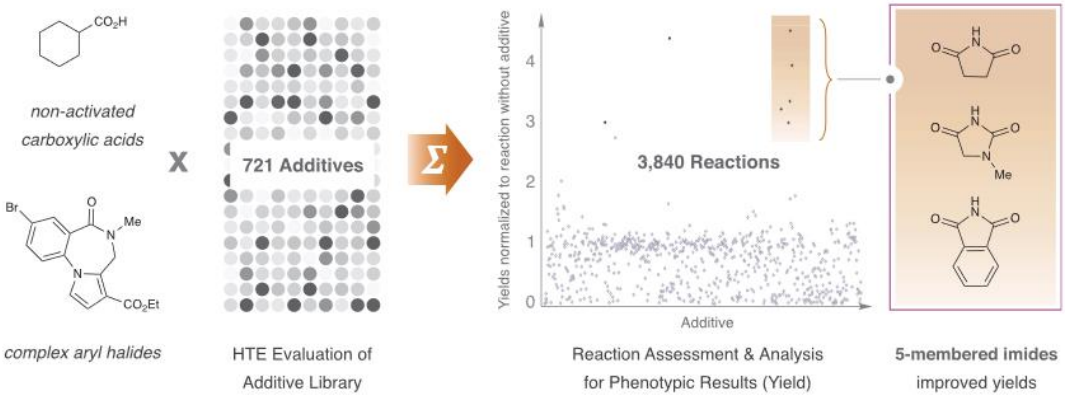

Figure 1-5: Phenotypic screening for reaction additive discovery using high-throughput experimentation. Figure reproduced from literature. [120]

Investigation of phthalimide addition over a broad range of carboxylic acids and aryl bromides (384 of each) demonstrated that inclusion of phthalimide significantly improved decarboxylative coupling product formation in most cases, significantly improving the scope of the reaction. Investigations revealed that the inclusion of phthalimide limited the amount of dehalogenation by-product, and dramatically improved the yields of non-activated carboxylic acid substrates, substantially enhancing the scope of the reaction.

Advances in machine learning, and other data driven approaches to chemistry have seen progress in recent years, coupled with increased access to more computational power.[121,122] The Doyle group recently applied Bayesian reaction optimization to demonstrate the power of data driven approaches,[123] showing that the optimizer yielded better performance than humans in optimizing reaction parameters. Similarly, Aspuru-Guzik and co-workers recently used a combination of ChemSpeed platform containing an in-line HPLC, and an optimizer for closed loop optimization of a reaction.[124] By performing HTE inside a well plate and analysing yields with inline HPLC (Figure **1-6**).

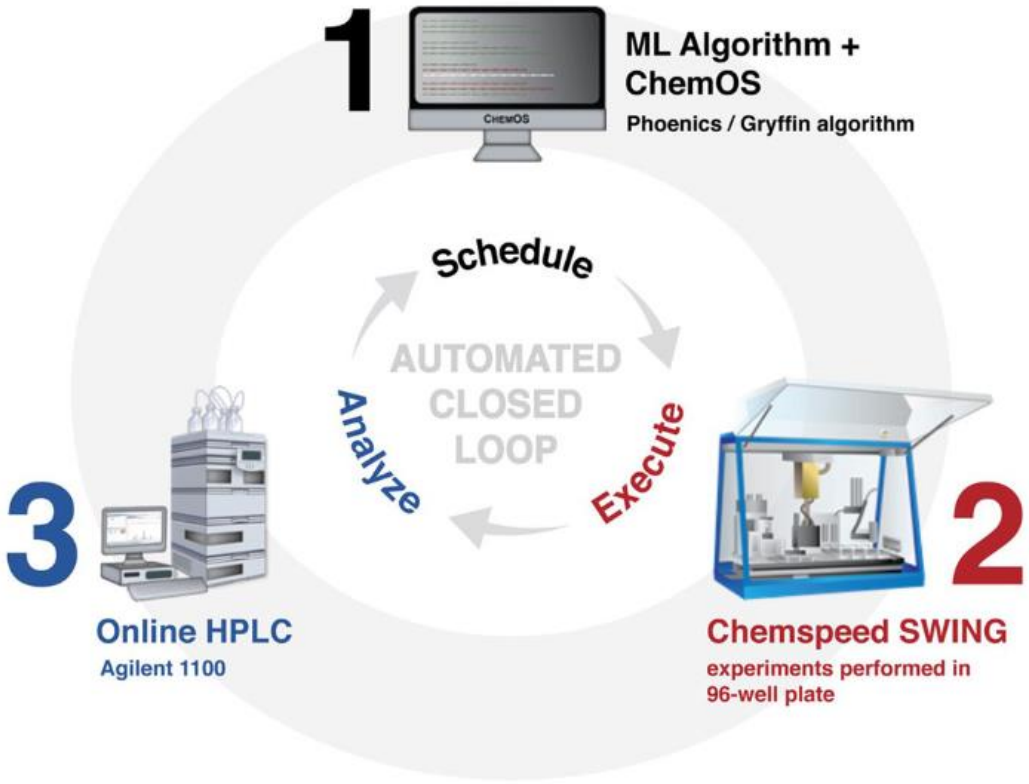

Figure 1-6: Autonomous reaction optimization using inline HPLC for HTE analysis. Figure reproduced from literature. [124]

The Cooper group has extensively used high-throughput experimentation for the discovery of new materials. Using a combination of computational pre-screening and experimentation with robotic platforms, Cooper and co-workers synthesized 170 polymers (Figure **1-7**) and used HTE to evaluate them for photocatalytic water splitting.[125] Through this workflow, a new polymer, P64, was discovered to be highly active for sacrificial hydrogen evolution, maintaining catalytic performance over 30 hours of irradiation.

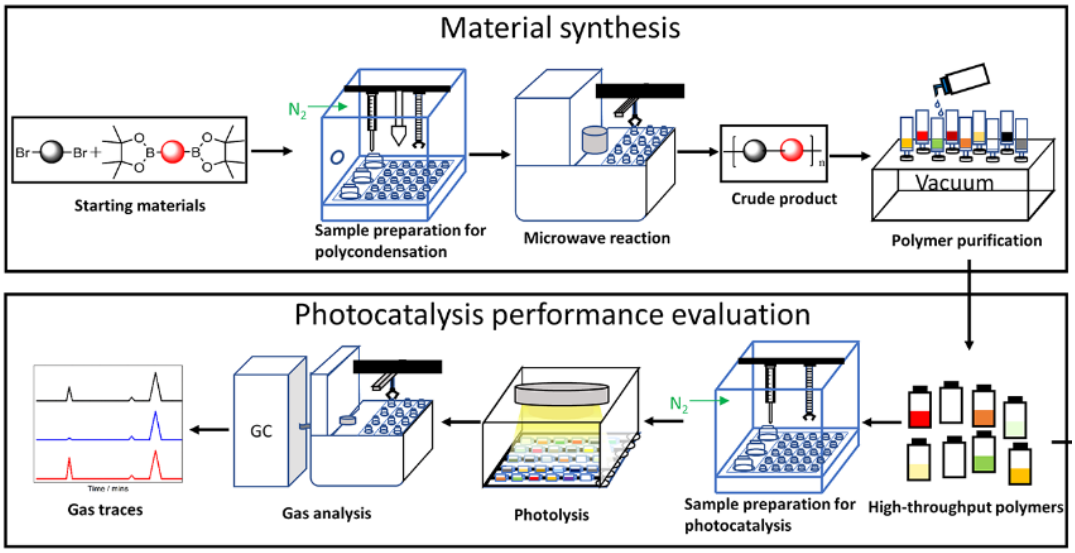

Figure 1-7: High-Throughput discovery of polymers for photocatalytic water splitting. Figure reproduced from literature. [125]

Cooper and co-workers have applied the use of mobile robotics towards optimization of hydrogen evolution,[126] using a KUKA platform to search for optimal conditions for sacrificial water splitting using a polymer photocatalyst. After days of unattended operation, the platform discovered a combination of components several times more active than the initial formulation over a total of 688 experiments (Figure **1-8**). Multivariate exploration of reaction space can no doubt offer benefits over traditional approaches such as one-variable-at-a-time or factorial design of experiments. Binary and ternary mixtures of reaction parameters, such as solvents for example, are often not explored for optimization due to practical constraints and could offer improved yields over using any one solvent alone.

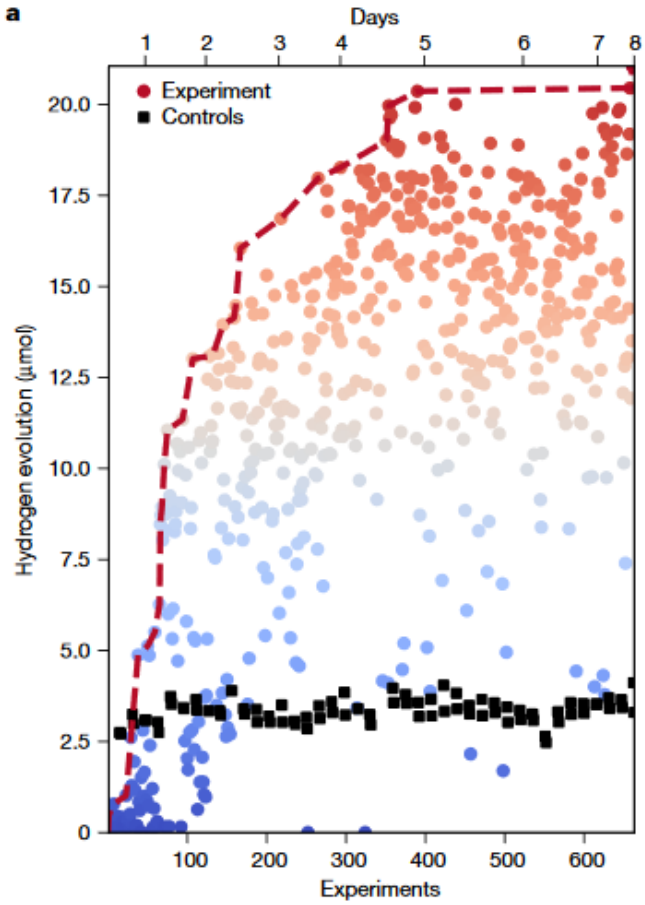

Figure 1-8: HTE using a mobile robot for optimization of hydrogen evolution. Figure reproduced from literature. [126]

Conclusions and Outlook:

The resurgence of modern photocatalysis has enabled the development of reactions with mild conditions, and allowed for unique reaction pathways. The ability to use inexpensive LEDs with visible light emission, over UV reactors, has drastically improved accessibility. However, its full potential is hindered by the prohibitive cost of commonly used precious metal transition metal complexes, or synthetically elaborate dyes. While much progress has been made in creating recyclable photocatalysts many reactions have never been catalysed by a heterogeneous photocatalyst. The development of sustainable catalysts will no doubt aid its wider adoption, particularly in industrial settings. HTE has seen great success in accelerating discovery, and these techniques could be translated to synthetic photochemistry.

References

1. Shaw, M. H., Twilton, J. & MacMillan, D. W. C. Photoredox Catalysis in Organic Chemistry. *J. Org. Chem.* **81**, 6898–6926 (2016).
2. Buglioni, L., Raymenants, F., Slattery, A., Zondag, S. D. A. & Noël, T. Technological Innovations in Photochemistry for Organic Synthesis: Flow Chemistry, High-Throughput Experimentation, Scale-up, and Photoelectrochemistry. *Chem. Rev.* **122**, 2752–2906 (2022).
3. Nicewicz, D. A. & MacMillan, D. W. C. Merging Photoredox Catalysis with Organocatalysis: The Direct Asymmetric Alkylation of Aldehydes. *Science* **322**, 77–80 (2008).
4. Ischay, M. A., Anzovino, M. E., Du, J. & Yoon, T. P. Efficient Visible Light Photocatalysis of [2+2] Enone Cycloadditions. *J. Am. Chem. Soc.* **130**, 12886–12887 (2008).
5. Narayanam, J. M. R., Tucker, J. W. & Stephenson, C. R. J. Electron-Transfer Photoredox Catalysis: Development of a Tin-Free Reductive Dehalogenation Reaction. *J. Am. Chem. Soc.* **131**, 8756–8757 (2009).
6. Zhou, Q., Zou, Y., Lu, L. & Xiao, W. Visible-Light-Induced Organic Photochemical Reactions through Energy-Transfer Pathways. *Angew. Chem. Int. Ed.* **58**, 1586–1604 (2019).
7. Le, C. “Chip” *et al.* A General Small-Scale Reactor To Enable Standardization and Acceleration of Photocatalytic Reactions. *ACS Cent. Sci.* **3**, 647–653 (2017).
8. McNally, A., Prier, C. K. & MacMillan, D. W. C. Discovery of an -Amino C-H Arylation Reaction Using the Strategy of Accelerated Serendipity. *Science* **334**, 1114–1117 (2011).
9. DeHovitz, J. S. *et al.* Static to inducibly dynamic stereocontrol: The convergent use of racemic β-substituted ketones. *Science* **369**, 1113–1118 (2020).
10. Proctor, R. S. J., Davis, H. J. & Phipps, R. J. Catalytic enantioselective Minisci-type addition to heteroarenes. *Science* **360**, 419–422 (2018).
11. Fu, M.-C., Shang, R., Zhao, B., Wang, B. & Fu, Y. Photocatalytic decarboxylative alkylations mediated by triphenylphosphine and sodium iodide. *Science* **363**, 1429–1434 (2019).

12. Qiu, G. & Wu, J. Transition metal-catalyzed direct remote C–H functionalization of alkyl groups via C(sp ^{3})–H bond activation. *Org. Chem. Front.* **2**, 169–178 (2015).
13. Zuo, Z. & Macmillan, D. W. C. Decarboxylative Arylation of a-Amino Acids via Photoredox Catalysis: A One-Step Conversion of Biomass to Drug Pharmacophore Zhiwei Zuo and David W. C. MacMillan*. *J. Am. Chem. Soc.* **136**, 5257 (2014).
14. Terrett, J. A., Clift, M. D. & MaCmillan, D. W. C. Direct β-alkylation of aldehydes via photoredox organocatalysis. *J. Am. Chem. Soc.* **136**, 6858–6861 (2014).
15. Petronijević, F. R., Nappi, M. & MacMillan, D. W. C. Direct β-Functionalization of Cyclic Ketones with Aryl Ketones via the Merger of Photoredox and Organocatalysis. *J. Am. Chem. Soc.* **135**, 18323–18326 (2013).
16. Jeffrey, J. L., Petronijević, F. R. & Macmillan, D. W. C. Selective Radical-Radical Cross-Couplings: Design of a Formal β-Mannich Reaction. *J. Am. Chem. Soc.* **137**, 8404–8407 (2015).
17. Pirnot, M. T., Rankic, D. A., Martin, D. B. C. & MacMillan, D. W. C. Photoredox Activation for the Direct -Arylation of Ketones and Aldehydes. *Science* **339**, 1593–1596 (2013).
18. Prier, C. K., Rankic, D. A. & MacMillan, D. W. C. Visible Light Photoredox Catalysis with Transition Metal Complexes: Applications in Organic Synthesis. *Chem. Rev.* **113**, 5322–5363 (2013).
19. Zuo, Z. *et al.* Merging photoredox with nickel catalysis: Coupling of α-carboxyl sp 3 -carbons with aryl halides. *Science* **345**, 437–440 (2014).
20. Johnston, C. P., Smith, R. T., Allmendinger, S. & MacMillan, D. W. C. Metallaphotoredox-catalysed sp3–sp3 cross-coupling of carboxylic acids with alkyl halides. *Nature* **536**, 322–325 (2016).
21. Perry, I. B. *et al.* Direct arylation of strong aliphatic C–H bonds. *Nature* **560**, 70–75 (2018).
22. Laudadio, G. *et al.* C(sp^3)–H functionalizations of light hydrocarbons using decatungstate photocatalysis in flow. *Science* **369**, 92–96 (2020).

23. Laudadio, G. *et al.* Selective C(sp ^{3})−H Aerobic Oxidation Enabled by Decatungstate Photocatalysis in Flow. *Angew. Chem. Int. Ed.* **57**, 4078–4082 (2018).
24. Harper, K. C. *et al.* Commercial-Scale Visible Light Trifluoromethylation of 2-Chlorothiophenol Using CF_3I Gas. *Org. Process Res. Dev.* **26**, 404–412 (2022).
25. Chen, M. *et al.* Highly efficient solution processed OLEDs based on iridium complexes with steric phenylpyridazine derivative. *Inorganica Chim. Acta* **516**, 516:120100 (2021).
26. Dold, B. Sustainability in metal mining: from exploration, over processing to mine waste management. *Rev. Environ. Sci. Biotechnol.* **7**, 275–285 (2008).
27. Romero, N. A. & Nicewicz, D. A. Organic Photoredox Catalysis. *Chem. Rev.* **116**, 10075–10166 (2016).
28. Skubi, K. L., Blum, T. R. & Yoon, T. P. Dual Catalysis Strategies in Photochemical Synthesis. *Chem. Rev.* **116**, 10035–10074 (2016).
29. Chen, Y. Z., Li, W. H., Li, L. & Wang, L. N. Progress in organic photocatalysts. *Rare Met.* **37**, 1–12 (2018).
30. Corrigan, N., Shanmugam, S., Xu, J. & Boyer, C. Photocatalysis in organic and polymer synthesis. *Chem. Soc. Rev.* **45**, 6165–6212 (2016).
31. Joshi-Pangu, A. *et al.* Acridinium-Based Photocatalysts: A Sustainable Option in Photoredox Catalysis. *J. Org. Chem.* **81**, 7244–7249 (2016).
32. Romero, N. A., Margrey, K. A., Tay, N. E. & Nicewicz, D. A. Site-selective arene C-H amination via photoredox catalysis. *Science* **349**, 1326–1330 (2015).
33. McManus, J. B. & Nicewicz, D. A. Direct C-H Cyanation of Arenes via Organic Photoredox Catalysis. *J. Am. Chem. Soc.* **139**, 2880–2883 (2017).
34. Tay, N. E. S. & Nicewicz, D. A. Cation Radical Accelerated Nucleophilic Aromatic Substitution via Organic Photoredox Catalysis. *J. Am. Chem. Soc.* **139**, 16100–16104 (2017).
35. MacKenzie, I. A. *et al.* Discovery and characterization of an acridine radical photoreductant. *Nature* **580**, 76–80 (2020).
36. Srivastava, V. & Singh, P. P. Eosin y catalysed photoredox synthesis: A review. *RSC Adv.* **7**, 31377–31392 (2017).

37. Hari, D. P. & König, B. Synthetic applications of eosin y in photoredox catalysis. *Chem. Commun.* **50**, 6688–6699 (2014).
38. Yan, D.-M., Chen, J.-R. & Xiao, W.-J. New Roles for Photoexcited Eosin Y in Photochemical Reactions. *Angew. Chem. Int. Ed.* **58**, 378–380 (2019).
39. Fan, X. Z. *et al.* Eosin Y as a Direct Hydrogen-Atom Transfer Photocatalyst for the Functionalization of C−H Bonds. *Angew. Chem. - Int. Ed.* **57**, 8514–8518 (2018).
40. Hari, D. P., Schroll, P. & König, B. Metal-Free, Visible-Light-Mediated Direct C–H Arylation of Heteroarenes with Aryl Diazonium Salts. *J. Am. Chem. Soc.* **134**, 2958–2961 (2012).
41. Neumann, M., Füldner, S., König, B. & Zeitler, K. Metal-free, cooperative asymmetric organophotoredox catalysis with visible light. *Angew. Chem. Int. Ed.* **50**, 951–954 (2011).
42. Kudisch, M., Lim, C. H., Thordarson, P. & Miyake, G. M. Energy Transfer to Ni-Amine Complexes in Dual Catalytic, Light-Driven C-N Cross-Coupling Reactions. *J. Am. Chem. Soc.* **141**, 19479–19486 (2019).
43. Rao, H., Lim, C.-H., Bonin, J., Miyake, G. M. & Robert, M. Visible-Light-Driven Conversion of CO_2 to CH_4 with an Organic Sensitizer and an Iron Porphyrin Catalyst. *J. Am. Chem. Soc.* **140**, 17830–17834 (2018).
44. Pearson, R. M., Lim, C.-H., McCarthy, B. G., Musgrave, C. B. & Miyake, G. M. Organocatalyzed Atom Transfer Radical Polymerization Using N -Aryl Phenoxazines as Photoredox Catalysts. *J. Am. Chem. Soc.* **138**, 11399–11407 (2016).
45. Theriot, J. C. *et al.* Organocatalyzed atom transfer radical polymerization driven by visible light. *Science* **352**, 1082–1086 (2016).
46. McCarthy, B. G. *et al.* Structure-property relationships for tailoring phenoxazines as reducing photoredox catalysts. *J. Am. Chem. Soc.* **140**, 5088–5101 (2018).
47. Du, Y. *et al.* Strongly Reducing, Visible-Light Organic Photoredox Catalysts as Sustainable Alternatives to Precious Metals. *Chem. Eur. J.* **23**, 10962–10968 (2017).
48. Tlahuext-Aca, A., Candish, L., Garza-Sanchez, R. A. & Glorius, F. Decarboxylative Olefination of Activated Aliphatic Acids Enabled by Dual Organophotoredox/Copper Catalysis. *ACS Catal.* **8**, 1715–1719 (2018).

49. Luo, J. & Zhang, J. Donor-Acceptor Fluorophores for Visible-Light-Promoted Organic Synthesis: Photoredox/Ni Dual Catalytic C(sp3)-C(sp2) Cross-Coupling. *ACS Catal.* **6**, 873–877 (2016).
50. Sherwood, T. C., Li, N., Yazdani, A. N. & Dhar, T. G. M. Organocatalyzed, Visible-Light Photoredox-Mediated, One-Pot Minisci Reaction Using Carboxylic Acids via N-(Acyloxy)phthalimides. *J. Org. Chem.* **83**, 3000–3012 (2018).
51. Shu, C., Mega, R. S., Andreassen, B. J., Noble, A. & Aggarwal, V. K. Synthesis of Functionalized Cyclopropanes from Carboxylic Acids by a Radical Addition–Polar Cyclization Cascade. *Angew. Chem. Int. Ed.* **57**, 15430–15434 (2018).
52. Lévêque, C., Chenneberg, L., Corcé, V., Ollivier, C. & Fensterbank, L. Organic photoredox catalysis for the oxidation of silicates: Applications in radical synthesis and dual catalysis. *Chem. Commun.* **52**, 9877–9880 (2016).
53. Rahman, M. Z., Kibria, M. G. & Mullins, C. B. Metal-free photocatalysts for hydrogen evolution. *Chem. Soc. Rev.* **49**, 1887–1931 (2020).
54. Zhang, G., Lan, Z. A. & Wang, X. Conjugated Polymers: Catalysts for Photocatalytic Hydrogen Evolution. *Angew. Chem. Int. Ed.* **55**, 15712–15727 (2016).
55. Pachfule, P. *et al.* Diacetylene Functionalized Covalent Organic Framework (COF) for Photocatalytic Hydrogen Generation. *J. Am. Chem. Soc.* **140**, 1423–1427 (2018).
56. Kuecken, S. *et al.* Fast tuning of covalent triazine frameworks for photocatalytic hydrogen evolution. *Chem. Commun.* **53**, 5854–5857 (2017).
57. Sprick, R. S. *et al.* Tunable organic photocatalysts for visible-light-driven hydrogen evolution. *J. Am. Chem. Soc.* **137**, 3265–3270 (2015).
58. Sprick, R. S. *et al.* Extended conjugated microporous polymers for photocatalytic hydrogen evolution from water. *Chem. Commun.* **52**, 10008–10011 (2016).
59. Lau, V. W. H. *et al.* Low-molecular-weight carbon nitrides for solar hydrogen evolution. *J. Am. Chem. Soc.* **137**, 1064–1072 (2015).

60. Yang, C. *et al.* Molecular Engineering of Conjugated Polybenzothiadiazoles for Enhanced Hydrogen Production by Photosynthesis. *Angew. Chem. Int. Ed.* **55**, 9202–9206 (2016).
61. Sachs, M. *et al.* Understanding structure-activity relationships in linear polymer photocatalysts for hydrogen evolution. *Nat. Commun.* **9**, 9:4968 (2018).
62. Wang, X. *et al.* Sulfone-containing covalent organic frameworks for photocatalytic hydrogen evolution from water. *Nat. Chem.* **10**, 1180–1189 (2018).
63. Fang, Y. & Wang, X. Photocatalytic CO2 conversion by polymeric carbon nitrides. *Chem. Commun.* **54**, 5674–5687 (2018).
64. Nguyen, H. L. Reticular Materials for Artificial Photoreduction of CO2. *Adv. Energy Mater.* **10**, 1–23 (2020).
65. Li, K., Peng, B. & Peng, T. Recent Advances in Heterogeneous Photocatalytic CO2 Conversion to Solar Fuels. *ACS Catal.* **6**, 7485–7527 (2016).
66. Yang, S. *et al.* 2D Covalent Organic Frameworks as Intrinsic Photocatalysts for Visible Light-Driven CO2 Reduction. *J. Am. Chem. Soc.* **140**, 14614–14618 (2018).
67. Savateev, A. & Antonietti, M. Heterogeneous Organocatalysis for Photoredox Chemistry. *ACS Catal.* **8**, 9790–9808 (2018).
68. Wang, X., Blechert, S. & Antonietti, M. Polymeric graphitic carbon nitride for heterogeneous photocatalysis. *ACS Catal.* **2**, 1596–1606 (2012).
69. Savateev, A., Ghosh, I., König, B. & Antonietti, M. Photoredox Catalytic Organic Transformations using Heterogeneous Carbon Nitrides. *Angew. Chem. - Int. Ed.* **57**, 15936–15947 (2018).
70. Gisbertz, S. & Pieber, B. Heterogeneous Photocatalysis in Organic Synthesis. *ChemPhotoChem* **4**, 456–475 (2020).
71. Zhou, Y. B. & Zhan, Z. P. Conjugated Microporous Polymers for Heterogeneous Catalysis. *Chem. Asian J.* **13**, 9–19 (2018).
72. Qian, Z., Wang, Z. J. & Zhang, K. A. I. Covalent Triazine Frameworks as Emerging Heterogeneous Photocatalysts. *Chem. Mater.* **33**, 1909–1926 (2021).

73. Bloh, J. Z. & Marschall, R. Heterogeneous Photoredox Catalysis: Reactions, Materials, and Reaction Engineering. *Eur. J. Org. Chem.* **2017**, 2085–2094 (2017).
74. Chen, J., Cen, J., Xu, X. & Li, X. The application of heterogeneous visible light photocatalysts in organic synthesis. *Catal. Sci. Technol.* **6**, 349–362 (2016).
75. Cheng, L., Zhang, H., Li, X., Fan, J. & Xiang, Q. Carbon–Graphitic Carbon Nitride Hybrids for Heterogeneous Photocatalysis. *Small* **17**, 1–22 (2021).
76. Möhlmann, L. *et al.* Carbon nitride-catalyzed photoredox C-C bond formation with N-aryltetrahydroisoquinolines. *Adv. Synth. Catal.* **354**, 1909–1913 (2012).
77. Pieber, B. *et al.* Semi-heterogeneous Dual Nickel/Photocatalysis using Carbon Nitrides: Esterification of Carboxylic Acids with Aryl Halides. *Angew. Chem. Int. Ed.* **58**, 9575–9580 (2019).
78. Mazzanti, S. & Savateev, A. Emerging Concepts in Carbon Nitride Organic Photocatalysis. *ChemPlusChem* **85**, 2499–2517 (2020).
79. Schwinghammer, K. *et al.* Triazine-based carbon nitrides for visible-light-driven hydrogen evolution. *Angew. Chem. Int. Ed.* **52**, 2435–2439 (2013).
80. Ghosh, I. *et al.* Organic semiconductor photocatalyst can bifunctionalize arenes and heteroarenes. *Science* **365**, 360–366 (2019).
81. Vijeta, A., Casadevall, C., Roy, S. & Reisner, E. Visible-Light Promoted C–O Bond Formation with an Integrated Carbon Nitride–Nickel Heterogeneous Photocatalyst. *Angew. Chem. Int. Ed.* **60**, 8494–8499 (2021).
82. Vijeta, A., Casadevall, C. & Reisner, E. An Integrated Carbon Nitride-Nickel Photocatalyst for the Amination of Aryl Halides Using Sodium Azide. *Angew. Chem. Int. Ed.* **61**, (2022).
83. Cai, Y. *et al.* Heterogeneous Visible-Light Photoredox Catalysis with Graphitic Carbon Nitride for α-Aminoalkyl Radical Additions, Allylations, and Heteroarylations. *ACS Catal.* **8**, 9471–9476 (2018).
84. Pieber, B., Shalom, M., Antonietti, M., Seeberger, P. H. & Gilmore, K. Continuous Heterogeneous Photocatalysis in Serial Micro-Batch Reactors. *Angew. Chem. Int. Ed.* **57**, 9976–9979 (2018).

85. Yang, Q. *et al.* Remarkable Activity of Potassium-Modified Carbon Nitride for Heterogeneous Photocatalytic Decarboxylative Alkyl/Acyl Radical Addition and Reductive Dimerization of para-Quinone Methides. *ACS Sustain. Chem. Eng.* **9**, 2367–2377 (2021).
86. Shi, J., Yuan, T., Wang, R., Zheng, M. & Wang, X. Boron carbonitride photocatalysts for direct decarboxylation: The construction of C(sp3)-N or C(sp3)-C(sp2) bonds with visible light. *Green Chem.* **23**, 3945–3949 (2021).
87. Li, R. *et al.* Poly(benzothiadiazoles) and Their Derivatives as Heterogeneous Photocatalysts for Visible-Light-Driven Chemical Transformations. *ACS Catal.* **8**, 4735–4750 (2018).
88. Wang, Z. J., Ghasimi, S., Landfester, K. & Zhang, K. A. I. Highly porous conjugated polymers for selective oxidation of organic sulfides under visible light. *Chem. Commun.* **50**, 8177–8180 (2014).
89. Wang, Z. J., Li, R., Landfester, K. & Zhang, K. A. I. Porous conjugated polymer via metal-free synthesis for visible light-promoted oxidative hydroxylation of arylboronic acids. *Polymer* **126**, 291–295 (2017).
90. Li, R. *et al.* Photocatalytic Selective Bromination of Electron-Rich Aromatic Compounds Using Microporous Organic Polymers with Visible Light. *ACS Catal.* **6**, 1113–1121 (2016).
91. Huang, W. *et al.* A fixed-bed photoreactor using conjugated nanoporous polymer-coated glass fibers for visible light-promoted continuous photoredox reactions. *J. Mater. Chem. A* **5**, 3792–3797 (2017).
92. Huang, W. *et al.* Asymmetric Covalent Triazine Framework for Enhanced Visible-Light Photoredox Catalysis via Energy Transfer Cascade. *Angew. Chem. Int. Ed.* **57**, 8316–8320 (2018).
93. Zou, Y. *et al.* Red edge effect and chromoselective photocatalysis with amorphous covalent triazine-based frameworks. *Nat. Commun.* **13**, 13:2171 (2022).
94. Bi, J. *et al.* Covalent Triazine-Based Frameworks as Visible Light Photocatalysts for the Splitting of Water. *Macromol. Rapid Commun.* **36**, 1799–1805 (2015).

95. Cheng, Z. *et al.* Efficient Visible-Light-Driven Photocatalytic Hydrogen Evolution on Phosphorus-Doped Covalent Triazine-Based Frameworks. *ACS Appl. Mater. Interfaces* **10**, 41415–41421 (2018).
96. Xie, J. *et al.* Efficient visible light-driven water oxidation and proton reduction by an ordered covalent triazine-based framework. *Energy Environ. Sci.* **11**, 1617–1624 (2018).
97. Sun, R. & Tan, B. Covalent Triazine Frameworks(CTFs) for Photocatalytic Applications. *Chem. Res. Chin. Univ.* **38**, 310–324 (2022).
98. Guo, L. *et al.* Engineering heteroatoms with atomic precision in donor-acceptor covalent triazine frameworks to boost photocatalytic hydrogen production. *J. Mater. Chem. A* **6**, 19775–19781 (2018).
99. Sun, R., Wang, X., Wang, X. & Tan, B. Three-Dimensional Crystalline Covalent Triazine Frameworks via a Polycondensation Approach. *Angew. Chem. Int. Ed.* **61**, e202117668, (2022).
100. Kuhn, P., Antonietti, M. & Thomas, A. Porous, Covalent Triazine-Based Frameworks Prepared by Ionothermal Synthesis. *Angew. Chem. Int. Ed.* **47**, 3450–3453 (2008).
101. Jiang, J. X. *et al.* Conjugated microporous polymers with rose bengal dye for highly efficient heterogeneous organo-photocatalysis. *Macromolecules* **46**, 8779–8783 (2013).
102. Wang, C.-A., Li, Y.-W., Cheng, X.-L., Zhang, J.-P. & Han, Y.-F. Eosin Y dye-based porous organic polymers for highly efficient heterogeneous photocatalytic dehydrogenative coupling reaction. *RSC Adv* **7**, 408–414 (2017).
103. Yu, X. *et al.* Eosin Y-Functionalized Conjugated Organic Polymers for Visible-Light-Driven CO 2 Reduction with H 2 O to CO with High Efficiency. *Angew. Chem. Int. Ed.* **58**, 632–636 (2019).
104. Thomson, C. G. *et al.* Continuous-flow synthesis and application of polymer-supported BODIPY Photosensitisers for the generation of singlet oxygen; process optimised by in-line NMR spectroscopy. *J. Flow Chem.* **10**, 327–345 (2020).
105. Bassan, E., Gualandi, A., Cozzi, P. G. & Ceroni, P. Design of BODIPY dyes as triplet photosensitizers: electronic properties tailored for solar energy

conversion, photoredox catalysis and photodynamic therapy. *Chem. Sci.* **12**, 6607–6628 (2021).

106. Tobin, J. M. *et al.* Polymer-Supported Photosensitizers for Oxidative Organic Transformations in Flow and under Visible Light Irradiation. *ACS Catal.* **7**, 4602–4612 (2017).
107. López-Magano, A. *et al.* Photoredox Heterobimetallic Dual Catalysis Using Engineered Covalent Organic Frameworks. *ACS Catal.* **11**, 12344–12354 (2021).
108. Jati, A. *et al.* Dual Metalation in a Two-Dimensional Covalent Organic Framework for Photocatalytic C-N Cross-Coupling Reactions. *J. Am. Chem. Soc.* **144**, 7822–7833 (2022).
109. Traxler, M. *et al.* Acridine-Functionalized Covalent Organic Frameworks (COFs) as Photocatalysts for Metallaphotocatalytic C−N Cross-Coupling. *Angew. Chem. Int. Ed.* **61**, (2022).
110. Ni, M., Leung, M. K. H., Leung, D. Y. C. & Sumathy, K. A review and recent developments in photocatalytic water-splitting using TiO2 for hydrogen production. *Renew. Sustain. Energy Rev.* **11**, 401–425 (2007).
111. Huang, Z. *et al.* Enhanced photocatalytic alkane production from fatty acid decarboxylation via inhibition of radical oligomerization. *Nat. Catal.* **3**, 170–178 (2020).
112. Zhu, Q. & Nocera, D. G. Photocatalytic Hydromethylation and Hydroalkylation of Olefins Enabled by Titanium Dioxide Mediated Decarboxylation. *J. Am. Chem. Soc.* **142**, 17913–17918 (2020).
113. Diaz-Angulo, J. *et al.* Visible-light activation of TiO_2 by dye-sensitization for degradation of pharmaceutical compounds. *Photochem. Photobiol. Sci.* **18**, 897–904 (2019).
114. Liu, Y. Y., Liang, D., Lu, L. Q. & Xiao, W. J. Practical heterogeneous photoredox/nickel dual catalysis for C-N and C-O coupling reactions. *Chem. Commun.* **55**, 4853–4856 (2019).
115. Caputo, J. A. *et al.* General and Efficient C-C Bond Forming Photoredox Catalysis with Semiconductor Quantum Dots. *J. Am. Chem. Soc.* **139**, 4250–4253 (2017).

116. Biyani, S. A., Moriuchi, Y. W. & Thompson, D. H. Advancement in Organic Synthesis Through High Throughput Experimentation. *Chemistry–Methods* **1**, 323–339 (2021).
117. Mennen, S. M. *et al.* The Evolution of High-Throughput Experimentation in Pharmaceutical Development and Perspectives on the Future. *Org. Process Res. Dev.* **23**, 1213–1242 (2019).
118. Shevlin, M. Practical High-Throughput Experimentation for Chemists. *ACS Med. Chem. Lett.* **8**, 601–607 (2017).
119. Stevens, J. M. *et al.* Leveraging High-Throughput Experimentation to Drive Pharmaceutical Route Invention: A Four-Step Commercial Synthesis of Branebrutinib (BMS-986195). *Org. Process Res. Dev.* **26**, 1174–1183 (2022).
120. Prieto Kullmer, C. N. *et al.* Accelerating reaction generality and mechanistic insight through additive mapping. *Science* **376**, 532–539 (2022).
121. Williams, W. L. *et al.* The Evolution of Data-Driven Modeling in Organic Chemistry. *ACS Cent. Sci.* **7**, 1622–1637 (2021).
122. Meuwly, M. Machine Learning for Chemical Reactions. *Chem. Rev.* **121**, 10218–10239 (2021).
123. Shields, B. J. *et al.* Bayesian reaction optimization as a tool for chemical synthesis. *Nature* **590**, 89–96 (2021).
124. Christensen, M. *et al.* Data-science driven autonomous process optimization. *Commun. Chem.* **4**, 112 (2021).
125. Bai, Y. *et al.* Accelerated Discovery of Organic Polymer Photocatalysts for Hydrogen Evolution from Water through the Integration of Experiment and Theory. *J. Am. Chem. Soc.* **141**, 9063–9071 (2019).
126. Burger, B. *et al.* A mobile robotic chemist. *Nature* **583**, 237–241 (2020).

Chapter 2

High Throughput Discovery of Novel Heterogeneous Photocatalysts

Author Contributions

All the work described in this chapter has been performed by the thesis author except for the following:

Cyanopyridine compounds **2.15** and **2.16** were synthesized and provided by Dr. Xiaobo Li. Dr. Xiaobo Li provided the initial material of CTF-2M. 2,4,6-tris(4-bromophenyl)-1,3,5-triazine was provided by Dr. Kewei Wang.

Parts of this chapter have been published in the following[1]

Discovery of a Covalent Triazine Framework Photocatalyst for Visible-Light-Driven Chemical Synthesis using High Throughput Screening ACS Catalysis **2022**, 12, 10057−1006

Sriram Vijayakrishnan, John Ward, Andrew Cooper.

Introduction

As discussed in **Chapter 1** – there are significant challenges associated with photoredox catalysis, such as the elaborate synthetic steps required to access many of the organic photoredox catalysts, and the cost of the transition metal complexes, along with their precious earth metal cores – which makes them difficult to scale for uses such as in large scale industrial production.

We recognized that heterogeneous photoredox catalysts could offer an alternative to this and could provide stable, recyclable, organic materials that could be scaled up, and could be significantly cheaper than iridium photoredox catalysts. However, development of these heterogeneous catalysts is still very limited, and many reactions that are catalysed by a homogeneous photocatalyst have no heterogeneous counterpart, and many of the reported examples of heterogeneous photoredox catalysis have limited synthetic applicability – particularly in C-C bond formation.

With few examples to start our search, we developed a strategy for targeted high throughput discovery of novel photoredox catalysts augmented through the use of robotic platforms. The Cooper group has previously reported on the synthesis of microporous polymers through the heterogenization of organic molecular dye Rose Bengal, for Aza-Henry reaction of tetrahydroisoquinolines,[2] and this has been also applied to the dye Eosin Y[3]. Building upon this work, we envisioned a strategy for discovery of new photocatalysts based on creating polymeric analogues of photoactive small molecules.

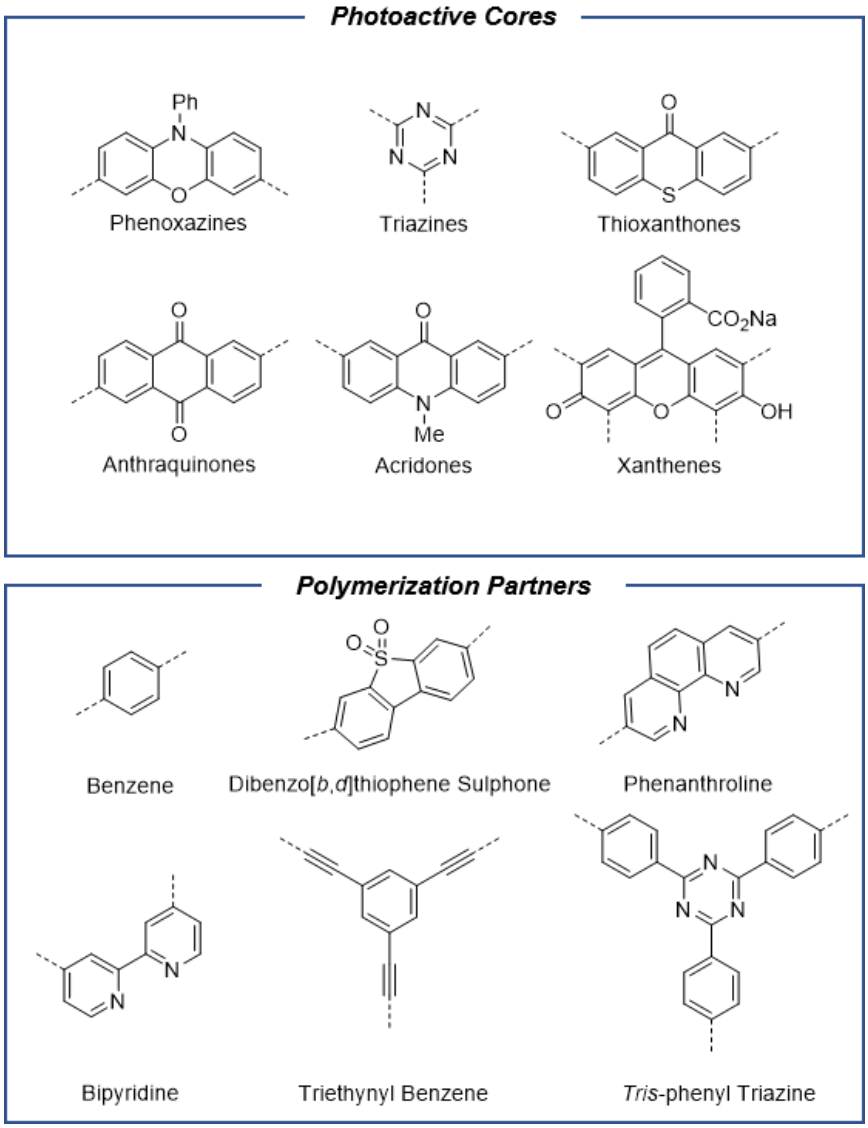

Figure 2-1: Photoactive cores and co-polymerization partners targeted for discovery of photocatalysts.

We began by identifying small organic molecules that were active in homogeneous photocatalysis, whether in organic synthesis, or in other applications such as water splitting. We identified xanthenes, phenoxazine, anthraquinone, triazines, and thioxanthones, among others, as starting points to create our initial pool of polymers to screen (Figure **2-1**). We also created our workflow for high-throughput screening of novel photocatalysts, screening our pool of polymer candidates against known reactions that are traditionally catalysed by transition metal complexes.

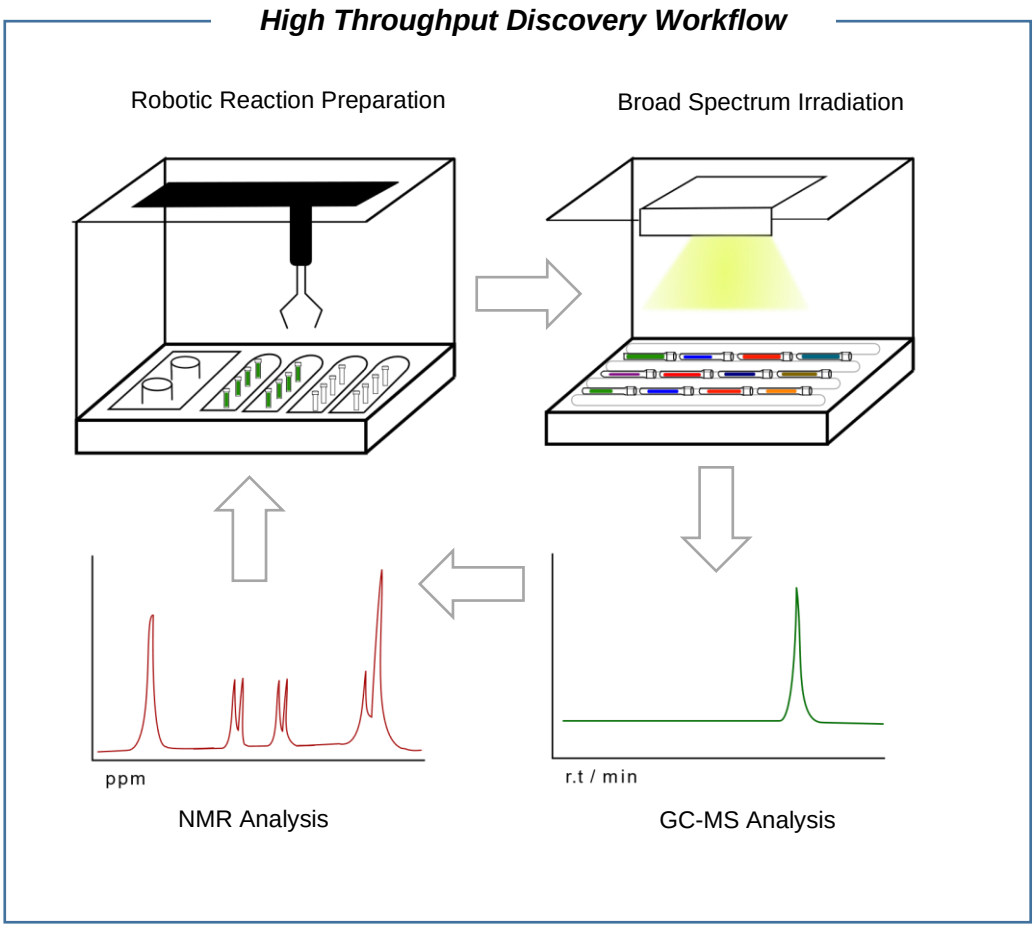

Figure 2-2: High-Throughput workflow for photocatalyst discovery.

Using Chemspeed platforms, we would utilize the robotic dispensing capabilities in order to dispense stock solutions of various reagents into vials charged with all our trial polymer candidates, along with any insoluble reagent under an inert nitrogen atmosphere (Figure **2-2**). From there vials would be crimp sealed and manually transferred out of the Chemspeed. The vials are then irradiated using broad spectrum white LEDs for several days, using rollers for agitation of the reactions. After irradiation (3 days) the samples would then be diluted, and then reformatting into autosampler vials, using the same robotic liquid handling capabilities. The reformatted vials could then be directly analysed by GC-MS in order to compare the performance of the polymers and determine whether there was any catalytic product formation. Using the combination of rollers and LED irradiation, our capacity was up to 48 reactions in parallel.

Following the detection of a successful polymer hit for a valuable reaction catalysed by a specific homogeneous photocatalyst, we could then proceed to take this result and then begin to optimize it further, if necessary, to develop the reaction so that we could obtain an appropriate substrate scope. From there, we would also test it against various other reactions that were catalysed by that same homogeneous photocatalyst. In an ideal scenario, we would discover a polymer that would be a heterogeneous equivalent to a commonly used transition metal photocatalyst and would be able to catalyse multiple reactions performed by that same transition metal photocatalyst.

Results and Discussion

Polymer Synthesis

Our group has previously used similar approaches[4] for the discovery of linear polymer photocatalysts for hydrogen evolution and have found that photocatalytic performance cannot be fully rationalized by any single property. The performance is found to be correlated to a combination of multiple factors, including ionization potential, optical gap, electron affinity, and transmission. We made a strategic choice to perform reaction screening on our polymers with minimal characterization. This would maximize the reactions that we could screen with our trial polymer candidates and minimize the precursor and polymer synthesis required. Fourier-Transform infrared spectroscopy (FT-IR) could identify the presence of key functional groups and consumption of starting material, where applicable. Meanwhile, UV-visible absorption spectroscopy (diffuse reflectance) would infer the synthesis of a conjugated material that absorbs in visible light, which is critical given that we exclusively irradiated with visible light, with broad spectrum white LEDs. Polymers that showed promise and were taken further for optimization and scope exploration would then be further characterized.

We first began our synthesis of the trial polymer candidates by converting several dyes that are known to photocatalyze different reactions directly into polymers in one step (Scheme **2-1**). 4CzIPN is a widely utilized homogeneous photocatalyst that has been used in a host of reactions,[5] and we used Scholl coupling to polymerize it using $FeCl_3$. Similarly, Rose Bengal and Eosin[6–9] are known to be organic photocatalysts, and we created polymer analogues of them using Sonogashira coupling with triethynyl benzene.

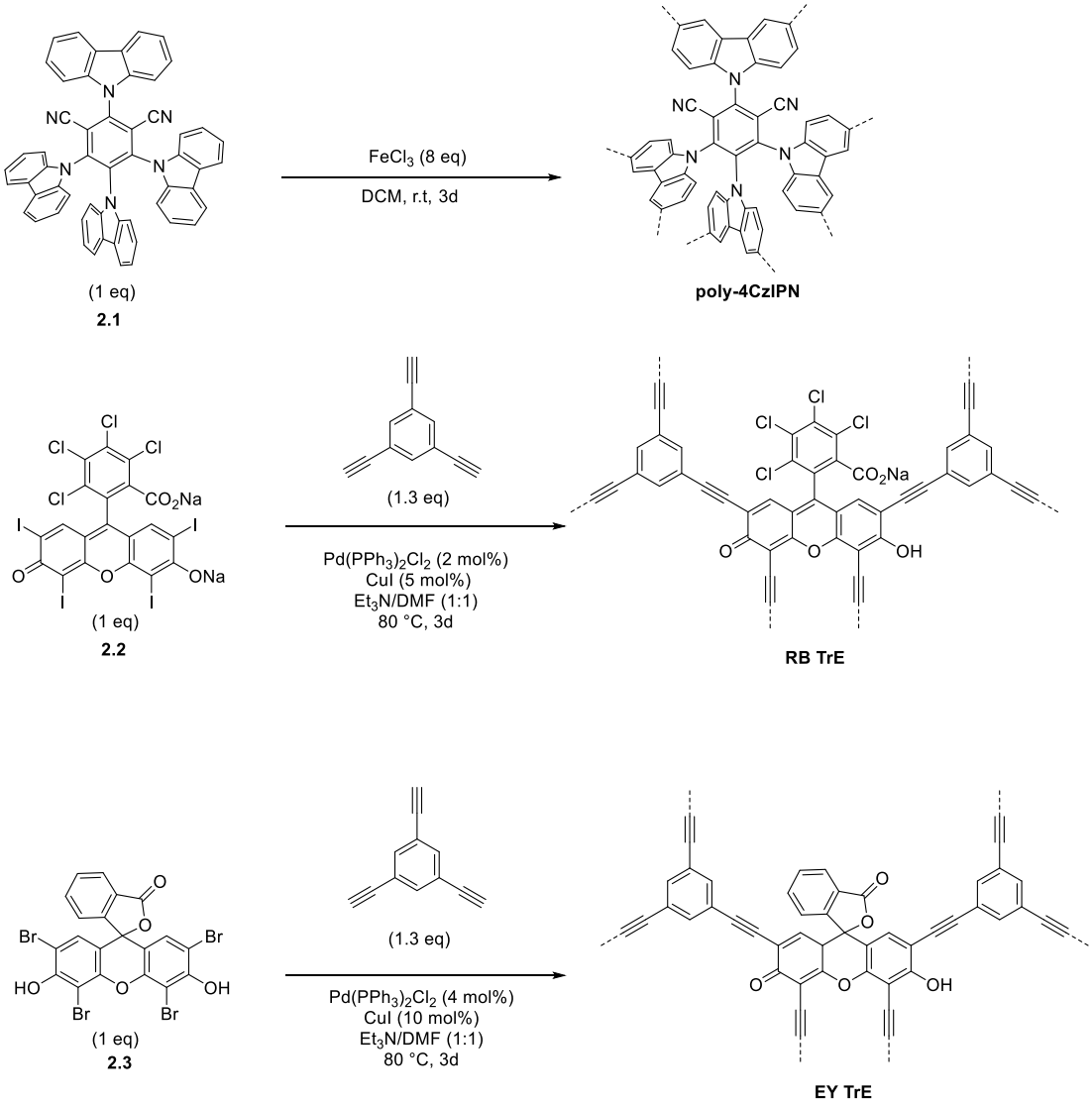

Scheme 2-1: Synthesis of xanthene and 4CzIPN based polymers

UV-Visible absorption spectrum of RB-TrE and EY-TrE (Figure **2-3**) demonstrated that the polymeric material broadly absorbed in visible light from 400-800 nm. In comparison, both Eosin Y and Rose Bengal dyes are known to have comparatively narrow absorption windows and do not absorb strongly near 400 nm[10,11], indicating the impact of the extended conjugation of the polymeric material. UV-Visible absorption spectra of poly-4CzIPN polymer was unable to be measured due to insufficient material and was not resynthesized due to generally poor performance in all tested photoredox reactions. However, this polymer has been previously synthesized by Zhang and co-workers[12] and known to absorb in visible light.

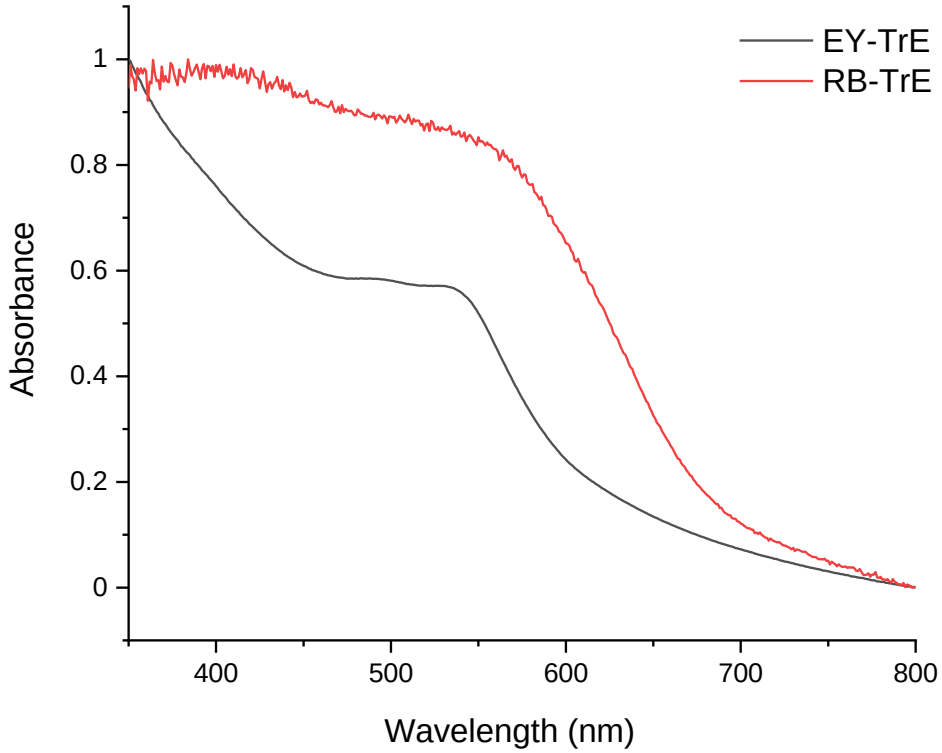

Figure 2-3: UV-Visible absorption spectra of xanthene based polymers.

FT-IR spectra (Figure **2-4**) of RB-TrE and EY-TrE showed bands corresponding to the carbonyl peaks at 1770 cm^{-1}, while no significant presence of alkyne C-H stretching bands near ~3300 cm^{-1} from the triethynylbenzene monomer was observed, indicating its absence in the insoluble, polymeric, material. Alkyne C≡C stretching was not readily visible, although aromatic C=C bands were visible near 1600 cm^{-1}. Poly-4CzIPN meanwhile showed strong aromatic C=C peaks at 1445 cm^{-1} and C-H bending signals at 741 cm^{-1}.

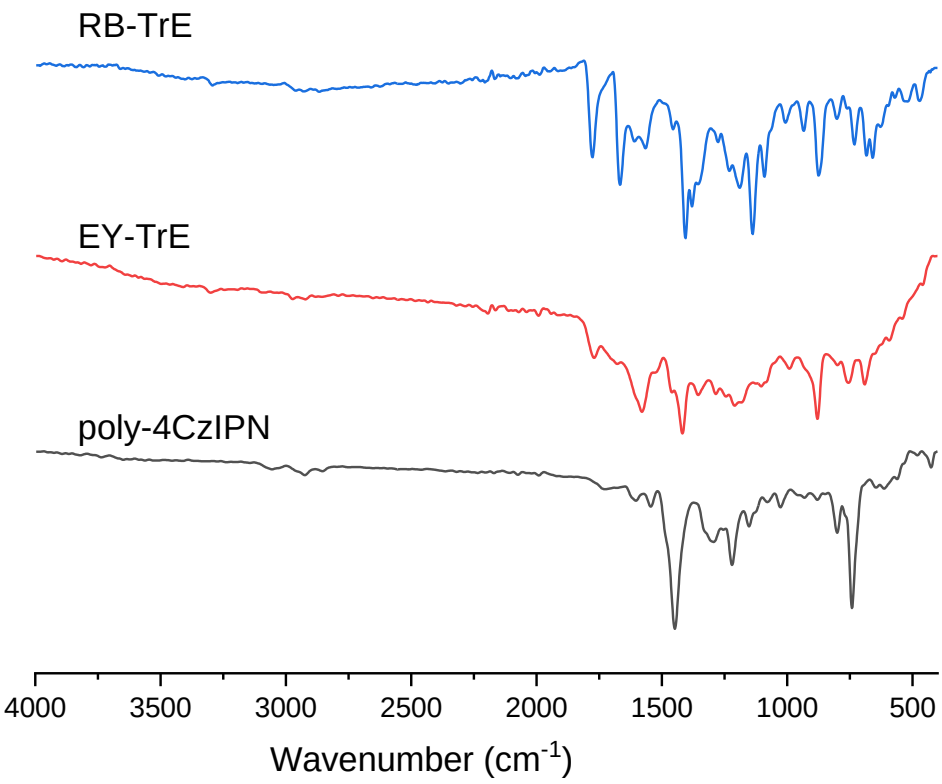

Figure 2-4: FT-IR spectra of poly-4CzIPN and xanthene polymers.

Our next polymer core of interest was N-phenyl phenoxazine. Phenoxazines have been successfully used as replacements for iridium and ruthenium photoredox catalysts as highly reducing organic molecules,[13,14] whose redox potentials can exceed that of the iridium catalysts. Our hope was that the polymer analogues would be mimic reactions catalysed by reducing photocatalysts such as $Ir(ppy)_3$. Installation of the phenyl group on phenoxazine was easily performed to yield **2.4**. From there dibromo intermediate **2.5** could be synthesized, which was then converted to boronate ester **2.6**, albeit only in modest 34% yield (Scheme **2-2**).

Using the phenoxazine core, we synthesized a series of trial polymers using relevant coupling partners. We selected coupling partners based on a combination of synthetic accessibility, and relevance towards applications in photocatalysis. We first synthesized simple POX Ph using Suzuki coupling of **2.5** (Scheme **2-2**), followed by the triazine polymer POX TAZ (Scheme **2-3**) and alkyne polymer POX TrE (Scheme **2-4**).

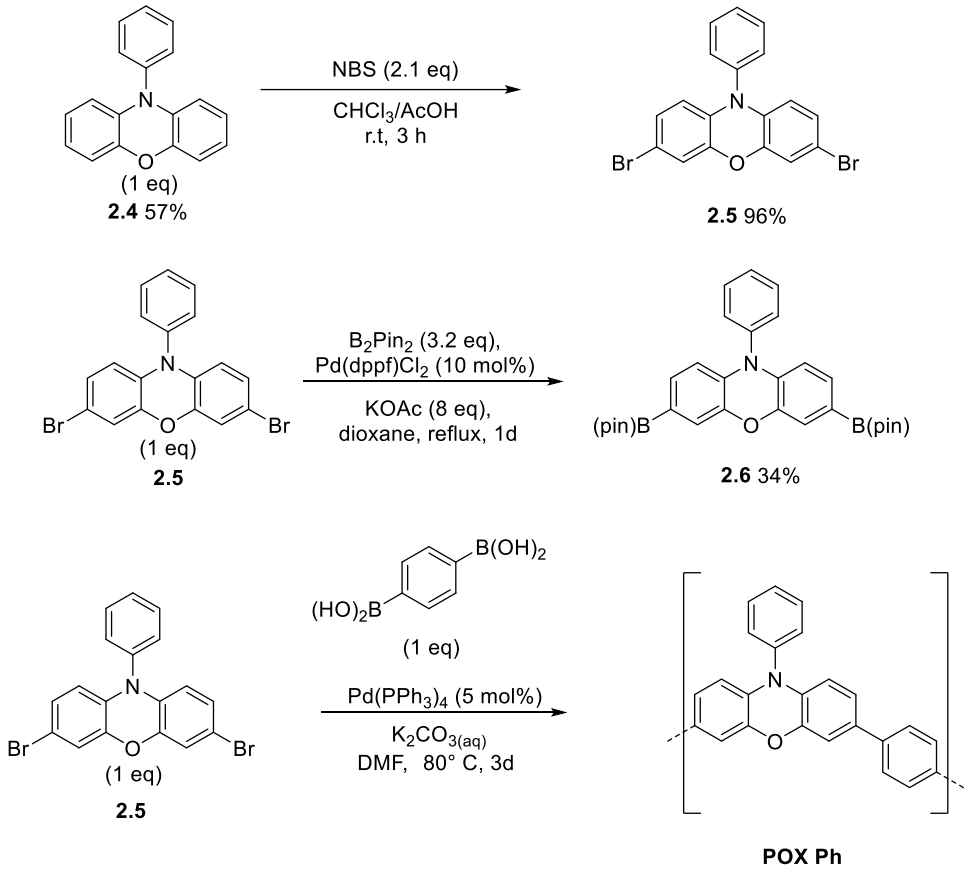

Scheme 2-2: Synthesis of POX polymer precursors and POX Ph

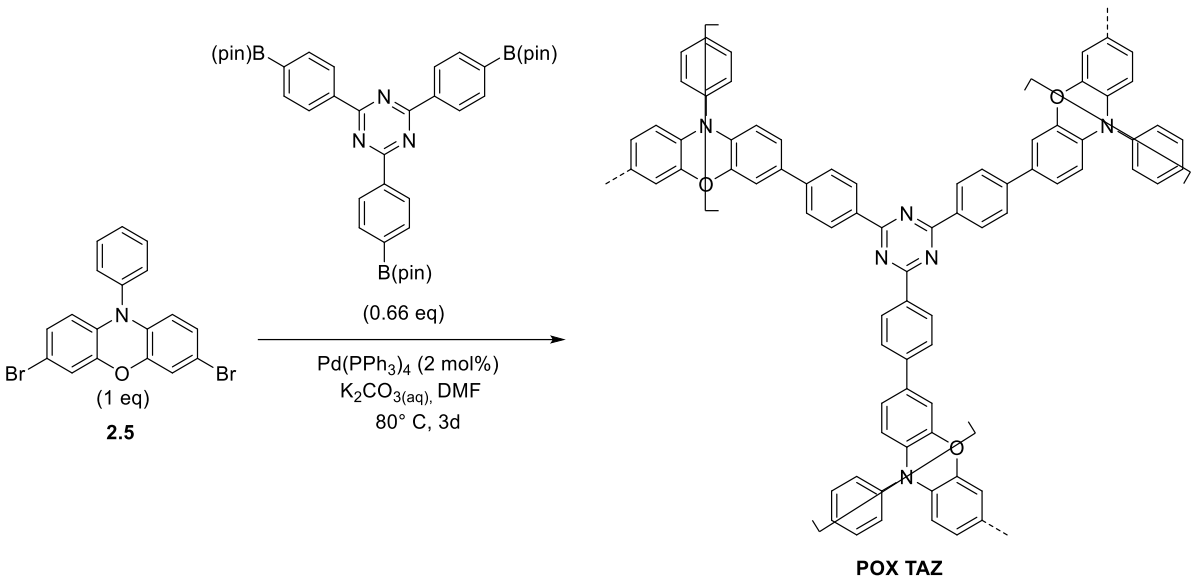

Scheme 2-3: Synthesis of POX TAZ polymer

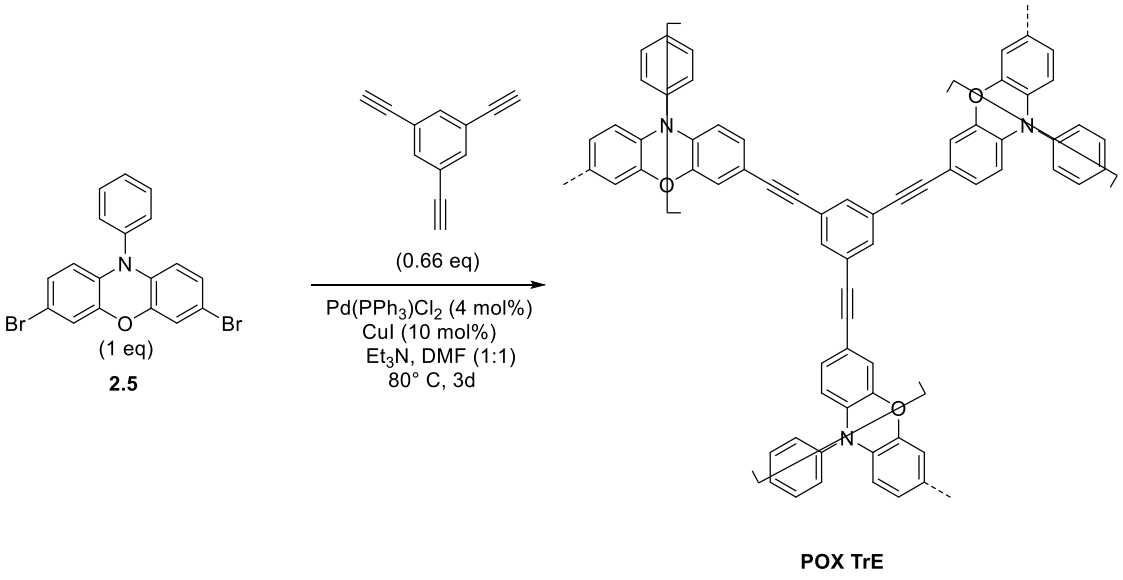

Scheme 2-4: Synthesis of POX TrE polymer

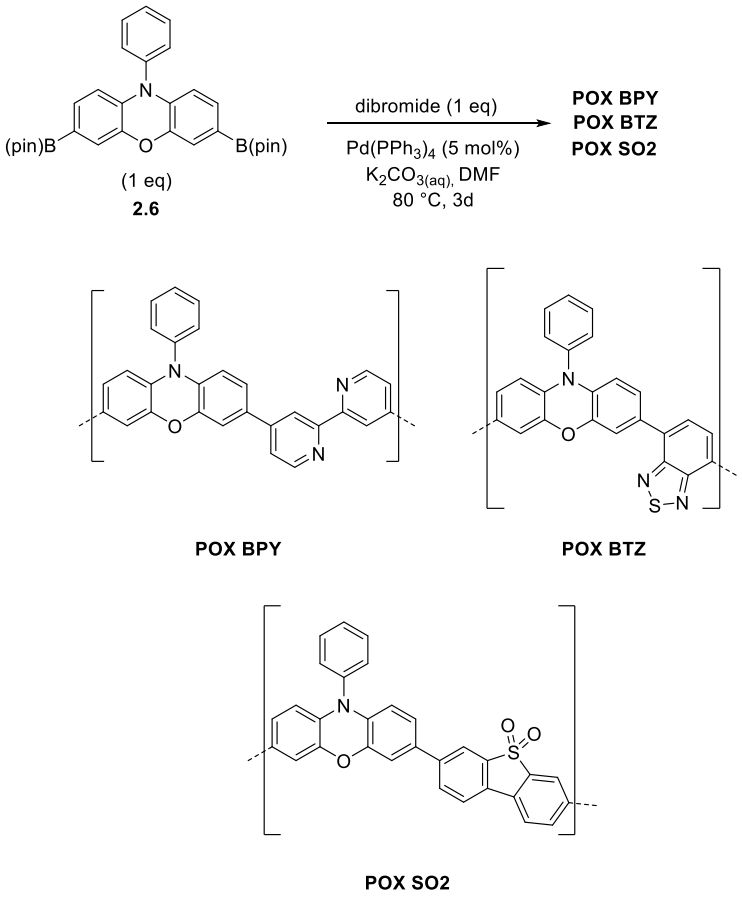

Scheme 2-5: Sythesis of POX SO2, POX BTZ, and POX BPy polymers

We then used boronate ester **2.6** for Suzuki polymerization with a variety of aryl bromide coupling partners (Scheme **2-5**). For example, dibenzothiophene 5,5-dioxide (sulphone) based polymers have been successfully used for efficient sacrificial hydrogen evolution.[15–17] Benzothiadiazole polymers have been successfully used for various photochemical reactions, and we wondered whether their inclusion could be beneficial.

UV-Visible spectra of the phenoxazine polymers (Figure **2-5**) revealed that all the materials broadly absorbed in visible light. In comparison, polymer core **2.4** absorbs poorly at similar wavelengths,[18] and the broad absorbance is a consequence of the extended conjugation. POX-BTZ, a dark purple material, absorbed strongly at 600 nm, and could potentially be a viable catalyst with red-light instead of typically used high-energy blue LED irradiation.

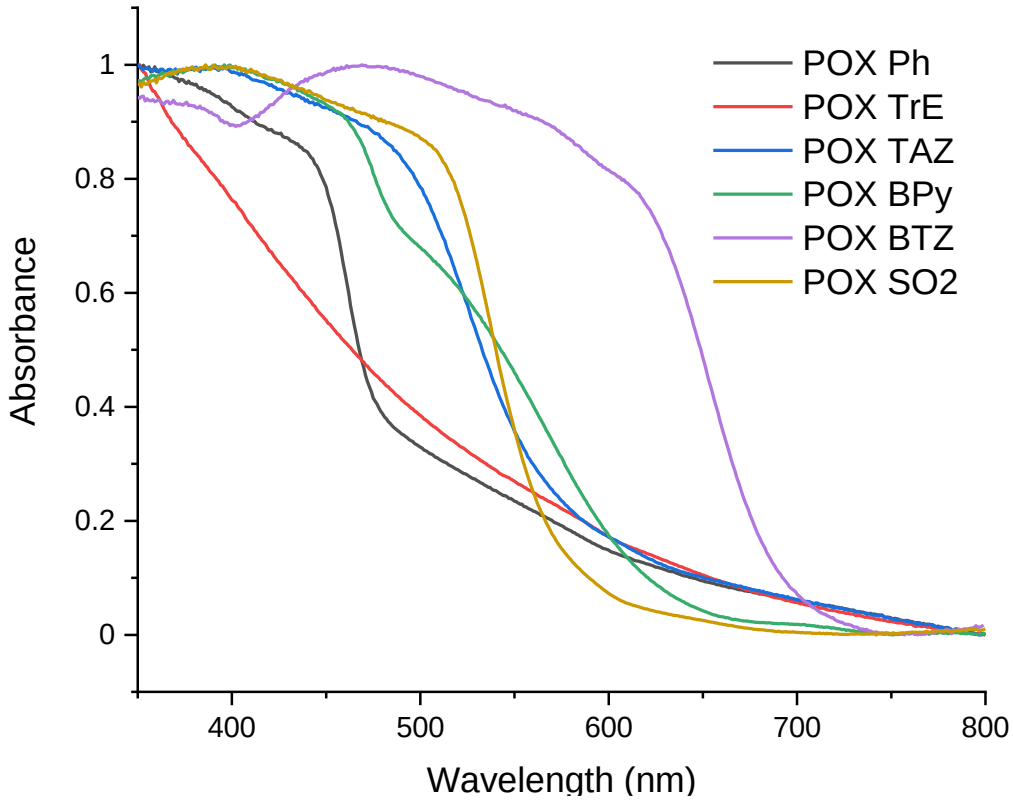

Figure 2-5: UV-Visible absorption spectra of phenoxazine based polymers

FT-IR spectra of the phenoxazine polymers (Figure **2-6**) showed strong peaks consistent with the expected aromatic C=C stretches of the phenoxazine core and their aromatic coupling partners. Notably, the FT-IR spectrum of POX-SO_2 had strong signals at 1153 cm^{-1} and 1302 cm^{-1}, which is likely indicative of the sulphone moiety. POX TAZ showed a strong band near 1500 cm^{-1} and 1350 cm^{-1}, which are characteristic in triazine rings.[19]

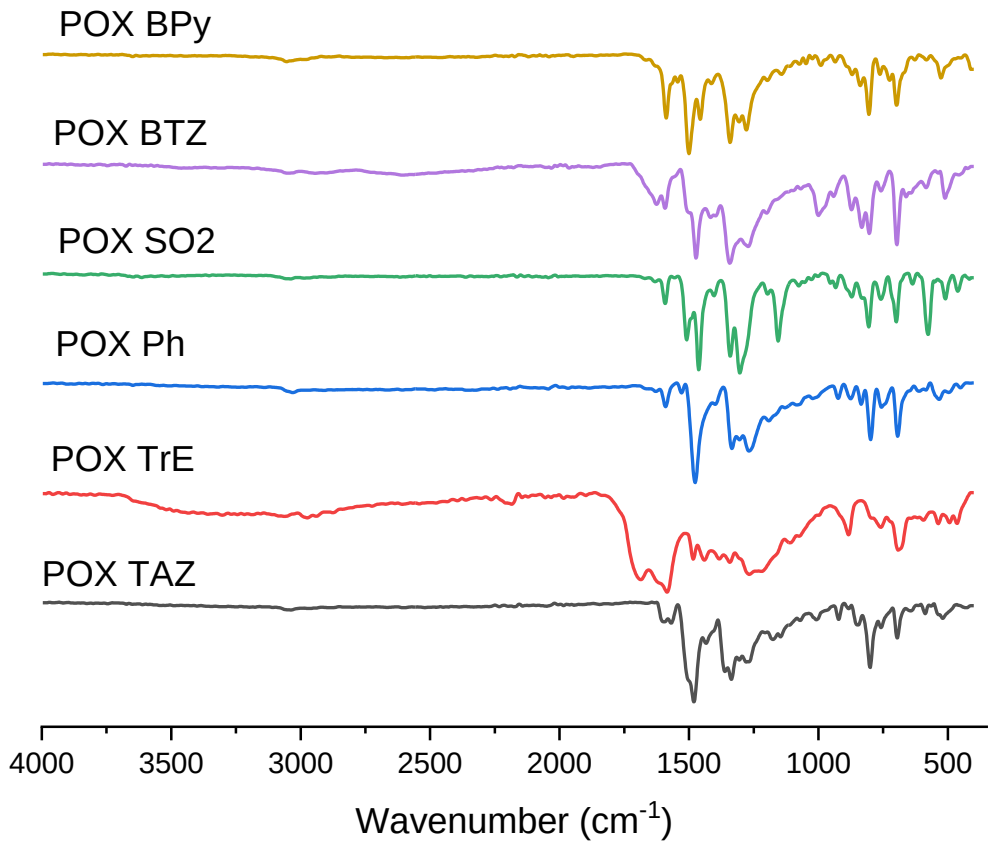

Figure 2-6: FT-IR spectra of phenoxazine based polymers.

The next major class of photoactive cores we were interested in targeting were aryl ketones. Anthraquinones,[20,21] acridones,[22] and thioxanthones have all been successfully used as homogeneous photocatalysts, particularly as hydrogen atom transfer (HAT) reagents or triplet energy transfer photocatalysts[23], and we were hopeful that this reactivity would be preserved in a heterogeneous polymer form. Borylation of commercially available dibromo anthraquinone proceeded smoothly (Scheme **2-6**) and allowed for the production of a number of candidate polymers from monomer **2.8** (Scheme **2-7**).

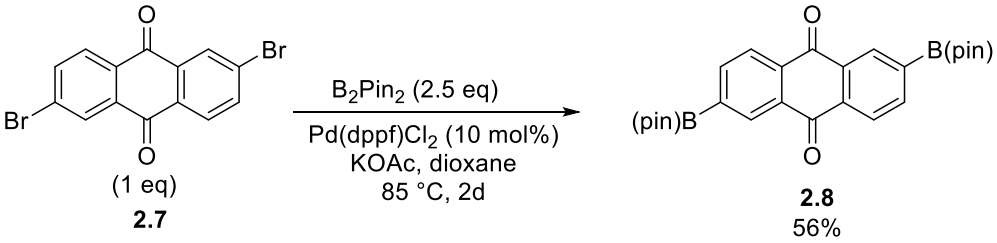

Scheme 2-6: Borylation of 2,6 dibromo anthraquinone.

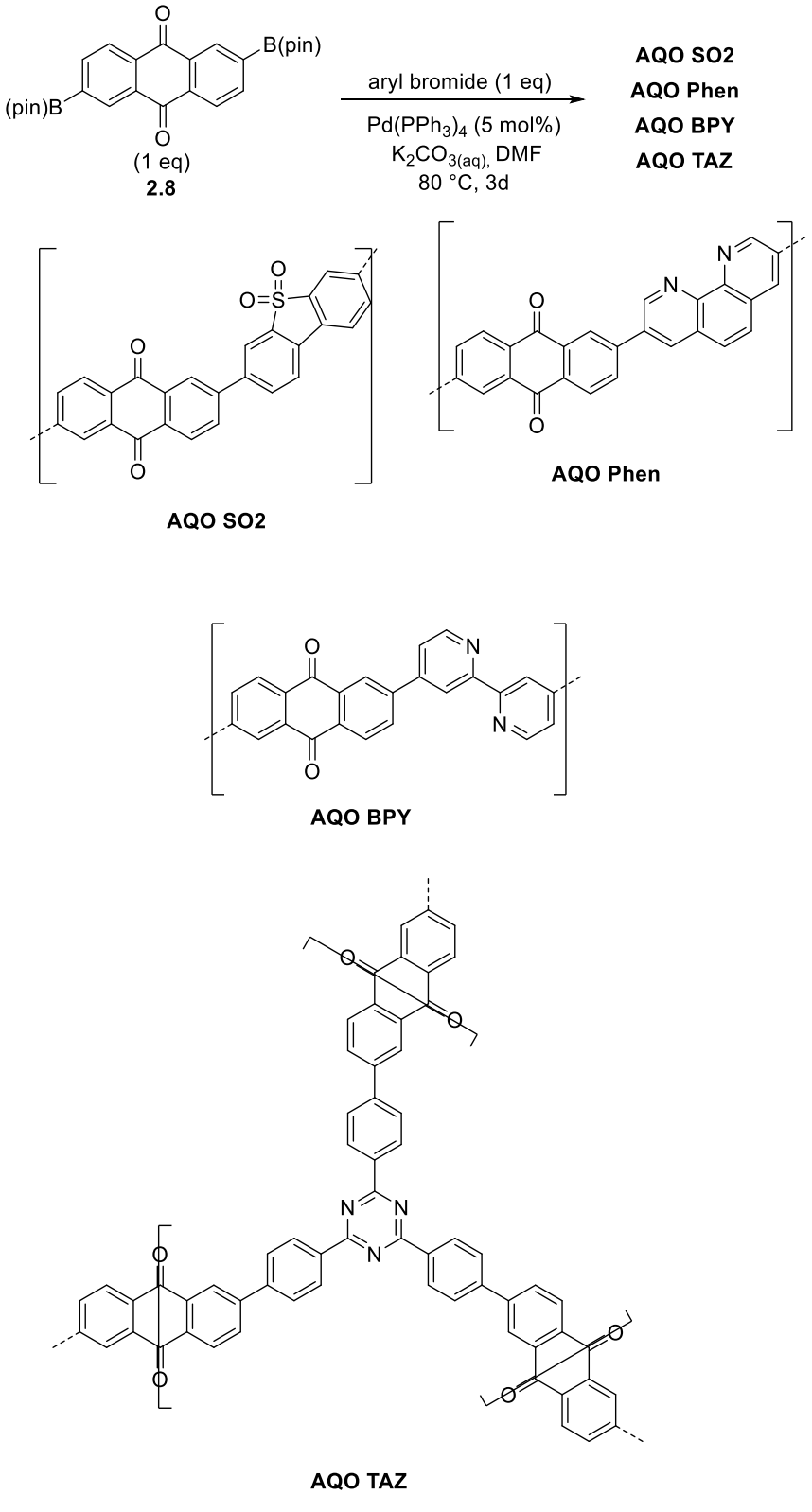

Scheme 2-7: Synthesis of anthraquinone polymers.

Similar to the phenoxazine based polymers, we also used dibromide **2.7** in Suzuki and Sonogashira polymerization to synthesize AQO Ph and AQO TrE polymers respectively (Scheme **2-8**)

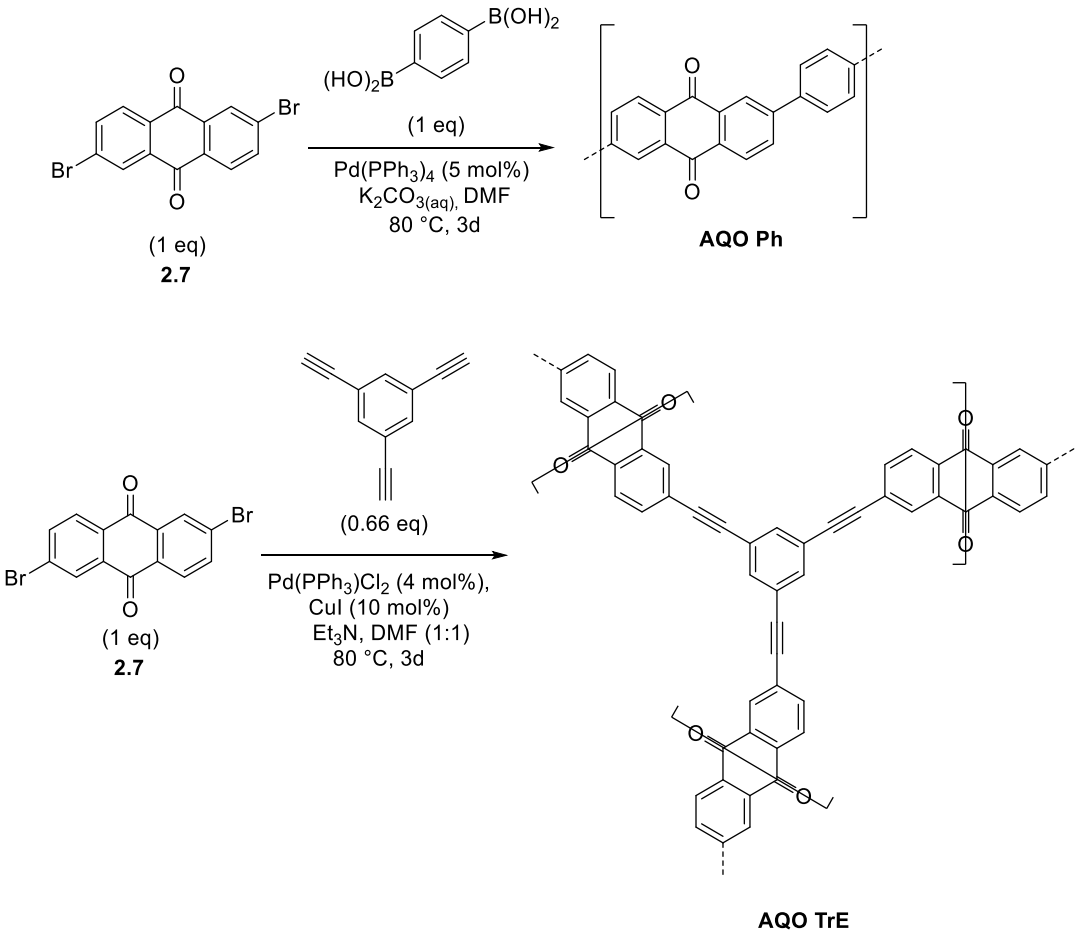

Scheme 2-8: Synthesis of AQO Ph and AQO TrE polymers.

The anthraquinone-based polymers all displayed broad visible light absorption from 400 – 800 nm (Figure **2-7**). Anthraquinone does not absorb in visible light, and UV-irradiation is often used when utilizing aryl ketones as homogeneous photocatalysts, [24] and it is possible that the conjugated analogues may be able to function efficiently in visible light instead.

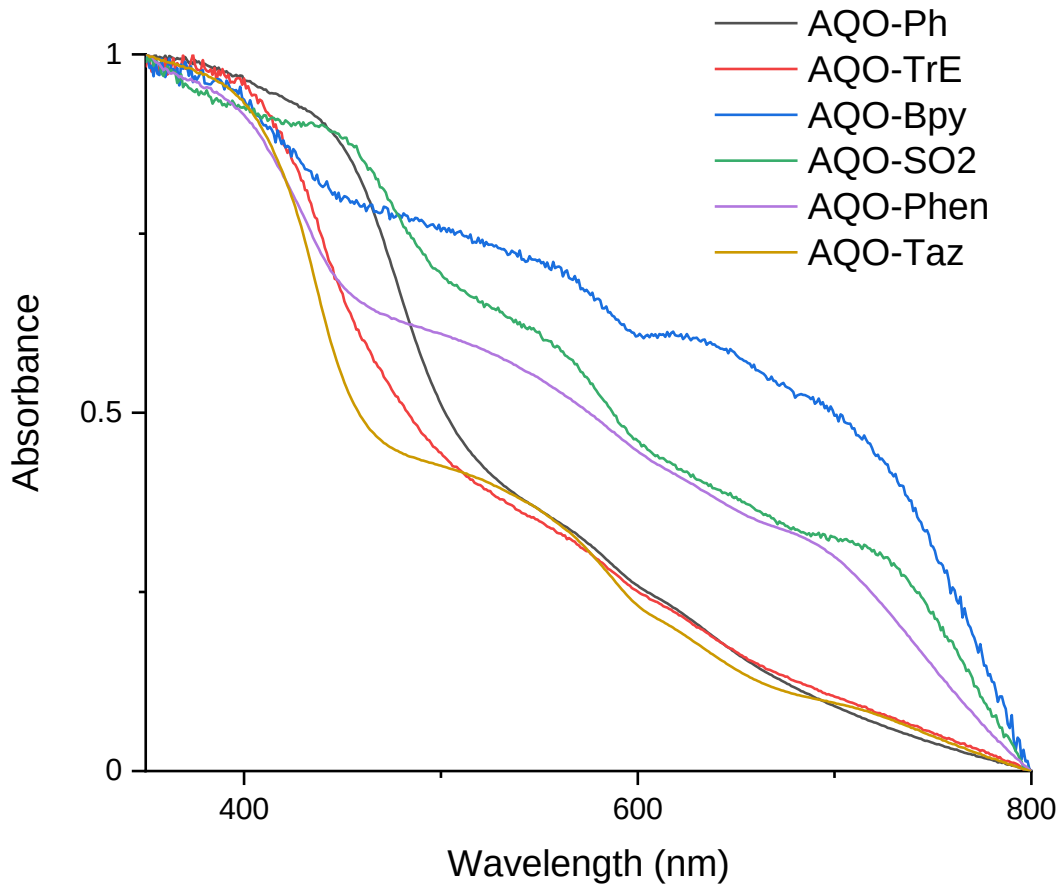

Figure 2-7: UV-Visible absorption spectra of anthraquinone based polymers.

FT-IR spectra of the anthraquinone polymers (Figure **2-8**) showed consistent peaks near 1670 cm^{-1} and 1580 cm^{-1}, corresponding to the C=O and C=C stretching vibrations respectively. Similar to POX-SO_2, the FT-IR spectrum of AQO-SO_2 displayed a peak at 1142 cm^{-1} which likely corresponds to the stretching vibration of the sulphone moiety. AQO-TAZ also showed a strong absorption band at 1503 cm^{-1}, indicative of the triazine ring[19].

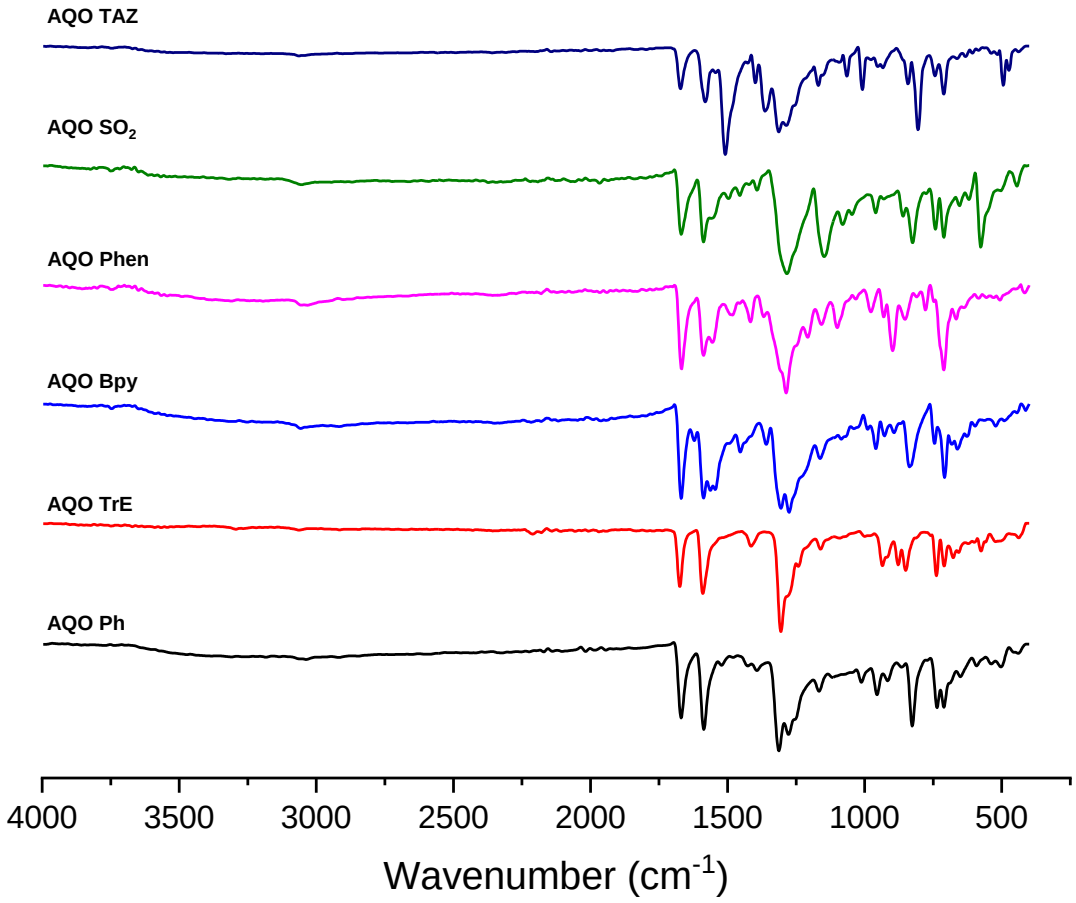

Figure 2-8: FT-IR spectra of anthraquinone based polymers.

Using acridone monomer **2.9**, we similarly synthesized NMeA Ph and NMeA TrE polymers using Suzuki and Sonogashira coupling respectively (Scheme **2-9**) Thioxanthone proved difficult to brominate in good yields, and we instead proceeded to use it directly to produce a hyper-crosslinked polymer (HCP), which has successfully been used as a radical initiator previously (Scheme **2-9**).[25]

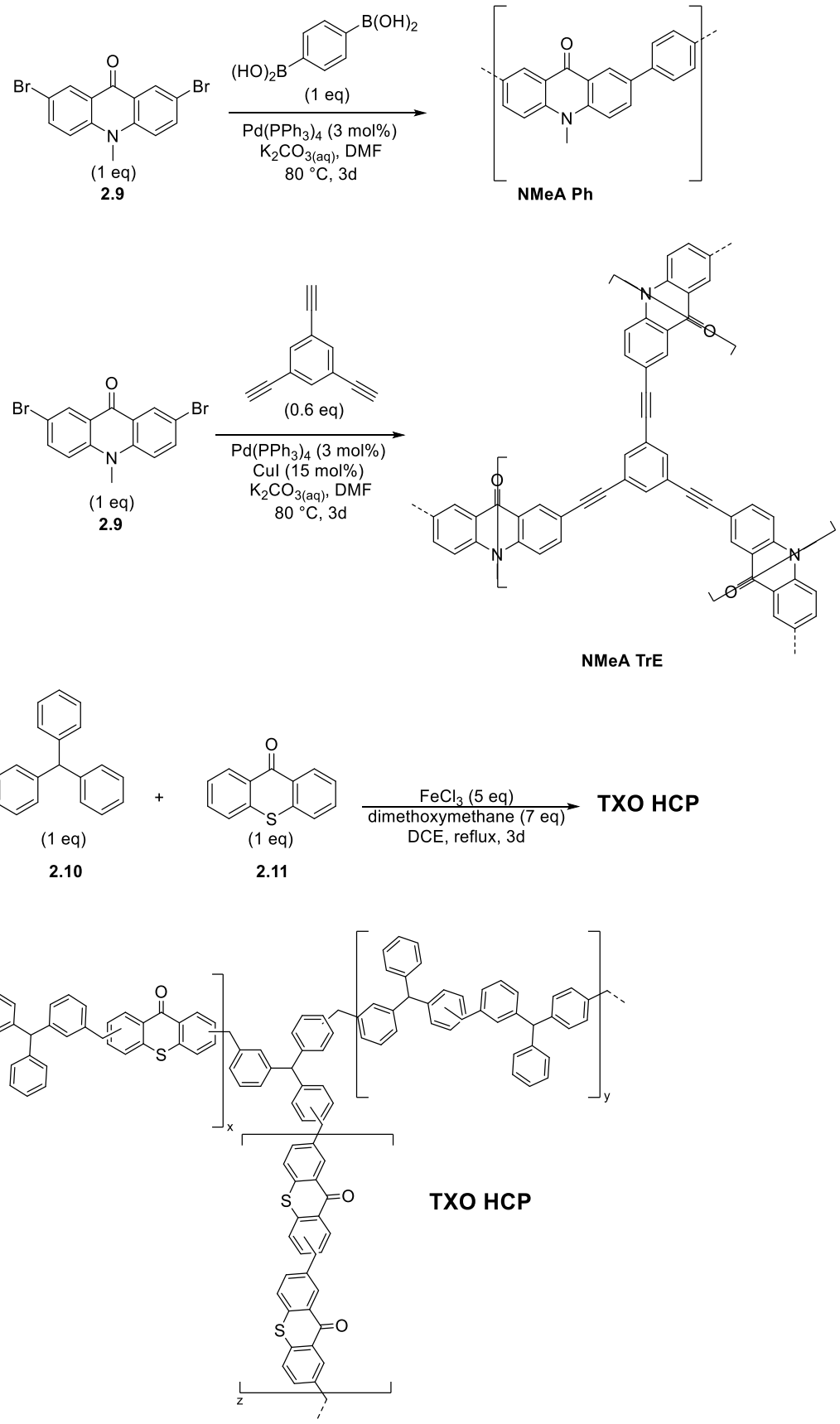

Scheme 2-9: Synthesis of N-Methyl acridone and thioxanthone polymers.

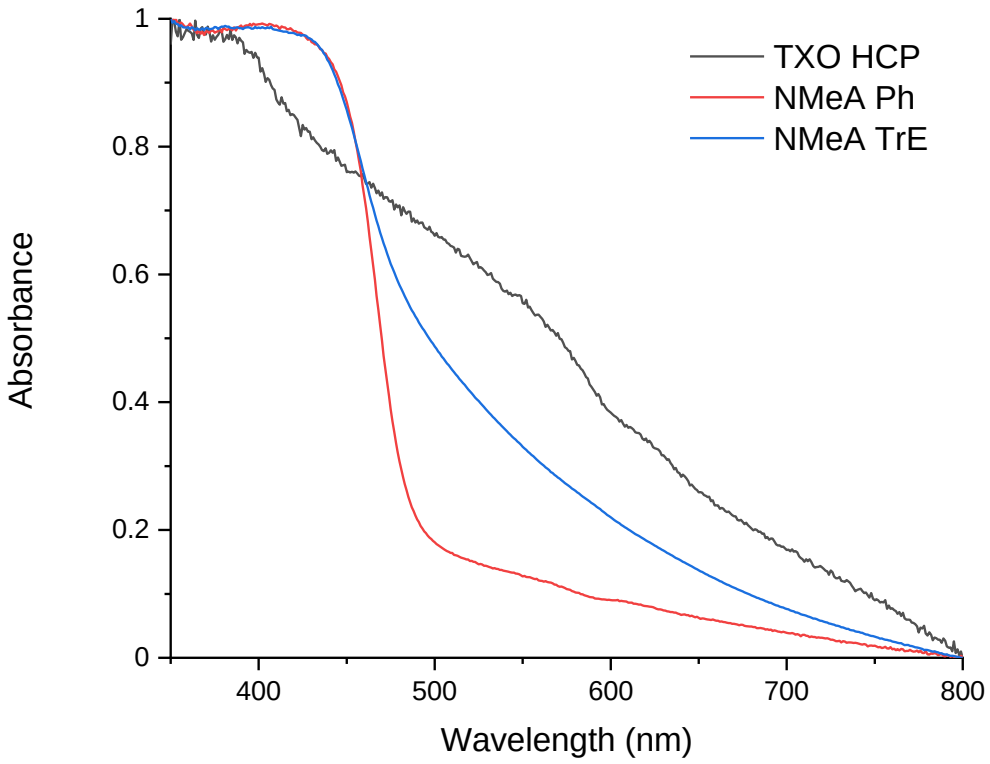

Figure 2-9: UV-Visible absorption spectra of N-Methyl acridone and Thioxanthone polymers.

Solid state UV-visible absorption spectra of TXO-HCP, NMeA-Ph, and NMeA-TrE (Figure **2-9**) revealed that each of the polymers were capable of absorbing in visible light. Despite neither the thioxanthone nor triphenylmethane monomers having no significant absorption in visible light, the hyper-crosslinked polymer TXO-HCP showed significant absorption in visible light, despite not being a fully conjugated polymer. Absorption of visible light by NMeA-Ph fell sharply at wavelengths longer than 450 nm, which could possibly be an indication that photocatalytic performance may be inefficient with 500 – 800 nm irradiation.

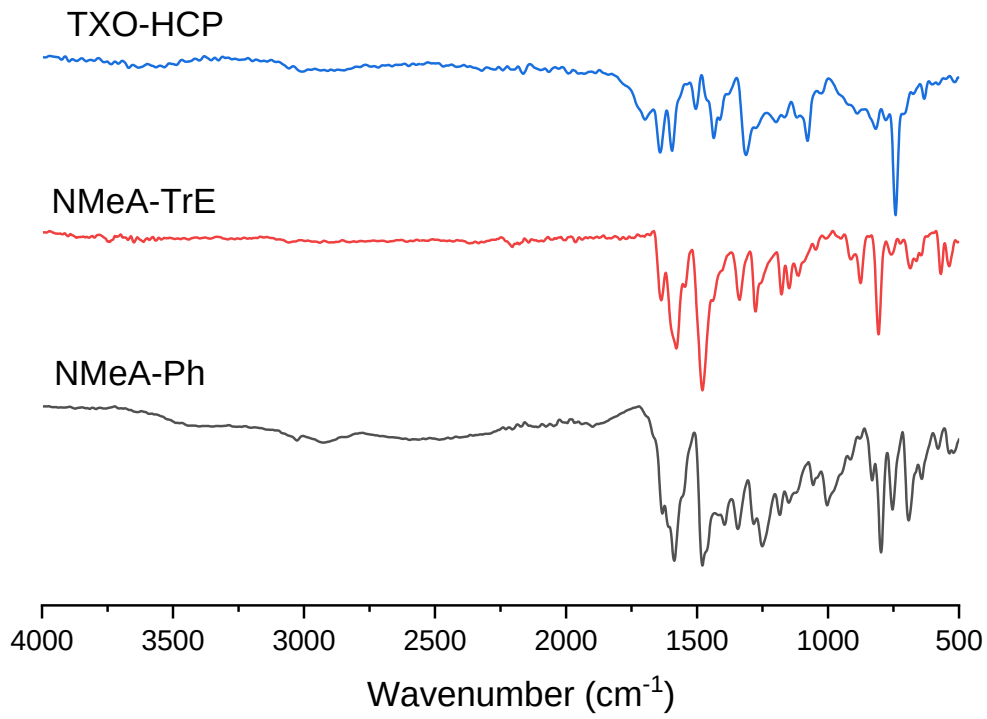

Figure 2-10:FT-IR spectra of thioxanthone and N-Methyl acridone polymers.

FT-IR spectra of TXO-HCP, NMeA-Ph, and NMeA-TrE (Figure **2-10**) displayed bands near 1630 cm^{-1}, followed by strong signals at 1580 cm^{-1}, and 1480 cm^{-1} which could correlate to the stretching of the carbonyl and aromatic C=C moieties respectively. Bands near 800 cm^{-1} corresponding to aryl C-H bending were clearly visible with all 3 polymers.

We also synthesized some miscellaneous polymers such as CTF-2, TAA, and Cz which have been successfully used in hydrogen evolution and are easily scalable (Scheme **2-10**). CTF-2, is an active hydrogen evolution catalyst, is synthetically accessible, synthesized in one step from commercially available materials.[26]

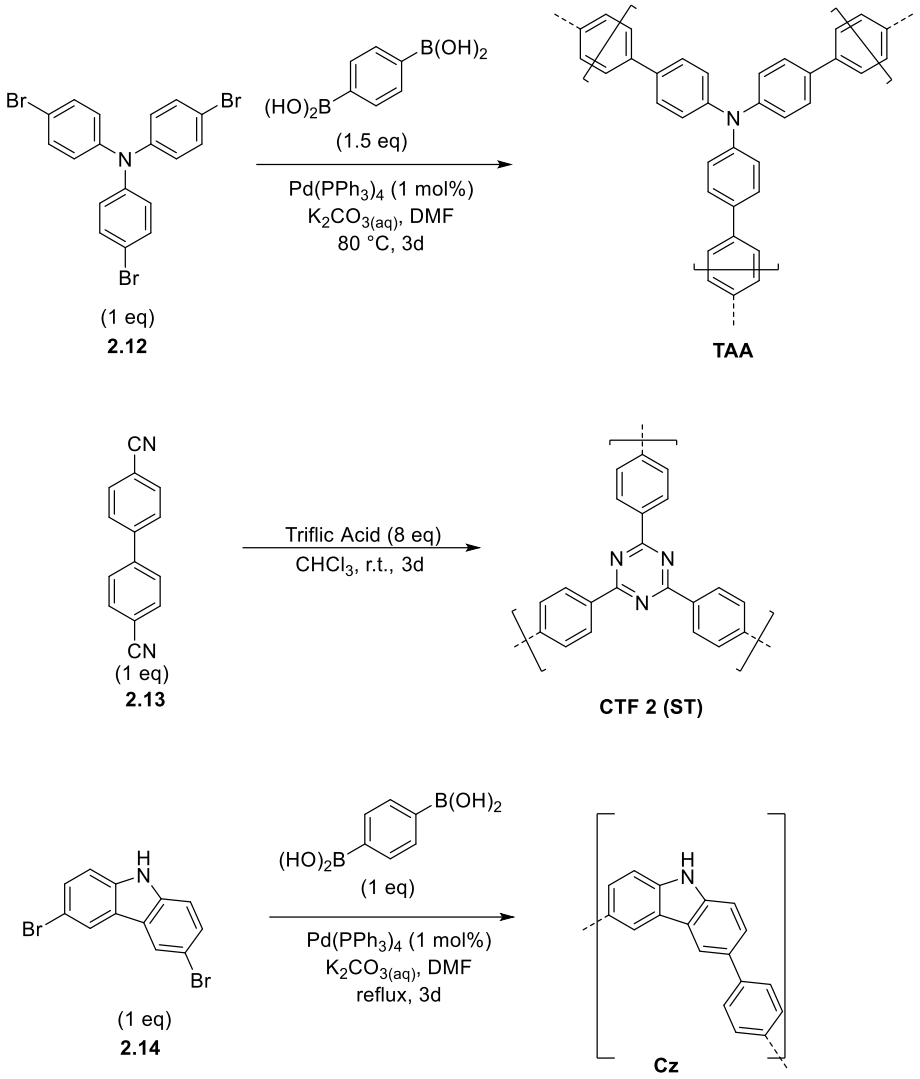

Scheme 2-10: Synthesis of TAA, CTF-2, and Cz polymers.

UV-visible absorption spectra of TAA and Cz polymers (Figure **2-11**) revealed that they had sharp decreases in absorption after 400 nm and 450 nm respectively, suggesting that both polymers may be inefficient without blue/purple LED irradiation, and compared the AQO and POX polymers narrow absorbed from 400-800 nm. CTF-2 also absorbed in visible light, as a result of the triflic acid catalysed polymerization. In comparison, monomer **2.13** does not absorb in visible light.[27]

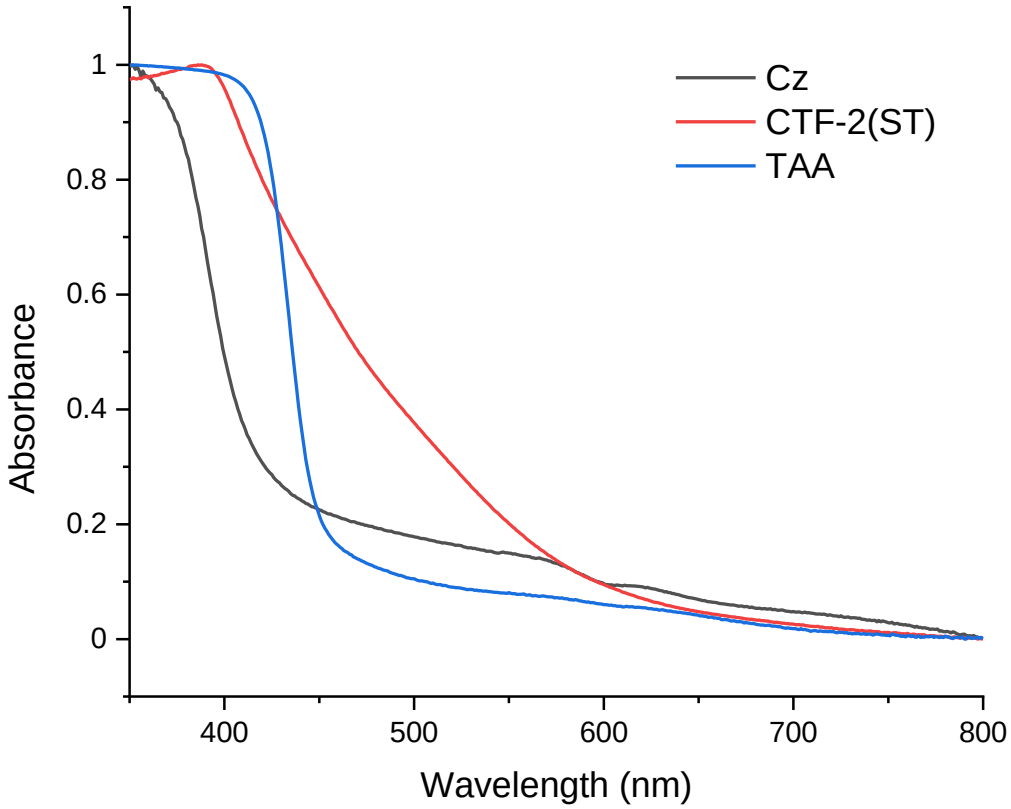

Figure 2-11: UV-Visible absorption spectra of Cz, CTF-2, and TAA polymers.

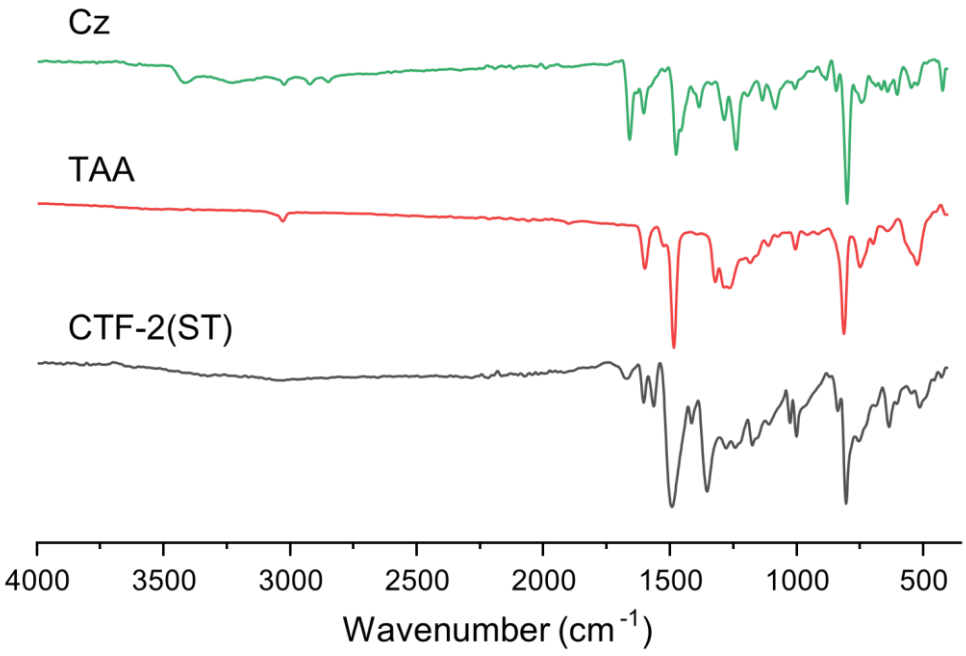

Figure 2-12:FT-IR spectra of Cz, TAA, and CTF-2 polymers.

The FT-IR spectrum (Figure **2-12**) of Cz displayed bands at 1658 cm^{-1}, and 1238 cm^{-1} which likely correlates to N-H bending and C-N stretching respectively. Cz, CTF-2, and TAA all displayed aromatic C-H bending signals near 800 cm^{-1}, as expected. No nitrile stretching band near 2250 cm^{-1} was observed in the FT-IR spectrum of CTF-2, suggesting that negligible amounts of if the dicarbonitrile monomer remained in the polymer. FT-IR spectrum of CTF-2 also displayed the expected strong absorption bands near 1500 and 1350 cm^{-1}, which are indicative of the triazine ring.

Internally, we also discovered that dicyanopyridine derivatives are active for photocatalytic hydrogen evolution, and we synthesized polymer versions of these to explore whether they would be active for organic photochemistry (Scheme **2-11**). Using monomers **2.15** and **2.16** we constructed polymer analogues using triazine and benzene coupling partners.

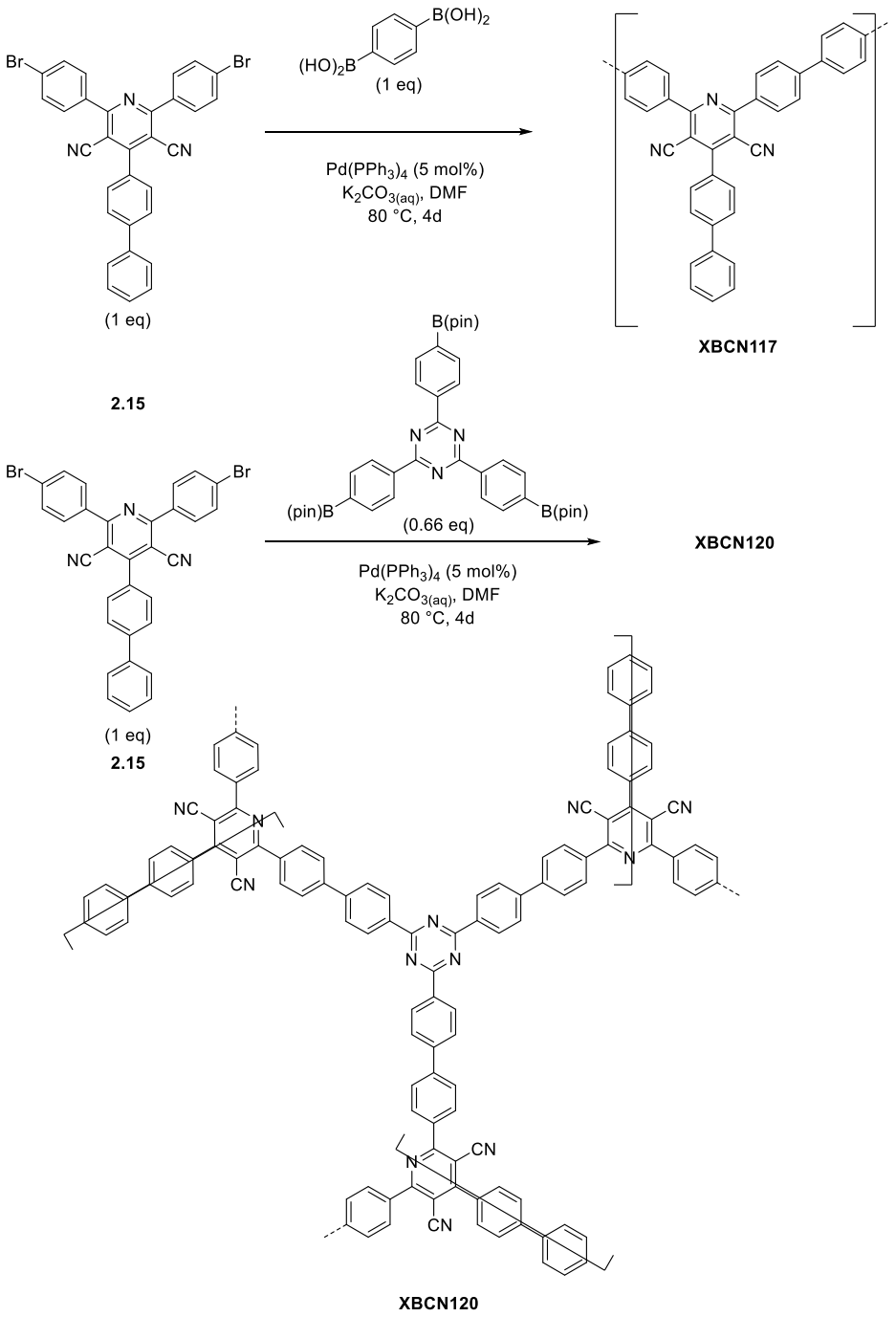

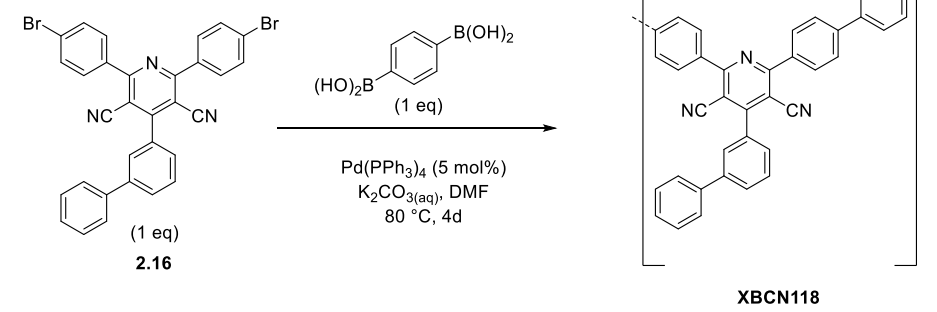

Scheme 2-11: Synthesis of dicyanopyridine polymers.

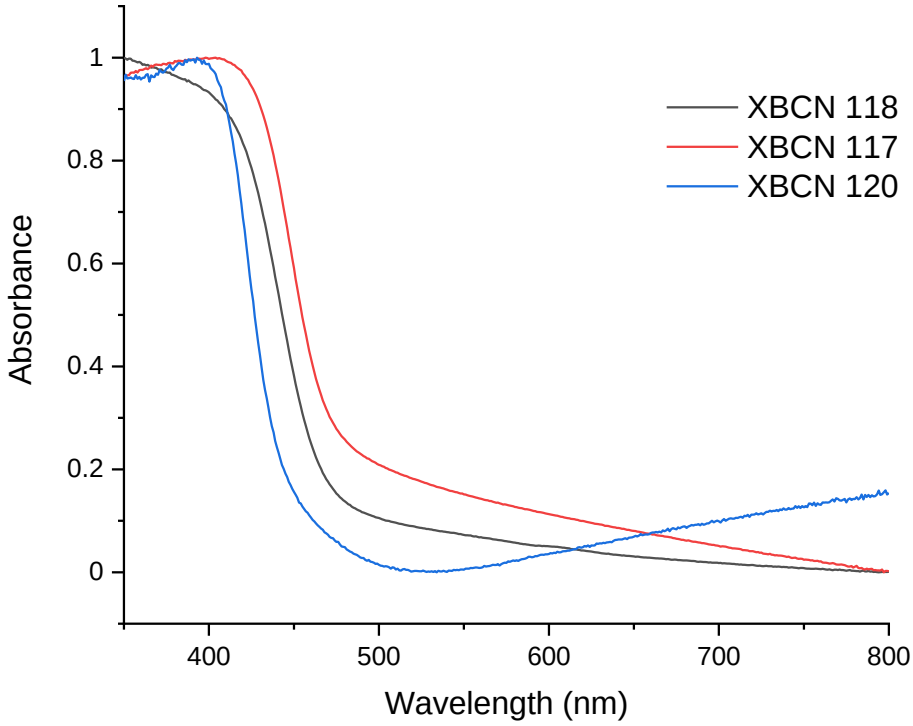

Figure 2-13: UV-Visible absorption spectra of cyanopyridine polymers.

UV-Visible absorption spectra of all 3 cyanopyridine polymers (Figure **2-13**) show significant falloffs in absorption after 450 nm, again suggesting that high-energy visible light irradiation might be critical for any photocatalytic activity.

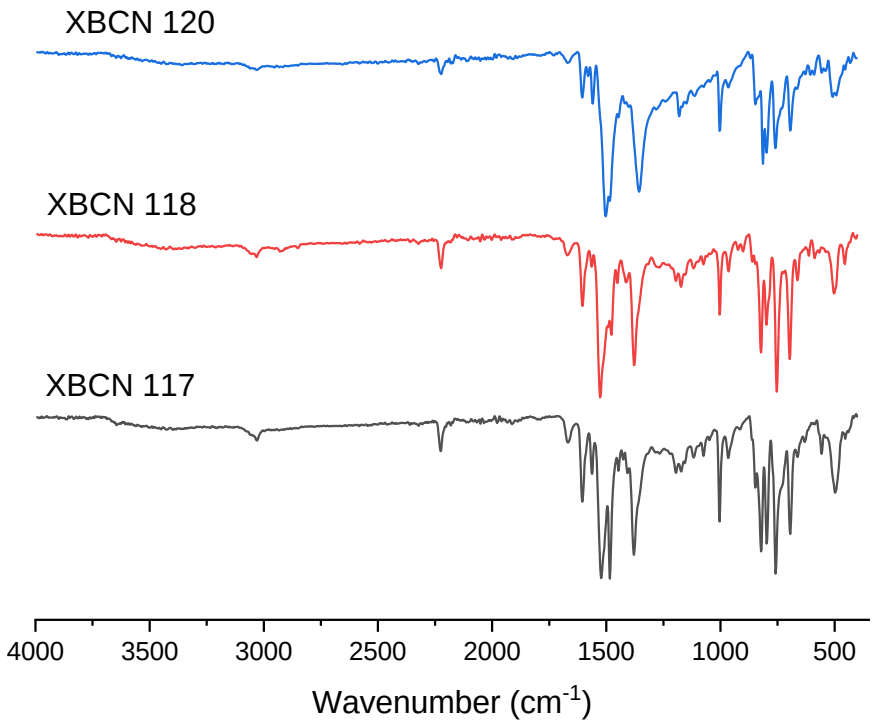

Figure 2-14: FT-IR spectra of cyanopyridine polymers.

XBCN118, 117, and 120 all displayed bands near 2250 cm^{-1} in their FT-IR spectra (Figure **2-14**), corresponding to the dicyanopyridine core, along with aromatic C=C stretching, while weak bands at ~3000 cm^{-1} could be attributed to C-H stretching vibrations.

High-Throughput Photocatalyst Discovery

With our initial library of polymers synthesized, we started testing on these candidate materials using our discovery process. 10 mL crimp seal headspace vials were loaded with polymer, and any insoluble reagents, and were placed inside either a ChemSpeed ISynth or Swing platform along with nitrogen sparged stock solutions of the organic reagents in septa screw top vials, and the robotic platform was closed, and purged with nitrogen for ~2 hours. The degassed stock solutions were then dispensed to each vial, and the vials were subsequently crimp sealed. The vials were manually transferred to our photoreactor setup and were irradiated for 3 days using a 400W white LED floodlight along with fan cooling. The vials were then transferred back to the ChemSpeed platform, and were diluted with ethyl acetate, and an aliquot of each was reformatted to a GC-MS filter vial. The GC-MS vials were then queued on the autosampler of a GC-MS instrument, and was directly analysed by GC-MS. In each case, blank reaction was performed to see the conversion in the absence of an exogeneous photocatalyst.

Direct C-H Trifluoromethylation

The method for C-H trifluoromethylation of arenes and heteroarenes (Scheme **2-12**) was previously reported by MacMillan and co-workers,[28] using a $Ru(Phen)Cl_2$ photocatalyst. Direct trifluoromethylation is particularly valuable in avenues such as medicinal or pharmaceutical chemistry. The mono- and di-trifluoromethylated products of dimethyl pyrazine were easily observed by GC-MS. Unfortunately, the mono- and di- trifluoromethylated products were unable to be completely separated through analytical GC, and accurate distributions of both species were unable to be calculated.

Surprisingly, we found that in the trifluoromethylation reaction resulted in 33% conversion without any catalyst (Figure **2-15**). This could be because of photocatalytic degradation of the trifluoromethylating agent to the trifluoromethyl radical. Several polymers were able to successfully catalyse this reaction – although we noted that polymers containing triethynyl benzene inhibited the reaction. The best performing polymer for this reaction, was POX-SO_2, which showed 83% GC-MS conversion from starting material. During our studies, however, a report by König and co-workers demonstrated an efficient method for C-H trifluoromethylation using polymeric carbon nitride in high yields.[29] Given that carbon nitride is a cheap, scalable, material that can be synthesized without metal coupling, we determined that it was unlikely to find a heterogeneous material that would offer substantial improvements and we discontinued further work on this reaction.

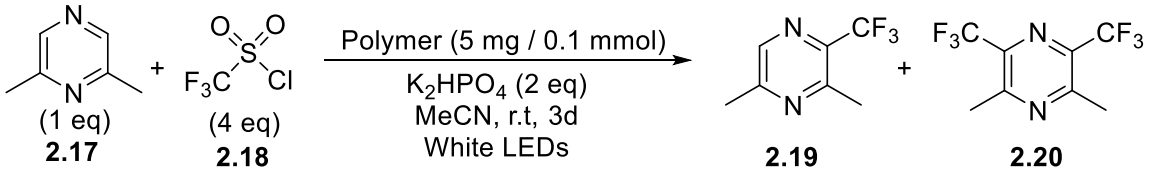

Scheme 2-12: Polymer catalysed C-H trifluoromethylation of heteroarenes.

Polymer	Conversion / %
Blank	33
CTF – 2 (ST)	51
TAA	45
POX TrE	trace
POX TAZ	42
EY - TrE	trace
poly-4CzIPN	71
NMeA – Ph	70
POX – Ph	62
POX – SO_2	83
POX - BTZ	73
POX - Bpy	73
NMeA - TrE	trace
Cz	42
RB - TrE	trace

Figure 2-15: Screening results for C-H trifluoromethylation of heteroarenes. Combination of mono- and di-trifluoromethylation products. Conversions based on dimethylpyrazine starting material.

Beta Ketone Addition of Carbonyls:

MacMillan and co-workers have reported on the direct beta addition of ketones (Scheme **2-13**), using a combination of a photocatalyst and amine catalyst,[30] enabling functionalization of a typically inert species. The photocatalyst used in for this reaction is $[Ir(ppy)_2(dtbbpy)][PF_6]$. From screening our library of polymers, we found that NMeA-Ph was particularly active for this reaction (Figure **2-16**), enabling 52% conversion, while TAA, and NMeA-TrE were also successful. No conversion was observed in the absence of a photocatalyst.

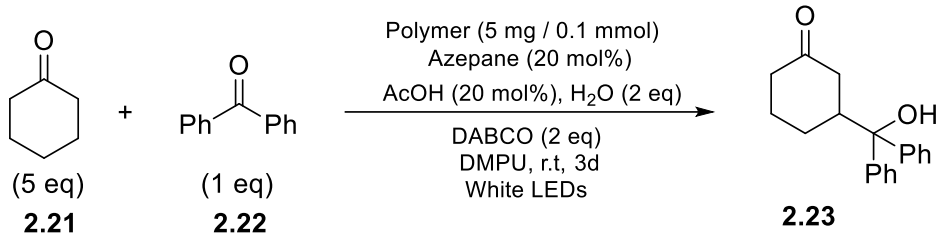

(5 eq) **2.21** (1 eq) **2.22** **2.23**

Scheme 2-13: Polymer catalyzed regioselective addition of aryl ketones to cyclic ketones.

Polymer	Conversion / %
Blank	0
CTF – 2 (ST)	0
TAA	36
EY - TrE	trace
POX TrE	12
POX TAZ	17
poly-4CzIPN	0
NMeA – Ph	52
POX – Ph	22
POX – SO_2	14
POX - BTZ	5
POX - Bpy	14
NMeA - TrE	28
Cz	trace
RB - TrE	0

Figure 2-16: Screening results for ketone addition to carbonyls. Conversions based relative to benzophenone starting material.

Decarboxylative Metallaphotoredox Arylation:

MacMillan and co-workers have successfully combined nickel cross-coupling catalysts in tandem with iridium photoredox catalysis for sp^3 arylation of carboxylic acids (Scheme **2-14**).[31] Carboxylic acids are relatively stable, inexpensive, and widely available – both commercially and in nature – and are attractive starting material, and an organic polymer able to catalyse this reaction could be valuable as a scalable material to convert feedstock chemicals. This reaction was originally reported with iridium catalyst $[Ir(dF(CF_3)ppy)_2(dtbbpy)][PF_6]$, which has been widely used in a variety of photoredox reactions, and we were ideally looking for a polymer that would be able to be able to mimic its capabilities. From our screening results (Figure **2-17**), while a few polymers such as CTF-2 and NMeA-TrE were able to successfully catalyse this decarboxylative arylation reaction, the conversions were very low (trace – 7% GC-MS yield), and several polymers appeared to produce large amounts of the dehalogenation side product instead.

As a benchmark, $[Ir(dF(CF_3)ppy)_2(dtbbpy)][PF_6]$ (2 mol% loading) under identical conditions in our photoreactor setup yielded 54% GC-MS yield (vs biphenyl) of the decarboxylative arylation product. Our hypothesis is that our pool of polymers struggled to perform the key oxidation of the carboxylic acid substrate to form the alkyl radical which is necessary to drive the arylation reaction.

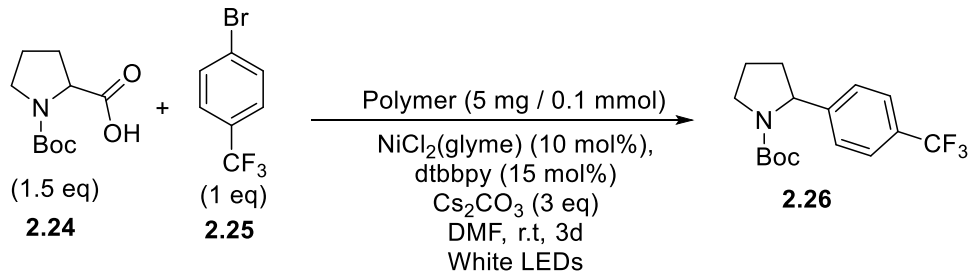

Scheme 2-14: Polymer catalysed metallaphotoredox decarboxylative arylation

Polymer	GC-MS Yield / %
Blank	0
CTF – 2 (ST)	6
TAA	2
EY - TrE	0
NMeA – Ph	4
POX – Ph	trace
POX – SO_2	trace
POX - BTZ	0
POX - Bpy	0
NMeA - TrE	7
Cz	0
RB - TrE	0
TXO HCP	4
AQO - Ph	0
AQO - TrE	0
AQO - Bpy	0
AQO - Phen	0
AQO - SO_2	0
AQO - TAZ	0
[Ir(dF(CF_3)ppy)$_2$(dtbbpy)][PF_6]	54

Figure 2-17: Screening results for metallaphotoredox decarboxylative arylation. GC-MS yields vs biphenyl.

Direct C-H Arylation of Tertiary Amines

Another reaction developed by the MacMillan group was the direct C-H arylation of tertiary arylamines with aryl cyanides (Scheme **2-15**), which MacMillan discovered with high throughput screening.[32] Alpha arylamines are widely present in many biologically relevant molecules, and a metal free synthesis method could prove valuable. The iridium photocatalyst originally used for this reaction was $Ir(ppy)_3$, a reducing photocatalyst. From our screening results (Figure **2-18**), we found, surprisingly, that the reaction appeared to show substantial product formation in the absence of any photocatalyst. This is possibly due to the formation of electron donor-acceptor (EDA) complexes that could initiate this reaction in the absence of any photocatalyst. Some of the polymers that we tested significantly improved the performance of the reaction, compared to the blank reaction. Polymers containing the phenoxazine (POX) core and NMeA – Ph showed > 60% GC-MS yield, while some polymers inhibited the reaction almost completely.

Recently, Jin and co-workers reported the ability to perform this reaction in the absence of an external photocatalyst,[33] using a combination of blue LED irradiation and Cs_2CO_3 to generate the arylated product in 43% yield, corroborating our findings. The attribute the reactivity to the formation of EDA complexes. While some polymers that we screened showed improved performance under white LED irradiation, the absence of any external catalyst at all is inherently superior, and blue LEDs are widely available. We recognized that any polymer photocatalyst we discovered for this reaction would be unlikely to yield substantial improvement over this reported procedure, and subsequently, we discontinued further work on developing this reaction.

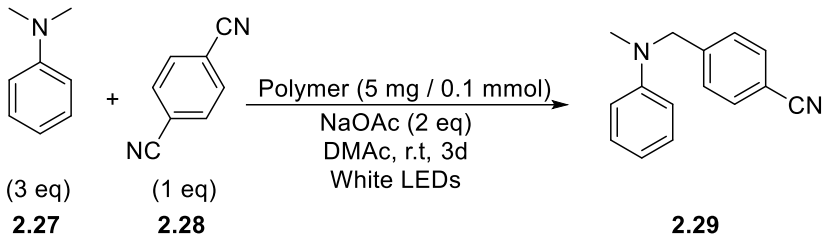

Scheme 2-15: Polymer catalyzed C-H arylation of tertiary arylamines.

Polymer	GC-MS Yield / %
Blank	20
CTF 2 (ST)	8
TAA	33
EY TrE	6
NMeA – Ph	60
POX Ph	63
POX SO2	65
POX BTZ	24
POX Bpy	63
NMeA – TrE	8
Cz	18
RB TrE	trace
TXO HCP	24
AQO Ph	trace
AQO TrE	trace
AQO Bpy	0
AQO Phen	trace
AQO SO2	0
AQO TAZ	0
XBCN-117	trace
XBCN-118	26
XBCN-120	18

Figure 2-18: Screening results of direct C-H arylation of tertiary arylamines. GC-MS yields vs biphenyl.

Metallaphotoredox C-H arylation of Tertiary Amines

The MacMillan group has also used [Ir(dF(CF_3)ppy)$_2$(dtbbpy)][PF_6] for the direct C-H arylation of arylamines (Scheme **2-16**).[31] Using our general screening approach, as described above – only two polymers showed yielded higher than trace product formation, CTF-2, and NMeA-Ph. This was disappointing, as we had hoped that the anthraquinone polymers would be capable of performing hydrogen abstraction and forming the requisite alkyl radical. We were surprised to see as well, that [Ir(dF(CF_3)ppy)$_2$(dtbbpy)][PF_6] only gave 15% GC-MS yield (Figure **2-19**), suggesting that there are significant improvements that could be made to our photoreactor station. In comparison, Macmillan and co-workers reported 84% isolated yield for this substrate. with No product formation was observed in the blank reaction, unlike the C-H arylation reaction of dimethylaniline with dicyanobenzene

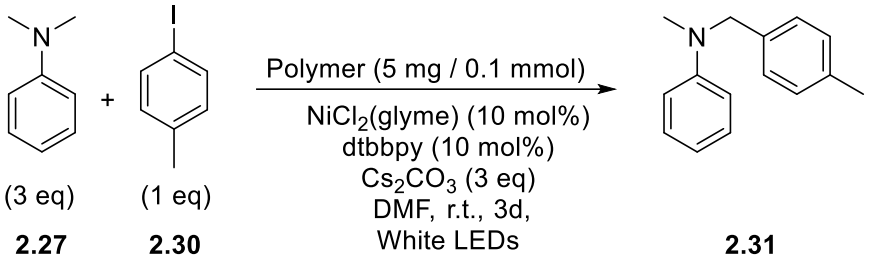

Scheme 2-16: Polymer catalysed metallaphotoredox C-H arylation of tertiary arylamines.

Polymer	GC-MS Yield / %
Blank	0
CTF – 2 (ST)	6
TAA	0
EY - TrE	0
NMeA – Ph	5
POX – Ph	0
POX – SO_2	trace
POX - BTZ	0
POX - Bpy	0
NMeA - TrE	trace
Cz	0
RB - TrE	0
TXO HCP	0
AQO Ph	0
AQO TrE	0
AQO Bpy	0
AQO Phen	0
AQO SO_2	0
AQO TAZ	0
[Ir(dF(CF_3)ppy)$_2$(dtbbpy)][PF_6] (2 mol%)	15

Figure 2-19: Screening results for metallaphotoredox C-H arylation of tertiary arylamines. GC-MS yields vs biphenyl.

Decarboxylative Conjugate Addition

Another decarboxylative reaction reported by MacMillan that we studied was the simple 1,4 conjugate addition reaction of carboxylic acids with Michael acceptors (Scheme **2-17**).[34] Applying our method for screening photocatalysts, we found that several polymers showed some product formation, AQO Phen, AQO Ph and CTF-2 (Figure **2-20**). While the yields were low compared to the iridium catalyst as a benchmark, under identical conditions, it was a good starting point – and a valuable C-C bond forming reaction that has seen limited exploration with heterogeneous photocatalysts. We deselected AQO-Phen and chose CTF-2 for further study.

CTF-2 can be synthesized without the use of palladium cross coupling, and in high yields from commercial materials. Furthermore, CTF-2 did show some activity in our screening of decarboxylative arylation (Figure **2-17**), and the direct C-H metallaphotoredox arylation (Figure **2-19**) while AQO-Phen showed only trace or no product formation in those reactions. Given that CTF-2 catalysed 3 different photochemical reactions performed by $[Ir(dF(CF_3)ppy)_2(dtbbpy)][PF_6]$, albeit in low yields, we hoped that CTF-2 would be able mimic the broad catalytic properties of this widely used photocatalyst in higher yields following further optimization and improvement.

Chapter 3 will focus on the development of this reaction.

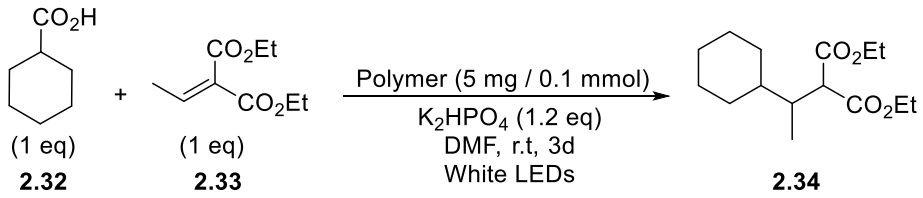

Scheme 2-17: Polymer catalysed decarboxylative conjugate addition

Polymer	GC-MS Yield
CTF-2 (M)	**19**
CTF-2 (ST)	**5**
EY TrE	0
POX Ph	0
POX SO2	0
POX BTZ	0
POX Bpy	trace
NMeA – TrE	trace
RB TrE	0
TXO HCP	trace
AQO Ph	6
AQO TrE	trace
AQO Bpy	0
AQO Phen	17
AQO SO2	trace
AQO TAZ	trace
Ir[(dFCF$_3$ppy)(dtbbpy)][PF$_6$] (2 mol%)	83

Figure 2-20: Screening results for decarboxylative conjugate addition. GC-MS yields vs biphenyl

Unsuccessful Reactions

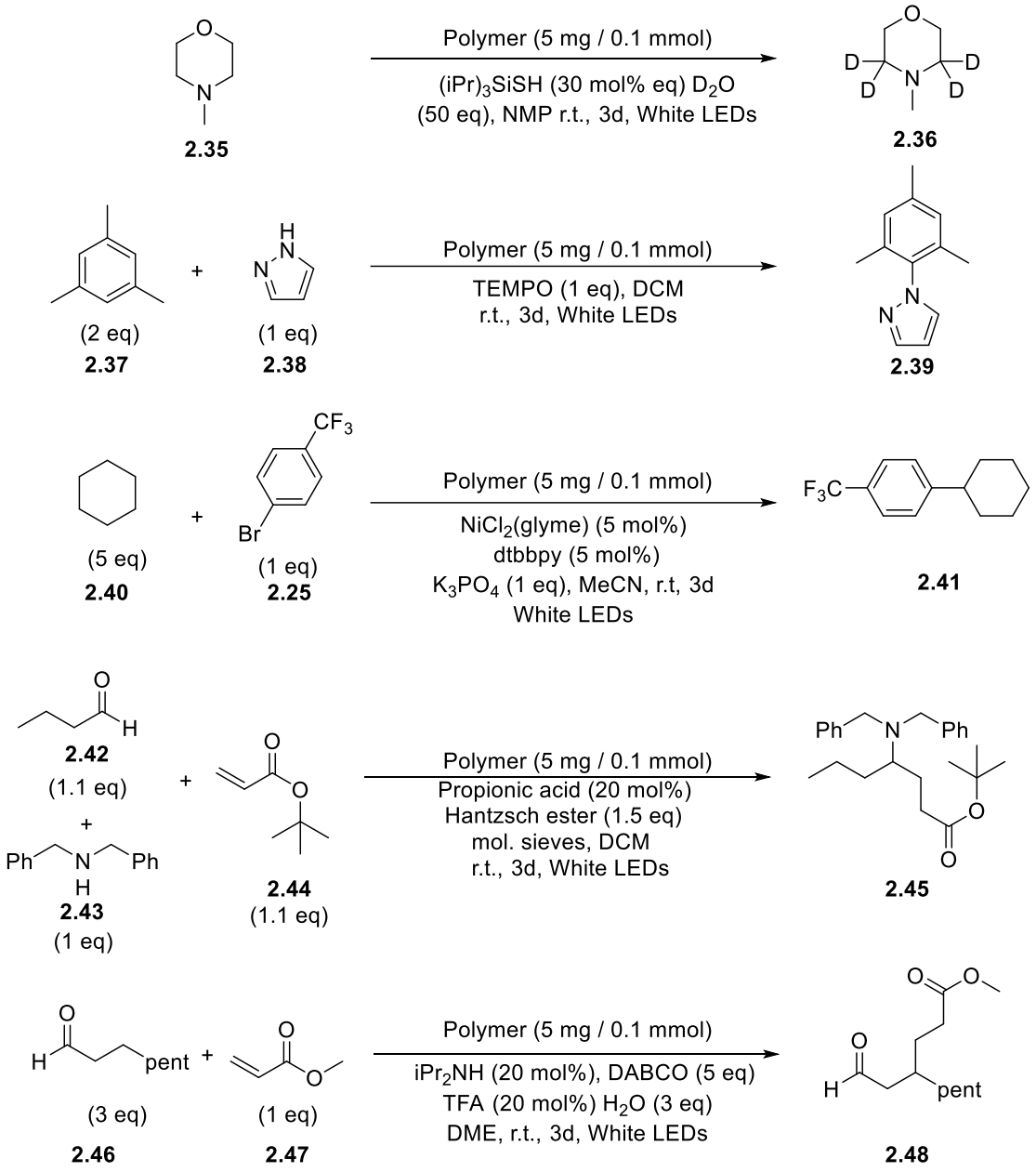

Scheme 2-18: Reactions that showed no product formation in any of the polymers screened

While several of the reactions that we tested were successfully catalysed by some of the polymers in our initial pool, other reactions[35–39] were unsuccessful in forming any product using all the polymers that we tested (Scheme **2-18**). Several of these reactions are already challenging to perform using transition metal photocatalysts. For several of these reactions, biphasic reaction mixtures, heterogeneous bases, or insoluble additives may create additional barriers for heterogeneous photocatalysts.

Conclusions

In summary, we developed a high throughput automation-augmented strategy for the discovery of novel heterogeneous organic photocatalysts. Using the robotic dispensing capabilities of ChemSpeed platforms, parallel sample irradiation, coupled with direct GC-MS analysis of reaction mixtures, we were able to test materials synthesized for several relevant photocatalytic reactions. With the photoreactor station we used for this workflow, we can run 48 samples in parallel.

This type of high-throughput process does have some distinct disadvantages, however. While it is relatively simple to screen whether a reaction has succeeded or not, it does not provide much insight into *why* it is successful (or unsuccessful). We also did not perform in depth characterization on deselected candidate polymers until they taken forward for further study.

In addition, GC-MS analysis is not compatible with substrates that have high boiling points, or are prone to decomposition at elevated temperatures, and this may limit the variety of reactions compatible. HPLC methods might be better suited in these cases, although this could necessitate lengthy method development. For comparison, little method development was required for our GC-MS analysis, beyond extending the run time at elevated temperatures in one case.

From our results, we discovered that CTF-2, a covalent triazine framework, was a promising material for decarboxylative conjugate addition, and potentially for other decarboxylative reactions as well. **Chapter 3** will focus on the optimization, development, and substrate scope of decarboxylative Michael addition reaction, and other related reactions.

Experimental

Monomer Synthesis

4CzIPN (2.1)

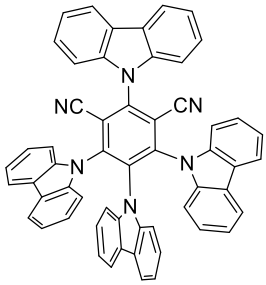

Carbazole (1.67 g, 10.0 mmol, 5 eq) is dissolved in dry THF (40 mL), followed by addition of sodium hydride (60% mineral oil dispersion) (0.6 g, 15 mmol, 7.5 eq). After 30 minutes of stirring, tetrafluoroisophtalonitrile (0.40 g. 2 mmol, 1 eq) is added, and the reaction is stirred at room temperature overnight. The reaction mixture is quenched with water, concentrated under reduced pressure, and filtered. The crude material is washed with ethanol, recrystallized from chloroform/acetone, and further purified by column chromatography in (DCM/hexane) to yield the product as a yellow powder (713 mg, 45% yield). Procedure was performed from reported methods. Data was consistent with previously reported values.[40,41]

^{1}H NMR (400 MHz, $CDCl_3$) δ 8.26 – 8.20 (m, 2H), 7.77 – 7.65 (m, 8H), 7.55 – 7.46 (m, 2H), 7.36 – 7.30 (m, 2H), 7.25 – 7.19 (m, 4H), 7.14 – 7.03 (m, 8H), 6.89 – 6.78 (m, 4H), 6.68 – 6.59 (m, 2H).

^{13}C NMR (101 MHz, $CDCl_3$) δ 145.36, 144.76, 140.12, 138.32, 137.10, 134.89, 127.11, 125.92, 125.10, 124.89, 124.68, 123.99, 122.54, 122.08, 121.55, 121.13, 120.57, 119.79, 116.50, 111.76, 110.09, 109.61, 109.56.

10-phenyl phenoxazine (2.4)

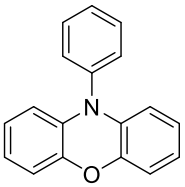

Phenoxazine (2.00 g, 10.9 mmol, 1 eq), copper powder (90 mg, 1.42 mmol, 13 mol %) iodobenzene (1.62 mL, 14.4 mmol, 1.3 eq) and potassium carbonate (1.52 g, 11.0 mmol, 1 eq) are placed under nitrogen and heated to reflux for 3 days. The reaction mixture is cooled, diluted with DCM, washed with dilute HCl, water, dried, and concentrated under reduced pressure. The crude product is purified by column chromatography (DCM/hexane) to yield the product as a white powder (1.61 g, 57% yield). Procedure was adapted from literature.[42–44] Data was consistent with previously reported values.

^{1}H NMR (400 MHz, $CDCl_3$) δ 7.63 – 7.57 (m, 2H), 7.51 – 7.45 (m, 1H), 7.38 – 7.33 (m, 2H), 6.70 (dd, *J* = 7.8, 1.7 Hz, 2H), 6.72-6.56 (m, 6H), 5.91 (dd, *J* = 7.8, 1.6 Hz, 2H).

^{13}C NMR (101 MHz, $CDCl_3$) δ 144.06, 139.10, 134.57, 131.18, 130.96, 128.62, 123.35, 121.38, 115.52, 113.36.

3,7 dibromo-10H-phenyl phenoxazine (2.5)

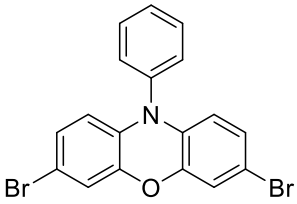

N-phenyl phenoxazine (2.00 g. 7.72 mmol, 1 eq) is dissolved in a solution of DCM/Acetic acid (100 mL, 1:1), followed by the slow addition of NBS (2.88 g, 16.2 mmol, 2.1 eq) over 15 minutes. The reaction mixture is stirred for 3 hours, diluted with DCM, and washed with saturated $NaHCO_3$, water, brine, and concentrated under reduced pressure. The crude product is purified by column chromatography (DCM/Hexane) to yield the product as white crystals (3.08 g, 96 % yield). Procedure was performed as in literature. [13]

^{1}H NMR (400 MHz, $CDCl_3$) δ 7.63 – 7.56 (m, 2H), 7.51 – 7.45 (m, 1H), 7.31 – 7.26 (m, 2H), 6.80 (d, *J* = 2.2 Hz, 2H), 6.68 (dd, *J* = 8.6, 2.2 Hz, 2H), 5.75 (d, *J* = 8.5 Hz, 2H).

^{13}C NMR (101 MHz, $CDCl_3$) δ 144.12, 138.14, 133.29, 131.36, 130.37, 129.01, 126.27, 118.63, 114.41, 112.84.

10-phenyl-3,7-bis(4,4,5,5-tetramethyl-1,3,2-dioxaborolan-2-yl)-10H-phenoxazine (2.6)

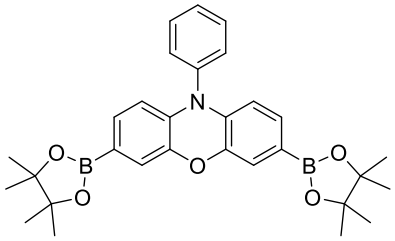

3,7 dibromo-10H-phenyl phenoxazine (3.00 g, 7.19 mmol, 1 eq), potassium acetate (5.84 g, 59.5 mmol, 8 eq), bispinacolato diboron (5.86 g, 23.1 mmol, 3.2 eq), and Pd(dppf)Cl_2 (0.528 g, 0.721 mmol, 0.1 eq) are suspended in dioxane (72 ml) and heated to reflux overnight under nitrogen. The reaction mixture is cooled and filtered through alumina eluting with ether. The crude solution is concentrated under reduced pressure and purified via column chromatography (DCM/Hexane), recrystallized, filtered and washed with hexane to yield the title compound as pale brown crystals (1.23 g, 34 % yield). Procedure adapted from a reported procedure. [45]

^{1}H NMR (400 MHz, $CDCl_3$) δ 7.64 – 7.55 (m, 2H), 7.52 – 7.46 (m, 1H), 7.33 – 7.27 (m, 2H), 7.07 (d, *J* = 1.3 Hz, 2H), 7.02 (dd, *J* = 7.9, 1.3 Hz, 2H), 5.85 (d, *J* = 7.9 Hz, 2H), 1.30 (s, 24H).

^{13}C NMR (101 MHz, $CDCl_3$) δ 143.66, 138.30, 136.59, 131.12, 130.49, 130.44, 128.74, 121.16, 112.75, 83.58, 24.80.

HRMS (+ESI): m/z calculated for $[M+H]^+$: 512.2774; found: 512.2787

2,6-bis(4,4,5,5-tetramethyl-1,3,2-dioxaborolan-2-yl)anthracene-9,10-dione (2.8)

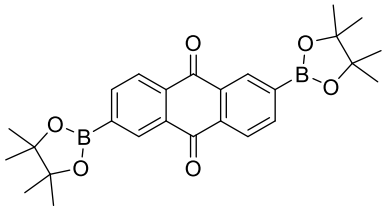

Dibromoanthraquinone (3.00 g, 8.20 mmol, 1 eq), potassium acetate (2.95 g, 30.0 mmol, 3.7 eq), bispinacolato diboron (5.21 g, 20.5 mmol, 2.5 eq), and Pd(dppf)Cl_2 (603 mg, 0.82 mmol, 0.1 eq) are suspended in dioxane (50 mL) and heated to 85 °C for 2 days. The reaction mixture is diluted with DCM, filtered through silica, washed with water, brine, concentrated, purified via column chromatography (DCM/EtOAc), and washed with hexane to yield the product as a pale brown solid (2.12 g, 56 % yield). Procedure adapted from literature.[46]

^{1}H NMR (400 MHz, $CDCl_3$) δ 8.74 (d, *J* = 0.6 Hz, 2H), 8.30 (dd, *J* = 7.7, 0.5 Hz, 2H), 8.20 (dd, *J* = 7.7, 1.2 Hz, 2H), 1.38 (s, 24H).

^{13}C NMR (101 MHz, $CDCl_3$) δ 183.42, 140.12, 135.17, 133.78, 132.55, 126.23, 84.58, 24.92.

Data is consistent with literature values. [47]

3,7-dibromodibenzo[b,d]thiophene 5,5-dioxide (2.50)

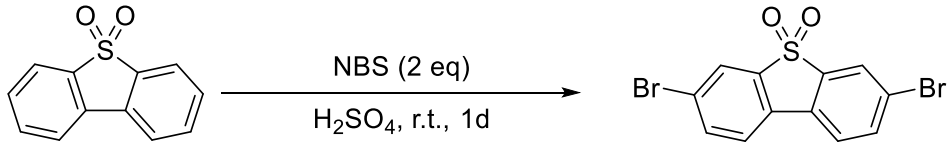

2.49 **2.50**
34%

Dibenzo[b,d]thiophene 5,5-dioxide (4.60 g, 21.3 mmol, 1 eq) is dissolved in concentrated sulphuric acid (100 mL), followed by addition of NBS (7.50 g, 42.1 mmol, 2 eq). The reaction mixture was stirred overnight, slowly added to ice, filtered, and washed with water. The crude material was recrystallized from chloroform to yield the compound as white crystals. (2.72 g, 34% yield). Procedure was adapted from literature.[48] Data was consistent with previously reported values.

^{1}H NMR (400 MHz, $CDCl_3$) δ 7.95 – 7.91 (m, 2H), 7.77 (dd, *J* = 8.2, 1.8 Hz, 2H), 7.63 (d, *J* = 8.2 Hz, 2H).

^{13}C NMR (101 MHz, $CDCl_3$) δ 139.05, 137.29, 129.74, 125.74, 124.75, 123.06.

2,4,6-tris(4-(4,4,5,5-tetramethyl-1,3,2-dioxaborolan-2-yl)phenyl)-1,3,5-triazine (2.52)

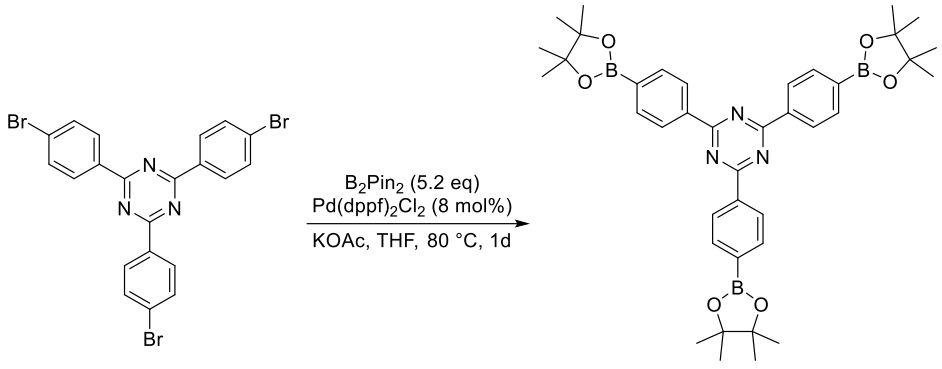

2,4,6-tris(4-bromophenyl)-1,3,5-triazine (2g, 3.66 mmol, 1 eq), B_2Pin_2 (4.84 g, 19.1 mmol, 5.2 eq), $Pd(dppf)_2Cl_2$ (218 mg, 0.30 mmol, 8 %), and KOAc (1.68 g, 17.1 mmol, 4.7 eq), were suspended in THF and heated overnight at 80 °C. The reaction mixture was cooled, diluted with water, filtered, and washed with hot acetonitrile to yield the product as a grey solid (2.02 g, 80% yield). Procedure was adapted from a reported procedure in the literature. [20]

^{1}H NMR (400 MHz, $CDCl_3$) δ 8.68 (d, *J* = 8.0 Hz, 6H), 7.94 (d, *J* = 7.8 Hz, 6H), 1.33 (s, 36H).

^{13}C NMR (101 MHz, $CDCl_3$) δ 171.94, 138.71, 135.15, 128.23, 84.23, 25.08.

Polymer Synthesis

TAA

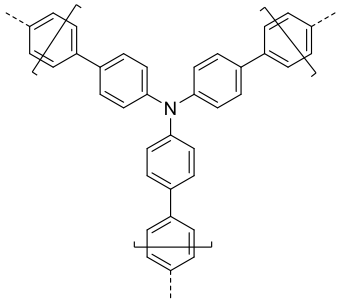

Tris(4-bromophenyl) amine (1.00 g, 2.07 mmol, 1 eq), benzene-1,4-diboronic acid (0.516 g, 3.11 mmol, 1.5 eq), $Pd(PPh_3)_4$ (32 mg, 0.028 mmol, 1.4%), and K_2CO_3 solution (2M, 7.5 ml, 15 mmol) are suspended in DMF (40 ml) and heated for 4 days at 80 °C under nitrogen. The reaction mixture is cooled, diluted with water, and filtered. The filtered material is washed with water, chloroform, methanol, acetone, and dried in a vacuum oven to yield the polymer as a pale green powder (754 mg)

poly-4CzIPN

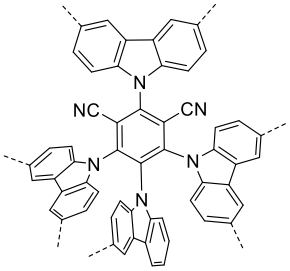

4CzIPN (0.100 g, 0.127 mmol, 1 eq) and $FeCl_3$ (164 mg, 1.0 mmol, 8 eq) are combined in DCM (30 ml) and stirred for 3 days at room temperature. Methanol (20 ml) is added, and the reaction mixture is stirred for 1 hour, followed by addition of excess conc. HCl and stirred for 2 hours. The reaction mixture is filtered and washed with water and THF followed by drying in a vacuum oven to yield the polymer as a yellow solid (76.9 mg). Procedure was adapted from literature.[49]

Cz

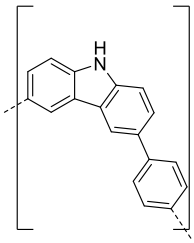

Dibromocarbazole (1.00 g, 3.08 mmol, 1 eq) benzene-1,4-diboronic acid (0.511 g, 3.08 mmol, 1 eq), $Pd(PPh_3)_4$ (46.5 mg, 0.040 mmol, 1.3 %) , and K_2CO_3 solution (2M, 9.2 mL) are suspended in DMF (46 ml) and heated to reflux for 3 days. The filtered material is washed with water, chloroform, methanol, acetone, and dried in a vacuum oven to yield the polymer as a grey powder. Procedure adapted from literature.[15]

EY TrE

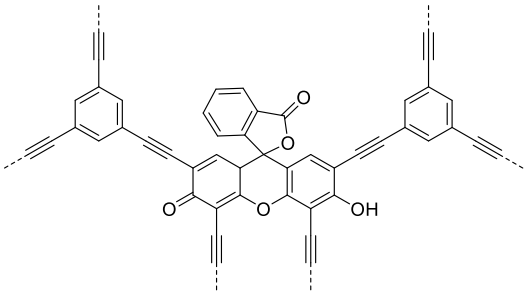

Eosin Y (1.00 g, 1.54 mmol, 1 eq), triethynyl benzene (0.308 g, 2.05 mmol, 1.33 eq), CuI (29 mg, 0.154 mmol, 0.1 eq), $Pd(PPh_3)Cl_2$ (43.4 mg, 0.0612 mmol, 4%), and Et_3N (15 mL) was suspended in DMF (15 mL) and heated to 80 °C under nitrogen for 3 days. The reaction mixture was cooled, diluted with water (100 mL), and filtered. The filtered material was washed with water (100 mL), chloroform (100 mL), methanol (100 mL), acetone (100 mL), and dried in a vacuum oven to yield EY-TrE polymer as a red powder (576 mg). This procedure was adapted from literature.[3]

POX Ph

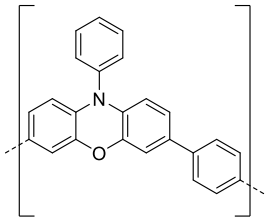

2,7 dibromo N-phenyl phenoxazine (0.300 g, 0.719 mmol, 1 eq), benzene-1,4-diboronic acid (0.119 g, 0.719 mmol, 1 eq), $Pd(PPh_3)_4$ (42 mg, 0.036 mmol, 5%), and aqueous 2M K_2CO_3 solution (2.5 mL) were suspended in DMF (15 mL) and heated for 3 days at 80 °C under nitrogen. The reaction mixture was cooled, diluted with water (100 mL), and filtered. The filtered material was washed with water (100 mL), chloroform (100 mL), methanol (100 mL), acetone (100 mL), and dried in a vacuum oven to yield the polymer as a green powder (144 mg).

CTF – 2 (ST)

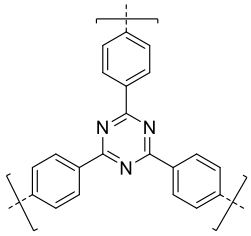

Trifluoromethanesulfonic acid (2.83 ml, 32 mmol, 8 eq) is diluted in chloroform (5 ml) under nitrogen. Biphenyl dicarbonitrile (0.814 g, 4 mmol, 1 eq) is dissolved in chloroform (40 ml) and added dropwise (2 mL/ min) and stirred for 3 days under nitrogen. The reaction mixture is neutralized with ammonia solution, stirred for 1 hour, and filtered. The filtered solid is washed with dichloromethane, water, acetone, and methanol and dried in a vacuum oven to yield CTF-2 as a pale-yellow powder (613 mg). Procedure followed as in literature. [26]

RB TrE

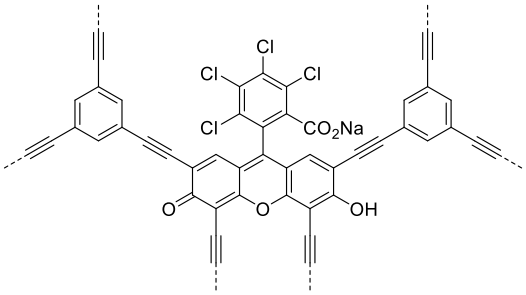

Rose Bengal (763 mg, 0.75 mmol, 0.75 eq), triethynyl benzene (0.150 mg 1.0 mmol, 1 eq), CuI (10 mg, 0.05 mmol, 5%), triethylamine (5 mL) and $Pd(PPh_3)_2Cl_2$ (15 mg, 0.021 mmol, 2%) were suspended in DMF (5 mL) and heated heated for 3 days at 80 °C under nitrogen. The reaction mixture was cooled, diluted with water (100 mL), and filtered. The filtered material was washed with water (100 mL), chloroform (100 mL), methanol (100 mL), acetone (100 mL), and dried in a vacuum oven to yield the polymer as a red powder (620 mg). This procedure was adapted from literature.[2]

POX SO_2

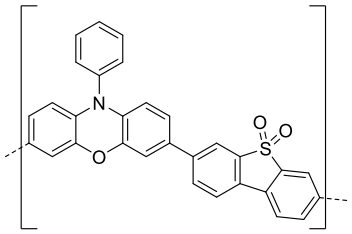

10-phenyl-3,7-bis(4,4,5,5-tetramethyl-1,3,2-dioxaborolan-2-yl)-10H-phenoxazine (0.275 g, 0.587 mmol, 1 eq) 3,7-dibromodibenzo[b,d]thiophene 5,5-dioxide (0.201 g, 0.587 mmol, 1 eq), $Pd(PPh_3)_4$, (34 mg, 0.0294 mmol, 5%) and aqueous 2M K_2CO_3 solution (2.1 mL) were suspended in DMF (12 mL) and heated to 80 °C for 3 days under nitrogen. The reaction mixture was cooled, diluted with water (100 mL), and filtered. The filtered material was washed with water (100 mL), chloroform (100 mL), methanol (100 mL), acetone (100 mL), and dried in a vacuum oven to yield the polymer as an orange powder (219 mg).

POX TrE

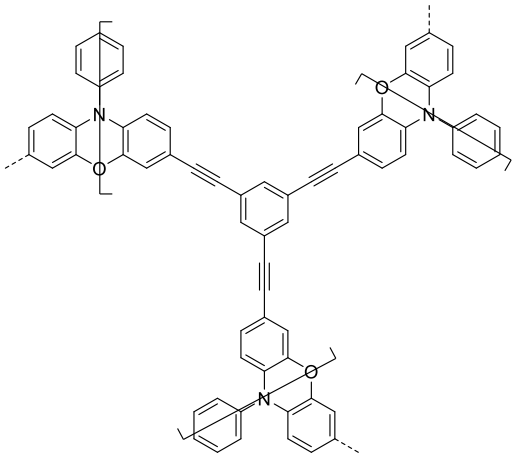

2,7 dibromo N-phenyl phenoxazine (100 mg, 0.240 mmol, 1 eq), triethynyl benzene (54 mg, 0.360 mmol, 1.5 eq), CuI (4.8 mg, 0.025 mmol, 10%), $Pd(PPh_3)_2Cl_2$ (7.2 mg, 0.0103 mmol, 4%), and triethylamine (4 ml) are suspended in DMF (4 ml) and heated to 80C for 3 days under nitrogen. The filtered material is washed with water, chloroform, methanol, acetone, and dried in a vacuum oven to yield the polymer is a brown solid (37.2 mg).

POX TAZ

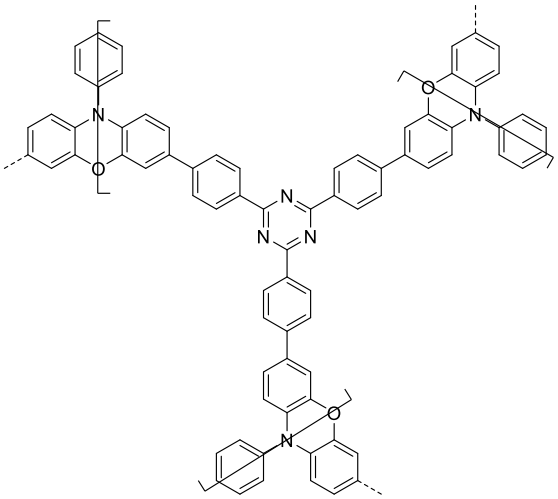

2,7 dibromo N-phenyl phenoxazine (100 mg, 0.240 mmol, 1 eq), 2,4,6-tris[4-(4,4,5,5-tetramethyl-1,3,2-dioxaborolan-2-yl)phenyl]-1,3,5-triazine (110 mg, 0.160 mmol, 0.66 eq), $Pd(PPh_3)_4$ (5 mg, 0.004 mmol, 1.7%) and K_2CO_3 solution (2M, 0.72 mL) are suspended in DMF (3 ml) and heated to 80 °C for 3 days under nitrogen.. The filtered material is washed with water, chloroform, methanol, acetone, and dried in a vacuum oven to yield the polymer as an orange solid (31.5 mg).

POX General Procedure A

10-phenyl-3,7-bis(4,4,5,5-tetramethyl-1,3,2-dioxaborolan-2-yl)-10H-phenoxazine (0.3 g, 0.587 mmol, 1 eq), bromide coupling partner, $Pd(PPh_3)_4$ (34 mg, 0.0294 mmol, 5%), and aqueous 2M K_2CO_3 solution (2.1 mL) were suspended in DMF (12 mL), degassed, and heated at 80 °C for 3 days under nitrogen followed by dilution with water (100 mL) and filtration. The filtered material was washed thoroughly with water (100 mL), chloroform (100 mL), methanol (100 mL), acetone (100 mL), and dried in a vacuum oven to yield the respective polymer.

POX BTZ

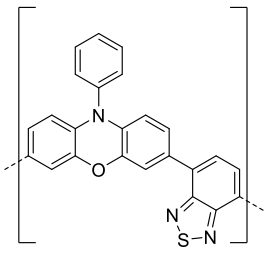

Synthesized using POX general procedure A using 4,7-dibromobenzo[c][1,2,5]thiadiazole (174 mg, 0.587 mmol, 1 eq) to yield the polymer as a dark purple powder (228 mg).

POX Bpy

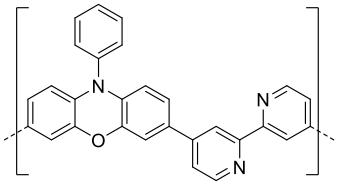

Synthesized using POX general procedure A using 4,4'-dibromo-2,2'-bipyridine (184 mg, 0.587 mmol, 1 eq) to yield the polymer as a brown powder (155 mg).

AQO General Procedure A

2,6-bis(4,4,5,5-tetramethyl-1,3,2-dioxaborolan-2-yl)anthracene-9,10-dione (0.300 g, 0.652 mmol, 1 eq), bromide coupling partner, $Pd(PPh_3)_4$ (38 mg, 0.0327 mmol, 5%), and aqueous 2M K_2CO_3 solution (2.5 mL) were suspended in DMF (12 mL), degassed, and heated at 80 °C for 3 days under nitrogen, followed by dilution with water and filtration. The filtered material is washed thoroughly with water (100 mL), chloroform (100 mL), methanol (100 mL), acetone (100 mL), and dried in a vacuum oven to yield the respective polymer.

AQO Bpy

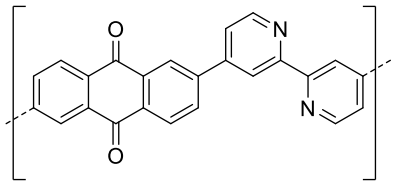

Synthesized using AQO general procedure A using 4,4 dibromo bipyridine (0.208 g, 0.652 mmol, 1 eq) to yield the polymer as a black powder (131 mg).

AQO SO_2

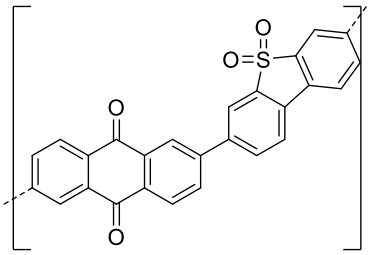

Synthesized using AQO general procedure A 3,7-dibromodibenzo[b,d]thiophene 5,5-dioxide (0.244 g, 0.652 mmol, 1 eq) to yield the polymer as a brown powder (281 mg).

AQO TAZ

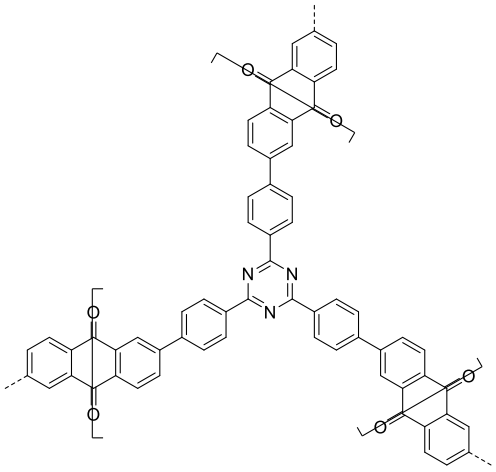

Synthesized using AQO general procedure A using tris(4-bromophenyl) triazine (0.237 g, 0.652 mmol, 1 eq) to yield the polymer as a brown powder (293 mg).

AQO Phen

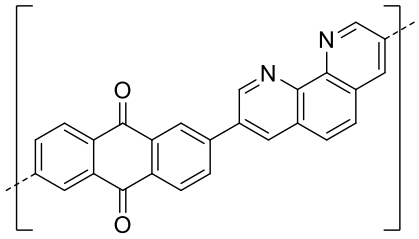

Synthesized using AQO general procedure A using 3,8-dibromo-1,10-phenanthroline (0.220 g, 0.652 mmol, 1 eq) to yield the polymer as a black powder (47.4 mg).

AQO Ph

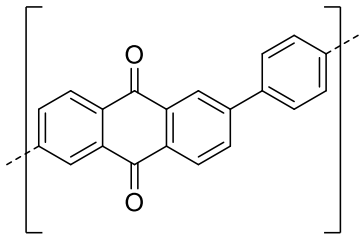

2,6 Dibromoanthraquinone (1.00 g, 2.73 mmol, 1 eq), benzene-1,4-diboronic acid (0.454 g, 2.74 mmol, 1 eq), $Pd(PPh_3)_4$ (158 mg, 0.137 mmol, 5%), and aqueous 2M K_2CO_3 solution (9 mL) were suspended in DMF (30 mL) and heated at 80 °C for 3 days under nitrogen. The filtered material was washed with water (100 mL), chloroform (100 mL), methanol (100 mL), acetone (100 mL), and dried in a vacuum oven to yield the polymer as a brown powder (799 mg).

AQO TrE

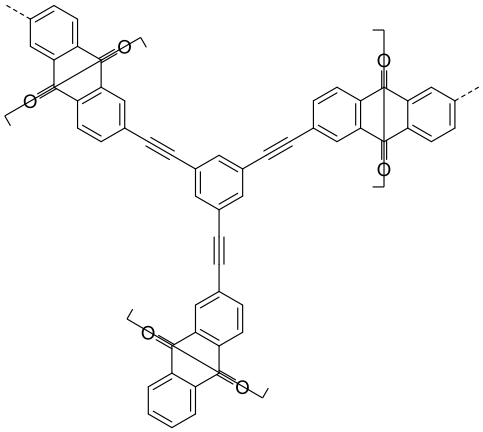

Dibromoanthraquinone (1.00 g, 2.73 mmol, 1 eq), triethynyl benzene (0.273 g, 1.82 mmol, 0.66 eq), CuI (53 mg, 0.28 mmol, 0.1 eq), $Pd(PPh_3)_2Cl_2$ (84 mg, 0.120 mmol, 4%), and Et_3N (15 mL) were suspended in DMF (15 mL) and heated at 80 °C for 3 days under nitrogen. The filtered material was washed with water (100 mL), chloroform (100 mL), methanol (100 mL), acetone (100 mL), and dried in a vacuum oven to yield the polymer as a brown powder (848 mg).

NMeA Ph

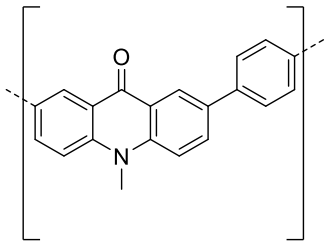

Dibromo N-Methyl acridone (0.50 g, 1.36 mmol, 1 eq), benzene-1,4-diboronic acid (0.226 g, 1.36 mmol, 1 eq), $Pd(PPh_3)_4$ (40 mg, 0.03 mmol, 2.6%), and aqueous 2M K_2CO_3 solution (4 mL) were suspended in DMF (20 mL) and heated at 80 °C for 3 days under nitrogen. The filtered material was washed with water (100 mL), chloroform (100 mL), methanol (100 mL), acetone (100 mL), and dried in a vacuum oven to yield the polymer as a dark green powder (169 mg).

NMeA TrE

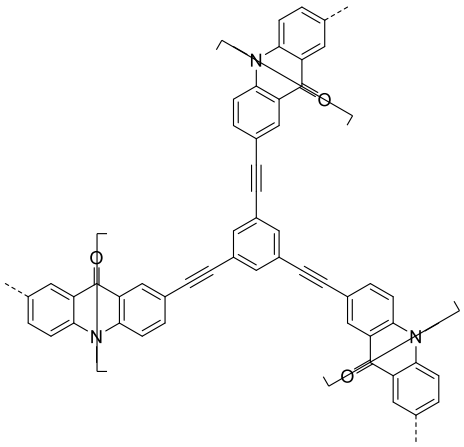

Dibromo N-Methyl acridone (0.3 g, 0.817 mmol), triethynyl benzene (82 mg, 0.545 mmol), $Pd(PPh_3)_4$ (25 mg, 0.022 mmol, 2.7%), CuI (18 mg, 0.12 mmol, 15%), DMF (7.5 mL), and triethylamine (7.5 mL) were combined and heated at 80 °C under nitrogen for 3 days. The reaction mixture was diluted with water, filtered, and washed with water (100 mL), chloroform (100 mL), methanol (100 mL), and acetone (100 mL) to yield a brown powder (262 mg).

TXO HCP

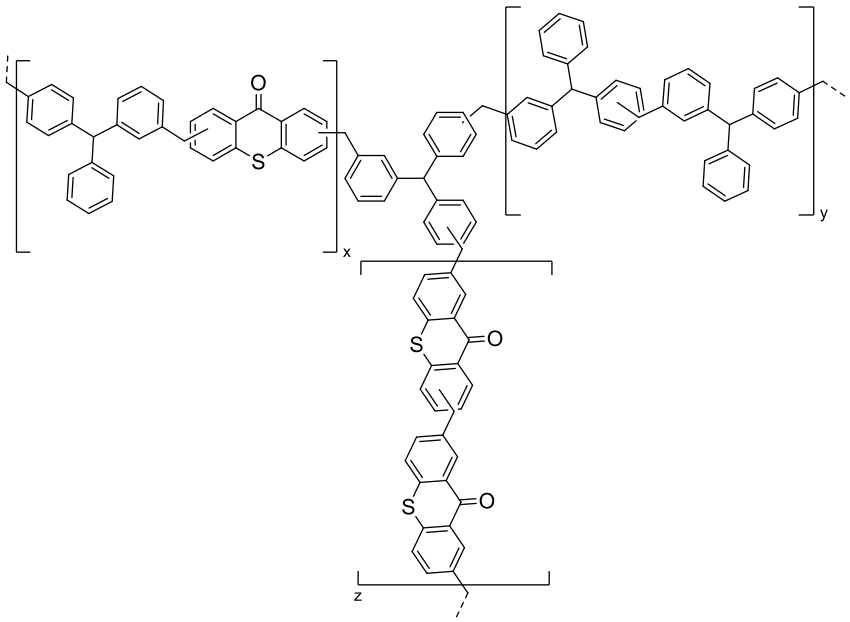

Thioxanthone (1 g, 4.72 mmol, 1 eq), triphenylmethane (1.22 g, 5.0 mmol, 1.1 eq), dimethoxymethane (2.66 g, 35 mmol, 7.4 eq), and $FeCl_3$ (5.67 g, 35 mmol, 4.7 eq) were suspended in dichloroethane (20 mL) and refluxed for 3 days. The reaction mixture was cooled, filtered washed with water (100 mL), methanol (100 mL), and further purified using Soxhlet extraction using methanol to yield the hyper crosslinked polymer as a black solid (1.93 g). This procedure was adapted from literature.[25]

XBCN General Procedure A

4-([1,1'-biphenyl]-4-yl)-2,6-bis(4-bromophenyl)pyridine-3,5-dicarbonitrile (0.3 g, 0.508 mmol 1 eq), coupling partner (1 eq), $Pd(PPh_3)_4$ (30 mg, 0.0254 mmol 5 mol%), K_2CO_3 (2.1 mL, 2M) are suspended in DMF (10 mL) and heated for 4 days under nitrogen at 80 °C. The filtered material was washed with water (100 mL), chloroform (100 mL), methanol (100 mL), acetone (100 mL), and dried in a vacuum oven to yield the respective polymer

XBCN117

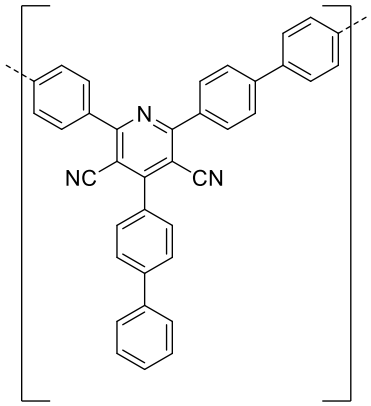

Performed using XBCN General Procedure A to yield the polymer as a green solid (220 mg).

XBCN118

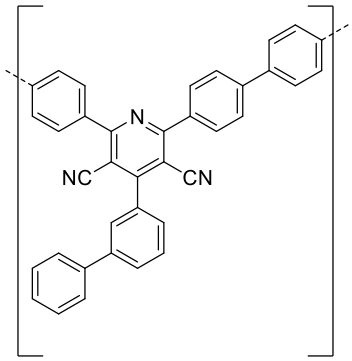

Performed using XBCN General Procedure A, but using 4-([1,1'-biphenyl]-3-yl)-2,6-bis(4-bromophenyl)pyridine-3,5-dicarbonitrile as the coupling partner to yield the polymer as a green solid (242 mg)

XBCN120

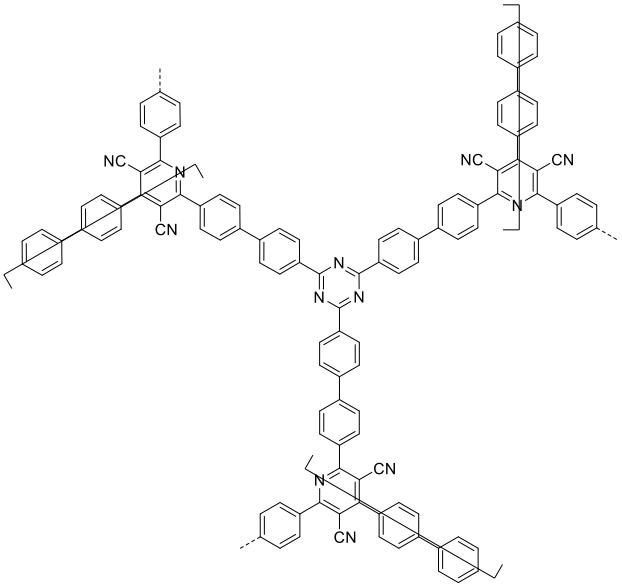

Performed using XBCN General Procedure A to yield the polymer as a grey solid (328 mg) with a minor modification – 0.66 eq of the boronate ester coupling partner was used instead.

General Photoredox Screening Procedure

Polymers (5 mg) were weighed into vials along with any inorganic bases or insoluble additives. Separately, a homogeneous stock solution of reagents and co-catalysts, if any, was prepared, sonicated, and degassed with nitrogen. Equal amounts of the stock solution were dispensed into the vials, which were crimped under nitrogen. The vials were irradiated for 3 days, then diluted with an ethyl acetate and filtered for GC-MS analysis. Reactions were run on 0.1 mmol scale, and at 0.2 M concentration except for some reactions, which were run at 0.1 M due to poor solubility of reagents.

References

1. Vijayakrishnan, S., Ward, J. W. & Cooper, A. I. Discovery of a Covalent Triazine Framework Photocatalyst for Visible-Light-Driven Chemical Synthesis using High-Throughput Screening. *ACS Catal.* **12**, 10057–10064 (2022).
2. Jiang, J. X. *et al.* Conjugated microporous polymers with rose bengal dye for highly efficient heterogeneous organo-photocatalysis. *Macromolecules* **46**, 8779–8783 (2013).
3. Wang, C.-A., Li, Y.-W., Cheng, X.-L., Zhang, J.-P. & Han, Y.-F. Eosin Y dye-based porous organic polymers for highly efficient heterogeneous photocatalytic dehydrogenative coupling reaction. *RSC Adv* **7**, 408–414 (2017).
4. Bai, Y. *et al.* Accelerated Discovery of Organic Polymer Photocatalysts for Hydrogen Evolution from Water through the Integration of Experiment and Theory. *J. Am. Chem. Soc.* **141**, 9063–9071 (2019).
5. Speckmeier, E., Fischer, T. G. & Zeitler, K. A Toolbox Approach To Construct Broadly Applicable Metal-Free Catalysts for Photoredox Chemistry: Deliberate Tuning of Redox Potentials and Importance of Halogens in Donor–Acceptor Cyanoarenes. *J. Am. Chem. Soc.* **140**, 15353–15365 (2018).
6. Srivastava, V. & Singh, P. P. Eosin y catalysed photoredox synthesis: A review. *RSC Adv.* **7**, 31377–31392 (2017).
7. Hari, D. P. & König, B. Synthetic applications of eosin Y in photoredox catalysis. *Chem Commun* **50**, 6688–6699 (2014).
8. Yan, D.-M., Chen, J.-R. & Xiao, W.-J. New Roles for Photoexcited Eosin Y in Photochemical Reactions. *Angew. Chem. Int. Ed.* **58**, 378–380 (2019).
9. Fan, X. Z. *et al.* Eosin Y as a Direct Hydrogen-Atom Transfer Photocatalyst for the Functionalization of C−H Bonds. *Angew. Chem. Int. Ed.* **57**, 8514–8518 (2018).
10. Koegl, M., Weiß, C. & Zigan, L. Fluorescence Spectroscopy for Studying Evaporating Droplets Using the Dye Eosin-Y. *Sensors* **20**, 20:5985 (2020).
11. Rauf, M. A., Graham, J. P., Bukallah, S. B. & Al-Saedi, M. A. S. Solvatochromic behavior on the absorption and fluorescence spectra of

Rose Bengal dye in various solvents. *Spectrochim. Acta. A. Mol. Biomol. Spectrosc.* **72**, 133–137 (2009).

12. Luo, J., Zhang, X., Lu, J. & Zhang, J. Fine Tuning the Redox Potentials of Carbazolic Porous Organic Frameworks for Visible-Light Photoredox Catalytic Degradation of Lignin β-O-4 Models. *ACS Catal.* **7**, 5062–5070 (2017).
13. McCarthy, B. G. *et al.* Structure-property relationships for tailoring phenoxazines as reducing photoredox catalysts. *J. Am. Chem. Soc.* **140**, 5088–5101 (2018).
14. Du, Y. *et al.* Strongly Reducing, Visible-Light Organic Photoredox Catalysts as Sustainable Alternatives to Precious Metals. *Chem. Eur. J.* **23**, 10962–10968 (2017).
15. Sprick, R. S. *et al.* Visible-Light-Driven Hydrogen Evolution Using Planarized Conjugated Polymer Photocatalysts. *Angew. Chem. Int. Ed.* **55**, 1792–1796 (2016).
16. Ye, H. *et al.* Bandgap engineering of novel peryleno[1,12- *bcd*]thiophene sulfone-based conjugated co-polymers for significantly enhanced hydrogen evolution without co-catalyst. *J. Mater. Chem. A* **8**, 20062–20071 (2020).
17. Sprick, R. S. *et al.* Photocatalytic Hydrogen Evolution from Water Using Fluorene and Dibenzothiophene Sulfone-Conjugated Microporous and Linear Polymers. *Chem. Mater.* **31**, 305–313 (2019).
18. Pearson, R. M., Lim, C.-H., McCarthy, B. G., Musgrave, C. B. & Miyake, G. M. Organocatalyzed Atom Transfer Radical Polymerization Using N -Aryl Phenoxazines as Photoredox Catalysts. *J. Am. Chem. Soc.* **138**, 11399–11407 (2016).
19. Kuhn, P., Antonietti, M. & Thomas, A. Porous, Covalent Triazine-Based Frameworks Prepared by Ionothermal Synthesis. *Angew. Chem. Int. Ed.* **47**, 3450–3453 (2008).
20. Bardagi, J. I., Ghosh, I., Schmalzbauer, M., Ghosh, T. & König, B. Anthraquinones as Photoredox Catalysts for the Reductive Activation of Aryl Halides. *Eur. J. Org. Chem.* **2018**, 34–40 (2018).
21. Capaldo, L. & Ravelli, D. Hydrogen Atom Transfer (HAT): A Versatile Strategy for Substrate Activation in Photocatalyzed Organic Synthesis. *Eur. J. Org. Chem.* **2017**, 2056–2071 (2017).

22. Chen, K. *et al.* N-substituted-3(10H)-acridones as visible-light photosensitizers for organic photoredox catalysis. *Tetrahedron* **74**, 483–489 (2018).
23. Dewanji, A., Krach, P. E. & Rueping, M. The Dual Role of Benzophenone in Visible-Light/Nickel Photoredox-Catalyzed C−H Arylations: Hydrogen-Atom Transfer and Energy Transfer. *Angew. Chem. Int. Ed.* **58**, 3566–3570 (2019).
24. Shen, Y., Gu, Y. & Martin, R. Sp3 C-H Arylation and Alkylation Enabled by the Synergy of Triplet Excited Ketones and Nickel Catalysts. *J. Am. Chem. Soc.* **140**, 12200–12209 (2018).
25. Dadashi-Silab, S., Bildirir, H., Dawson, R., Thomas, A. & Yagci, Y. Microporous Thioxanthone Polymers as Heterogeneous Photoinitiators for Visible Light Induced Free Radical and Cationic Polymerizations. *Macromolecules* **47**, 4607–4614 (2014).
26. Meier, C. B. *et al.* Structure-property relationships for covalent triazine-based frameworks: The effect of spacer length on photocatalytic hydrogen evolution from water. *Polymer* **126**, 283–290 (2017).
27. Vonlanthen, D. *et al.* Conformationally Controlled Electron Delocalization in n-Type Rods: Synthesis, Structure, and Optical, Electrochemical, and Spectroelectrochemical Properties of Dicyanocyclophanes. *Chem. Eur. J.* **17**, 7236–7250 (2011).
28. Nagib, D. A. & Macmillan, D. W. C. Trifluoromethylation of arenes and heteroarenes by means of photoredox catalysis. *Nature* **480**, 224–228 (2011).
29. Ghosh, I. *et al.* Organic semiconductor photocatalyst can bifunctionalize arenes and heteroarenes. *Science* **365**, 360–366 (2019).
30. Petronijević, F. R., Nappi, M. & MacMillan, D. W. C. Direct β-Functionalization of Cyclic Ketones with Aryl Ketones via the Merger of Photoredox and Organocatalysis. *J. Am. Chem. Soc.* **135**, 18323–18326 (2013).
31. Zuo, Z. *et al.* Merging photoredox with nickel catalysis: Coupling of α-carboxyl sp 3 -carbons with aryl halides. *Science* **345**, 437–440 (2014).

32. McNally, A., Prier, C. K. & MacMillan, D. W. C. Discovery of an -Amino C-H Arylation Reaction Using the Strategy of Accelerated Serendipity. *Science* **334**, 1114–1117 (2011).
33. Xu, C., Shen, F.-Q., Feng, G. & Jin, J. Visible-Light-Induced α-Amino C–H Bond Arylation Enabled by Electron Donor–Acceptor Complexes. *Org. Lett.* **23**, 3913–3918 (2021).
34. Chu, L., Ohta, C., Zuo, Z. & MacMillan, D. W. C. Carboxylic Acids as A Traceless Activation Group for Conjugate Additions: A Three-Step Synthesis of (±)-Pregabalin. *J. Am. Chem. Soc.* **136**, 10886–10889 (2014).
35. Trowbridge, A., Reich, D. & Gaunt, M. J. Multicomponent synthesis of tertiary alkylamines by photocatalytic olefin-hydroaminoalkylation. *Nature* **561**, 522–527 (2018).
36. Perry, I. B. *et al.* Direct arylation of strong aliphatic C–H bonds. *Nature* **560**, 70–75 (2018).
37. Romero, N. A., Margrey, K. A., Tay, N. E. & Nicewicz, D. A. Site-selective arene C-H amination via photoredox catalysis. *Science* **349**, 1326–1330 (2015).
38. Terrett, J. A., Clift, M. D. & MaCmillan, D. W. C. Direct β-alkylation of aldehydes via photoredox organocatalysis. *J. Am. Chem. Soc.* **136**, 6858–6861 (2014).
39. Loh, Y. Y. *et al.* Photoredox-catalyzed deuteration and tritiation of pharmaceutical compounds. *Science* **358**, 1182–1187 (2017).
40. Luo, J. & Zhang, J. Donor-Acceptor Fluorophores for Visible-Light-Promoted Organic Synthesis: Photoredox/Ni Dual Catalytic C(sp3)-C(sp2) Cross-Coupling. *ACS Catal.* **6**, 873–877 (2016).
41. Lima, F. *et al.* Organic photocatalysis for the radical couplings of boronic acid derivatives in batch and flow. *Chem. Commun.* **54**, 5606–5609 (2018).
42. Gilman, H. & Moore, L. O. The Preparation of Some 10-Substituted Phenoxazines 1. *J. Am. Chem. Soc.* **79**, 3485–3487 (1957).
43. Tian, Z. Y., Ming, X. X., Teng, H. B., Hu, Y. T. & Zhang, C. P. Transition-Metal-Free N-Arylation of Amines by Triarylsulfonium Triflates. *Chem. - Eur. J.* **24**, 13744–13748 (2018).

44. Zhu, Y., Kulkarni, A. P. & Jenekhe, S. A. Phenoxazine-based emissive donor-acceptor materials for efficient organic light-emitting diodes. *Chem. Mater.* **17**, 5225–5227 (2005).
45. Heil, H.; Burkhart, B.; Rodriguez, L.-I.; Meyer, S. Phenoxazine Derivatives For Organic Electroluminescent Devices, WO 2017/028941 A1, 2017
46. Liu, S. *et al.* Strategies to Enhance the Photosensitization: Polymerization and the Donor–Acceptor Even–Odd Effect. *Angew. Chem. Int. Ed.* **57**, 15189–15193 (2018).
47. Kuwabara, T., Orii, J., Segawa, Y. & Itami, K. Curved Oligophenylenes as Donors in Shape-Persistent Donor-Acceptor Macrocycles with Solvatofluorochromic Properties. *Angew. Chem. Int. Ed.* **54**, 9646–9649 (2015).
48. Wang, Z. *et al.* Dibenzothiophene Dioxide Based Conjugated Microporous Polymers for Visible-Light-Driven Hydrogen Production. *ACS Catal.* **8**, 8590–8596 (2018).
49. Luo, J., Zhang, X. & Zhang, J. Carbazolic porous organic framework as an efficient, metal-free visible-light photocatalyst for organic synthesis. *ACS Catal.* **5**, 2250–2254 (2015).

Chapter 3

Covalent Triazine Frameworks for Organic Photoredox Catalysis

Author Contributions

All the work described in this chapter has been performed by the thesis author except for the following: Dr. Xiaobo Li provided g-C_3N_4 and the initial batch of CTF-2(M). Ms. Xue Wang performed SEM imaging of CTF-2 and assisted in the microwave digestion of CTF-2 for ICP-OES analysis. Surface area analysis of CTF2 synthesized at 50 – 130 °C was performed by Dr. Alex James. Mr. Rob Clowes assisted with the setup of the Chemspeed programs, and Dr. Veronica Del Angel Hernandez assisted with the electrochemical characterization of CTF-2.

This chapter is based on the following publication:[1]

Discovery of a Covalent Triazine Framework Photocatalyst for Visible-Light-Driven Chemical Synthesis using High Throughput Screening. ACS Catalysis **2022**, 12, 10057−10064.

Sriram Vijayakrishnan, John W. Ward, Andrew I. Cooper.

Introduction

In **Chapter 2**, we used a high-throughput strategy to discover CTF-2 as a promising heterogeneous organic photoredox catalyst for decarboxylative conjugate addition of carboxylic acids. Previously, this reaction has been performed in visible light using the iridium catalyst $[Ir(dF(CF_3)ppy)_2(dtbbpy)][PF_6]$,[2] or using homogeneous organic dyes such as 4CzIPN[3] or acridiniums,[4] which are capable of driving alkyl radical formation through photocatalytic decarboxylation.

There are several distinct advantages for using carboxylic acids in organic synthesis that motivated us. Carboxylic acids are chemically stable, inexpensive, widely available from commercial sources, non-toxic, and are ubiquitous in nature – or can be synthesized from conversion of feedstock chemicals, making them promising candidates as sustainable carbon sources.

Compared to synthetic handles such as halides,[5] the by-product of the of the reaction, carbon dioxide, is benign. Direct activation of carboxylic acids[6,7] is also preferred to using redox active ester derivatives,[8,9] which requires stoichiometric amounts of activating agents or coupling reagents, resulting in low atom economy, or with costly agents such as HATU (1-[Bis(dimethylamino)methylene]-1H-1,2,3-triazolo[4,5-b]pyridinium 3-oxide hexafluorophosphate).[10]

Ultimately, efficient photodecarboxylative reactions could help deliver environmentally friendly synthetic routes. CO_2 reduction is an active area of research,[11,12] and it could be applied to producing carboxylic acid building blocks, either through direct carboxylation, or indirectly from carbon monoxide[13]. Biosynthesis and fermentation of building blocks such as amino acids are widely utilized in industry,[14,15] and these techniques could potentially be applied to produce these sustainable carbon sources.[16]

Results and Discussion

CTF-2 Synthesis and Characterization.

From our discovery workflow in **Chapter 2**, we found that CTF-2 could catalyse the decarboxylative conjugate addition of cyclohexanecarboxylic with diethyl ethylidenemalonate.

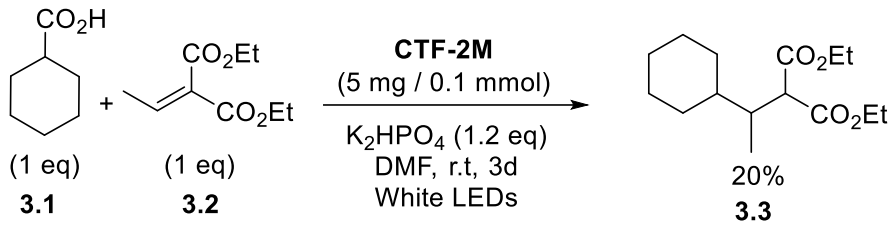

Scheme 3-1: Discovery hit for decarboxylative conjugate addition with CTF-2(M).

While the initial result was promising (Scheme **3-1**), the yield of the conjugate addition reaction was low, and we proceeded to optimize this result so that we could investigate the scope of this reaction. We first found that utilizing CTF-2 synthesized through microwave heating in triflic acid at 150 °C provided substantially higher yields (Figure **2-20**) than CTF-2 synthesized with solvothermal synthesis in chloroform at room temperature. As a result of these observations, we switched our general synthesis method for CTF-2 from to high-temperature microwave synthesis[17] (Scheme **3-2**).

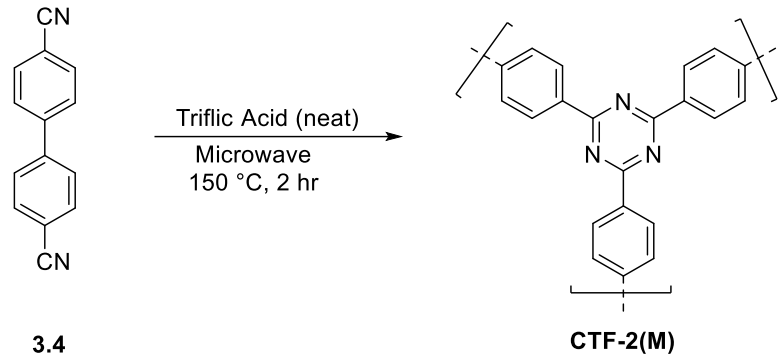

Scheme 3-2: Microwave synthesis of CTF-2.

We then proceeded to characterize CTF-2. The FT-IR spectrum of CTF-2 powder (Figure **3-1**) showed no nitrile bands at 2250 cm^{-1}, suggesting complete incorporation of the monomer into the extended framework. In addition, characteristic triazine bands[18] at around 1500 cm^{-1} and 1350 cm^{-1} were observed as expected. Due to the insolubility of CTF-2 in all compatible solvents, gel permeation chromatography (GPC) analysis was not possible to determine molar weight of the polymer or degree of polymerization. However, the recovered mass from the polymerization is near quantitative, suggesting virtually complete conversion of the monomer **3.4**.

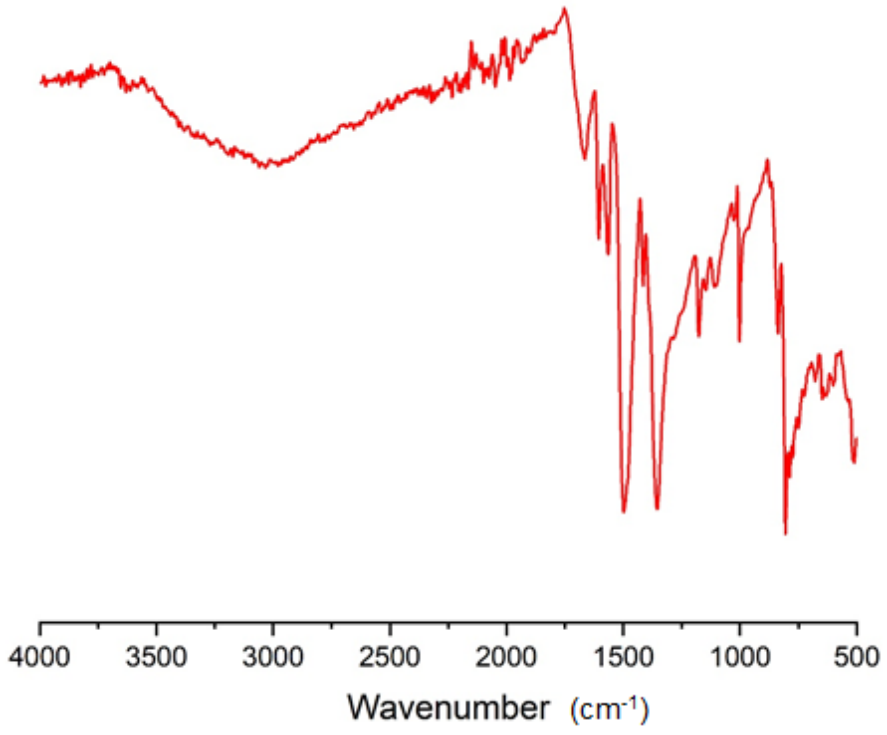

Figure 3-1: FT-IR spectrum of CTF-2 powder

The UV-visible absorption spectrum of CTF-2 (Figure **3-2**) revealed that it broadly absorbed visible light from 400 – 800 nm which is in contrast to monomer **3.4**[19] and is a consequence of the acid-catalysed trimerization forming the extended covalent framework and supports our observations that it is an active catalyst in visible light.

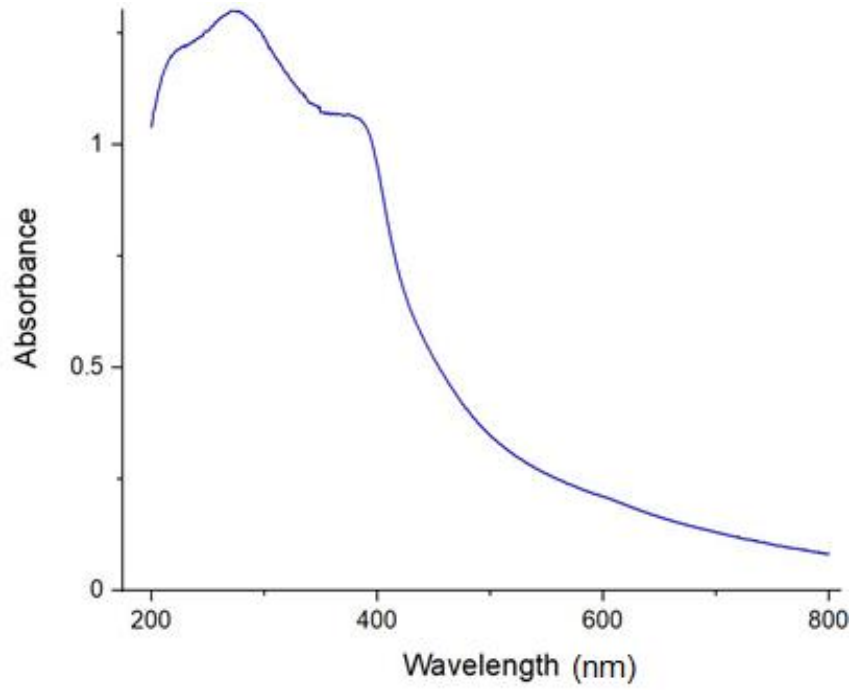

Figure 3-2: UV-visible absorption spectrum of CTF-2

From the UV-visible spectrum, a Tauc plot (Figure **3-3**) was constructed (assuming direct transition) to calculate estimate the optical band gap which was found 2.7 eV, which is similar to that of graphitic carbon nitride.[20] We also attempted to perform electrochemical characterization of CTF-2, to determine redox potentials, however we were significantly hindered by the dispersibility of CTF-2, which did generally not form stable suspensions, was insoluble common laboratory solvents, and had very low conductivity. While we were able to deposit CTF-2 on to carbon paper electrodes with the assistance of Nafion, the measured current following cyclic voltammetry (CV) measurements in acetonitrile were low and showed overlap with background current from the carbon paper in acetonitrile, and we were not able to obtain unambiguous, reproducible results. DFT calculations on CTF-2 have been previously reported and calculated by our group,[35] and give an indication of the redox window of CTF-2 in lieu of

experimental CV data - giving an ionization potential (IP) value of +1.69 V and an electron
affinity (EA) value of −1.68 V vs the standard hydrogen electrode (SHE) at pH 7. Conversion to the saturated calomel electrode (SCE) gives IP = +1.45 V and EA = −1.92 V. These potential values are in line with the required potentials to oxidize cyclohexanecarboxylic acid ($E_{1/2}$ = +1.16 V vs SCE)[2]

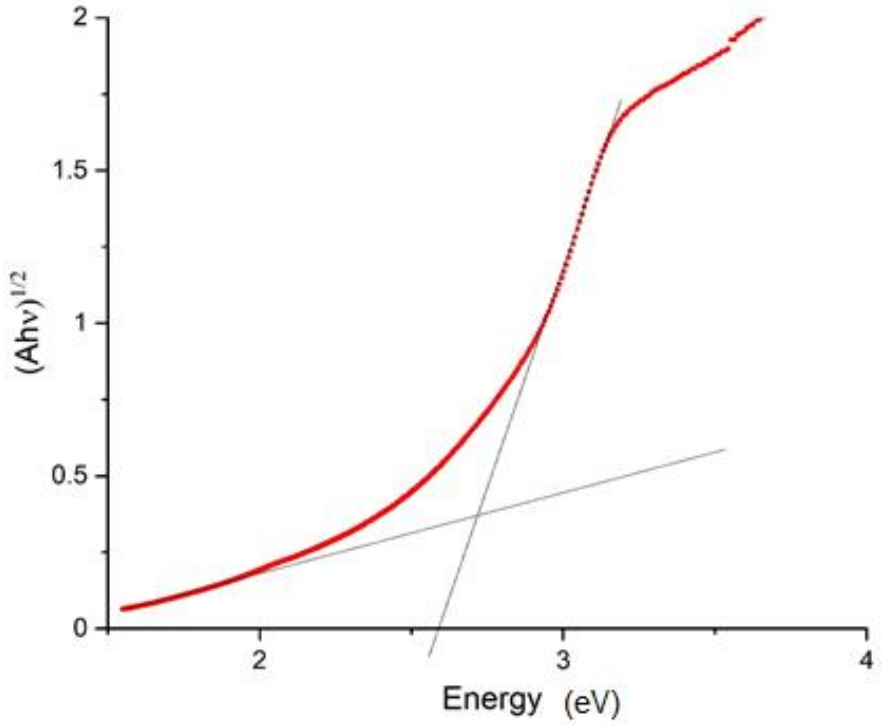

Figure 3-3: Tauc plot for CTF-2 assuming direct transition.

We then further examined the photophysical properties of CTF-2 using solid-state fluorescence spectroscopy to observe the excitation and emission spectra (Figure **3-4**), revealing an excitation maximum at 401 nm, and an emission maximum of 452 nm. While CTF-2 was photochemically active with broad spectrum white LED irradiation, we hypothesized that targeted irradiation near 400 nm could improve yields.

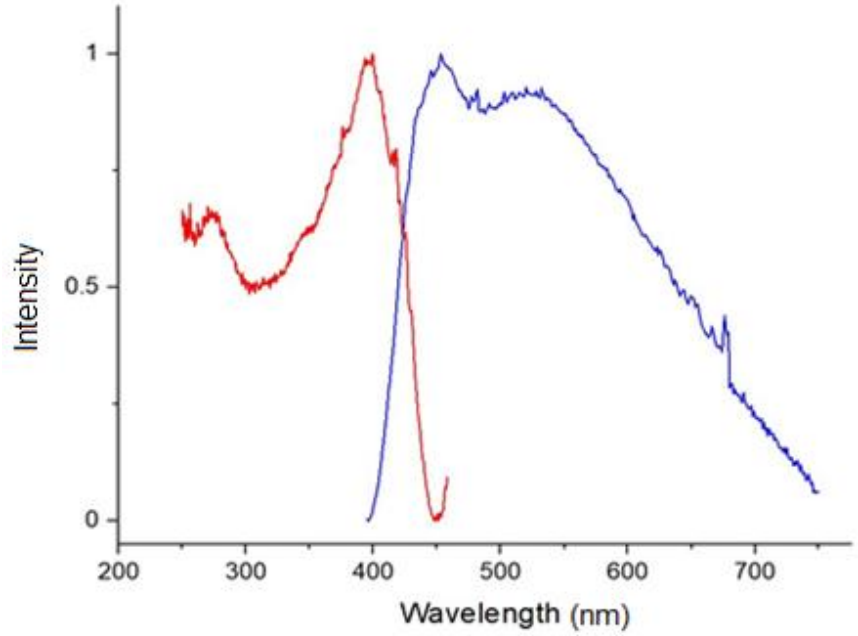

Figure 3-4: Excitation (red) and emission (blue) spectrum of CTF-2 powder.

From here, we investigated the fluorescence lifetime of CTF-2 using time correlated single photon counting (TCSPC) with 390 nm laser excitation. TCSPC experiments on CTF-2 in powder form revealed average weighted t_{avg} values of 1.65 ns and 0.65 ns for intensity and amplitude respectively after fitting was performed as a sum of 3 exponential terms (Figure **3-5** and **3-6**). These fluorescence lifetime values are generally in line with other covalent triazine frameworks synthesized by our group, which are typically < 10 ns. In comparison, homogeneous organic photocatalysts have also reported nanosecond fluorescence lifetimes. In contrast, however, transition metal photocatalysts are often reported to have excited state lifetimes of several microseconds.[21]

Parameter	**B_1**	**B_2**	**B_3**	**t_1**	**t_2**	**t_3**	**A**
Value	10659	1226	83	0.43	1.98	8.51	1.856
Error	99	55	8	0.00594	0.0639	0.385	
t_{avg} (Intensity): 1.65 ns (± 0.092) t_{avg} (amp): 0.65 ns (± 0.012) $\chi^2 = 1.22$							

Figure 3-5: Fitting parameters for TCSPC experiments as a sum of 3 exponential terms.

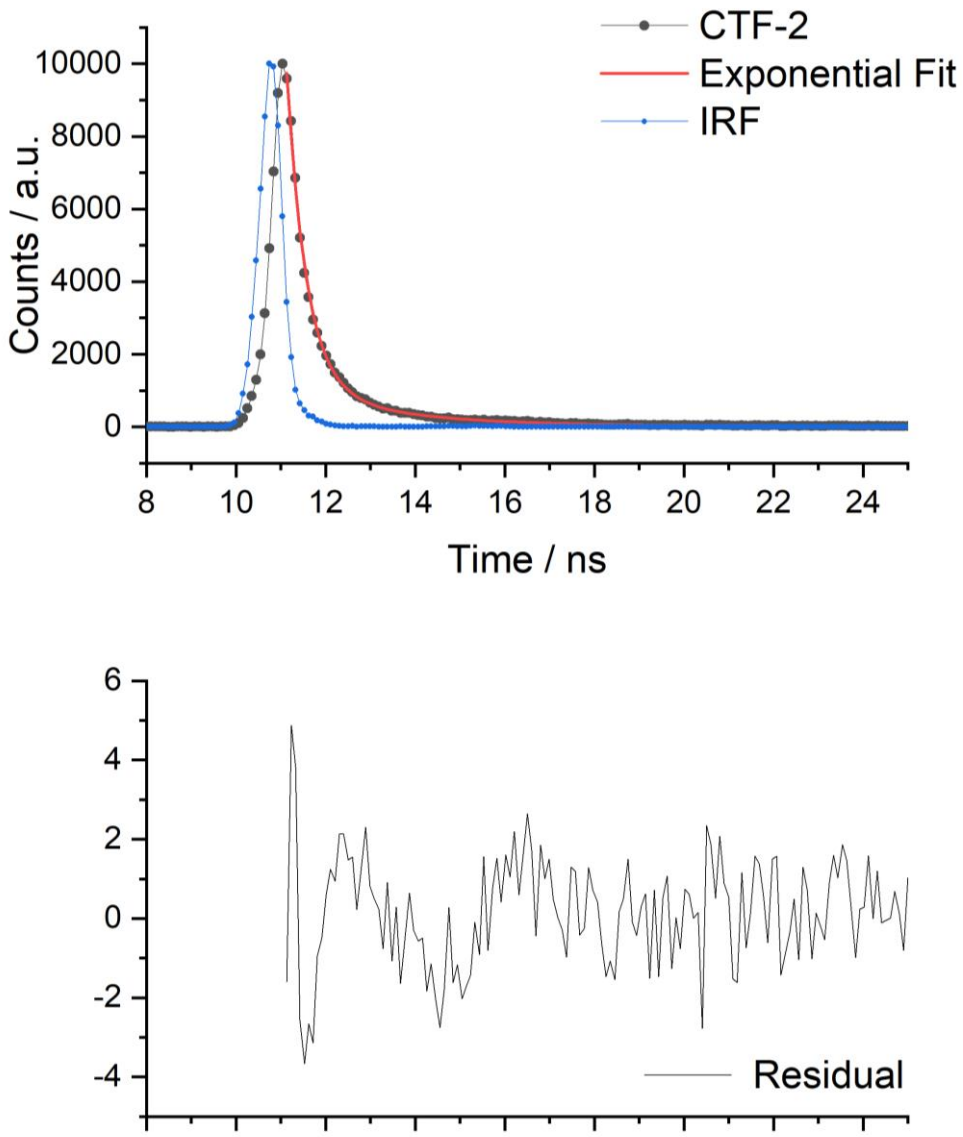

Figure 3-6: TCSPC lifetime analysis for CTF-2 powder (above) and residual for fitting (below)

From here, we then turned our attention to investigate the crystallinity and surface area of CTF-2. Powder X-ray diffraction measurements of the polymer (Figure **3-7**) revealed that microwave synthesized CTF-2 is an amorphous material, with no long-range order. Nitrogen sorption analysis of CTF-2 (Figure **3-8**) showed that it is an essentially non-porous material, with little to nitrogen uptake and a calculated BET surface area of 25 $m^2 g^{-1}$.

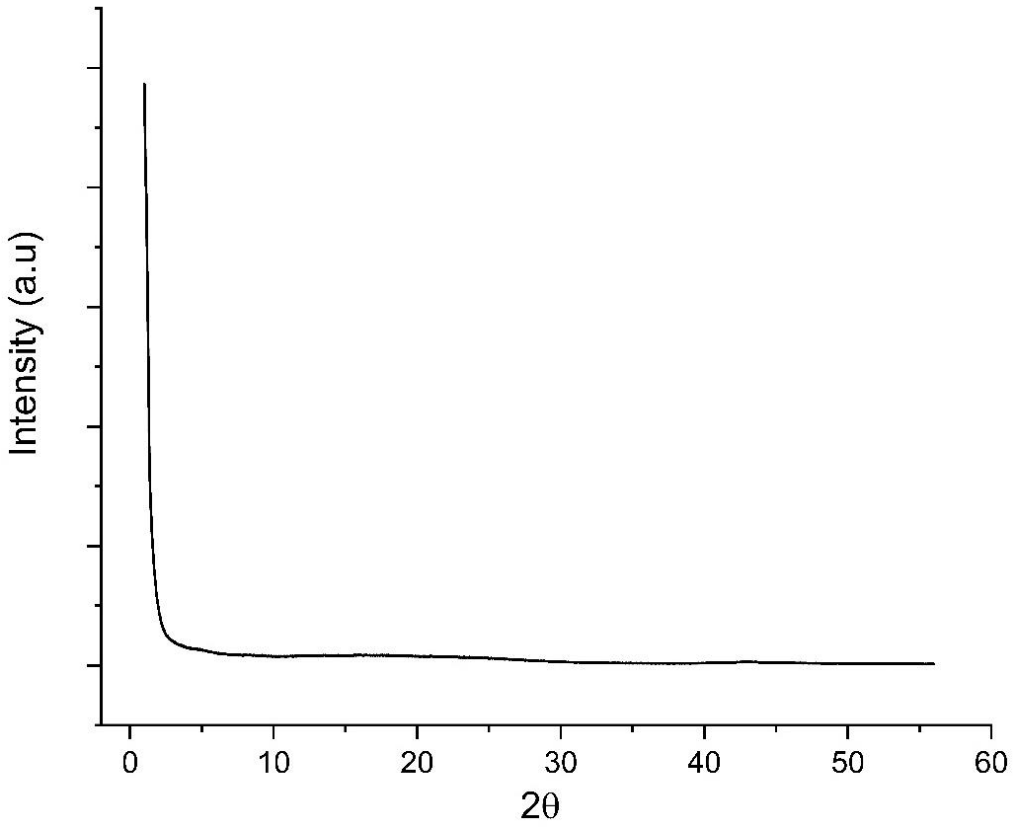

Figure 3-7: pXRD pattern for CTF-2 powder.

Both results are unexpected, since CTF-2 has been previously reported[22] to be a porous, with a surface area of 560 m^2 g^{-1}, and slightly crystalline material[17] when synthesized using triflic acid with microwave heating. We reattempted the microwave synthesis several times to obtain porous CTF-2, and rigorously purified the dicarbonitrile monomer prior to synthesis. Despite multiple attempts, we were unable to reproduce these previously reported results. However, it is evident that high surface area and crystallinity are not essential properties, although they might offer enhanced performance. In practical terms, however, this was beneficial for our high throughput workflow and made CTF-2 amenable for parallel optimization, since the polymerization was highly reproducible, and CTF-2 was able to be consistently synthesized in gram scale without concern for the crystallinity or surface area. In contrast, scaling materials such as COFs are challenging, and can be difficult to reproducibly synthesize these materials on gram scale, while retaining their crystallinity and high surface area.

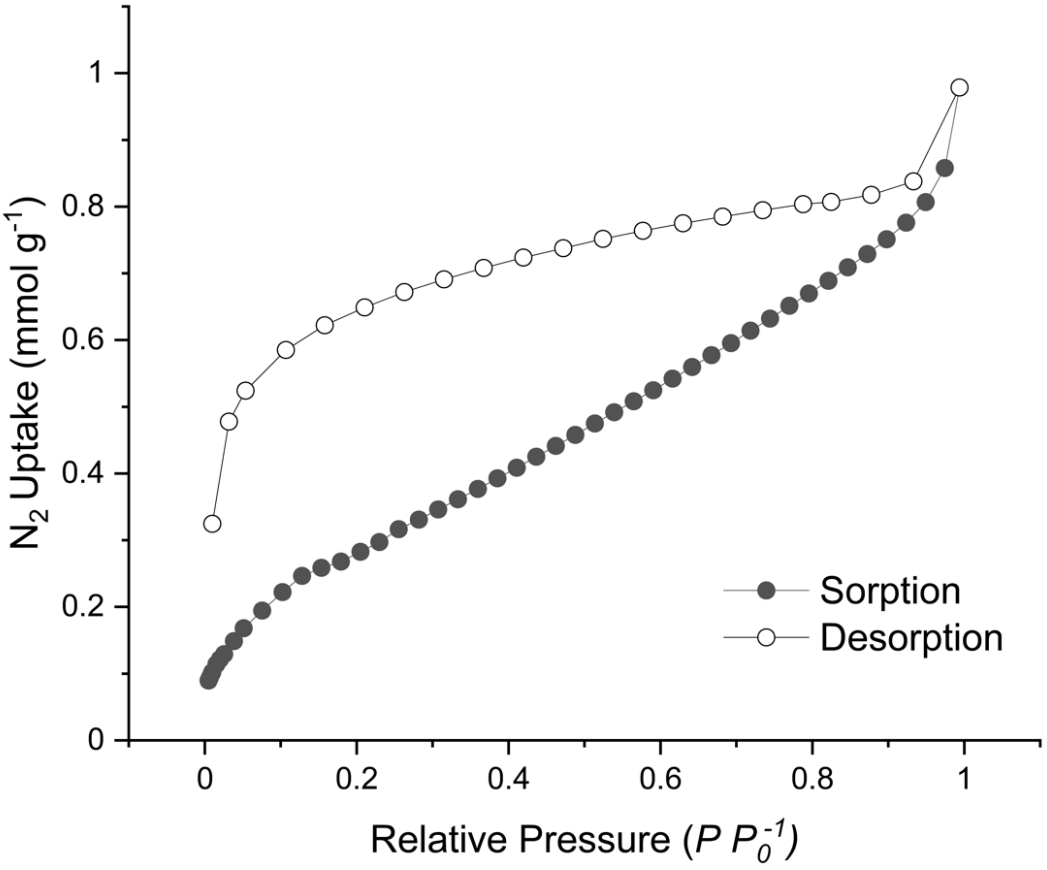

Figure 3-8: Sorption (filled circles) and desorption (unfilled circles) for CTF-2. BET surface area was calculated to be 25 m2g-1

We then examined the morphology and of CTF-2. SEM imaging of ball milled CTF-2 (Figure **3-9**) which largely showed irregular, non-uniform micrometre sized particles with no observable uniform or regular morphologies. There were however, several nanometre sized domains with roughly spherical particles, which is likely a result of the ball milling process, which has been reported to decrease particle size in CTFs.[22] Due to the very low dispersibility of CTF-2 before ball milling, we were unable to perform SEM imaging to compare morphologies before and after ball milling. Throughout our experiments, we found that the ball milling of CTF-2 had no observable impact on its performance in photocatalysis and was not required for catalysis. As a result, it is unlikely that the morphology of CTF-2 plays a major role in its role as a heterogeneous photoredox catalyst.

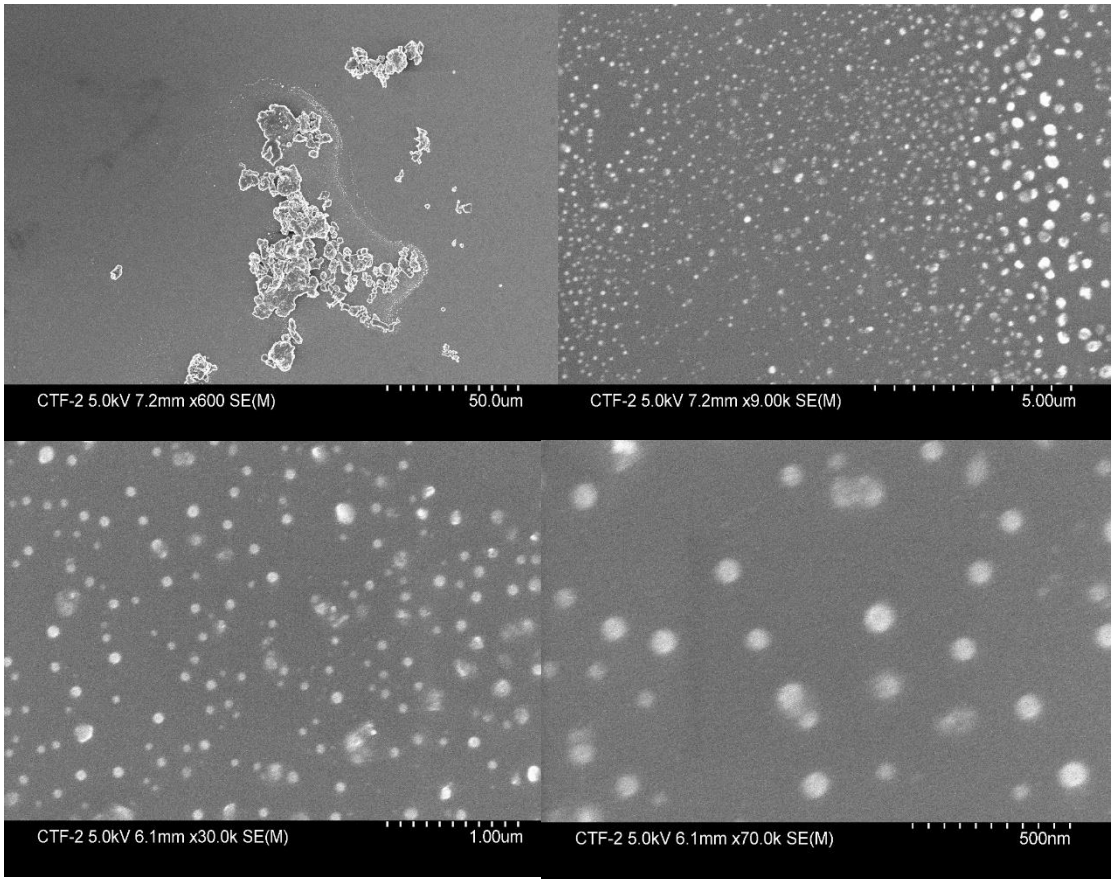

Figure 3-9: SEM images of ball-milled CTF-2. Clockwise from top left: 50 micrometre scale bar, 5 micrometre scale bar, 500 nm scale bar, and 1 micrometre scale bar.

Finally, we then examined the metal content of CTF-2 using Inductively Coupled Plasma Optical Emission spectroscopy (ICP-OES). While we intentionally avoided routes to CTF-2 involving metal catalysts such as palladium, we also wished to rule out any potential influence of trace metal content. ICP-OES analysis examining Co, Cu, Fe, Ir, Ni, Pd, Pt, and Ru content of CTF-2 following digestion in nitric acid revealed that the content of the tested metals were below detection limits or in very low (sub ppm) concentrations (Figure **3-10**). Copper and iron were present up to 0.07 mg L^{-1} in the CTF-2 sample, but these trace amounts are unlikely to be responsible for catalysis. In **Chapter 2**, we tested several polymers that had been synthesized using CuI, and $FeCl_3$ as catalysts (NMeA-TrE, and TXO-HCP respectively) which had poor performance in photocatalytic decarboxylative conjugate addition.

Date Time	Label	Element Label (nm)	Conc	%RSD	Unadjusted Conc
06/05/2022 15:20:31	CTF-2 Ram conc.	Co (228.615 nm)	0.00 (mg/L)	> 100.00	0.00 (mg/L)
06/05/2022 15:20:31	CTF-2 Ram conc.	Co (230.786 nm)	0.00 (mg/L)	77.17	0.00 (mg/L)
06/05/2022 15:20:31	CTF-2 Ram conc.	Co (231.160 nm)	0.00 (mg/L)	47.89	0.00 (mg/L)
06/05/2022 15:20:31	CTF-2 Ram conc.	Co (237.863 nm)	0.00 (mg/L)	31.28	0.00 (mg/L)
06/05/2022 15:20:31	CTF-2 Ram conc.	Cu (213.598 nm)	0.06 (mg/L)	1.24	0.06 (mg/L)
06/05/2022 15:20:31	CTF-2 Ram conc.	Cu (223.009 nm)	0.07 (mg/L)	1.71	0.07 (mg/L)
06/05/2022 15:20:31	CTF-2 Ram conc.	Cu (224.700 nm)	0.06 (mg/L)	1.43	0.06 (mg/L)
06/05/2022 15:20:31	CTF-2 Ram conc.	Cu (327.395 nm)	0.07 (mg/L)	1.10	0.07 (mg/L)
06/05/2022 15:20:31	CTF-2 Ram conc.	Fe (234.350 nm)	0.07 (mg/L)	0.68	0.07 (mg/L)
06/05/2022 15:20:31	CTF-2 Ram conc.	Fe (238.204 nm)	0.07 (mg/L)	0.34	0.07 (mg/L)
06/05/2022 15:20:31	CTF-2 Ram conc.	Fe (239.563 nm)	0.07 (mg/L)	0.99	0.07 (mg/L)

Date Time	Label	Element Label (nm)	Conc	%RSD	Unadjusted Conc
06/05/2022 15:20:31	CTF-2 Ram conc.	Fe (259.940 nm)	0.07 (mg/L)	0.50	0.07 (mg/L)
06/05/2022 15:20:31	CTF-2 Ram conc.	Ir (212.681 nm)	0.00 (mg/L)	95.30	0.00 (mg/L)
06/05/2022 15:20:31	CTF-2 Ram conc.	Ir (236.804 nm)	0.00 u (mg/L)	> 100.00	0.00 u (mg/L)
06/05/2022 15:20:31	CTF-2 Ram conc.	Ir (254.397 nm)	0.02 (mg/L)	25.88	0.02 (mg/L)
06/05/2022 15:20:31	CTF-2 Ram conc.	Ni (216.555 nm)	0.02 (mg/L)	2.18	0.02 (mg/L)
06/05/2022 15:20:31	CTF-2 Ram conc.	Ni (222.486 nm)	0.02 (mg/L)	8.06	0.02 (mg/L)
06/05/2022 15:20:31	CTF-2 Ram conc.	Ni (227.021 nm)	0.02 (mg/L)	0.20	0.02 (mg/L)
06/05/2022 15:20:31	CTF-2 Ram conc.	Ni (230.299 nm)	0.02 (mg/L)	0.42	0.02 (mg/L)
06/05/2022 15:20:31	CTF-2 Ram conc.	Pd (229.651 nm)	0.01 (mg/L)	11.10	0.01 (mg/L)
06/05/2022 15:20:31	CTF-2 Ram conc.	Pd (248.892 nm)	0.00 (mg/L)	52.15	0.00 (mg/L)
06/05/2022 15:20:31	CTF-2 Ram conc.	Pd (340.458 nm)	0.00 (mg/L)	65.31	0.00 (mg/L)
06/05/2022 15:20:31	CTF-2 Ram conc.	Pd (351.694 nm)	0.00 (mg/L)	41.95	0.00 (mg/L)
06/05/2022 15:20:31	CTF-2 Ram conc.	Pt (217.468 nm)	0.01 (mg/L)	11.91	0.01 (mg/L)
06/05/2022 15:20:31	CTF-2 Ram conc.	Pt (273.396 nm)	0.00 u (mg/L)	> 100.00	0.00 u (mg/L)
06/05/2022 15:20:31	CTF-2 Ram conc.	Pt (299.796 nm)	0.00 u (mg/L)	48.21	0.00 u (mg/L)
06/05/2022 15:20:31	CTF-2 Ram conc.	Ru (240.272 nm)	0.00 u (mg/L)	> 100.00	0.00 u (mg/L)
06/05/2022 15:20:31	CTF-2 Ram conc.	Ru (267.876 nm)	0.00 (mg/L)	5.79	0.00 (mg/L)
06/05/2022 15:20:31	CTF-2 Ram conc.	Ru (269.213 nm)	0.00 (mg/L)	57.73	0.00 (mg/L)
06/05/2022 15:20:31	CTF-2 Ram conc.	Ru (349.894 nm)	0.00 u (mg/L)	41.99	0.00 u (mg/L)

Figure 3-10: ICP-OES analysis results of CTF-2.

High-Throughput Optimization

Our attention then turned to optimizing the solvents and base for the decarboxylative conjugate addition of cyclohexanecarboxylic acid with diethyl ethylidenemalonate, seeking to improve the yields from our discovery workflow. Using our ChemSpeed platform, we screened a variety of solvents and bases in parallel, using GC-MS to evaluate performance of the reaction, as in our discovery workflow. Stock solutions of the substrates in each solvent were dispensed under nitrogen to vials charged with polymer and the respective base.

<table>
<tr><th></th><th>EtOAc</th><th>MeCN</th><th>MeOH</th><th>DMSO</th></tr>
<tr><td>(None)</td><td>trace</td><td>4</td><td rowspan="10">0 - trace</td><td>2</td></tr>
<tr><td>K_2HPO_4</td><td>27</td><td>28</td><td>15</td></tr>
<tr><td>NaOH</td><td>7</td><td>6</td><td>8</td></tr>
<tr><td>Cs_2CO_3</td><td rowspan="9">0 - trace</td><td>4</td><td>trace</td></tr>
<tr><td>DABCO</td><td>trace</td><td>0</td></tr>
<tr><td>DBU</td><td>trace</td><td>0</td></tr>
<tr><td>Lutidine</td><td>5</td><td>2</td></tr>
<tr><td>TEOA</td><td>trace</td><td>0</td></tr>
<tr><td>TMG</td><td>7</td><td>trace</td></tr>
<tr><td>BTTP</td><td>0</td><td>0</td></tr>
</table>

Figure 3-11: Optimization for decarboxylative conjugate addition with CTF-2 under white LED irradiation. GC-MS yields vs biphenyl standard.

Our screening results (Figure **3-11**) showed that a combination of MeCN, and K_2HPO_4 yielded slightly superior results to our initial conditions, while most other conditions inhibited the reaction. This was an improvement, but still far below the performance of the iridium photocatalyst. We then turned our attention to the light source. While CTF-2 absorbs well in the visible light region, we hypothesized that focused irradiation near the excitation maximum might improve yields and switched our light source to Blue LEDs using a commercial SynLED parallel photoreactor. We also switched the carboxylic acid substrate used in our screening to tetrahydrofuran-2-carboxylic acid (Scheme **3-3**), reasoning that the adjacent heteroatom might enable better radical stabilization, and consequently, result in higher yields of the conjugate addition product

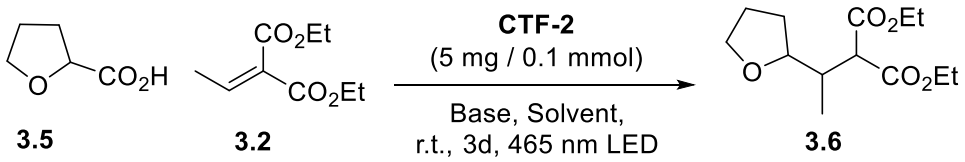

3.5 **3.2** **3.6**

Scheme 3-3: Base and solvent screening for decarboxylative conjugate addition of tetrahydofuran-2-carboxylic acid.

	EtOAc	MeOH	DMSO	MeCN
(None)	7	22	59	38
K_2HPO_4	28	0 – trace	69	81
Cs_2CO_3	9		trace	trace
DABCO	8		trace	4
DBU	13		trace	trace
K_3PO_4	0		0	trace
TEOA	35		trace	trace
TMG	9		23	8
BTTP	trace		0	trace
Ir[(dFCF$_3$ppy)$_2$(dtbbpy)][PF$_6$] (2 mol%) [(a)]	92			
Blank Experiment (no catalyst) [(a)]	0			
***tris*-biphenyl triazine [(a)]**	0			
Carbon Nitride (g-C_3N_4) [(a)]	13			

Figure 3-12: High-throughput optimization of decarboxylative conjugate addition of tetrahydrofuran-2-carboxylic acid. (a) – Performed in MeCN with K_2HPO_4 base.

Decarboxylative Conjugate Addition

We were delighted to observe that under blue LED irradiation, and using tetrahydrofuran-2-carboxylic acid, CTF-2 afforded the conjugate addition product at 81% GC-MS yield (Figure **3-12**). In comparison, under identical conditions, Ir[(dFCF$_3$ppy)$_2$(dtbbpy)][PF$_6$] (2 mol %) yielded in the conjugate addition product in 92% GC-MS yield. We performed a blank experiment to ensure that CTF-2 was required for catalysis, and similarly tested *tris*-biphenyl triazine. Under identical conditions, g-C$_3$N$_4$ yielded only 13% of the decarboxylative addition product.

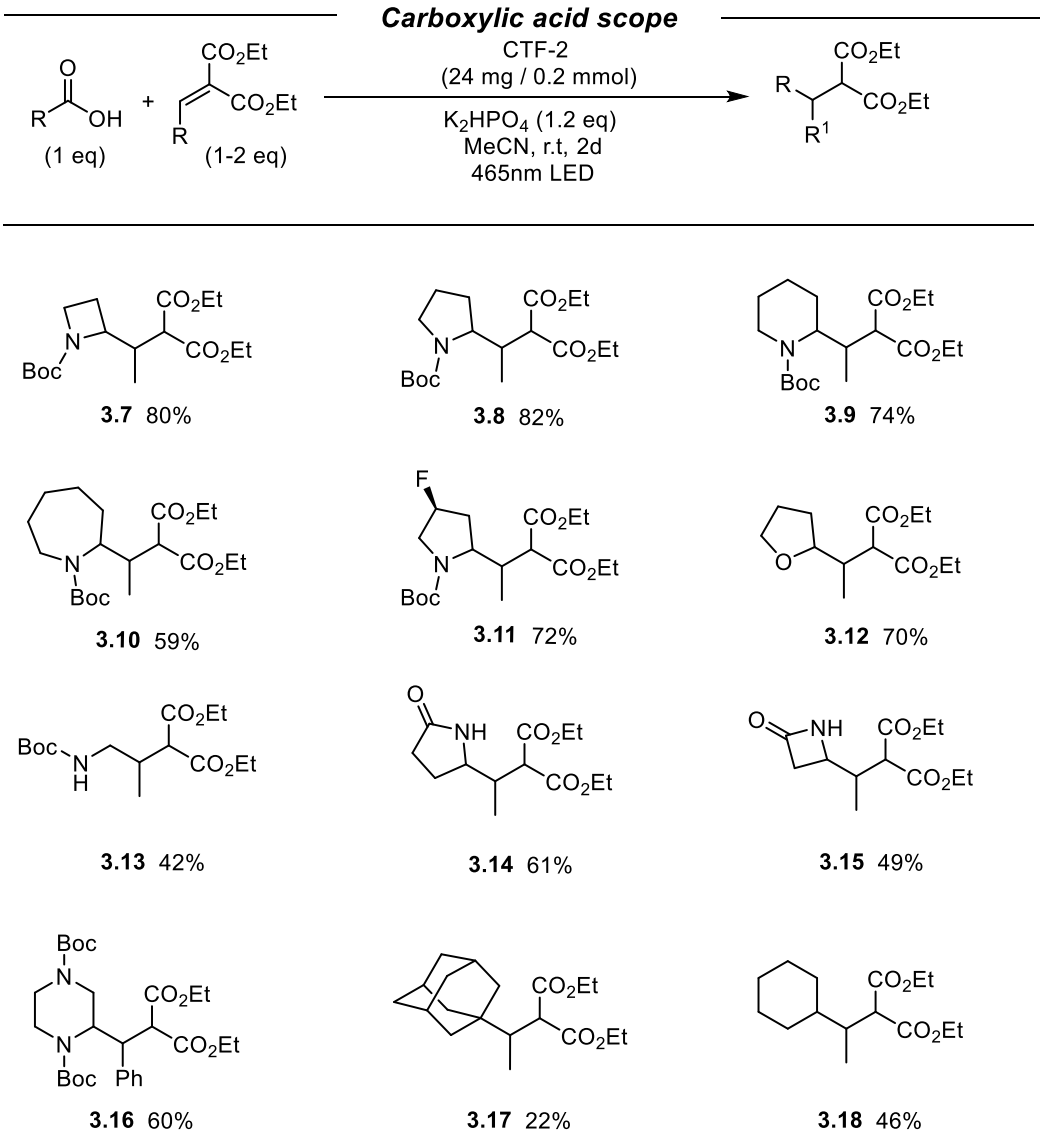

Scheme 3-4: Carboxylic acid scope of CTF-2 catalysed decarboxylative conjugate addition.

With our improved conditions, we probed the carboxylic acid scope for this reaction using CTF-2. 4, 5, 6, and 7-member heterocyclic carboxylic acids were smoothly functionalized (Scheme **3-4**). We were also pleased to see that unprotected lactams underwent conjugate addition, providing modular construction of these pharmaceutically relevant structures, along with protected piperazine. While cyclic carboxylic acids with an adjacent heteroatom were the most successful, substrates such as cyclohexane carboxylic acid also underwent conversion, although in modest yields.

We also attempted to demonstrate the functionalization of some pharmaceutically relevant molecules using CTF-2 as a photocatalyst (Figure **3-13**), however these were unsuccessful, providing starting material (**3.19**), hydrodecarboxylation (**3.20**), or decomposition (**3.21**) in each case. Efforts to use acetic acid (**3.22**) as a methyl radical source, similar to the work reported by Nocera using TiO_2,[23] were also unsuccessful, resulting in no methylation of the Michael acceptor. Substrates **3.19** and **3.22** may have been hindered by slow radical decarboxylation, while sulbactam (**3.21**) might have possibly undergone ring-opening side-reactions following radical decarboxylation.

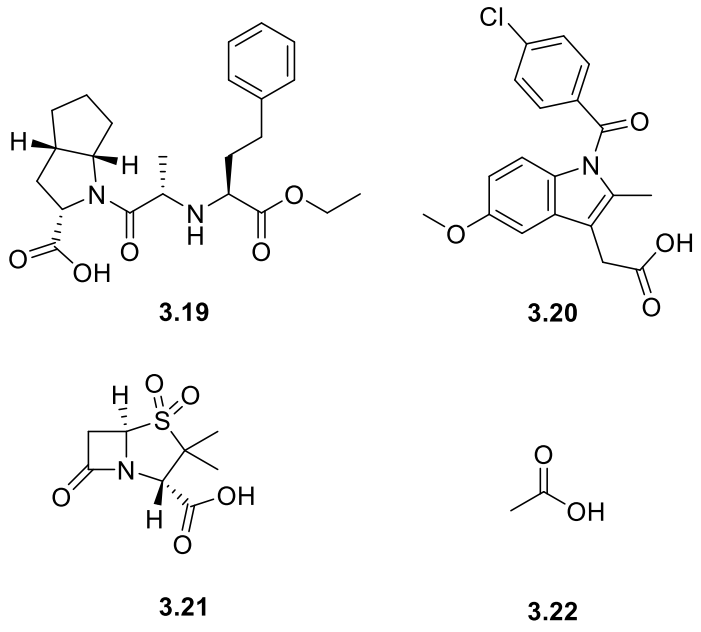

Figure 3-13: Unsuccessful carboxylic acid substrates for decarboxylative conjugate addition.

Showing the utility of CTF-2 in the functionalization of various carboxylic acids, we then explored the Michael acceptor scope for this reaction (Scheme **3-5**). A variety of Michael acceptors proved suitable for this reaction, including diethyl benzylidenemalonate, which was compatible 4,5, and 6-member heterocyclic carboxylic acids along with unprotected L-pyroglutamic acid. We also successfully used acyclic Boc-Gly-OH to synthesize **3.28**, which is a precursor to the pharmaceutical phenibut.

Michael acceptor scope

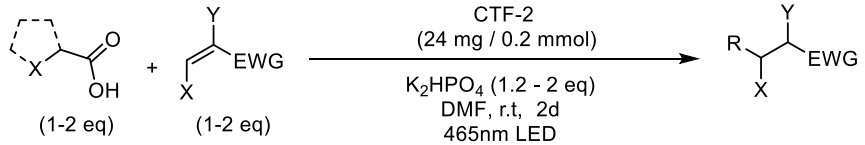

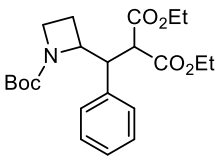

3.23 62%

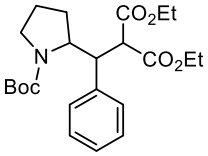

3.24 84%

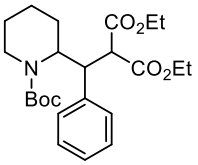

3.25 73%

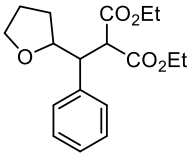

3.26 59%

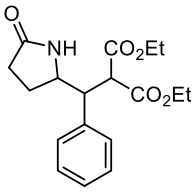

3.27 52%

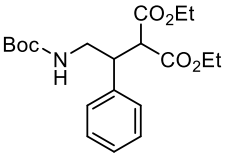

3.28 37%

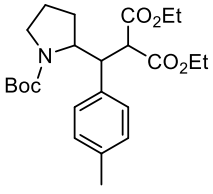

3.29 72%

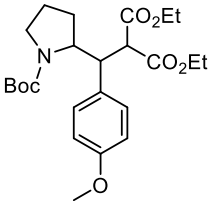

3.30 65%

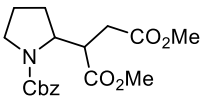

3.31 58%

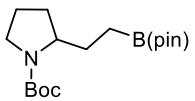

3.32 58%

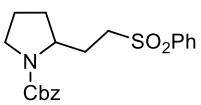

3.33 26%

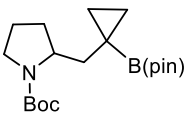

3.34 43%

Scheme 3-5: Michael acceptor scope for decarboxylative conjugate addition.

Dimethyl maleate, vinylboronic acid pinacol ester, and phenyl vinyl sulphone were also successful, yielding the conjugate addition products in modest to good yields. Given that we were successful in producing boronate ester **3.32**, we wondered if CTF-2 could catalyse cascade reactions, and we applied it for the synthesis of cyclopropanes reported by Aggarwal.[24] Applying CTF-2, we successfully produced the strained product (**3.34**) in 43% yield.

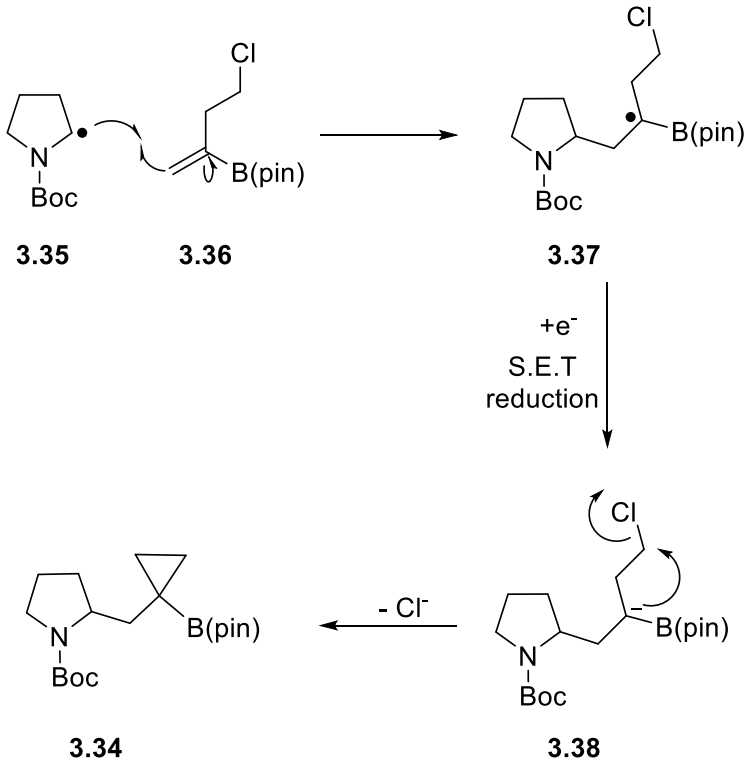

Scheme 3-6: Mechanism of radical cyclization cascade for synthesis of product 3.34.

In the proposed mechanism (Scheme **3-6**) reported by Aggarwal and co-workers, this cascade reaction is initiated by photodecarboxylative formation of radical **3.35**, which then undergoes addition Michael acceptor **3.36** to form intermediate **3.37**. From here, single electron transfer (S.E.T) reduction of intermediate **3.37** forms anion **3.38**, which rapidly undergoes *3-exo-tet* cyclization to form the cyclopropane product **3.34**. In our system, with CTF-2 as a heterogeneous photocatalyst, we believe that CTF-2 generates alkyl radical **3.35** through oxidative decarboxylation, and then reduces intermediate **3.37** through sequential S.E.T events.

We also attempted conjugate addition on a variety of other Michael acceptors (Figure **3-14**), however, these were unsuccessful, providing complex mixtures (**3.39** and **3.40**) of products or starting material (**3.41** and **3.42**) instead of the desired conjugate addition product. It is possible that unproductive polymerization side reactions may be taking place in the case of **3.39** and **3.40.** Michael acceptors **3.41** and **3.42** are known to be suitable coupling partners for decarboxylative conjugate addition, as reported by MacMillan[2], when using the iridium catalyst $Ir[(dFCF_3ppy)_2(dtbbpy)][PF_6]$. It is plausible that CTF-2 is unable to efficiently reduce radical intermediates such as **3.37** unless it is sufficiently stabilized as in the case of diethyl ethylidenemalonate (**3.2**).

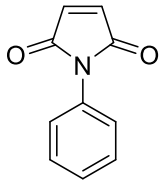

3.39

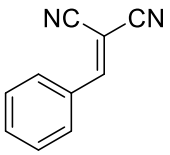

3.40

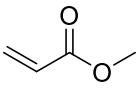

3.41

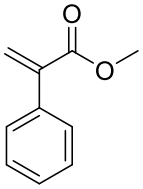

3.42

Figure 3-14: Unsuccessful Michael acceptor coupling partners.

In several cases, the diastereomeric ratios of the conjugate addition products were unable to be unambiguously determined due to the presence of rotamers and complex, overlapping peaks. However, the diastereomeric ratio of some products were identified by NMR: **3.7** (1:1), **3.12** (1:1.3), **3.14** (1:1), **3.15** (1:1) and **3.26** (1:1.1). These values are consistent with the diastereomeric ratios reported[2] by MacMillan and co-workers using a homogeneous iridium catalyst, who reported a range of 1:1 – 1:1.5, showing no significant influence from the use of CTF-2 in place a homogeneous catalyst. In the future, it could be worth exploring if the use of chiral, porous photocatalysts could enhance the diasteroselectivity of the conjugate addition product formation.

Unfortunately, the isolated yields of conjugate addition products synthesized with CTF-2 were consistently lower than those reported by MacMillan in co-workers. Cyclic, secondary, carboxylic acids with an adjacent heteroatom, such as **3.8** and **3.12** were competitive with good yields of 84% and 70% (compared to 97% and 92% with an iridium catalyst). However, tertiary carboxylic acids without an adjacent heteroatom (**3.17**) and primary carboxylic acids (**3.13**) had far lower yields with CTF-2 compared with reported values: 22% vs 93% and 42% vs 94% yield for products **3.17** and **3.13** respectively. This suggests that the radical stability seems to greatly impact the yield. Notably, we observed that several carboxylic acid substrates that resulted in low yields often had turbid reaction mixtures during irradiation, which likely had a detrimental effect on the irradiation of the photocatalyst, resulting in lower yields.

CTF-2 Reaction Scope

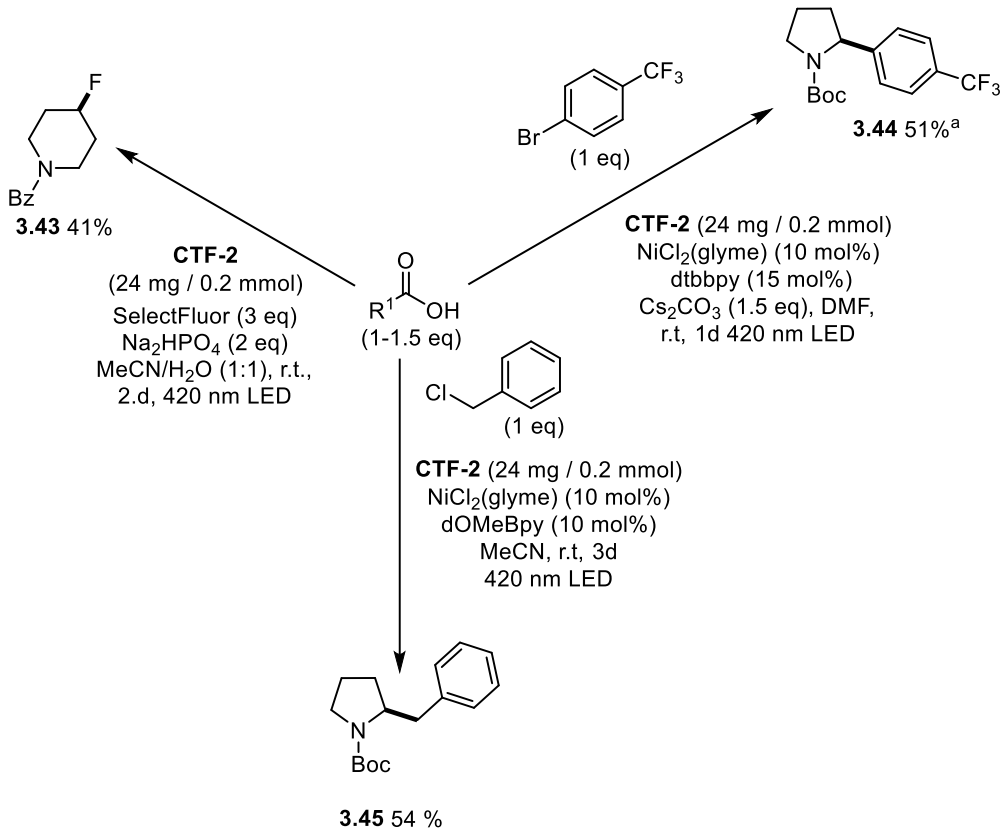

Scheme 3-7: Decarboxylative reaction scope of CTF-2.

Having successfully explored the scope of CTF-2 on a variety of conjugate addition reactions, we then explored the scope of reactions that could be performed with CTF-2 (Scheme **3-7**). Decarboxylative radical formation has been leveraged for a variety of reactions and we hypothesized that, similar to the iridium catalysts, we could substitute CTF-2 for a range of reactions. Using the reported literature conditions but substituting CTF-2 in place of the iridium catalyst, a variety of decarboxylative reactions were performed. CTF-2 provided the decarboxylative fluorination product **3.43** in 41% yield,[25]

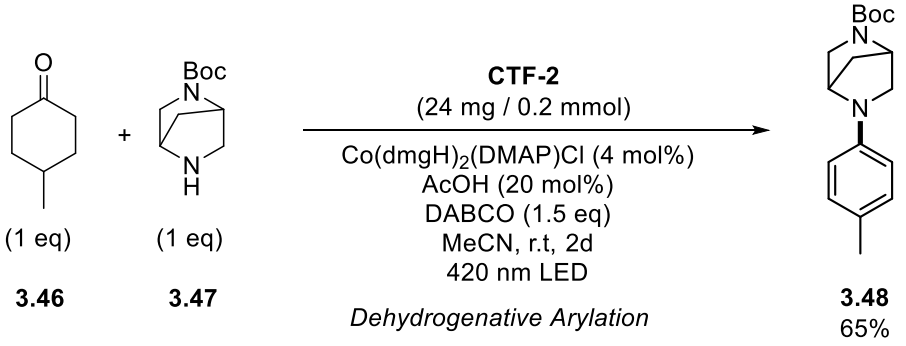

Scheme 3-8: Dehydrogenative arylation using CTF-2 as a heterogeneous photocatalyst.

decarboxylative arylation product[26] **3.44** in 51% yield (GC-MS vs biphenyl), and decarboxylative alkylation product[27] **3.45** in 54% yield. Demonstrating that CTF-2 is compatible with nickel cross-coupling catalysis, we wondered whether it would be possible to apply it in tandem with other cross coupling catalysts, such as cobalt. The Leonori group recently developed a dehydrogenative arylation strategy involving a cobalt dehydrogenation catalyst in tandem with an iridium co-catalyst.[28] Applying CTF-2 with the reported conditions, but with CTF-2 in place of the iridium catalyst (Scheme **3-8**), we were able to successfully produce the dehydrogenative arylation product **3.48** in 65% yield. To the best of our knowledge, this is the first time that metallaphotoredox decarboxylative arylation, alkylation, and dehydrogenative arylation have been performed with a fully organic polymer catalyst.

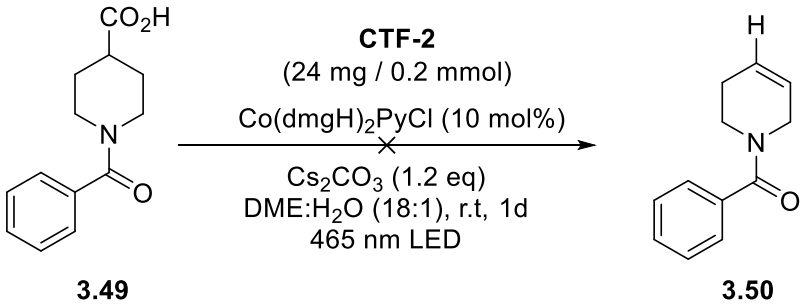

3.49 **3.50**

Scheme 3-9: Attempted decarboxylative olefination reaction with CTF-2.

We also attempted to apply CTF-2 for the decarboxylative olefination reaction procedure developed by Ritter which also utilized the same iridium catalyst (Scheme **3-9**).[29] Unfortunately, this did not appear to produce any of the olefin product. A major challenge for this reaction was the required solvent combination of H_2O/DME, which resulted in aggregation of CTF-2, and little to no dispersion of the material in the reaction mixture, providing no conversion. Attempts to perform this reaction in other solvents to improve the dispersibility were unsuccessful. Given that both cobalt catalysed dehydrogenation and decarboxylation have been independently performed by CTF-2, we are hopeful that this reaction will be successfully catalysed by CTF-2, or another heterogeneous photocatalyst, in the future. After demonstrating the reaction scope and the substrate scope for decarboxylative conjugate addition, we then

decided to demonstrate a potential application for CTF-2 photoredox catalysis in pharmaceutical synthesis (Scheme **3-10**). Inspired by the synthesis of pregabalin by MacMillan,[2] we developed a route to the antidepressant Rolipram. Traditionally, the synthesis of rolipram has involved toxic cyanide reagents followed by hydrogenation,[30] or the use of nitromethane[31,32].

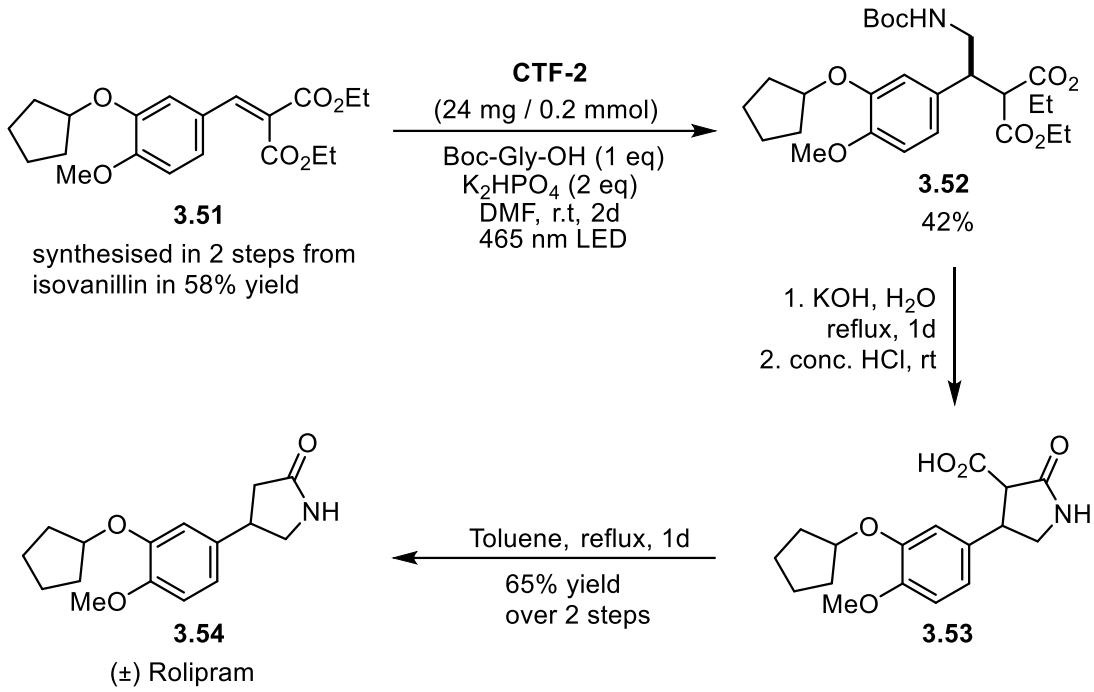

Scheme 3-10: Synthesis of antidepressant rolipram using CTF-2 for key C-C bond forming step.

Starting from isovanillin, we synthesized cyclopentyl derivative, followed by condensation with diethyl malonate to produce Michael acceptor (**3.51**) in 62% yield. Using CTF-2 as the key C-C bond forming step, reacting (**3.51**) with Boc-Gly-OH resulted in intermediate (**3.52**) in 42% yield. From here, we were able to directly convert the conjugate addition product to Rolipram (**3.54**) in 65% yield over 2 steps. Using Boc-Gly-OH, we were able to obviate the need for hydrogenation or cyanide reagents. While it is unlikely to be a cost-competitive route, it can offer a relatively mild alternative, and avoids the need for any transition metals and hazardous reagents such as nitromethane or cyanides.

Formation of the decarboxylative arylation product **3.44** is commendable since it demonstrates distinct properties of CTF-2 in comparison to other polymer photocatalysts such as carbon nitrides. A report by Seeberger and co-workers studying a variety of carbon nitrides demonstrated that they exclusively produced the ester product,[33] rather than the decarboxylative C-C bond forming product.

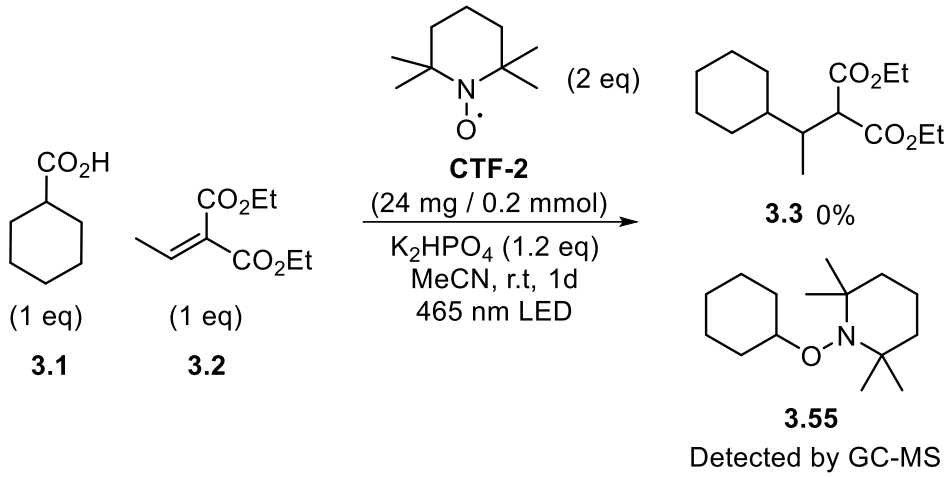

Scheme 3-11: Radical trap experiment for CTF-2 catalysed conjugate addition.

To further probe the mechanism of CTF-2 photocatalysis, we conducted mechanistic experiments using the radical trap (2,2,6,6-Tetramethylpiperidin-1-yl)oxyl (TEMPO). Performing the decarboxylative conjugate addition of cyclohexanecarboxylic acid with diethyl ethylidenemalonate in the presence of TEMPO, no formation of the conjugate addition product was observed by GC-MS (Scheme **3-11**). Instead, the TEMPO adduct of the cyclohexyl radical (**3.55**) was observed, suggesting that CTF-2 based photoredox catalysis undergoes a radical pathway, similar to iridium catalysts. Further experiments, and in-detailed experiments are required, but we have proposed a plausible mechanism for CTF-2 catalysed decarboxylative conjugate addition (Scheme **3-12**). Upon irradiation with visible light, the electron hole in the valence band of CTF-2 can oxidize carboxylate **(I)** to form the alkyl **(II)**, which then undergoes radical addition to form intermediate **(III)**, which is then reduced by the charge band of CTF-2, to form the conjugate addition product **(IV)**.

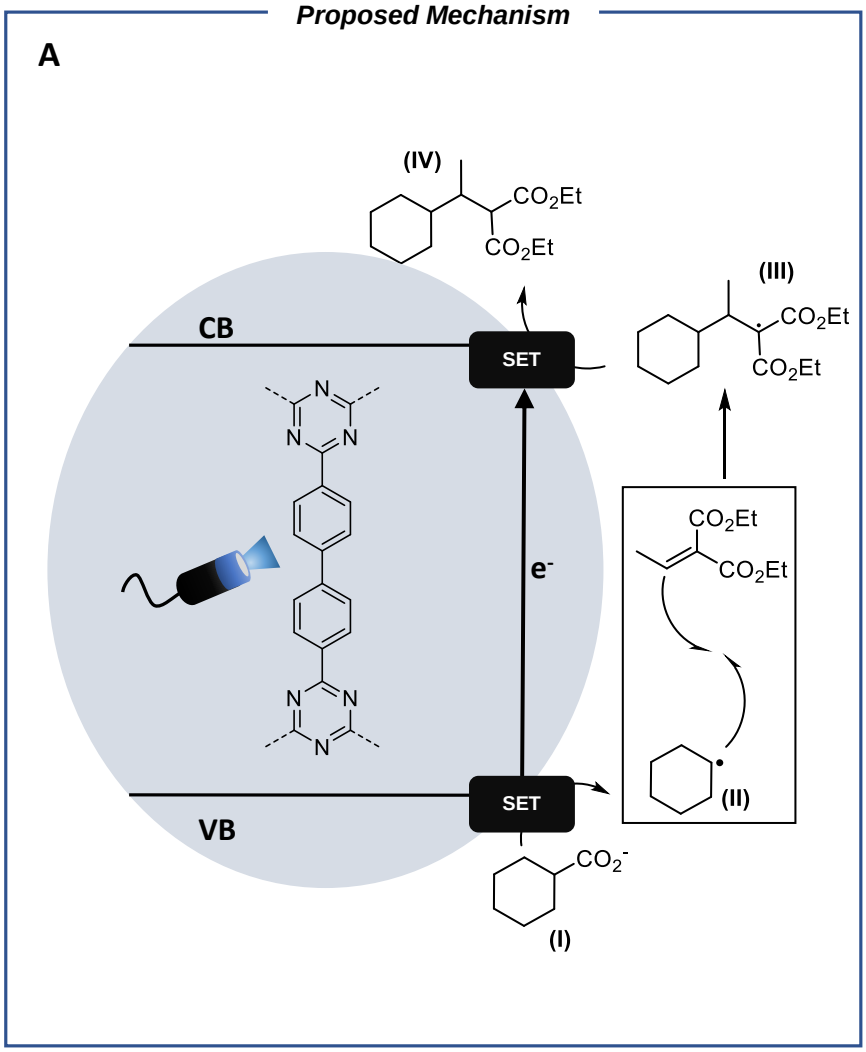

Scheme 3-12: Proposed mechanism for decarboxylative conjugate addition using CTF-2.

The use of structurally similar motifs to induce decarboxylative transformations has been previously described in homogeneous systems. Yoshimi has previously reported the use of biphenyl in combination with dicyanoarenes for decarboxylative transformations under UV irradiation.[34] Mechanistic experiments by Orr-Ewing and co-workers[35] on photocatalyzed decarboxylation using a combination of phenanthrene and dicyanobenzene under UV irradiation have indicated that photoexcited phenanthrene was oxidized by dicyanobenzene, and subsequently reduced by SET from the deprotonated carboxylic acid. It is plausible that CTF-2 might work under similar mechanism under visible light, with the triazine unit of the framework oxidizing the biphenyl unit,[36] which subsequently oxidizes the carboxylate. The reduced triazine moiety might then reduce intermediate **(III)** completing the catalytic cycle.[37]

Further experiments to evidence this mechanism are required, however. To investigate this, fluorescence quenching experiments could be performed, by observing the quenching (or lack of) in the fluorescence of CTF-2 following addition of the diethyl ethylidenemalonate, and the carboxylic acid in separate experiments. From our proposed mechanism, addition of the carboxylate should result in fluorescence quenching, while the addition of the Michael acceptor should have no effect. Unfortunately, we were only unable to perform fluorescence spectroscopy of CTF-2 in solid state, as we were unable to suspend CTF-2 in a compatible solvent.

Similarly, transient absorption spectroscopy might also be able to differentiate between an electron-transfer mechanism and an energy transfer process. By observing the change in excitation lifetime in the presence and absence of a quencher, oxidative electron transfer would result in accelerated lifetime decay, along with a return to a non-zero baseline. In comparison, an energy transfer process would return to a zero baseline. This could however be complicated by the fact that CTF-2 is a, irregular, non-uniform material with short excited-state lifetimes, compared to homogeneous organometallic catalysts with well-defined electronic states and long excited state lifetimes. Finally, cyclic voltammetry would also be able to provide experimental redox potentials, which should be in line with those required to oxidize carboxylate **(I)** and reduce intermediate **(III)**.

Recycling Experiments

One of the primary motivators for exploring heterogeneous polymers as replacements for transition metal complexes and organic dyes are their potential stability and recyclability. CTF-2 is a photostable polymer that has previously been demonstrated in our group to maintain photocatalytic activity for extended periods of time in hydrogen evolution.[22] Triazines themselves are known to be highly photostable. For example, *tris*-biphenyl triazine is an ingredient in sun-cream formulations as a UV-filter due to its high photostability.[38]

Exploring the reusability of CTF-2, we performed several recycling experiments to probe the performance of the polymer. Following a decarboxylative conjugate reaction between Boc-Proline and diethyl ethylidenemalonate to produce product **(3.8)**, the polymer was recycled by decantation of the diluted reaction mixture, and the polymer was subsequently washed repeatedly with water/acetone mixture and dried under a vacuum oven in the reaction vial and reused in the same vial. The higher density of CTF-2 allowed for trivial recovery of the insoluble polymer. Recycling experiments after several days demonstrated that CTF-2 showed consistent photocatalytic performance. We performed 4 cycles of CTF-2 photocatalysis utilizing our optimized conditions (Figure **3-15**), and there was no loss of catalytic performance in the material over time. Over the course of the 4 cycles, this totalled ~192 hours of blue LED irradiation on the same sample of CTF-2.

Catalyst Cycle	NMR Yield / %
1	87
2	92
3	92
4	92

Figure 3-15: NMR yields for CTF-2 recycling experiments for synthesis of product 3.8

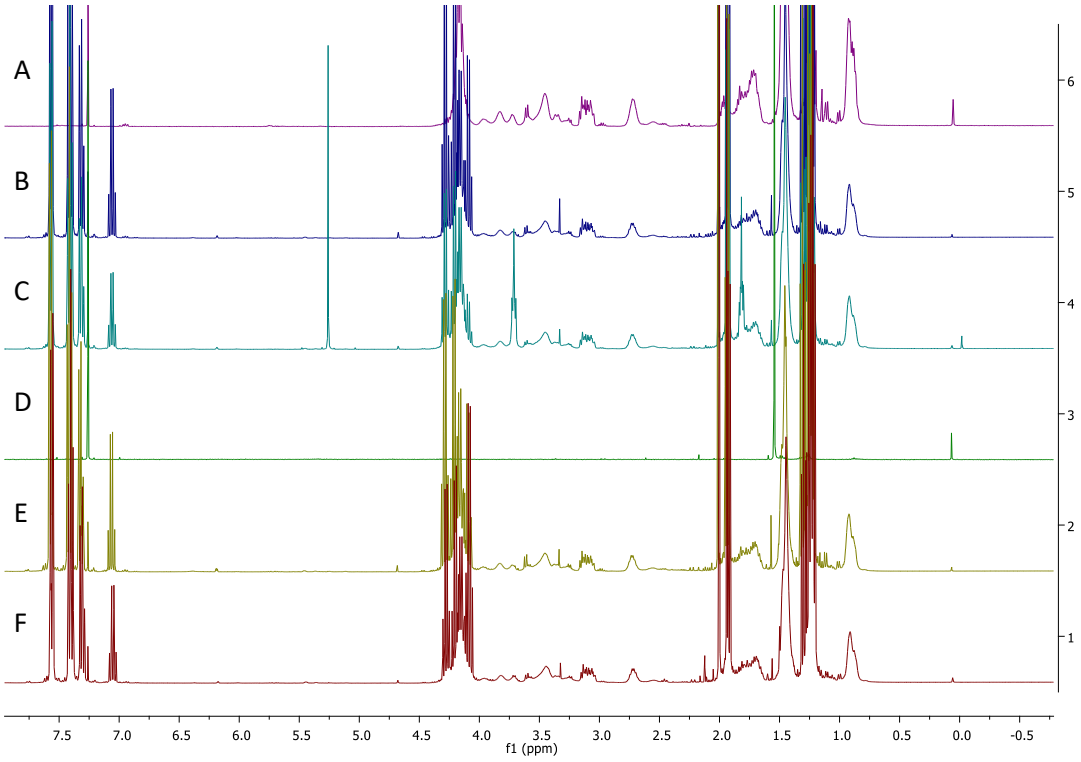

Figure 3-16: NMR traces of reaction mixtures of CTF-2 catalysed decarboxylative conjugate addition. A) purified Boc-Proline conjugate addition product; B) First cycle; C) Second cycle; D) NMR spectra of dried CTF-2 from cycle 2 rinsed with CDCl3, to ensure no residual conjugate addition product; E) Third cycle; F) Fourth cycle

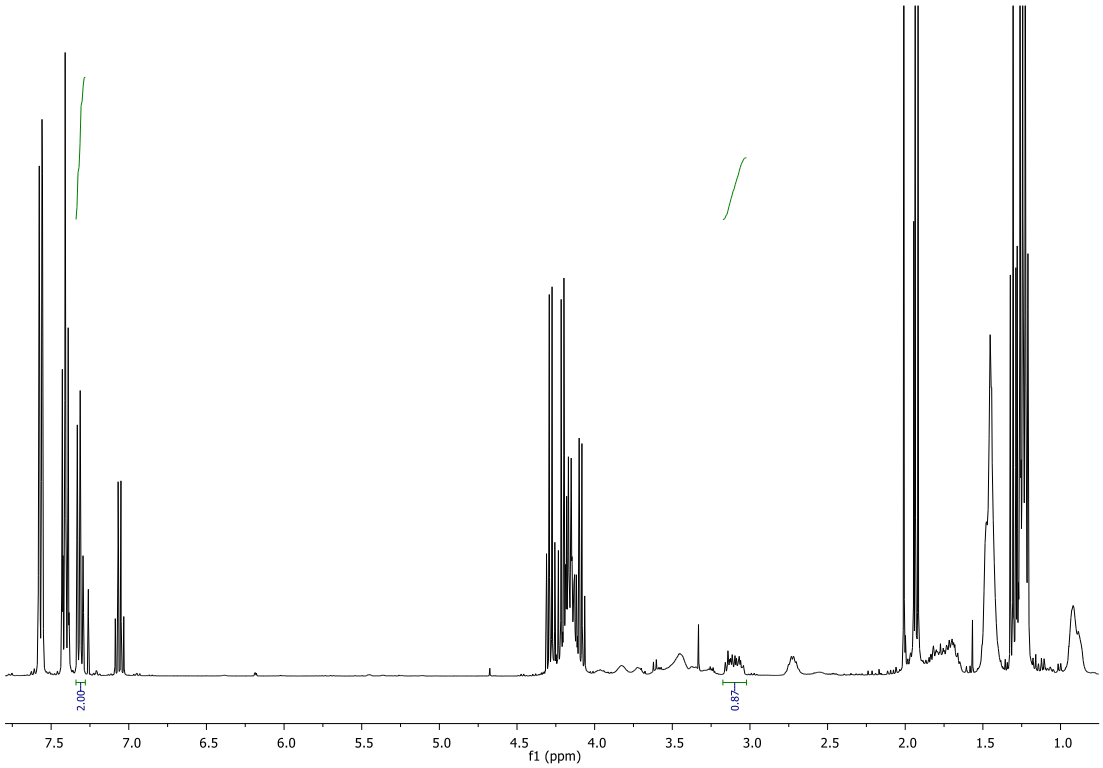

Figure 3-17: NMR plot of Cycle 1. Biphenyl signal from 7.34 - 7.28 ppm assumed to be 2 protons - Boc-Proline conjugate addition product signal from 3.17 - 3.02 ppm assumed to be 1 proton. Isolated yield for this reaction was 82%. All spectra were referenced to residual chloroform at 7.26 ppm in all cases

The trivial recovery, separation and high photostability of the catalyst are a significant benefit over iridium complexes or organic dyes, which are prone to degradation. These properties are an asset over transition metal complexes, where separation of dyes and their decomposition products from target molecules could cause issues, or in situations where metal toxicity is a concern.

Figure 3-18: CTF-2 settling in reaction mixtures for recovery and reuse.

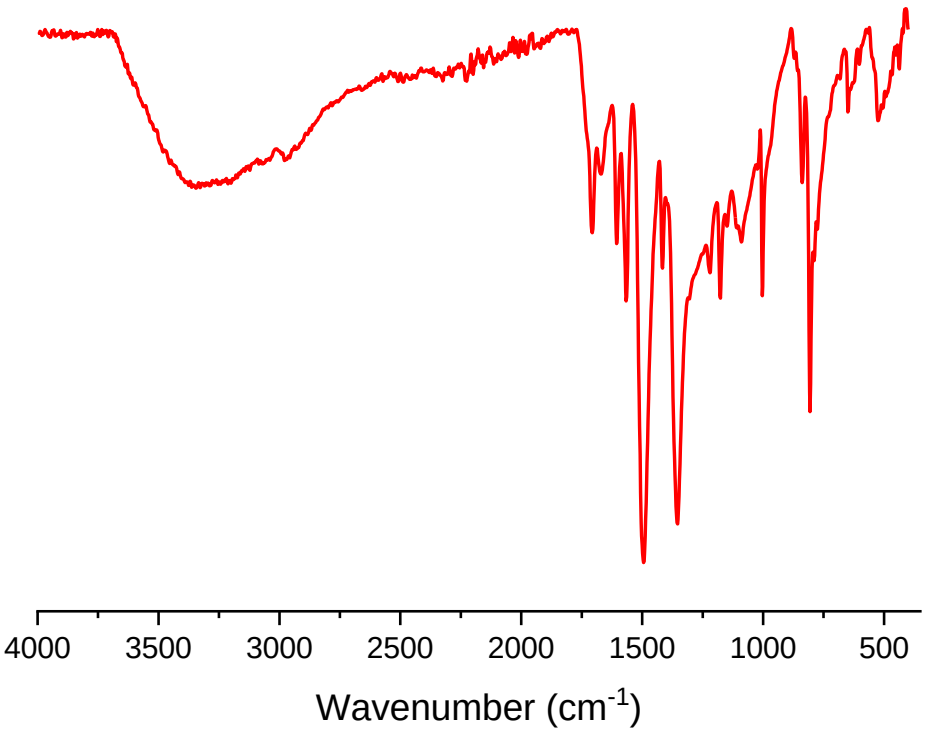

Figure 3-19: FT-IR spectrum of CTF-2 powder after photocatalysis (conjugate addition - 1 cycle)

Investigating the FT-IR spectrum of recovered CTF-2 powder following catalysis (Figure **3-19**), no substantial change was observed compared to the pristine material (Figure **3-1**) with strong bands corresponding to the triazine ring still present at 1500 cm^{-1} and 1350 cm^{-1}. No nitrile bands were observed, suggesting that the framework did not undergo depolymerization, and this is consistent with our previous work using CTF-2 as a hydrogen evolution catalyst, and the reported photostability of triazines.

Conclusions

In summary, this chapter has demonstrated the performance and capability of CTF-2 to catalyse decarboxylative photochemical reactions, along with dehydrogenative aniline synthesis. We have shown that CTF- 2 can be easily synthesized on large scale and could be used in recycling experiments for 4 total cycles without loss of catalytic discovery. To the best of our knowledge, this is the first time an organic polymer has been capable of performing decarboxylative arylation, alkylation, and dehydrogenative arylation. While the efficiency and yields of CTF-2 catalysis are lower than iridium complexes and homogeneous organic dyes,[21] it is still a significant accomplishment. The substantially lower cost, heterogeneous nature, photostability makes CTF-2 an attractive material. From our characterization experiments, we found that CTF-2 synthesized using this microwave method is a non-porous, amorphous material, and clearly neither of these properties are critical for effective catalysis.

These results have motivated further work on sustainable decarboxylative photocatalysis. While the decarboxylative olefination reaction reported by Ritter was unsuccessful with CTF-2 – the compatibility of CTF-2 to work in tandem with cobalt dehydrogenation catalysts is promising and we aim to develop methods for decarboxylative olefin synthesis, using CTF-2 or other heterogeneous polymers. Selective conversion of bio-renewable fatty acids into linear olefins using robust photocatalysts such as CTF-2 could allow for milder, low temperature alternatives to traditional production methods such as ethylene polymerization[39] or steam cracking.[40]

More broadly, we were also motivated to search for a wider range of reactions to be catalysed by heterogeneous organic polymers. Having shown that CTF-2 is compatible with nickel and cobalt co-catalysts, it may be possible to find polymers able of acting in tandem with copper-cocatalysts,[41] or potentially even enzymes[42] for highly enantioselective syntheses (Scheme **3-13**). Given the stable nature of triazine polymers, it may be possible to find reaction conditions, particularly in

aqueous environments, where polymers might be capable of outperforming transition metal complexes or organic dyes. We are also interested in developing metal doped or integrated polymers for unified heterogeneous metallaphotoredox catalysts,[43,44] which could potentially obviate the need for costly and synthetically elaborate external ligands in some synthetic routes.

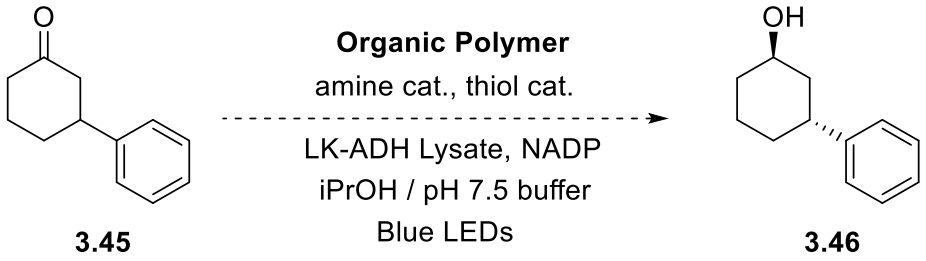

Scheme 3-13: Possible polymer and enzyme co-catalysed dynamic kinetic resolution for sustainable enantioselective production of chemicals.

Integrating these CTF-2, or other suitable polymers, into flow reactors [45–47] is a goal for us in the future to improve the yields and efficiencies. One of the primary disadvantages of heterogeneous photocatalysts is their decreased light penetration in reaction mixtures. While heterogeneous polymers might be scalable, suitably scaled reaction vessels and lights sources may not be easily accessible and could present significant engineering challenges.

By amplifying the irradiated surface area in flow reactors, polymer photocatalysts could provide substantial improvements to batch reactors. However, there are practical obstacles, such as potential blockages, and finding ways of adequately suspending polymers such as CTF-2 that have yet to be addressed, although there have been several reports in successfully using polymers such as carbon nitride in flow reactors for metallaphotoredox amination.[48]

Experimental

Reagents were purchased from Sigma Aldrich, Fluorochem, Alfa Aesar, Carbosynth, or TCI Chemicals and used were used without further purification unless otherwise specified. Chromatographic purification was performed on either using silica gel, or automated using prepacked columns on a Biotage Isolera purification system using gradient elution. Thin layer chromatography (TLC) plates were visualized using a combination of Ninhydrin stain, potassium permanganate, and UV fluorescence quenching as needed.

Photocatalysis experiments were performed using 400 W white LED floodlights for photocatalyst discovery experiments with rollers for agitation. Upscaled reactions for purifications were performed on either a SynLED Parallel Photoreactor (Z742680 – Sigma Aldrich UK), a PennOC Photoreactor with 420 nm irradiation at 100 % LED intensity, or using Kessil PR160L lights (max intensity, 3 cm distance from vial).

GC-MS analysis was performed on an Agilent 7890B GC system equipped with an Agilent 5977B Mass Spectrum Detector. UV-Vis measurements of polymer samples (powder form) were performed on Cary-5000 UV-VIS-NIR Spectrometer.

Automated dispensing of stock solutions was performed using liquid dispensing capabilities of a ChemSpeed Swing or ISynth platform, along with automated crimp sealing under nitrogen atmosphere. ^{1}H and ^{13}C NMR experiments were performed on a Bruker 400 MHz NMR instrument. Spectroscopic measurements are referenced to residual solvent signals at 7.26 ppm and 77.16 ppm, respectively, in $CDCl_3$, and processed in MestReNova.

Mass Spectrometry was performed by the University of Liverpool Analytical Services, or on a Waters Xevo G2-XS QToF. Excitation, emission, and lifetime experiments were performed on an Edinburgh Instruments Fluorescence Lifetime Spectrometer, with exponential fitting.

Powder X-Ray diffraction measurements were performed on a Panalytical Empyrean diffractometer equipped with a high throughput screening XYZ stage, an X-ray focusing mirror and a PIXcel detector with Cu Kα radiation.

Surface area measurements were performed on a Micromeritics ASAP 2020 Surface Area and Porosity Analyzer. IR spectra were recorded using a Bruker Tensor 27 FT-IR spectrometer with neat samples for novel products, or as powders for polymers. ICP-OES measurements were performed by the University of Liverpool Analytical Services following microwave digestion of CTF-2 in nitric acid.

Synthesis of CTF-2

[1,1'-biphenyl]-4,4'-dicarbonitrile (400 mg) was added to a microwave vial containing a stirrer bar. Triflic Acid (2.4 mL) was added in one portion and the vial was crimp sealed. The vial was heated at 150 °C in a Biotage Microwave Reactor for 2 hours and allowed to cool to room temperature. The vial was decapped, and the reaction mixture was quenched by slow addition (highly *exothermic*) of ammonia solution in water (100 mL, 3M) followed by stirring for 2 hours. The polymer was filtered and washed with water, acetone, and methanol. The washed polymer was roughly ground with a pestle and mortar and further purified by Soxhlet extraction with chloroform (overnight) and methanol (overnight) to remove any residual starting material or soluble oligomers. The purified material was further ground to a finer powder and dried in a vacuum oven at 180 °C to remove any traces of triflic acid to yield an orange-brown CTF-2 (794 mg, 99% yield, monomer basis– combination of 2 batches). **CHN Analysis:** Calculated % – C (82.30%), H (3.90%), N (13.70%); Analysis % - C (78.22%), H (3.95%), N (11.48%)

In general, multiple batches of 400 mg scale were queued on the microwave reactor's autosampler and combined after the microwave heating for convenience. Through the course of our studies, over 10 grams of CTF-2 was synthesized in this way. CTF-2 can also be synthesized without a microwave, by heating the above-described reaction mixture in a sand-bath for 3 days at 150 °C, however this resulted in lower yields of the framework, and for convenience, CTF-2 was synthesized in the microwave reactor.

CTF-2 synthesized at 50 – 130 °C was also performed analogously to the procedure above, and likewise resulted in non-porous polymeric material with a similar UV-Visible absorption spectra (Figure **3-20**) compared to batches synthesized at 150 °C. Sorption experiments for these polymers were performed by Dr. Alex James.

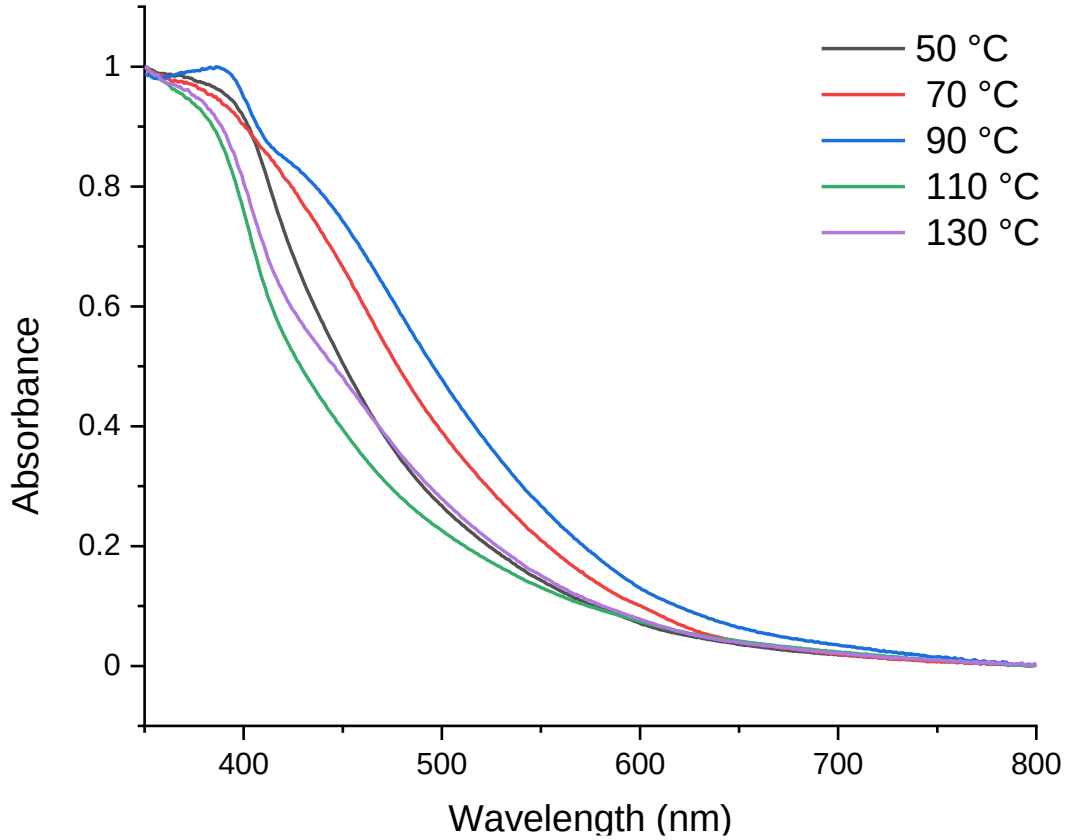

Figure 3-20: Normalized UV-Visible spectra of CTF-2 synthesized at increasing microwave temperatures.

Radical Trap Experiment

Cyclohexanecarboxylic acid, diethyl ethylidenemalonate, CTF-2, potassium phosphate dibasic, and TEMPO (2 eq) were combined as according to General Procedure A and irradiated for 2 days. The reaction mixture was diluted with ethyl acetate and directly analysed by GC-MS. The data for the radical trap experiment of cyclohexanecarboxylic acid was consistent with previous reports.[4]

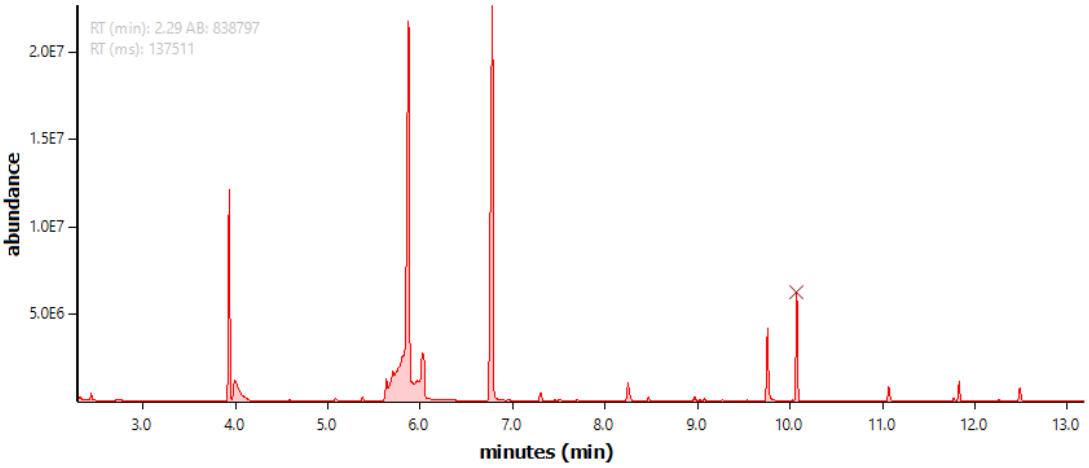

Figure 3-21: GC trace for decarboxylative conjugate addition in of cyclohexanecarboxylic acid in the presence of TEMPO. Adduct eluted at 10.1 mins, marked with X.

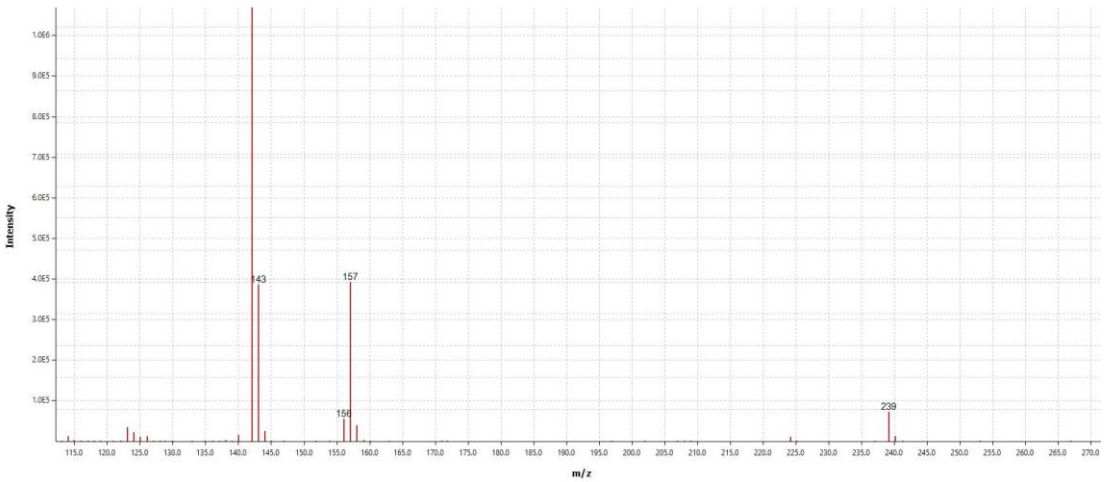

Figure 3-22: GC-MS Spectrum of TEMPO adduct of decarboxylated cyclohexanecarboxylic acid.

Product Characterization

General Procedure A – <u>Decarboxylative Conjugate Addition Scope</u>

CTF-2 (24 mg), carboxylic acid (0.20 mmol, 1 eq), Michael acceptor (0.4 mmol, 2 eq) and K_2HPO_4 (42 mg, 0.24 mmol, 1.2 eq) were combined in a 4 mL vial containing a stirrer bar. The vial was sealed with a septa screw cap and anhydrous acetonitrile (1 mL) was added. The reaction mixture was degassed by sparging with nitrogen and irradiated for 2 days with a SynLed Parallel photoreactor. The reaction mixtures were diluted repeatedly with ethyl acetate (4 mL x 3), and separated from the heterogeneous components by centrifugation, filtration, or decantation. The organic layers were then dried, concentrated, and purified by automated column chromatography in EtOAc or Et_2O with hexane or petroleum ether gradients, or 5% MeOH in DCM for polar compounds.

In some cases, reactions were performed in DMF due to the turbidity of the reaction mixture in acetonitrile after extended irradiation. In this case, the reaction vails were diluted with ethyl acetate (4 mL x 3), allowing for the polymer to settle to the bottom of the vial, extracted from water (20 mL), dried, concentrated under vacuum, and purified as above. In general, we found that carboxylic acid substrates containing secondary amines or lactams tended to have turbid reaction mixtures that adversely affected performance, presumably due to the poor light penetration that is already diminished by using a heterogeneous photocatalyst.

Diethyl 2-(1-(1-(tert-butoxycarbonyl)azetidin-2-yl)ethyl)malonate (3.7)

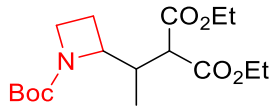

Performed according to General Procedure A to yield a colourless oil as an inseparable mixture of rotamers and diastereomers (55.2 mg, 80% yield).

^{1}H NMR (400 MHz, $CDCl_3$) δ 4.34 – 4.25 (m, 1H), 4.21 – 4.10 (m, 4H), 3.84 – 3.74 (m, 1H), 3.73 – 3.64 (m, 1H), 3.60 (d, *J* = 9.3 Hz, 0.5H), 3.37 (br s, 1H), 2.81 – 2.69 (m, 0.5H), 2.63 – 2.52 (m, 0.5H), 2.31 – 2.19 (m, 0.5H), 2.18 – 2.07 (m, 0.5H), 1.98 – 1.87 (m, 1H), 1.42 (d, *J* = 2.2 Hz, 9H), 1.27 – 1.22 (m, 6H), 1.04 (d, *J* = 7.0 Hz, 1.5H),0.99 (d, *J* = 7.0 Hz, 1.5H).

^{13}C NMR (101 MHz, $CDCl_3$) δ 168.95, 168.93, 168.76, 168.49, 157.16, 156.84, 79.84, 79.63, 64.50, 64.16, 61.37, 61.34, 61.32, 61.25, 54.25, 53.98, 46.66, 37.46, 36.35, 28.49, 28.46, 19.70, 18.36, 14.20, 14.17, 14.16, 14.13, 12.36, 11.03.

HRMS (ESI+): Found $M+Na^+$: 366.1905, $C_{17}H_{29}NNaO_6^+$ requires 366.1887

FT-IR (cm^{-1}): 2978, 2939, 1729, 1696, 1364, 1133, 1030

Diethyl 2-(1-(1-(tert-butoxycarbonyl)pyrrolidin-2-yl)ethyl)malonate (3.8)

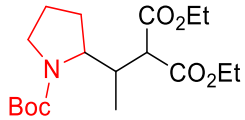

Performed according to General Procedure A to yield a pale-yellow oil as an inseparable mixture of rotamers and diastereomers (58.8 mg, 82% yield). Spectroscopic data was consistent with previously reported values.[2]

^{1}H NMR (400 MHz, $CDCl_3$) δ 4.25 – 4.09 (m, 4H), 4.06 – 3.20 (m, 3H), 3.19 – 3.03 (m, 1H), 2.80 – 2.42 (m, 1H), 2.06 – 1.60 (m, 4H), 1.56 – 1.33 (m, 9H), 1.28 – 1.21 (m, 6H), 0.97 – 0.82 (m, 3H).

^{13}C NMR (101 MHz, $CDCl_3$) δ 169.06, 168.53, 155.53, 154.99, 79.94, 79.35, 61.41, 61.28, 60.65, 60.39, 55.70, 54.91, 54.44, 54.19, 47.83, 47.29, 47.00, 37.17, 36.91, 28.60, 24.43, 23.96, 23.65, 23.45, 14.22, 13.57.

HRMS (ESI+): Found $M+Na^+$: 380.2047, $C_{18}H_{31}NNaO_6^+$ requires 380.2044

^{13}C NMR spectrum for this sample was processed with apodization in MestReNova (Exponential Function – 6.9Hz) for improved visual clarity.

Diethyl 2-(1-(1-(tert-butoxycarbonyl)piperidin-2-yl)ethyl)malonate (3.9)

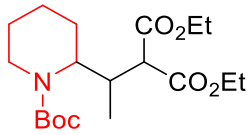

Performed according to General Procedure A to yield the product as a colorless oil as an inseparable mixture of rotamers and diastereomers (54.7 mg, 74 %). Spectroscopic data was consistent with previously reported values.[2]

^{1}H NMR (400 MHz, $CDCl_3$) δ 4.25 – 3.98 (m, 6H), 3.41 (d, *J* = 4.5 Hz, 1H), 2.79 – 2.61 (m, 2H), 1.81 – 1.65 (m, 1H), 1.64 – 1.45 (m, 5H), 1.42 (s, 9H), 1.29 – 1.22 (m, 6H), 1.05 (d, *J* = 6.9 Hz, 1.4H), 0.98 (d, *J* = 6.9 Hz, 1.6H).

^{13}C NMR (101 MHz, $CDCl_3$) δ 169.91, 169.29, 168.57, 168.29, 155.22, 155.20, 79.54, 79.43, 61.53, 61.43, 61.21, 60.95, 53.44, 53.20, 32.03, 31.77, 28.54, 28.50, 26.24, 26.15, 25.43, 19.09, 18.94, 14.25, 14.18, 14.15, 13.84, 12.95.

HRMS (ESI+): Found $M+Na^+$: 394.2232, $C_{19}H_{33}NNaO_6^+$ requires 394.2200

Diethyl 2-(1-(1-(tert-butoxycarbonyl)azepan-2-yl)ethyl)malonate (3.10)

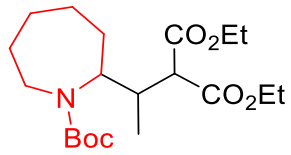

Performed according to General Procedure A in DMF and with 1.3 eq acceptor to yield a colourless oil as an inseparable mixture of rotamers and diastereomers (45.5 mg, 59% yield).

^{1}H NMR (400 MHz, $CDCl_3$) δ 4.29 – 3.91 (m, 5H), 3.83 – 3.55 (m, 1H), 3.46 (d, *J* = 2.1 Hz, 0.3H), 3.46 (d, *J* = 2.8 Hz, 0.4H), 3.35 (d, *J* = 7.9 Hz, 0.4H), 2.73 – 2.56 (m, 1H), 2.44 (s, 0.2H), 2.37 – 2.00 (m, 1.7H),1.88 – 1.65 (m, 2.3H), 1.64 - 1.52 (m, 1.7), 1.46 (s, 2H), 1,43 (s, 7H), 1.39 – 1.12 (m, 9H), 1.00 (d, *J* = 6.9 Hz, 0.8H), 0.96 (t, *J* = 6.5 Hz, 1.3H), 0.91 (d, *J* = 7.0 Hz, 0.8H).

^{13}C NMR ($CDCl_3$) δ 169.52, 169.30, 169.17, 169.14, 169.08, 168.97, 168.80, 168.50, 168.21, 156.77, 156.56, 156.08, 155.59, 79.89, 79.75, 79.25, 79.10, 61.62, 61.49, 61.41, 61.25, 61.22, 61.18, 60.99, 58.49, 57.26, 56.27, 54.84, 54.43, 54.40, 53.89, 43.58, 42.79, 38.49, 38.40, 38.34, 38.22, 33.19, 32.83, 32.78, 32.37, 30.20, 29.94, 29.20, 28.60, 28.56, 28.45, 28.02, 27.66, 25.41, 25.29, 24.84, 14.40, 14.33, 14.21, 14.18, 14.13, 14.09, 13.16, 12.73.

HRMS (ESI+): Found $M+Na^+$: 408.2359, $C_{20}H_{35}NNaO_6^+$ requires 408.2357; Found $[M\text{-}Boc+H]^+$: 286.2013, $C_{15}H_{28}NO_4^+$ requires 286.2013

FT-IR (cm^{-1}): 2976, 2929, 1729, 1686, 1366, 1158, 1028

Diethyl2-(1-((4S)-1-(tert-butoxycarbonyl)-4-fluoropyrrolidin-2-yl)ethyl)malonate (3.11)

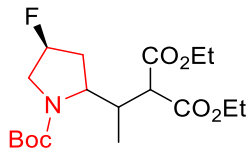

Performed according to General Procedure A in DMF with 1.3 eq acceptor to yield a yellow oil as an inseparable mixture of rotamers and diastereomers (54.0 mg, 72% yield).

^{1}H NMR (400 MHz, $CDCl_3$) δ 5.28 – 5.20 (m, 0.21H), 5.19 – 5.07 (m, 0.46H), 5.06 – 4.98 (m, 0.25H), 4.33 – 3.64 (m, 6H), 3.61 – 2.54 (m, 3H), 2.42 – 1.74 (m, 2H), 1.45 (s, 9H), 1.28 – 1.19 (m, 6H), 1.06 – 0.76 (m, 3H).

^{13}C NMR (101 MHz, $CDCl_3$) δ 169.13, 168.84, 168.68, 168.62, 168.28, 168.14, 155.54, 154.93, 92.85, 92.34, 91.16, 90.62, 80.67, 80.52, 80.03, 61.62, 61.40, 61.28, 60.27, 59.34, 58.89, 57.92, 55.82, 55.42, 55.00, 54.77, 54.53, 54.37, 53.76, 53.46, 37.90, 36.21, 35.52, 35.25, 35.11, 34.91, 28.50, 14.39, 14.19, 13.44, 10.98.

^{19}F NMR (376 MHz, $CDCl_3$) δ -169.37, -170.20, -170.46, -171.03, -176.78, -177.29, -177.51.

HRMS (ESI+): Found $M+Na^+$: 398.1955, $C_{18}H_{30}FNNaO_6^+$ requires 398.1949

FT-IR (cm^{-1}): 2980, 1729, 1691, 1387, 1366, 1160, 1030

^{13}C NMR spectrum for this sample was processed with apodization in MestReNova (Exponential Function - 5Hz) for improved visual clarity.

Diethyl 2-(1-(tetrahydrofuran-2-yl)ethyl)malonate (3.12)

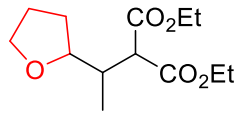

Performed according to General Procedure A to yield a colourless oil as an inseparable mixture of diastereomers (35.9 mg, 70% yield). Spectroscopic data was consistent with reported values. [2]

^{1}H NMR (400 MHz, $CDCl_3$) δ 4.21 – 4.13 (m, 4H), 3.87 – 3.65 (m, 3H), 3.59 (d, *J* = 6.4 Hz, 0.56H), 3.41 (d, *J* = 8.6 Hz, 0.42H), 2.53 – 2.42 (m, 0.44H), 2.34 – 2.22 (m, 0.55H), 2.04 – 1.76 (m, 3H), 1.65 – 1.48 (m, 1H), 1.28 – 1.22 (m, 6H), 0.97 (dd, *J* = 6.9, 5.4 Hz, 3H)

^{13}C NMR (101 MHz, $CDCl_3$) δ 169.46, 169.02, 168.98, 168.92, 81.40, 80.50, 68.45, 67.89, 61.36, 61.30, 61.22, 61.13, 55.08, 54.56, 39.22, 37.50, 30.12, 28.60, 26.11, 25.99, 14.26, 14.22, 14.18, 13.61, 12.45.

HRMS (ESI+): Found $M+Na^+$: 281.1375, $C_{13}H_{22}NNaO_5^+$ requires 281.1359

Diethyl 2-(1-((tert-butoxycarbonyl)amino)propan-2-yl)malonate (3.13)

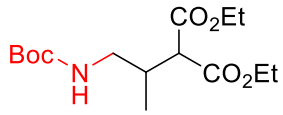

Performed according to General Procedure A to yield a colourless oil as a mixture of rotamers (26.5 mg, 42 % yield). Spectroscopic data was consistent with reported values.[2]

^{1}H NMR (400 MHz, $CDCl_3$) δ 4.72 (br s, 1H), 4.23 – 4.14 (m, 4H), 3.29 (d, *J* = 7.5 Hz, 1H), 3.22 – 3.09 (m, 2H), 2.48 – 2.40 (m, 1H), 1.42 (s, 9H), 1.26 (t, *J* = 7.2, 6H), 1.00 (d, *J* = 7.0 Hz, 3H).

^{13}C NMR (101 MHz, $CDCl_3$) δ 168.90, 168.68, 156.07, 79.36, 61.53, 61.47, 55.17, 44.33, 34.23, 28.50, 15.65, 14.21, 14.19.

HRMS (ESI+): Found $M+Na^+$: 340.1750, $C_{15}H_{27}NNaO_6^+$ requires 340.1731

Diethyl 2-(1-(5-oxopyrrolidin-2-yl)ethyl)malonate (3.14)

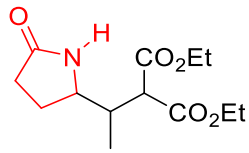

Performed according to General Procedure A in DMF to yield the product as a pale-yellow oil as an inseparable mixture of diastereomers (33.2 mg, 61% yield).

^{1}H NMR (400 MHz, $CDCl_3$) δ 6.27 (s, 1H), 6.17 (s, 0.4H), 4.24 – 4.15 (m, 0.5H), 3.82 – 3.71 (m, 0.5H), 3.66 – 3.54 (m, 0.5H), 3.37 (d, *J* = 6.1 Hz, 0.5H), 3.34 (d, *J* = 7.1 Hz, 0.5H), 2.45 – 2.13 (m, 4H), 1.86 – 1.73 (m, 1H), 1.26 (td, *J* = 7.1, 1.4 Hz, 6H), 1.00 (t, *J* = 6.8 Hz, 3H).

^{13}C NMR (101 MHz, $CDCl_3$) δ 178.23, 178.00, 168.96, 168.49, 168.41, 168.38, 61.88, 61.80, 61.75, 61.72, 56.56, 56.26, 55.12, 54.27, 38.46, 38.05, 30.11, 29.83, 25.21, 24.46, 14.19, 14.17, 14.14, 13.04, 12.13.

HRMS (ESI+): Found $M+Na^+$: 294.1318, $C_{13}H_{21}NNaO_5^+$ requires 294.1312

FT-IR (cm^{-1}): 3127, 2980, 1725, 1690, 1267, 1152, 1028, 731

Diethyl 2-(1-(4-oxoazetidin-2-yl)ethyl)malonate (3.15)

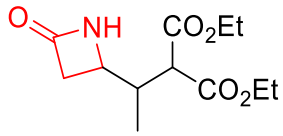

Performed according to General Procedure A in DMF to yield a pale-yellow oil as an inseparable mixture of diastereomers (25.3 mg, 49%).

^{1}H NMR (400 MHz, $CDCl_3$) δ 6.04 (s, 1H), 4.26 – 4.14 (m, 4H), 3.80-3.72 (m, 0.5H), 3.69 – 3.63 (m, 0.5H), 3.37 (d, *J* = 5.6 Hz, 0.5H), 3.32 (d, *J* = 6.6 Hz, 0.5H), 3.07 – 2.96 (m, 1H), 2.74 – 2.61 (m, 1H), 2.53 - 2.44 (m, 0.5H), 2.44 – 2.35 (m, 0.5H), 1.27 (t, *J* = 7.1 Hz, 6H), 1.05 (d, *J* = 6.9 Hz, 3H).

^{13}C NMR (101 MHz, $CDCl_3$) δ 168.67, 168.41, 168.38, 168.27, 167.55, 167.37, 61.84, 61.79, 61.78, 61.76, 54.96, 54.62, 50.45, 50.12, 42.38, 41.74, 38.32, 36.48, 14.22, 14.18, 14.15, 13.36, 12.79.

HRMS (ESI+): Found M+Na^{+}: 280.1159, $C_{12}H_{19}NNaO_5^{+}$ requires 280.1155

FT-IR (cm^{-1}): 3260, 2980, 1723, 1177, 1154, 1028, 730

Di-tert-butyl 2-(3-ethoxy-2-(ethoxycarbonyl)-3-oxo-1-phenylpropyl)piperazine-1,4 dicarboxylate (3.16)

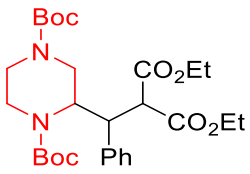

Performed according to General Procedure A in DMF with 1 eq acceptor to yield the product as a white paste as an inseparable mixture of rotamers and diastereomers (65.2 mg, 61 %).

^{1}H NMR (400 MHz, $CDCl_3$) δ 7.35 – 7.05 (m, 5H), 4.71 (s, 0.28H), 4.54 (s, 0.26H), 4.31 (s, 0.34H), 4.23 – 3.56 (m, 8H), 3.45 (d, *J* = 13.3 Hz, 1H), 3.30 – 2.26 (m, 3H), 1.55 – 1.22 (m, 17H), 1.17 (t, *J* = 7.2 Hz, 3H), 1.11 – 0.87 (m, 1.66H), 0.84 – 0.65 (m, 2.51H).

^{13}C NMR (101 MHz, $CDCl_3$) δ 168.41, 168.25, 168.14, 167.84, 167.66, 155.49, 155.10, 154.90, 154.55, 138.51, 136.85, 130.18, 129.51, 128.60, 127.97, 127.81, 127.67, 127.33, 80.99, 80.63, 80.04, 62.06, 61.69, 61.50, 61.34, 61.23, 56.02, 55.13, 54.38, 52.02, 45.53, 44.72, 44.17, 43.91, 43.39, 42.86, 42.50, 40.24, 39.43, 38.61, 37.78, 28.56, 28.46, 28.34, 14.12, 13.93, 13.62.

HRMS (ESI+): Found M+Na^{+}:557.2841, $C_{28}H_{42}N_2NaO_8^{+}$ requires 557.2833

FT-IR (cm^{-1}): 2977, 2933, 1731, 1690, 1364, 1160, 1098, 701

^{13}C NMR spectrum for this sample was processed with apodization in MestReNova (Exponential Function – 5.8Hz) for improved visual clarity.

Diethyl 2-(1-((3r,5r,7r)-adamantan-1-yl)ethyl)malonate (3.17)

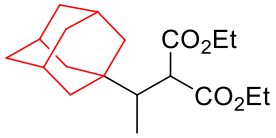

Performed according to General Procedure A to yield a colourless oil (13.9 mg, 22% yield). Spectroscopic data was consistent with previously reported values. [2]

^{1}H NMR: (400 MHz, $CDCl_3$) δ 4.22 – 4.13 (m, 4H), 3.56 (d, *J* = 5.2 Hz, 1H), 2.11 – 2.02 (m, 1H), 1.96 (s, 3H), 1.72 – 1.64 (m, 3H), 1.64 – 1.57 (m, 3H), 1.56 – 1.45 (m, 6H), 1.26 (td, *J* = 7.1, 5.9 Hz, 6H), 0.98 (d, *J* = 7.3 Hz, 3H).

^{13}C NMR (101 MHz, $CDCl_3$) δ 170.54, 169.94, 61.46, 61.02, 51.99, 43.23, 39.51, 37.17, 35.38, 28.76, 14.22, 14.18, 10.53.

HRMS (ESI+): Found $M+Na^+$: 345.2049 $C_{19}H_{30}NaO_4^+$ requires 345.2036

Diethyl 2-(1-cyclohexylethyl)malonate (3.18)

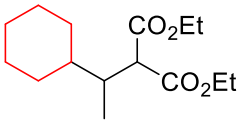

Performed as in General Procedure A to yield a colourless oil (25.1 mg, 46% yield). Spectroscopic data was consistent with previously reported values.[2]

^{1}H NMR (400 MHz, $CDCl_3$) δ 4.24 – 4.12 (m, 4H), 3.38 (d, *J* = 9.2 Hz, 1H), 2.22 – 2.11 (m, 1H), 1.77 – 1.68 (m, 2H), 1.67 – 1.54 (m, 3H), 1.28 – 1.08 (m, 11H), 0.99 – 0.90 (m, 1H), 0.89 (d, *J* = 7.0 Hz, 3H).

^{13}C NMR (101 MHz, $CDCl_3$) δ 169.45, 169.19, 61.26, 61.18, 55.95, 40.39, 38.69, 31.65, 27.54, 26.86, 26.67, 26.60, 14.25, 13.03.

HRMS (ESI+): Found $M+Na^+$: 293.1729, $C_{15}H_{26}NaO_4^+$ requires 293.1723

Diethyl 2-((1-(tert-butoxycarbonyl)azetidin-2-yl)(phenyl)methyl)malonate (3.23)

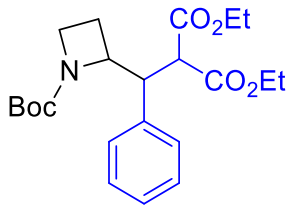

Performed according to General Procedure A with 1 eq acceptor in DMF to yield a colourless oil as an inseparable mixture of diastereomers and rotamers (50.2 mg, 62% yield).

^{1}H NMR (400 MHz, $CDCl_3$) δ 7.26 – 7.10 (m, 5H), 4.63 – 4.52 (m, 0.4H), 4.50 – 4.38 (m, 0.6H), 4.27 (d, *J* = 11.8 Hz, 0.4H), 4.21 – 4.07 (m, 2H), 4.01 – 3.89 (m, 1.1H), 3.83 – 3.70 (m, 2H), 3.66 – 3.50 (m, 1.4H), 3.32 (br s, 0.5H), 3.08 (td, *J* = 8.8, 5.8 Hz, 0.4H), 2.21 – 2.03 (m, 1H), 1.91 – 1.78 (m, 1H), 1.42 (s, 9H), 1.21 (td, *J* = 7.1, 4.8 Hz, 3H), 0.88 – 0.75 (m, 3H).

^{13}C NMR (101 MHz, $CDCl_3$) δ 168.71, 168.40, 168.17, 167.84, 156.99, 137.65, 136.93, 129.93, 129.33, 128.25, 128.16, 127.40, 127.34, 79.97, 64.37, 63.47, 61.61, 61.22, 61.15, 54.03, 48.88, 46.58, 28.55, 20.48 (br), 19.29, 14.16, 14.13, 13.73, 13.70.

HRMS (ESI+): Found $M+Na^+$: 428.2046, $C_{22}H_{31}NNaO_5^+$ requires 428.2044

FT-IR (cm^{-1}): 2976, 1731, 1694, 1364, 1136, 703

Diethyl-2-((1-(tert-butoxycarbonyl)pyrrolidin-2-yl)(phenyl)methyl)malonate (3.24)

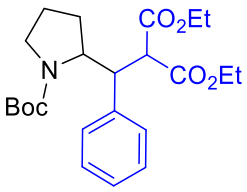

Performed according to General Procedure A with 1 eq acceptor and in DMF to yield a colourless viscous oil as an inseparable mixture of diastereomers and rotamers (70.7 mg, 84% yield).

^{1}H NMR (400 MHz, $CDCl_3$) δ 7.30 – 7.08 (m, 5H), 4.37 (s, 0.3H), 4.30 – 3.97 (m, 3.6H), 3.89 – 3.55 (m, 2.4H), 3.48 (d, *J* = 9.3 Hz, 0.3H), 3.46 (d, *J* = 9.2 Hz, 0.2H), 3.38 (br s, 0.2H), 3.28 – 3.08 (m, 0.8H), 3.01 – 2.87 (m, 0.5H), 2.73 – 2.63 (m, 0.4H), 2.06 – 1.79 (m, 1H), 1.78 – 1.66 (m, 1H), 1.61 – 1.52 (m, 3.7H), 1.51 – 1.36 (m, 6.4H), 1.26 – 1.15 (m, 3.5H), 0.88 – 0.68 (m, 3.5H).

^{13}C NMR (101 MHz, $CDCl_3$) δ 168.72, 168.57, 168.36, 168.18, 168.02, 156.21, 155.43, 155.03, 139.86, 139.68, 138.70, 138.34, 129.65, 129.31, 128.46, 128.30, 128.04, 127.32, 127.19, 80.35, 79.52, 79.30, 62.43, 62.28, 61.81, 61.47, 61.36, 61.17, 61.01, 60.34, 58.95, 54.96, 54.89, 54.73, 53.92, 50.56, 50.52, 50.37, 49.61, 47.97, 47.08, 46.67, 29.99, 29.61, 29.23, 28.71, 28.61, 23.70, 23.30, 22.73, 22.35, 14.21, 14.13, 13.66, 13.62.

HRMS (ESI+): Found $M+Na^+$: 442.2200, $C_{23}H_{33}NNaO_6^+$ requires 442.2200; Found $[M\text{-}Boc+H]^+$: 320.1856, $C_{18}H_{26}NO_4^+$ requires 320.1856

FT-IR (cm^{-1}): 2976, 1731, 1688, 1366, 1160, 1033, 703

Diethyl 2-((1-(tert-butoxycarbonyl)piperidin-2-yl)(phenyl)methyl)malonate (3.25)

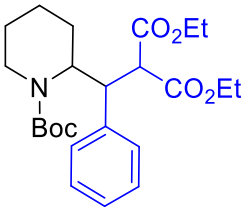

Performed according to General Procedure A with minor modifications. Reaction was performed with 1 eq acceptor and in DMF to yield a colourless oil as an inseparable mixture of diastereomers and rotamers (63.6 mg, 73% yield).

^{1}H NMR (400 MHz, $CDCl_3$) δ 7.31 – 7.04 (m, 5H), 4.71 – 4.50 (m, 0.67H), 4.39 (s, 0.32H), 4.24 – 3.95 (m, 2H), 3.93 – 3.56 (m, 4.6H), 3.51 (d, *J* = 13.3 Hz, 0.2H), 2.93 (t, *J* = 12.6 Hz, 0.2H), 2.75 (t, *J* = 12.8 Hz, 0.3H), 2.39 (q, *J* = 14.0 Hz, 0.4H), 1.79 – 1.06 (m, 18H), 0.94 – 0.80 (m, 1.3H), 0.76 (t, *J* = 7.1 Hz, 1.9H).

^{13}C NMR (101 MHz, $CDCl_3$) δ 168.79, 168.63, 168.14, 168.01, 167.85, 155.88, 154.91, 154.43, 139.61, 139.45, 138.41, 138.09, 129.72, 129.61, 128.55, 127.92, 127.67, 127.31, 127.21, 126.99, 80.04, 79.71, 79.53, 79.03, 61.97, 61.77, 61.60, 61.39, 61.21, 56.92, 56.76, 56.53, 55.28, 54.54, 52.92, 45.74, 45.32, 45.05, 40.55, 39.91, 38.90, 38.45, 28.63, 28.37, 27.45, 27.03, 26.70, 26.51, 25.51, 25.13, 24.88, 24.76, 19.22, 19.13, 14.12, 14.06, 13.71, 13.62.

HRMS (ESI+): Found $M+Na^+$: 456.2357, $C_{24}H_{35}NNaO_6^+$ requires 456.2357; Found $[M\text{-Boc}+H]^+$: 334.2013, $C_{19}H_{28}NO_4^+$ requires 334.2013

FT-IR (cm^{-1}): 2978, 2933, 1731, 1686, 1158, 1030, 701

Diethyl 2-(phenyl(tetrahydrofuran-2-yl)methyl)malonate (3.26)

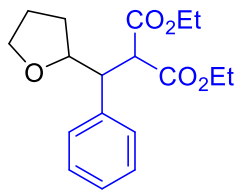

Performed as in General Procedure A with minor modifications. Reaction was performed with 1.2 eq carboxylic acid and 1 eq acceptor in DMF to yield the product as a clear oil as an inseparable mixture of diastereomers and rotamers (37.6 mg, 59% yield).

^{1}H NMR (400 MHz, $CDCl_3$) δ 7.27 – 7.10 (m, 5H), 4.22 – 4.04 (m, 3.5H), 3.83 – 3.72 (m, 2.5H), 3.72 – 3.61 (m, 1H), 3.60 – 3.49 (m, 1H), 3.45 (dd, *J* = 11.7, 2.9 Hz, 0.5H), 3.40 (t, *J* = 10.1 Hz, 0.5H), 1.90 – 1.66 (m, 1.5H), 1.64 – 1.52 (m, 1H), 1.51 – 1.41 (m, 0.5H), 1.40 – 1.30 (m, 0.5H), 1.29 – 1.16 (m, 3.5H), 0.82 (td, *J* = 7.0, 5.5 3H).

^{13}C NMR (101 MHz, $CDCl_3$) δ 168.68, 168.64, 168.15, 168.07, 138.88, 137.57, 130.26, 129.05, 128.48, 127.94, 127.32, 127.16, 82.31, 79.08, 68.65, 68.06, 61.67, 61.45, 61.17, 56.77, 55.12, 51.46, 49.33, 30.39, 28.96, 25.88, 25.42, 14.19, 14.14, 13.74, 13.72.

HRMS (ESI+): Found M+Na^+: 343.1537, $C_{18}H_{24}NaO_5^+$ requires 343.1516

FT-IR (cm^{-1}): 2980, 2873, 1729, 1257, 1173, 1033, 703

Diethyl-2-((5-oxopyrrolidin-2-yl)(phenyl)methyl)malonate (3.27)

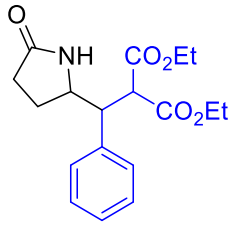

Performed according to General Procedure A with 1 eq acceptor in DMF to yield a pale-yellow oil as an inseperable mixture of diastereomers and rotamers (34.8 mg, 52% yield).

^{1}H NMR (400 MHz, $CDCl_3$) δ 7.30 – 7.08 (m, 5H), 6.42 – 6.09 (m, 1H), 4.23 – 4.13 (m, 2H), 4.06 – 4.00 (m, 0.5H), 3.99 – 3.91 (m, 1.5H), 3.91 – 3.78 (m, 1.5H), 3.74 (d, *J* = 8.3 Hz, 0.5H), 3.50 (t, *J* = 7.9 Hz, 1H), 3.42 (dd, *J* = 10.7, 5.2 Hz, 1H), 2.21 – 2.10 (m, 0.5H), 2.08 – 1.84 (m, 2H), 1.81 – 1.62 (m, 1H), 1.54 – 1.40 (m, 0.5H), 1.26 – 1.18 (m, 3H), 0.99 (t, *J* = 7.1 Hz, 1.5H), 0.90 (t, *J* = 7.1 Hz, 1.5H)

^{13}C NMR (101 MHz, $CDCl_3$) δ 178.49, 178.10, 168.71, 168.46, 167.79, 167.26, 137.63, 136.47, 129.45, 128.87, 128.72, 128.69, 127.92, 127.82, 62.18, 62.11, 61.92, 61.60, 56.40, 55.80, 55.38, 54.91, 50.21, 50.13, 29.57, 29.19, 25.26, 25.24, 14.13, 14.10, 13.85, 13.75.

HRMS (ESI+): Found $M+Na^+$: 356.1468, $C_{18}H_{23}NNaO_5^+$ requires 356.1468

FT-IR (cm^{-1}): 3238, 2959, 2916, 1727, 1688, 1259, 1024, 703

Diethyl 2-(2-((tert-butoxycarbonyl)amino)-1-phenylethyl)malonate (3.28)

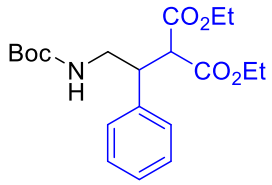

Performed according to General Procedure A with minor modifications. Reaction was performed in DMF with 2 eq carboxylic acid and 1 eq acceptor to yield a clear oil that turned to a white solid upon standing as an inseparable mixture of rotamers (28.1 mg, 37% yield). Spectroscopic data was consistent with previously reported values.[46]

^{1}H NMR (400 MHz, $CDCl_3$) δ 7.33 – 7.17 (m, 5H), 4.47 – 4.36 (m, 1H), 4.28 – 4.20 (q, *J* = 6.8 Hz, 2H), 3.95 – 3.85 (m, 2H), 3.74 - 3.67 (m, 1H), 3.65 – 3.47 (m, 2H), 3.45 – 3.28 (m, 1H), 1.37 (s, 9H), 1.29 (t, *J* = 7.1 Hz, 3H), 0.95 (d, *J* = 7.2 Hz, 3H).

^{13}C NMR (101 MHz, $CDCl_3$) δ 168.33, 167.66, 155.67, 139.01, 128.75, 128.50, 127.57, 79.43, 61.94, 61.46, 55.87, 45.53, 44.12, 28.44, 14.18, 13.82.

HRMS (ESI+): Found $M+Na^+$: 402.1888, $C_{15}H_{26}NaO_4^+$ requires 402.1887

Diethyl2-((1-(tert-butoxycarbonyl)pyrrolidin-2-yl)(p-tolyl)methyl)malonate (3.29)

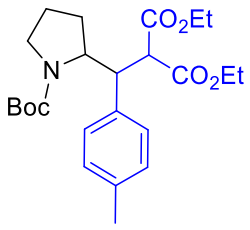

Performed according to General Procedure A with minor modifications. Reaction was performed with 1 eq acceptor on 0.242 mmol scale and in DMF with 5d irradiation to yield a colorless oil as an inseparable mixture of diastereoisomers and rotamers (75.3 mg, 72% yield).

^{1}H NMR (400 MHz, $CDCl_3$) δ 7.23 – 7.15 (d, *J* = 7.6 Hz, 0.4H), 7.14 – 6.97 (m, 3.5H), 4.39 (s, 0.2H), 4.34 – 4.24 (m, 0.7H), 4.22 – 4.01 (m, 3H), 3.90 – 3.66 (m, 2H), 3.65 – 3.56 (m, 0.2H), 3.54 – 3.45 (m, 0.5H), 3.43 (br s, 0.1H), 3.34 – 3.12 (m, 0.8H), 3.06 – 2.91 (m, 0.5H), 2.80 – 2.66 (m, 0.4H), 2.28 (s, 0.9H), 2.27 (s, 1.9H), 2.13 – 1.84 (m, 1.4H), 1.82 – 1.69 (m, 0.9H), 1.65 – 1.41 (m, 10.3H), 1.32 – 1.20 (m, 3.5H), 0.99 – 0.75 (m, 3.5H).

^{13}C NMR (101 MHz, $CDCl_3$) δ 168.77, 168.63, 168.55, 168.39, 168.24, 168.07, 156.19, 155.43, 155.04, 136.87, 136.72, 136.55, 135.58, 135.15, 129.47, 129.13, 128.97, 128.73, 80.29, 79.47, 79.24, 62.45, 62.29, 61.75, 61.42, 61.31, 61.13, 60.97, 60.40, 58.98, 54.96, 54.80, 53.98, 50.07, 49.89, 49.17, 47.98, 47.07, 46.65, 29.94, 29.59, 29.21, 28.70, 28.61, 23.74, 23.29, 22.36, 21.13, 21.12, 14.21, 14.13, 13.70, 13.64.

HRMS (ESI+): Found M+Na$^+$: 456.2357, $C_{24}H_{35}NNaO_6^+$ requires 456.2357; Found [M-Boc+H]$^+$: 334.2012, $C_{19}H_{28}NO_4^+$ requires 334.2013

FT-IR (cm^{-1}): 2976, 2937, 1731, 1688, 1366, 1162, 1096, 1033, 732

Diethyl 2-((1-(tert-butoxycarbonyl)pyrrolidin-2-yl)(4 methoxyphenyl) methyl)malonate (3.30)

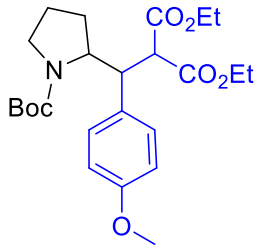

Performed according to General Procedure A with minor modifications. Reaction was performed with 1 eq acceptor on 0.223 mmol scale and in DMF with 5d irradiation to yield a colourless oil as an inseparable mixture of diastereomers and rotamers (65.4 mg, 65% yield).

^{1}H NMR (400 MHz, $CDCl_3$) δ 7.22 (d, *J* = 8.1 Hz, 0.4H), 7.16 – 7.03 (m, 1.5H), 6.84 – 6.73 (m, 2H), 4.39 (s, 0.3H), 4.32 – 4.00 (m, 3.6H), 3.87 – 3.66 (m, 5H), 3.63 – 3.44 (m, 1H), 3.42 – 3.12 (m, 1H), 3.05 – 2.89 (m, 0.5H), 2.77 – 2.66 (m,

0.4H), 2.10 – 1.67 (m, 2.3H), 1.64 – 1.36 (m, 10.4H), 1.30 – 1.15 (m, 3.5H), 0.94 – 0.75 (m, 3.5H).

^{13}C NMR (101 MHz, $CDCl_3$) δ 168.81, 168.63, 168.44, 168.23, 168.11, 158.79, 158.76, 156.20, 155.03, 131.81, 131.55, 130.61, 130.45, 130.24, 113.86, 113.67, 113.46, 80.30, 79.49, 79.27, 62.43, 62.32, 61.77, 61.64, 61.45, 61.32, 61.16, 61.00, 60.19, 58.89, 58.45, 55.28, 55.23, 55.04, 54.88, 54.27, 49.69, 49.62, 49.04, 47.96, 47.08, 46.66, 30.40, 30.12, 29.53, 29.18, 28.71, 28.62, 23.74, 23.30, 23.18, 22.38, 14.22, 14.14, 13.78, 13.74.

HRMS (ESI+): Found $M+Na^+$: 472.2307, $C_{24}H_{35}NNaO_7^+$ requires 472.2306; Found $[M\text{-Boc}+H]^+$: 350.1962, $C_{19}H_{28}NO_5^+$ requires 350.1962

FT-IR (cm^{-1}): 2976, 1731, 1688, 1366, 1247, 1162, 1033, 730

Dimethyl 2-(1-((benzyloxy)carbonyl)pyrrolidin-2-yl)succinate (3.31)

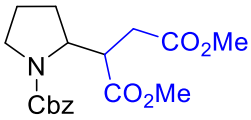

Performed according to General Procedure A to yield a colourless oil as an inseparable mixture of rotamers and diastereomers (40.5 mg, 58% yield). Spectroscopic data was consistent with previously reported values.[2]

^{1}H NMR (400 MHz, $CDCl_3$) δ 7.47 – 7.27 (m, 5H), 5.27 – 5.04 (m, 2H), 4.34 – 4.25 (m, 0.5H), 4.19 – 4.06 (m, 0.5H), 3.74 – 3.43 (m, 8H), 3.40 – 3.30 (m, 1H), 3.29 – 3.16 (m, 1H), 2.88 – 2.65 (m, 1H), 2.58 – 2.23 (m, 1H), 2.02 – 1.67 (m, 4H).

^{13}C NMR (101 MHz, $CDCl_3$) δ 173.64, 173.31, 173.09, 172.42, 172.35, 172.19, 155.46, 155.09, 136.95, 136.83, 136.63, 128.57, 128.40, 128.27, 128.08, 128.05, 127.91, 67.28, 66.93, 59.08, 58.42, 58.31, 57.50, 52.17, 52.15, 51.92, 47.84, 47.25, 47.01, 46.65, 44.65, 44.38, 44.22, 43.72, 33.67, 31.22, 30.61, 29.21, 28.17, 27.49, 24.22, 23.70, 23.63, 22.91.

HRMS (ESI+): Found $M+Na^+$: 372.1422, $C_{18}H_{23}NNaO_6^+$ requires 372.1418

Tert-butyl2-(2-(4,4,5,5-tetramethyl-1,3,2-dioxaborolan-2-yl)ethyl)pyrrolidine-1-carboxylate (3.32)

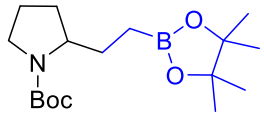

Performed according to General Procedure A in DMF with minor modifications. Reaction was performed using Cs_2CO_3 as base to yield the product as a mixture of rotamers (37.6 mg, 58%). Spectroscopic data was consistent with previously reported values.[49]

Vinyl boronic acid pinacol ester was distilled before use on a Kugelrohr under reduced pressure to remove residual inhibitor.

^{1}H NMR (400 MHz, $CDCl_3$) δ 3.86 – 3.53 (m, 1H), 3.46 – 3.10 (m, 2H), 1.95 – 1.58 (m, 5H), 1.44 (s, 9H), 1.22 (s, 12H), 0.80 – 0.62 (m, 2H).

^{13}C NMR (101 MHz, $CDCl_3$) δ 154.85, 83.09, 78.97, 59.24, 46.58, 46.24, 30.15, 29.21, 28.71, 28.11, 24.95, 24.93, 23.78, 23.14, 7.81 (br).

HRMS (ESI+): Found $M+Na^+$: 348.2331, $C_{17}H_{32}NBNaO_4^+$ requires 348.2317

Benzyl 2-(2-(phenylsulfonyl)ethyl)pyrrolidine-1-carboxylate (3.33)

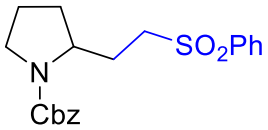

Performed according to General Procedure A with minor modifications. Reaction was performed with 1.5 eq carboxylic acid with 1 eq acceptor and using Cs_2CO_3 as base to yield a pale-yellow solid as a mixture of rotamers (19.1 mg, 26% yield). Spectroscopic data was consistent with previously reported values.[2]

^{1}H NMR (400 MHz, $CDCl_3$) δ 7.97 – 7.72 (m, 2H), 7.70 – 7.60 (m, 1H), 7.58 – 7.49 (m, 2H), 7.40 – 7.22 (m, 5H), 5.18 – 4.89 (m, 2H), 3.94 (s, 1H), 3.57 – 3.27 (m, 2H), 3.25 – 3.10 (m, 1H), 3.09 – 2.92 (m, 1H), 2.12 – 1.92 (m, 2H), 1.90 – 1.75 (m, 3H), 1.67 – 1.57 (m, 1H).

^{13}C NMR (101 MHz, $CDCl_3$) δ 155.52, 155.10, 139.26, 136.86, 136.51, 133.81, 129.41, 128.65, 128.14, 127.95, 67.26, 66.94, 56.54, 55.96, 53.98, 53.72, 46.89, 46.59, 31.19, 30.77, 27.94, 23.80, 23.10.

HRMS (ESI+): Found $M+Na^+$: 396.1250, $C_{20}H_{23}NNaO_4S^+$ requires 396.1240

Tert-butyl-2-((1-(4,4,5,5-tetramethyl-1,3,2-dioxaborolanyl)cyclopropyl)methyl)pyrrolidine-1-carboxylate (3.34)

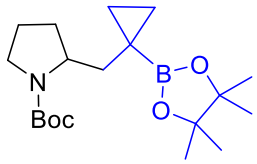

2-(4-chlorobut-1-en-2-yl)-4,4,5,5-tetramethyl-1,3,2-dioxaborolane (61 µL, 0.3 mmol, 1.5 eq) Boc-Pro-OH (43.0 mg, 0.2 mmol), CTF-2 (100 mg), and Cs_2CO_3 (78 mg, 0.24 mmol, 1.2 eq) were suspended in DMF (4 mL), sparged with nitrogen, and irradiated on a PennOC Photoreactor at 420nm for 48 hours. The reaction mixture was diluted with ethyl acetate (3 × 4 mL) and washed with water (20 mL). The organic layer was dried with $MgSO_4$, filtered and concentrated under vacuum. The crude residue was purified by column chromatography to yield the product as a colourless oil (30.4 mg, 43% yield). Spectroscopic data was consistent previously reported values.[24]

^{1}H NMR (400 MHz, $CDCl_3$) δ 4.07 – 3.76 (m, 1H), 3.41 – 3.19 (m, 2H), 2.10 – 1.50 (m, 6H), 1.43 (s, 9H), 1.20 (s, 6H), 1.18 (s, 6H), 0.76 – 0.53 (m, 2H), 0.52 – 0.27 (m, 2H).

^{13}C NMR (101 MHz, $CDCl_3$) δ 154.74, 83.09, 78.94, 78.67, 57.81, 57.36, 46.27, 45.92, 39.87, 39.34, 29.88, 28.76, 24.83, 24.67, 23.74, 23.05, 13.60, 13.27, 10.13, 1.79 (br).

^{11}B NMR (128 MHz, $CDCl_3$) δ 33.51.

HRMS (ESI+): Found $M+Na^+$: 374.2486, $C_{19}H_{34}NBNaO_4^+$ requires 374.2474

N.B: While the reaction was also successful on the SynLED parallel photoreactor with 24 mg / 0.2mmol substrate loading of CTF-2, it also appeared to result in significant formation of the ester alkylation product that was difficult to separate from the decarboxylative cyclopropanated product. We found that using 420nm LEDs on a PennOC photoreactor (along with dilution) led to higher yields, presumably due to better radical decarboxylation. 2-(4-chlorobut-1-en-2-yl)-4,4,5,5-tetramethyl-1,3,2-dioxaborolane was prepared according to the method described by Aggarwal *et al.* [24]

(4-Fluoropiperidin-1-yl)(phenyl)methanone (3.43)

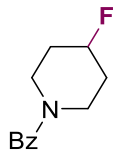

1-benzoylpiperidine-4-carboxylic acid (46.6 mg, 0.2 mmol, 1 eq), NaH_2PO_4 (57 mg, 0.4 mmol, 2 eq), and SelectFluor (212 mg, 0.6 mmol, 3 eq) was suspended in MeCN/H_2O (1mL, 1:1 v/v) and irradiated for 2 days at 420 nm using a PennOC photoreactor. The reaction mixture was concentrated under vacuum and purified by column chromatography (diethyl ether/petroleum ether) to yield product as a colourless oil (17.0 mg, 41% yield). Spectroscopic data is consistent with previously reported values.[25]

^{1}H NMR (400 MHz, $CDCl_3$) δ 7.44 – 7.36 (m, 5H), 4.99 – 4.80 (m, 1H), 4.13 – 3.83 (m, 1H), 3.78 – 3.22 (m, 3H), 2.12 – 1.71 (m, 4H).

^{13}C NMR (101 MHz, $CDCl_3$) δ 170.62, 135.97, 129.86, 128.67, 126.94, 87.79 (^{1}C-F) (d, *J* = 171 Hz), 43.68, 38.16.

^{19}F NMR (376 MHz, $CDCl_3$) δ -183.17.

HRMS (ESI+): Found $M+H^+$: 208.1161, $C_{12}H_{15}FNO^+$ requires 208.1132

Tert-butyl 2-(4-(trifluoromethyl)phenyl)pyrrolidine-1-carboxylate (3.44)

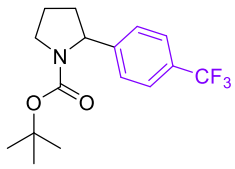

Boc-Pro-OH (32 mg, 0.15 mmol, 1.5 eq), 4-bromobenzo trifluoride (14 µL, 0.1 mmol, 1 eq), CTF-2 (12 mg), $NiCl_2$(glyme) (2.2 mg, 0.1 eq), di-tert butyl bipyridine (4 mg, 0.15 eq) and Cs_2CO_3 (50 mg) were suspended in DMF (0.5 mL) and irradiated for 1 day with at 420nm irradiation in a PennOC photoreactor. The reaction mixture was diluted with ethyl acetate (5 mL) and biphenyl standard (1 eq) and analysed by GC-MS. (51% GC-MS yield, relative to biphenyl standard). The GC-MS traces were compared to authentic product and with the reaction mixture of $Ir[(dFCF_3ppy)_2(dtbbpy)][PF_6]$ under White LED floodlights using our discovery workflow. We were unable to isolate this product cleanly by column chromatography.

GCMS (TIC): 315 [M], 214 [M-Boc]

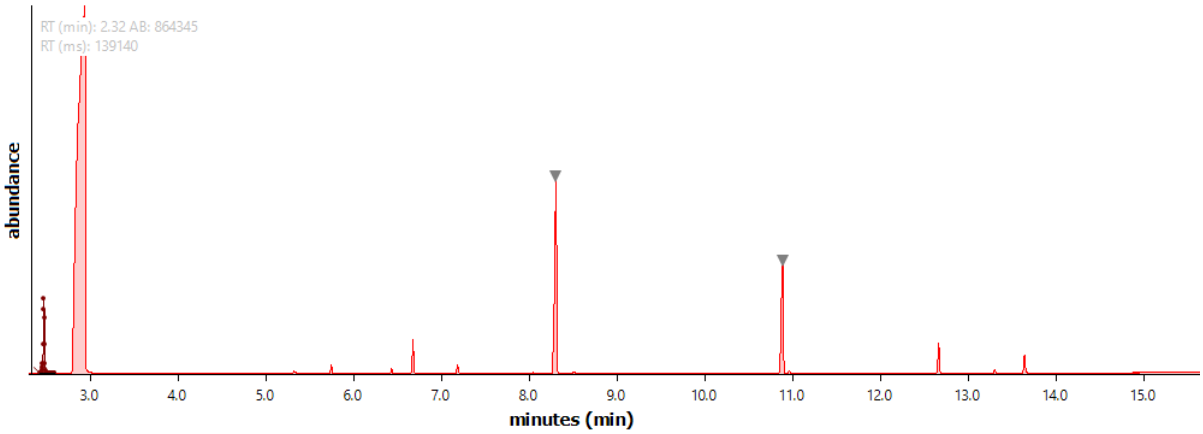

Figure 3-23: GC-Trace of decarboxylative conjugate addition reaction.

RT (min)	Area
8.301	98879724
10.887	50593567

Figure 3-24: Areas of GC-MS spectrum of biphenyl (8.3 min elution) and decarboxylative arylation product (10.9 min elution)

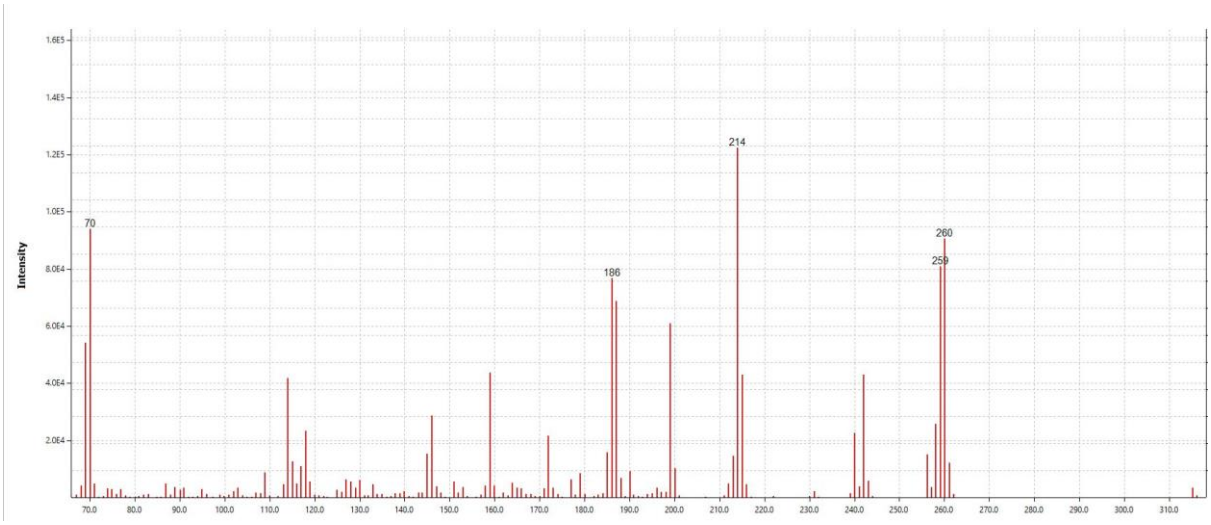

Figure 3-25: GC-MS spectrum of decarboxylative arylation product

Tert-butyl-2-benzylpyrrolidine-1-carboxylate (3.45)

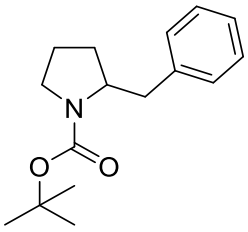

Boc-Pro-OH (161 mg, 0.75 mmol, 1.5 eq), benzyl chloride (58 µL, 0.50 mmol, 1 eq), CTF-2 (60 mg), K_2CO_3 (138 mg, 1 mmol, 2 eq) $NiCl_2$(glyme) (11 mg, 0.05 mmol, 0.1 eq), H_2O (180 µL, 10 mmol, 20 eq), and dimethoxy bipyridine (11 mg, 0.05 mmol, 0.1 eq) were suspended in MeCN (5 mL) and irradiated for 3 days with 427nm irradiation using Kessil lamps. The reaction mixture was repeatedly diluted with diethyl ether (8 mL x 3), allowed to settle, decanted and concentrated under vacuum. Column chromatography using diethyl ether/hexane afforded the product as a colourless oil (70.4 mg, 54% yield). Spectroscopic data was consistent with previously reported values.[27]

^{1}H NMR (400 MHz, $CDCl_3$) δ 7.35 – 7.10 (m, 5H), 4.12 – 3.87 (m, 1H), 3.45 – 3.21 (m, 2H), 3.10 (m, 1H), 2.63 – 2.46 (m, 1H), 1.74 (s, 4H), 1.51 (s, 9H).

^{13}C NMR (101 MHz, $CDCl_3$) δ 154.64, 139.30, 129.67, 129.47, 128.48, 128.35, 126.29, 126.16, 79.35, 79.08, 58.95, 58.78, 46.89, 46.39, 40.68, 39.66, 29.73, 28.95, 28.70, 23.50, 22.73.

HRMS (ESI+): Found M-OtBu: 188.1086, $C_{12}H_{13}NO^+$ requires 188.1075; Found $M+Na^+$: 284.1632, $C_{16}H_{23}NNaO_2^+$ requires 284.1621

N.B – Sonication before irradiation, and vigorous stirring was essential for this reaction. The addition of water often caused aggregation of CTF-2 with the potassium carbonate base.

Tert-butyl 5-(p-tolyl)-2,5-diazabicyclo[2.2.1]heptane-2-carboxylate (3.48)

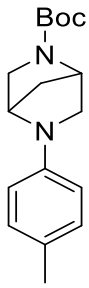

tert-butyl 2,5-diazabicyclo[2.2.1]heptane-2-carboxylate (79.2 mg, 0.4 mmol), $[Co(dmgH)_2(DMAP)][Cl]$ (7.2 mg, 4mol%), AcOH (5µL, 0.2 eq), DABCO (68 mg, 0.6 mmol, 1.5 eq), CTF-2 (48 mg), 4-methyl cyclohexanone (49µL, 0.4 mmol), and acetonitrile (2 mL) are combined under nitrogen, sparged, and irradiated for 3 days under 427nm irradiation with Kessil lamps. The mixture was repeatedly diluted with diethyl ether (8 mL x 3), shaken thoroughly, the polymer allowed to settle to the bottom, and the supernatant removed. The combined ether layers were concentrated under vacuum and purified by column chromatography using diethyl ether/hexane to afford the product as an off-white solid as a mixture of rotamers (75.4 mg, 65% yield). Spectroscopic data was consistent with previously reported values.[28]

^{1}H NMR (400 MHz, $CDCl_3$) δ 7.14 – 6.98 (m, 2H), 6.52 (d, *J* = 5.7 Hz, 2H), 4.62 (s, 0.5H), 4.47 (s, 0.4H), 4.35 (s, 1H), 3.59 (d, *J* = 8.1 Hz, 1H), 3.53 – 3.28 (m, 2H), 3.19 (d, *J* = 8.5 Hz, 0.6H), 3.10 (d, *J* = 8.6 Hz, 0.4H), 2.26 (s, 3H), 2.07 – 1.82 (m, 2H), 1.45 (s, 4H), 1.40 (s, 5H).

^{13}C NMR (101 MHz, $CDCl_3$) δ 154.19, 144.36, 130.03, 126.50, 113.08, 79.72, 57.49, 57.18, 56.49, 50.95, 50.58, 37.82, 37.40, 28.65, 28.56, 20.45.

HRMS (ESI+): Found $M+H^+$: 289.1920, $C_{17}H_{25}N_2O_2^+$ requires 289.1911

^{13}C NMR spectrum for this sample was processed with apodization in MestReNova (Exponential Function – 6.8Hz) for improved visual clarity.

Diethyl 2-(3-(cyclopentyloxy)-4-methoxybenzylidene)malonate (3.51)

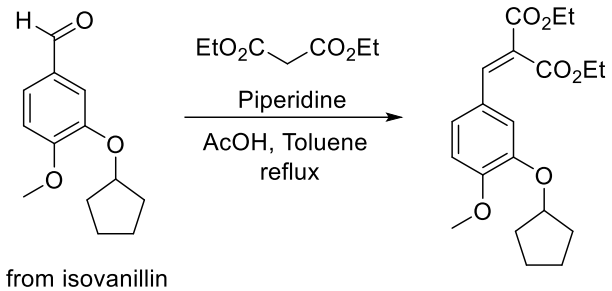

from isovanillin

3-(cyclopentyloxy)-4-methoxybenzaldehyde was synthesized from isovanillin exactly as reported by Aggarwal et al[50] in 94% yield.

3-(cyclopentyloxy)-4-methoxybenzaldehyde (1226 mg, 5.57 mmol, 1 eq), diethyl malonate (0.85 mL, 5.57 mmol, 1.1 eq), piperidine (28 µl) and acetic acid (0.14 mL) were dissolved in toluene (7 mL) and refluxed using a Dean-Stark apparatus. The reaction mixture was then concentrated, and further portions of piperidine (0.28 mL) acetic acid (0.92 mL), diethyl malonate (0.94 mL, 1.1 eq), and toluene (7 mL) were added, and refluxed for another 3 days without a Dean-Stark apparatus. The reaction mixture was concentrated and purified directly by column chromatography using diethyl ether/hexane to yield the product as a pale-yellow oil that solidified to a white solid under extended vacuum. (1254 mg, 62% yield). Method was adapted from a reported procedure.[51]

^{1}H NMR (400 MHz, $CDCl_3$) δ 7.63 (s, 1H), 7.08 – 7.00 (m, 2H), 6.84 (d, *J* = 8.3 Hz, 1H), 4.75 – 4.68 (m, 1H), 4.34 (q, *J* = 7.1 Hz, 2H), 4.28 (q, *J* = 7.1 Hz, 2H), 3.86 (s, 3H), 2.00 – 1.76 (m, 6H), 1.68 – 1.58 (m, 2H), 1.32 (t, *J* = 7.1 Hz, 6H).

^{13}C NMR (101 MHz, $CDCl_3$) δ 167.41, 164.65, 152.45, 147.76, 142.27, 125.59, 124.25, 123.62, 115.31, 111.56, 80.66, 61.72, 61.56, 56.11, 32.88, 24.17, 14.30, 14.12.

HRMS (ESI+): Found $M+Na^+$: 385.1621, $C_{20}H_{26}NaO_6^+$ requires 385.1622

Diethyl2-(2-((tert-butoxycarbonyl)amino)-1-(3-(cyclopentyloxy)-4 methoxyphenyl)ethyl)malonate (3.52)

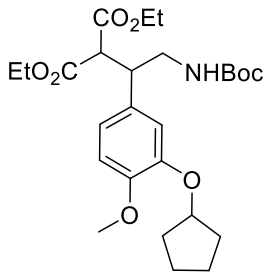

Diethyl 2-(3-(cyclopentyloxy)-4-methoxybenzylidene)malonate (64.9 mg, 0.179 mmol, 1 eq), Boc-Gly-OH (31.3 mg, 0.179 mmol, 1 eq), K_2HPO_4 (62 mg, 2 eq), and CTF-2 (22 mg) were suspended in DMF (0.9 mL) and irradiated for 2 days with a SynLED photoreactor. The reaction mixture was diluted with ethyl acetate (4 mL × 3) and extracted from water. The organic layer was dried with $MgSO_4$, filtered and concentrated under vacuum. The crude residue was purified by column chromatography (EtOAc/Petrol Ether gradient) to yield the product as a colourless oil that turned to a white solid upon standing (41.8 mg, 42% yield).

^{1}H NMR (400 MHz, $CDCl_3$) δ 6.81 – 6.77 (m, 1H), 6.76 – 6.66 (m, 2H), 4.75 (dq, *J* = 9.4, 3.2 Hz, 1H), 4.39 (s, 1H), 4.24 (q, *J* = 7.1 Hz, 2H), 3.99 – 3.88 (m, 2H), 3.81 (s, 3H), 3.65 (d, *J* = 10.0 Hz, 1H), 3.57 – 3.45 (m, 2H), 3.41 – 3.25 (m, 1H), 2.00 – 1.77 (m, 6H), 1.67 - 1.60 (m, 2H), 1.38 (s, 9H), 1.29 (t, *J* = 7.1 Hz, 3H), 0.99 (t, *J* = 7.1 Hz, 3H).

^{13}C NMR (101 MHz, $CDCl_3$) δ 168.35, 167.73, 155.71, 149.40, 147.69, 131.20, 120.53, 115.31, 112.12, 80.51, 61.93, 61.47, 56.18, 56.07, 45.06, 44.19, 32.94, 32.91, 28.48, 24.18, 14.21, 13.94.

HRMS (ESI+): Found M+Na^+: 516.2574, $C_{26}H_{39}NNaO_8^+$ requires 516.2568

FT-IR (cm^{-1}): 3384, 2945, 2868, 1722, 1683, 1512, 1160, 1016

(±) Rolipram (3.54)

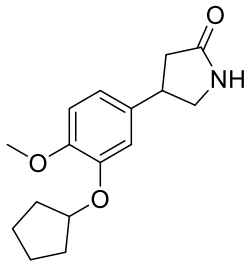

Diethyl2-(2-((tert-butoxycarbonyl)amino)-1-(3-(cyclopentyloxy)-4 methoxyphenyl)ethyl)malonate (67.7 mg, 0.137 mmol) was suspended with KOH (2 eq) solution in water (5 mL) and heated to reflux. The solution was acidified with slow addition of concentrated HCl, stirred, and extracted with ethyl acetate (4 mL × 3). The concentrated residue was dissolved in toluene (7 mL) and refluxed at 110 °C overnight. The concentrated residue was purified by column chromatography (5% MeOH in DCM) to yield the product as a white solid (24.4 mg, 65% yield). Spectroscopic data was consistent with previously reported values. [52]

^{1}H NMR (400 MHz, $CDCl_3$) δ 6.90 – 6.70 (m, 3H), 6.20 (s, 1H), 4.83 – 4.70 (m, 1H), 3.83 (s, 3H), 3.75 (t, *J* = 8.7 Hz, 1H), 3.68 – 3.56 (m, 1H), 3.38 (dd, *J* = 9.2, 7.5 Hz, 1H), 2.71 (dd, *J* = 16.9, 8.9 Hz, 1H), 2.47 (dd, *J* = 16.9, 8.9 Hz, 1H), 1.96 – 1.78 (m, 6H), 1.66 – 1.56 (m, 2H).

^{13}C NMR (101 MHz, $CDCl_3$) δ 177.82, 149.34, 148.05, 134.65, 118.94, 113.96, 112.35, 80.74, 56.29, 49.87, 40.13, 38.19, 32.95, 24.15

HRMS (ESI+): Found $M+H^+$: 276.1619, $C_{16}H_{22}NO_3^+$ requires 276.1594

NMR Spectra of Products

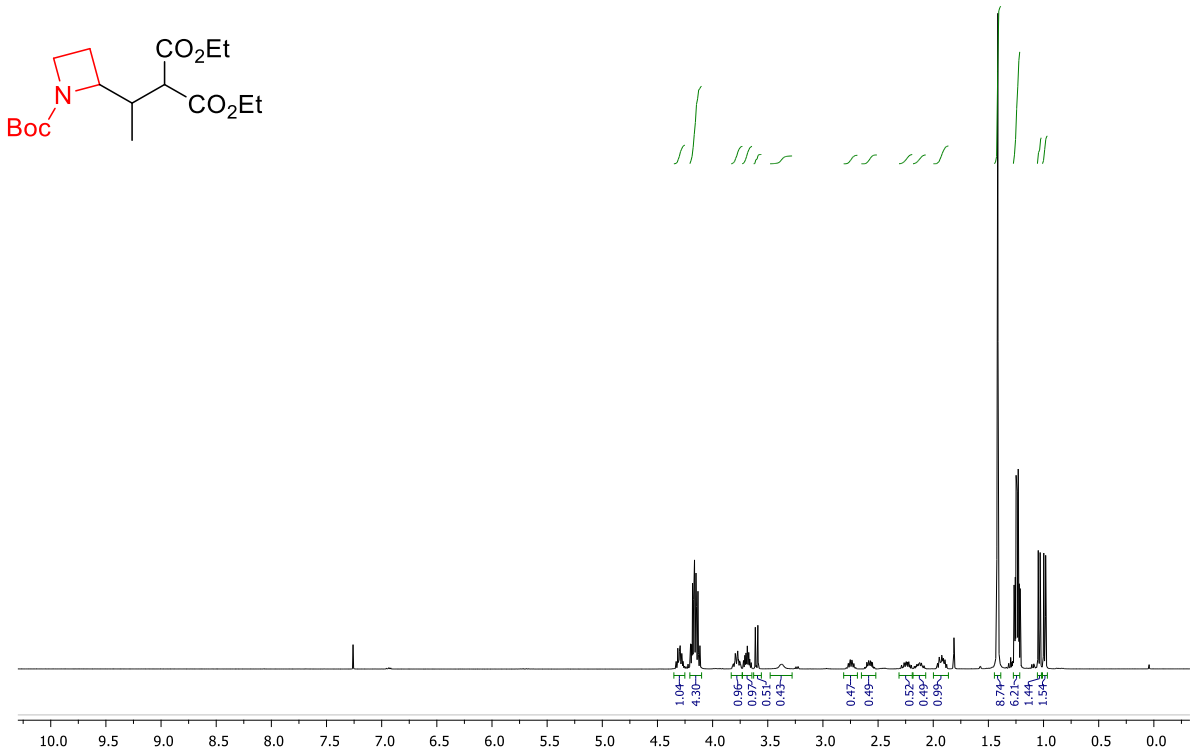

Figure 3-26: 1H NMR spectrum of product 3.7

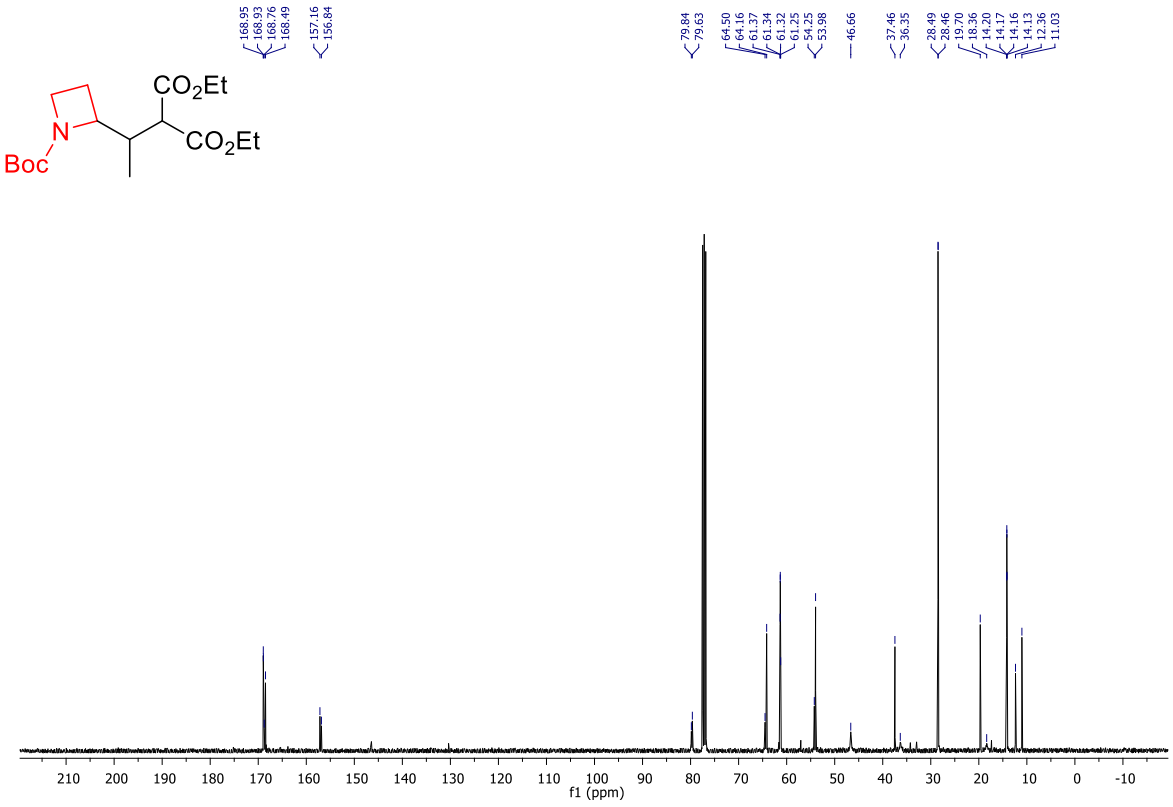

Figure 3-27: 13C NMR spectrum of product 3.7

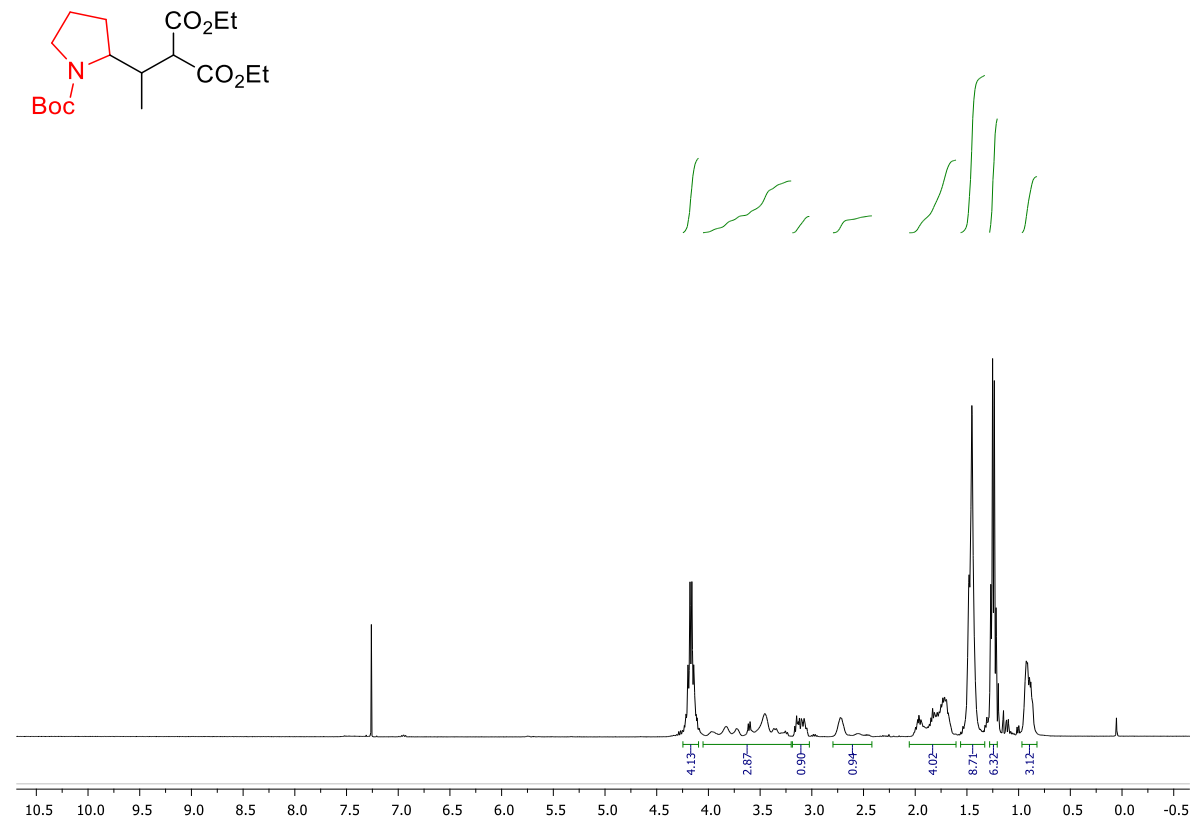

Figure 3-28: 1H NMR spectrum of product 3.8

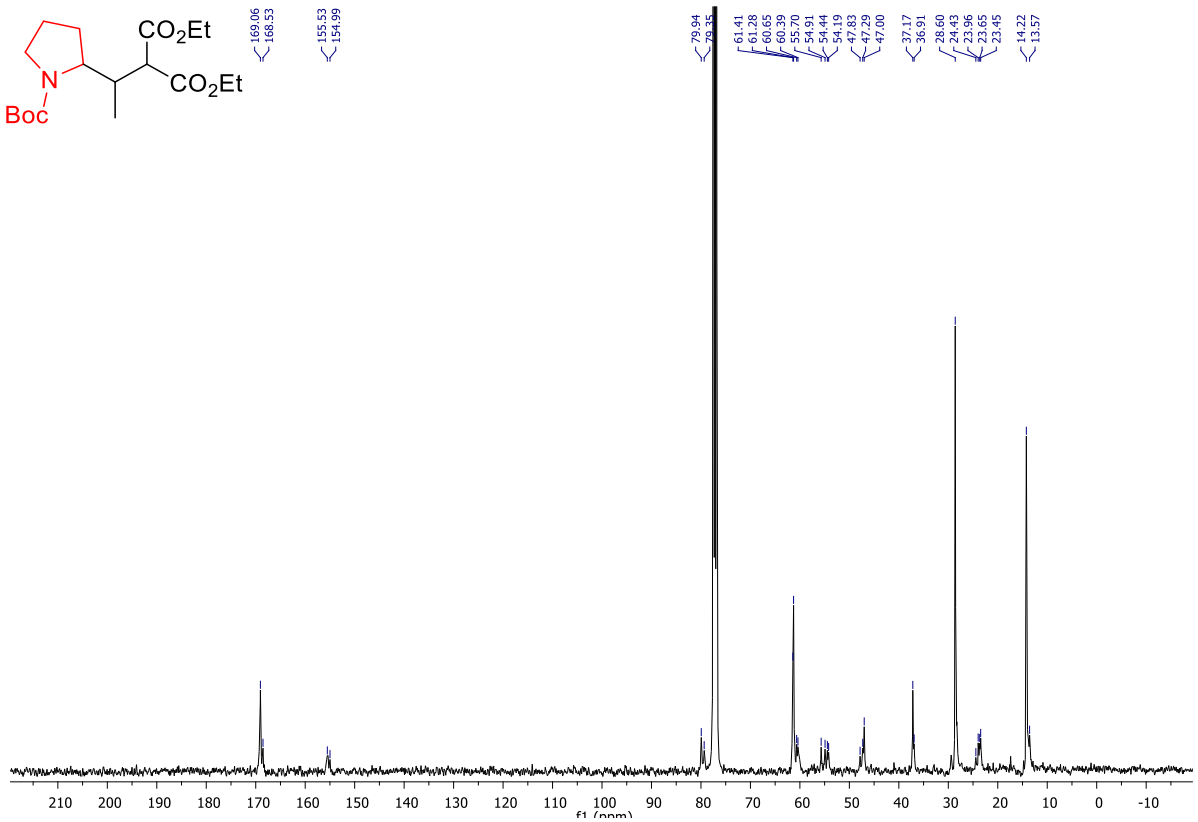

Figure 3-29: 13C NMR spectrum of product 3.8

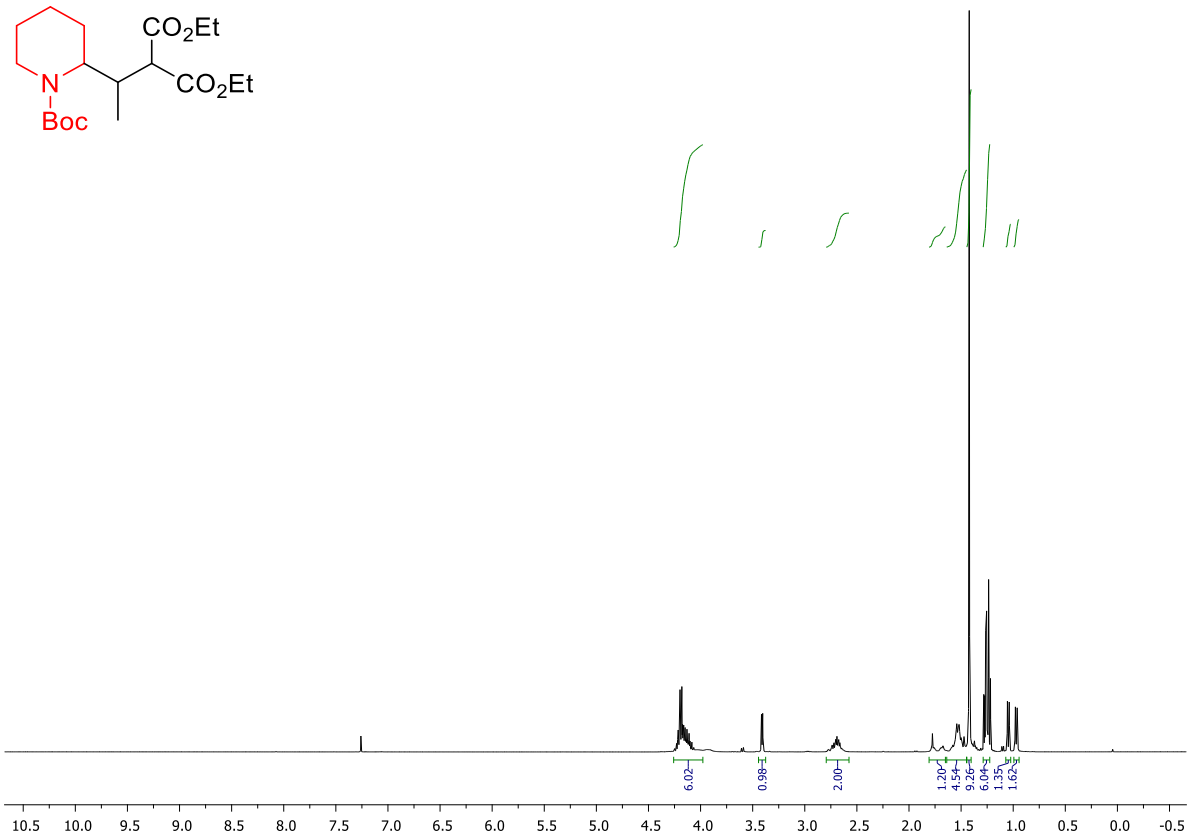

Figure 3-30: 1H NMR spectrum of product 3.9

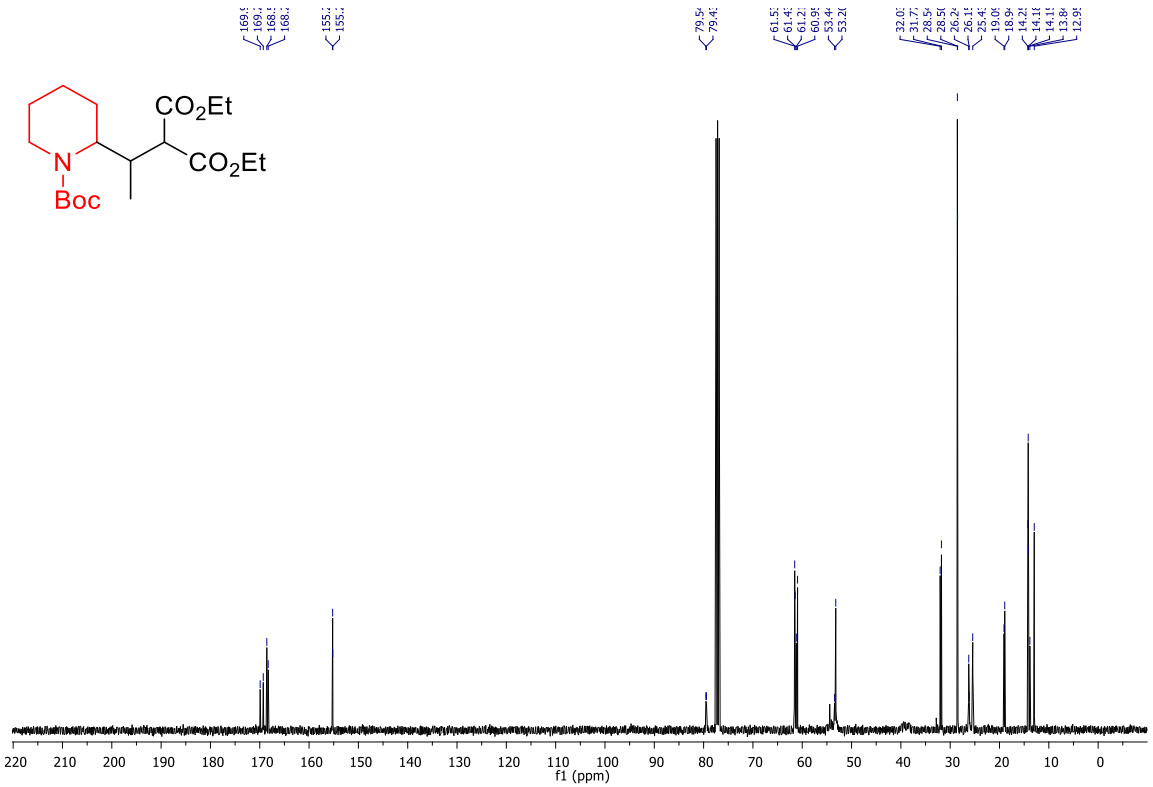

Figure 3-31: Figure 3 39: 13C NMR spectrum of product 3.9

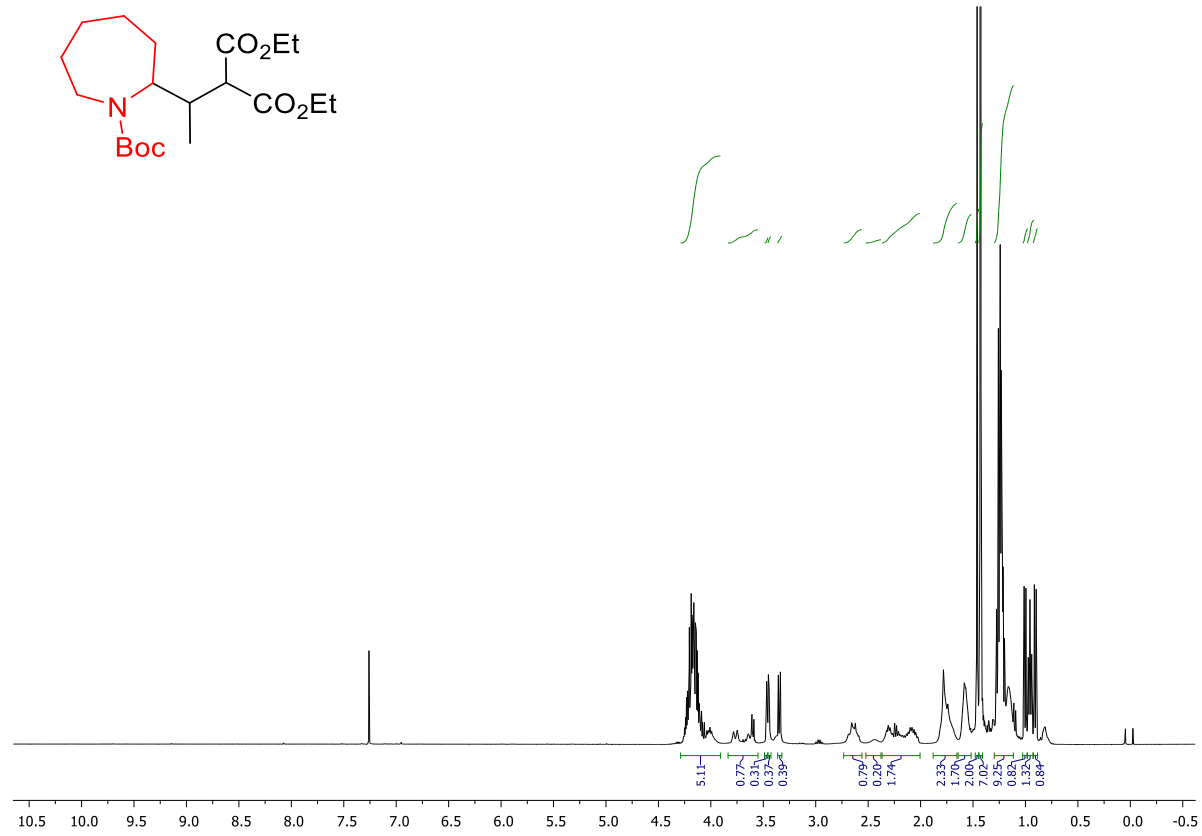

Figure 3-32: 1H NMR spectrum of product 3.10

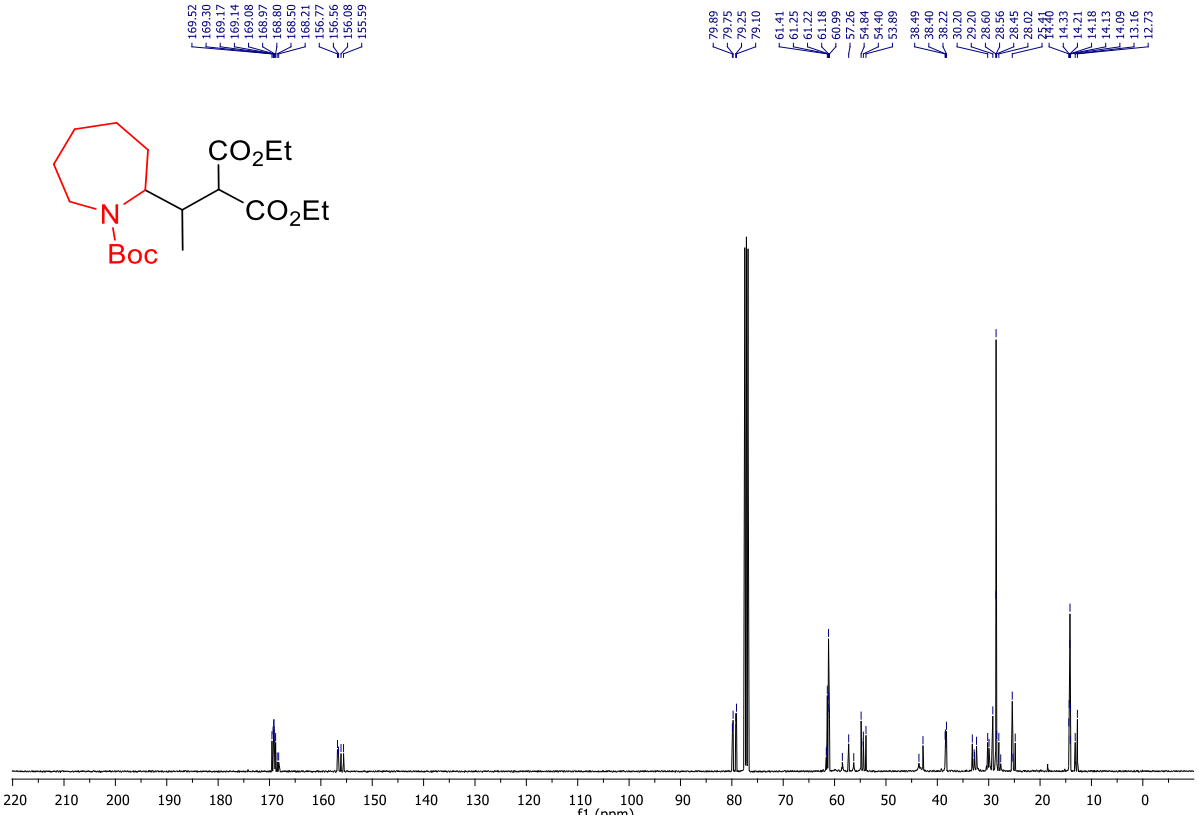

Figure 3-33: 13C NMR spectrum of product 3.10

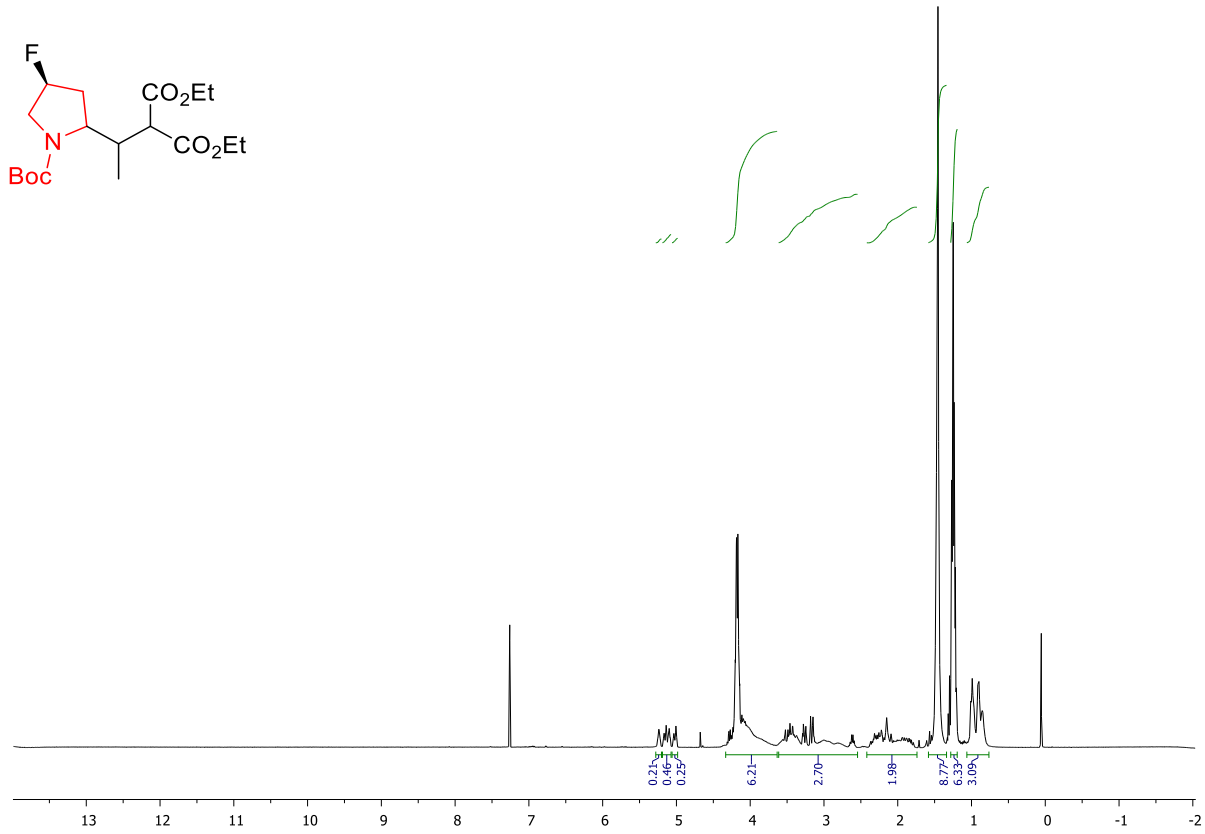

Figure 3-34: 1H NMR spectrum of product 3.11

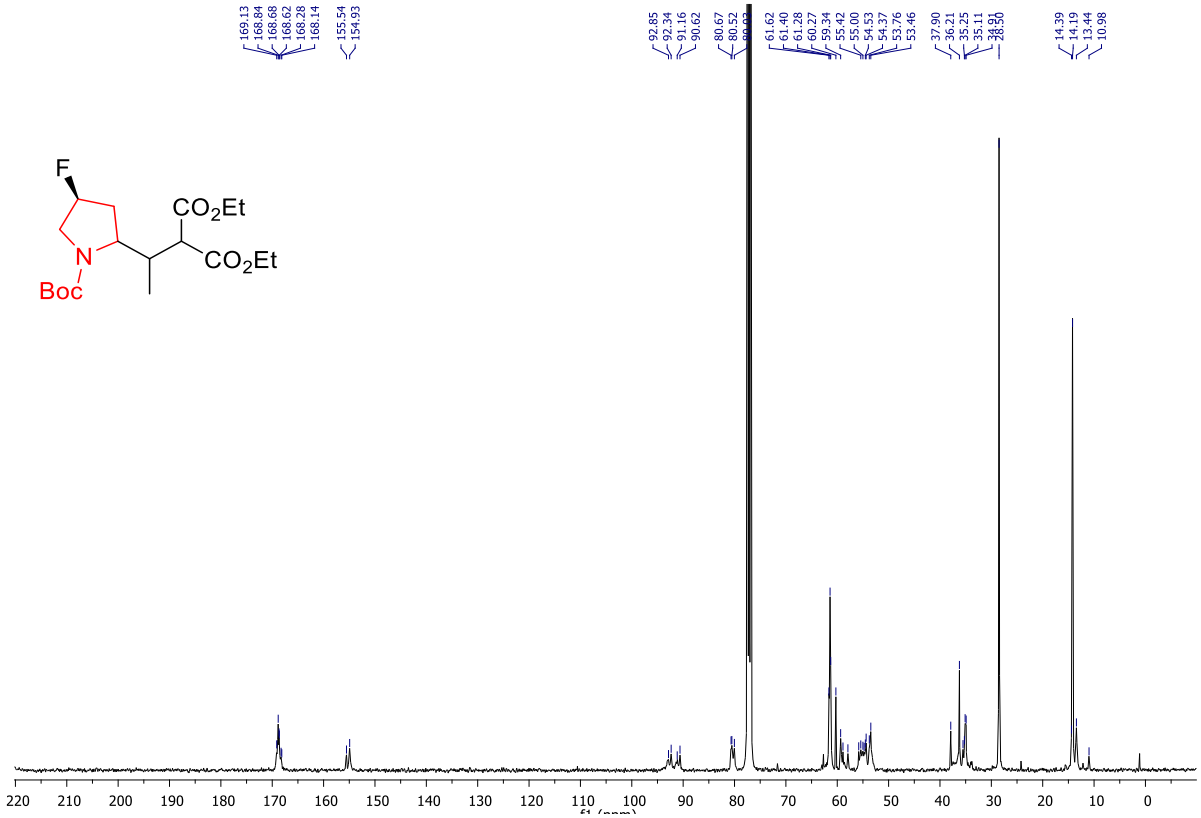

Figure 3-35: 13C NMR spectrum of product 3.11

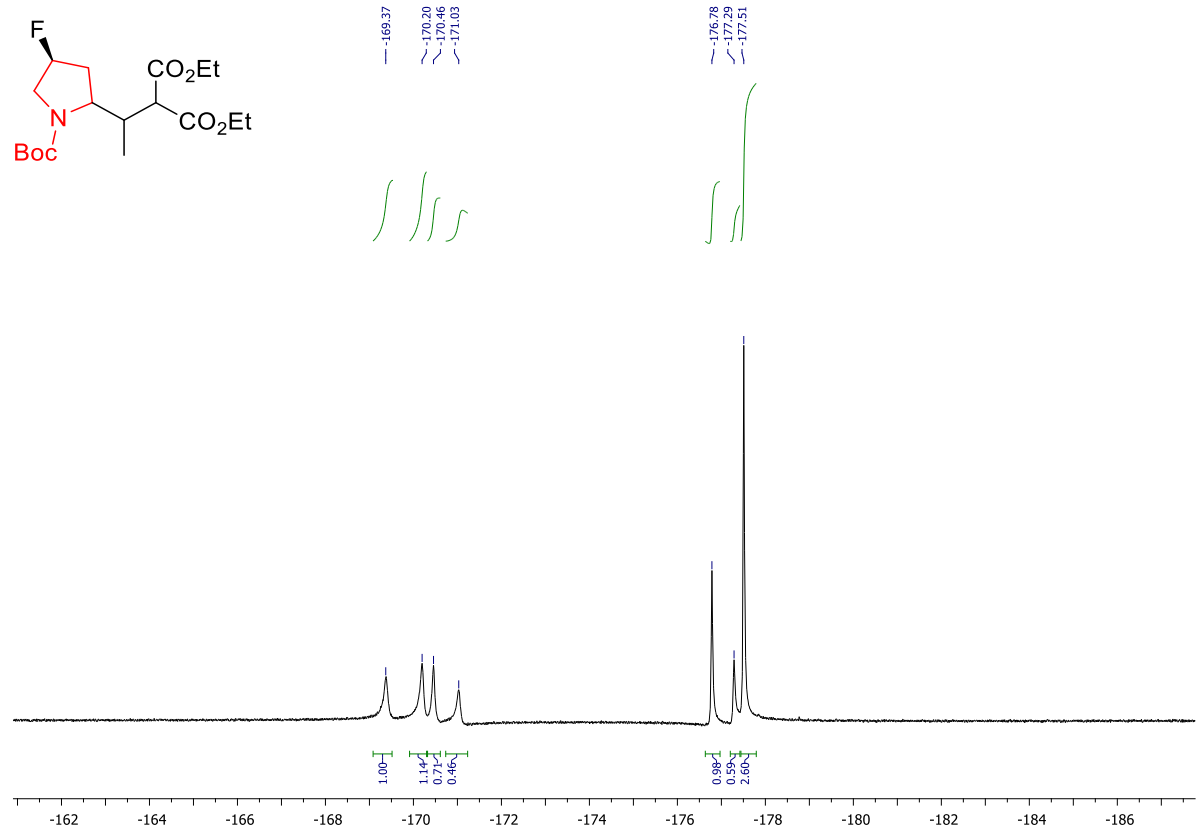

Figure 3-36: 19F NMR spectrum of product 3.11

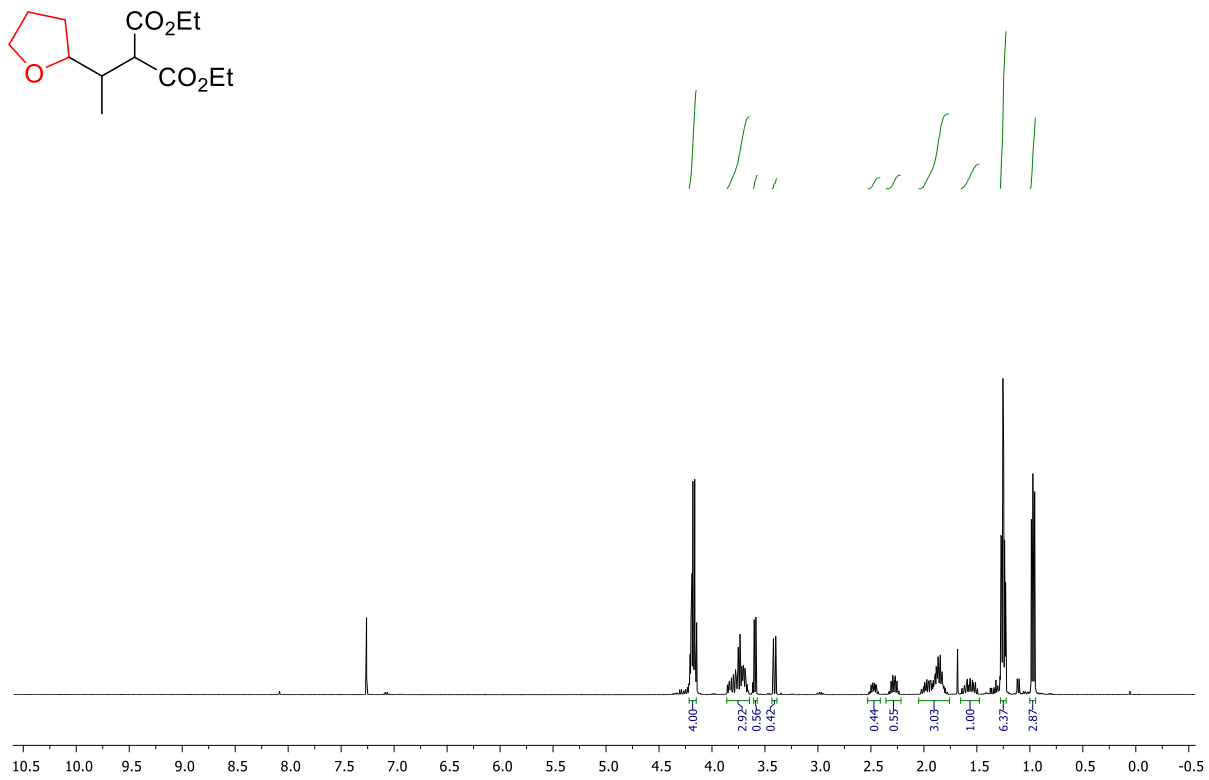

Figure 3-37: 1H NMR spectrum of product 3.12

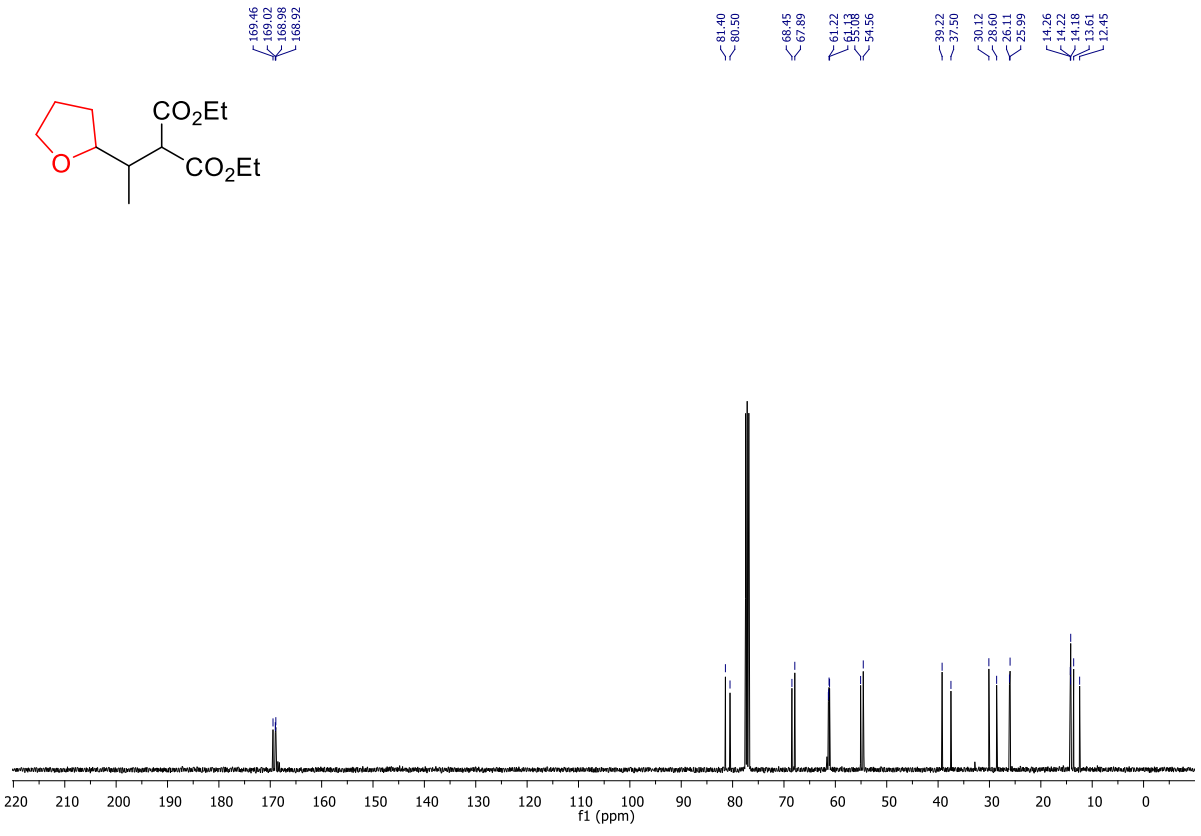

Figure 3-38: 13C NMR spectrum of product 3.12

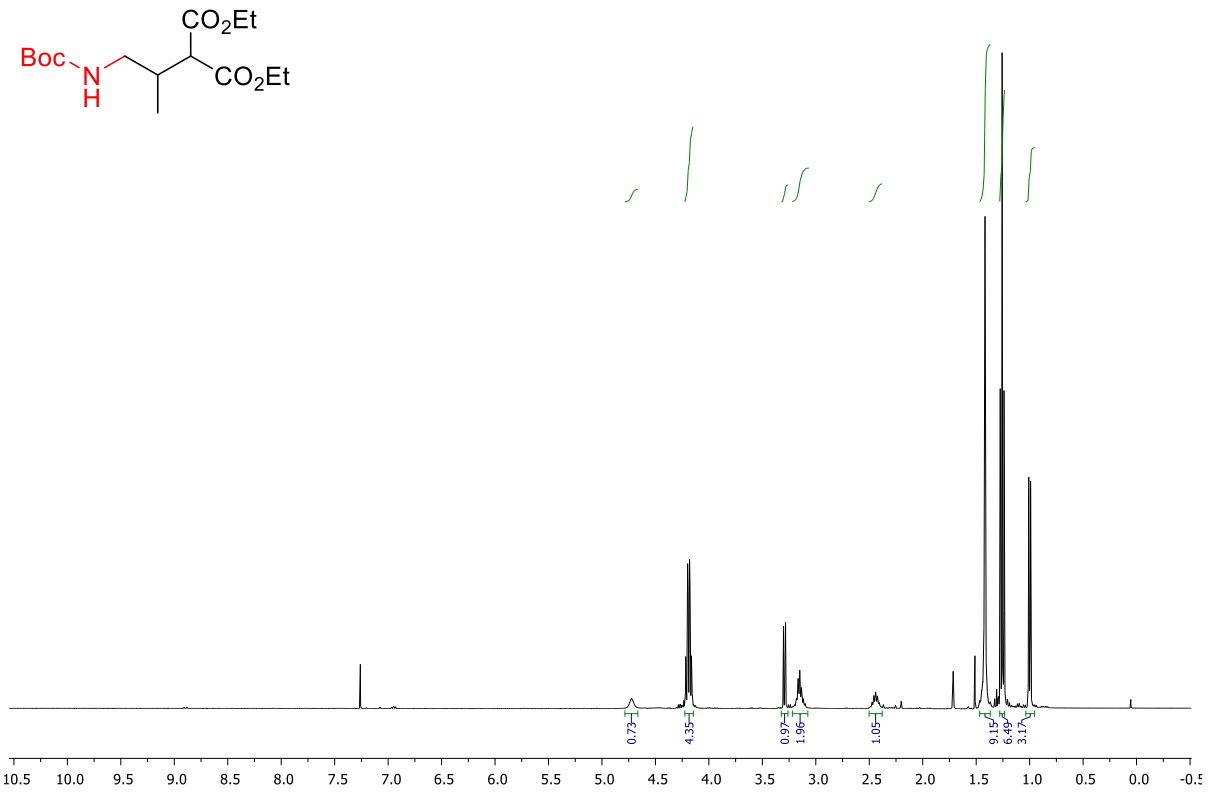

Figure 3-39: 1H NMR spectrum of product 3.13

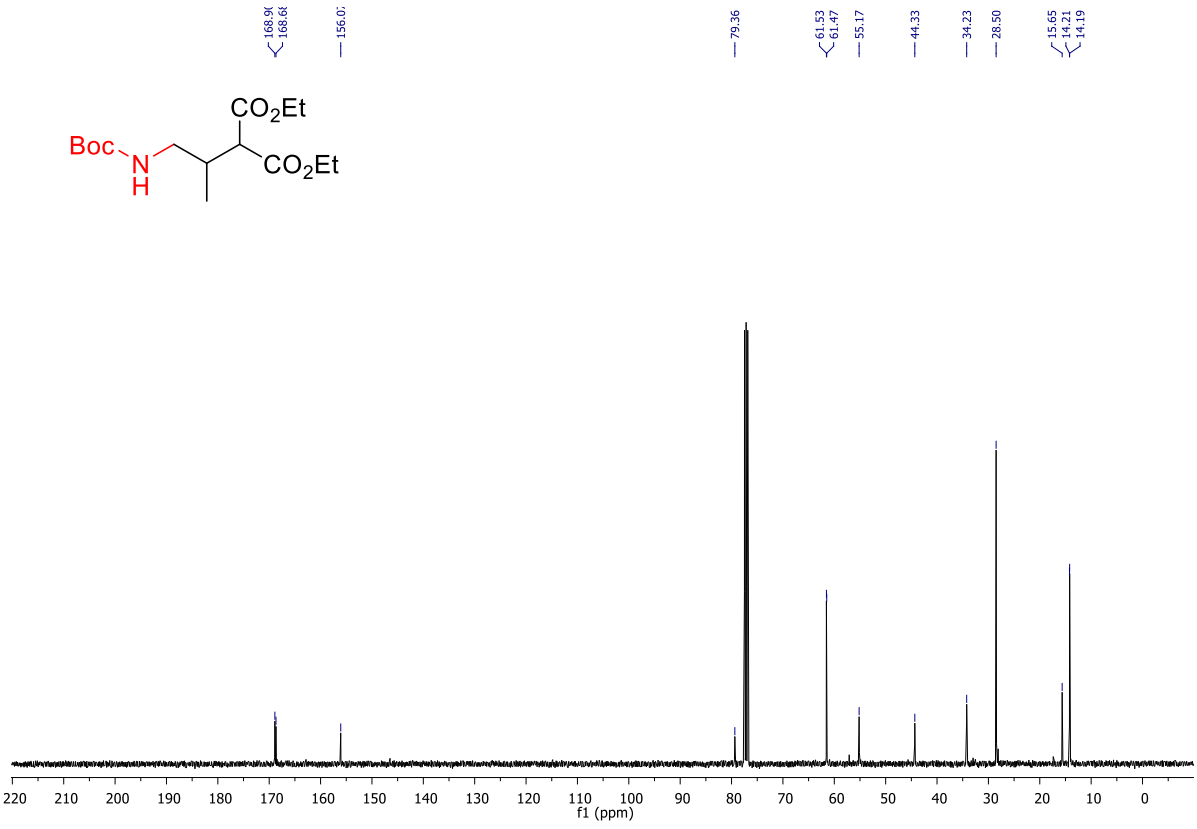

Figure 3-40: 13C NMR spectrum of product 3.13

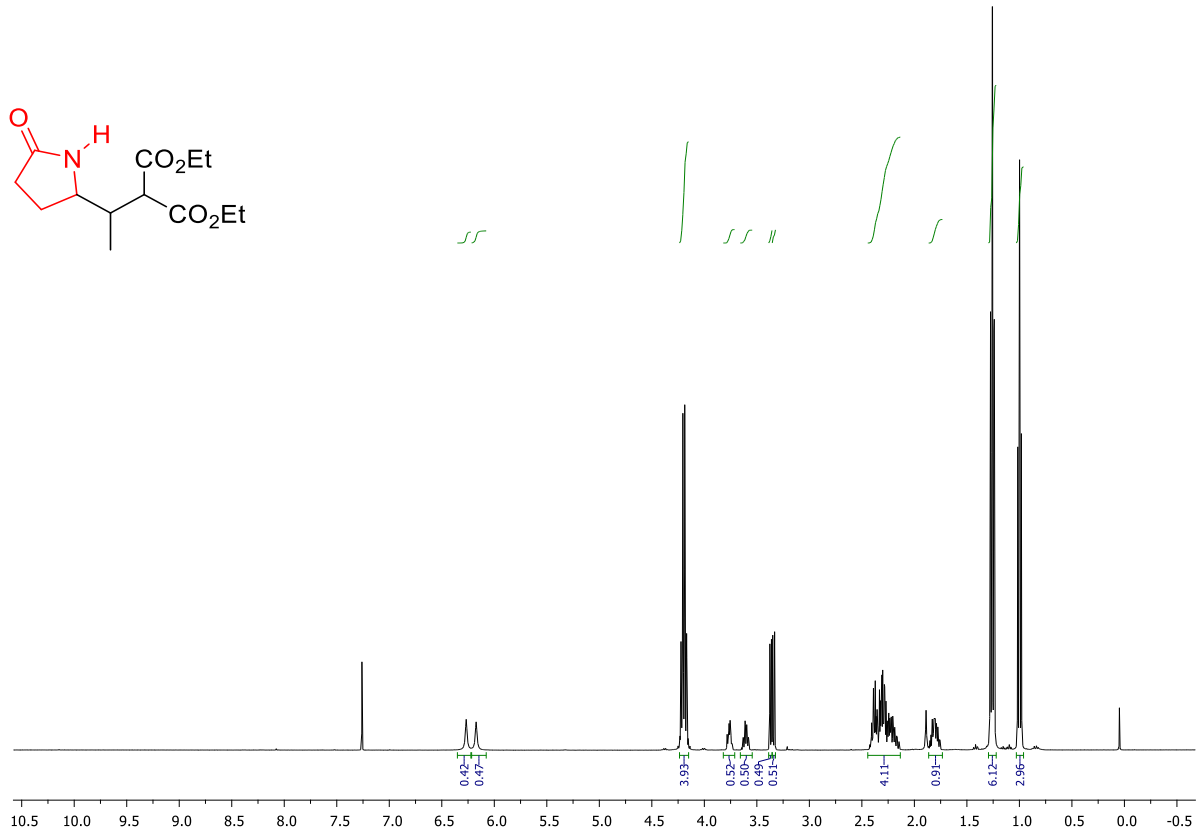

Figure 3-41: 1H NMR spectrum of product 3.14

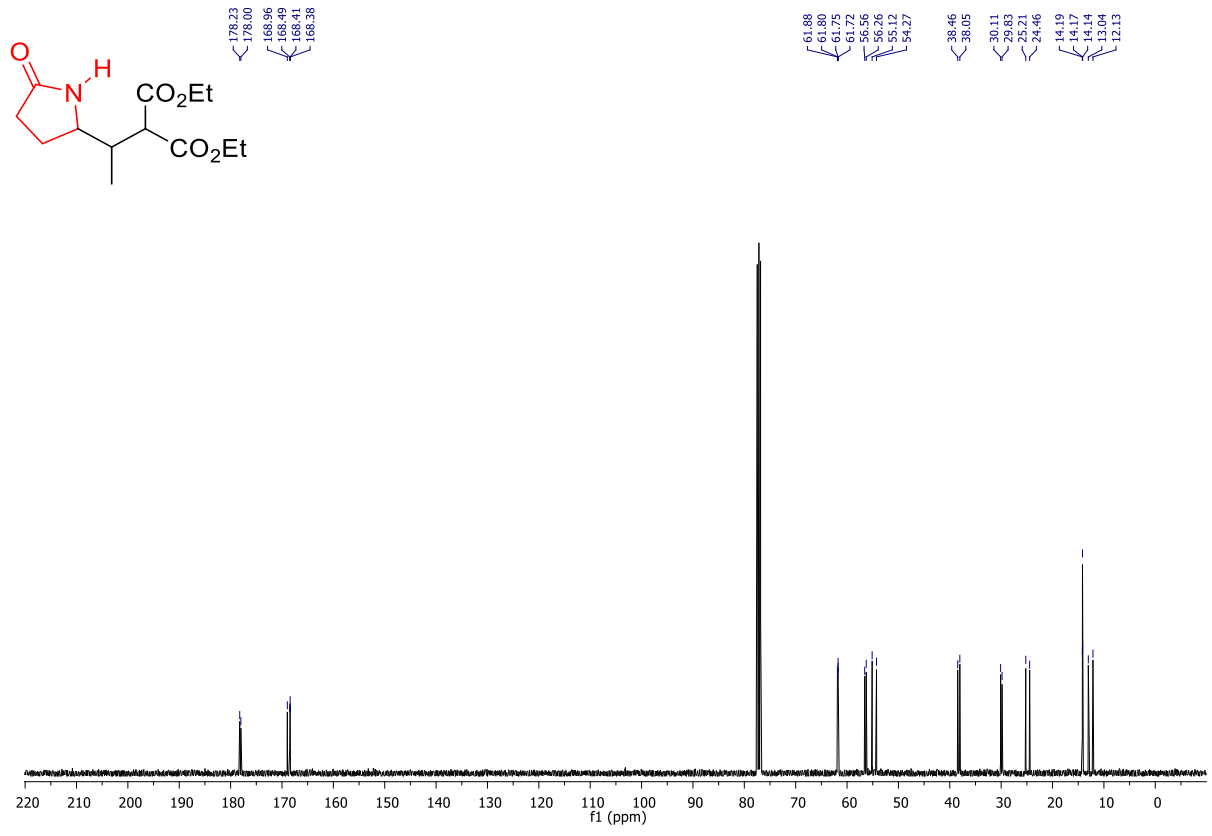

Figure 3-42: 13C NMR spectrum of product 3.14

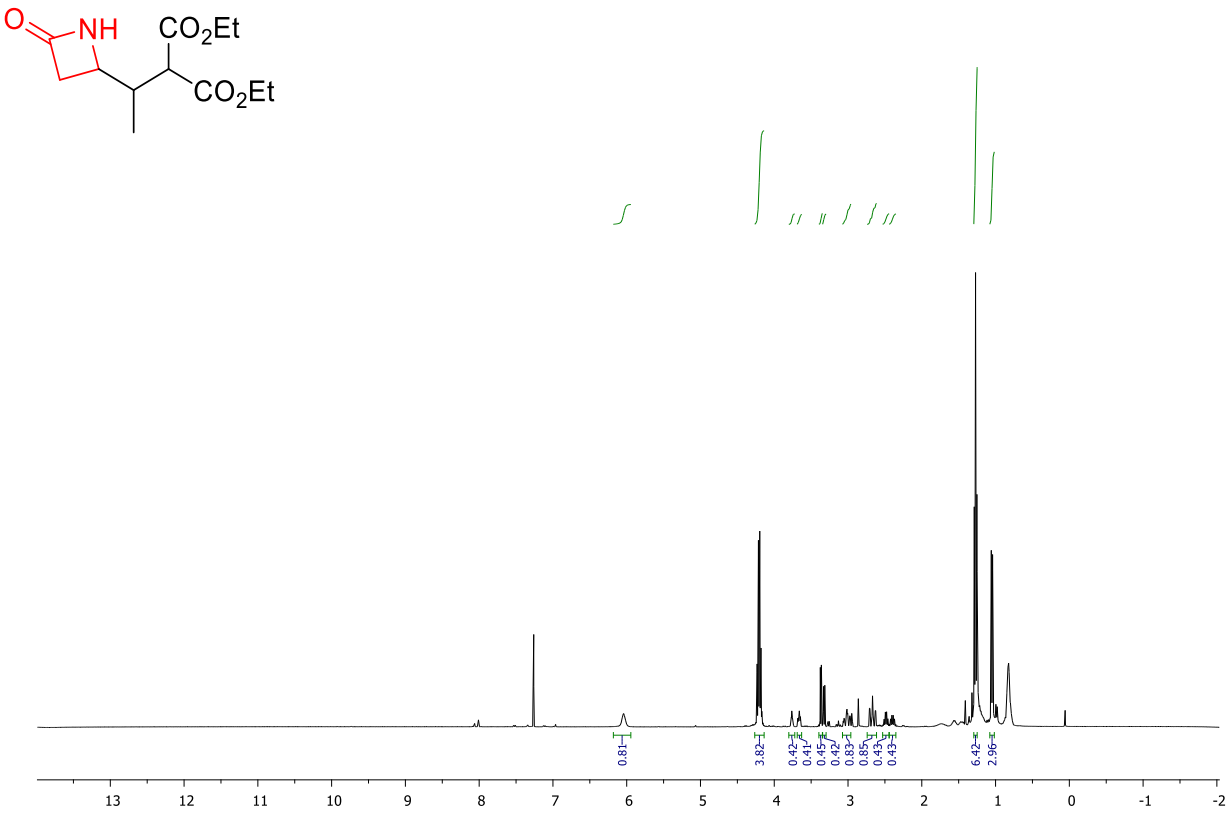

Figure 3-43: 1H NMR spectrum of product 3.15

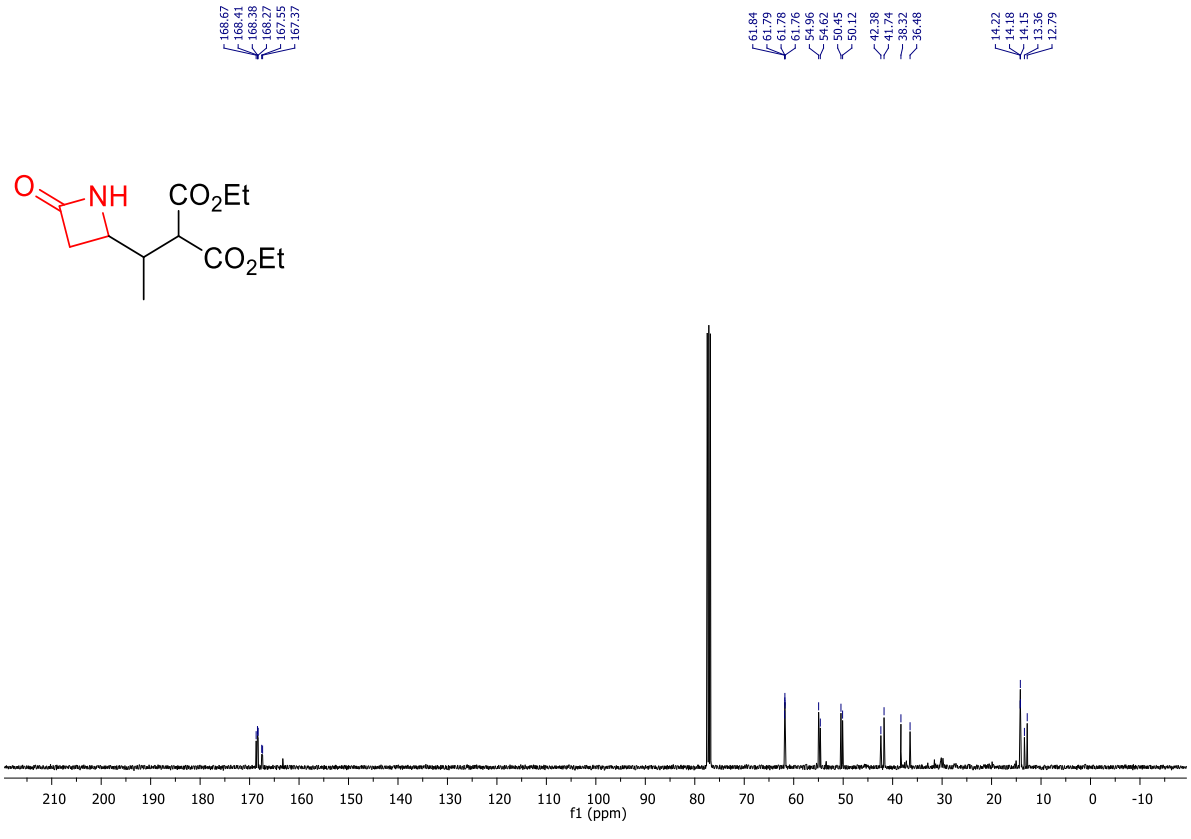

Figure 3-44: 13C NMR spectrum of product 3.15

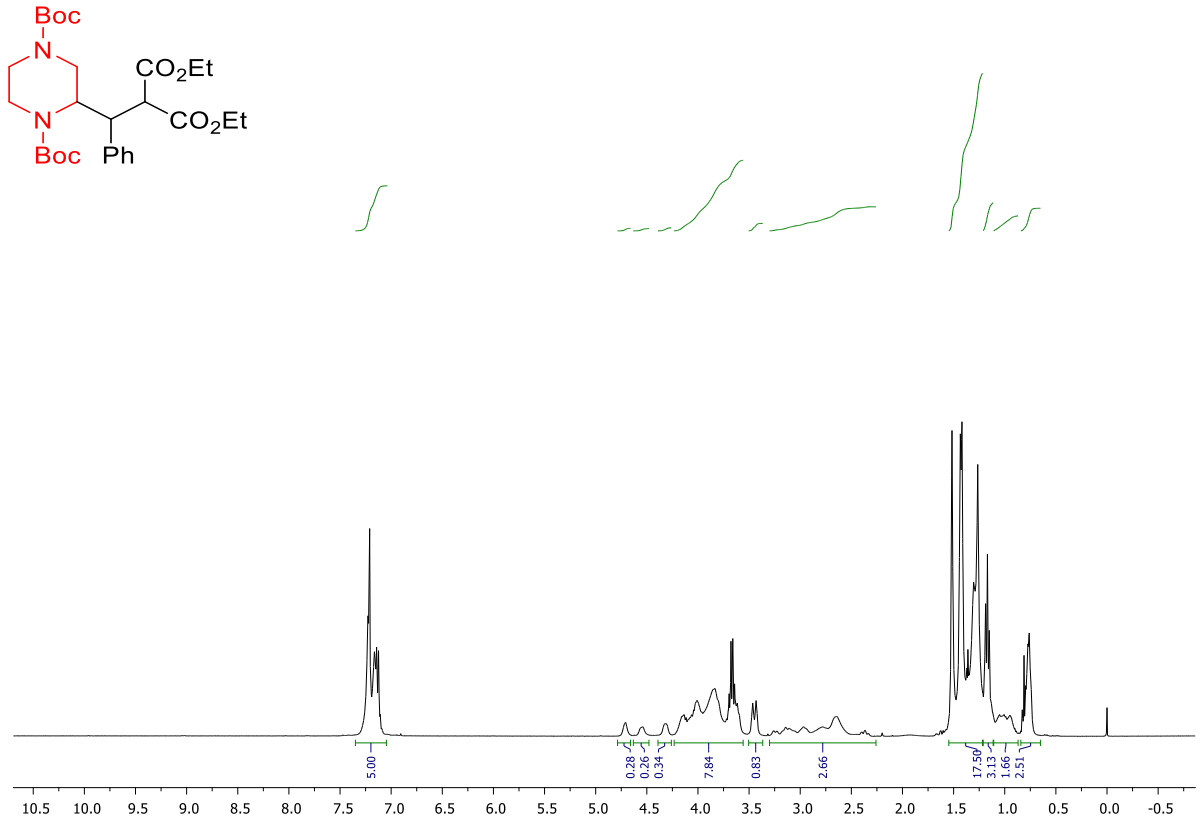

Figure 3-45: 1H NMR spectrum of product 3.16

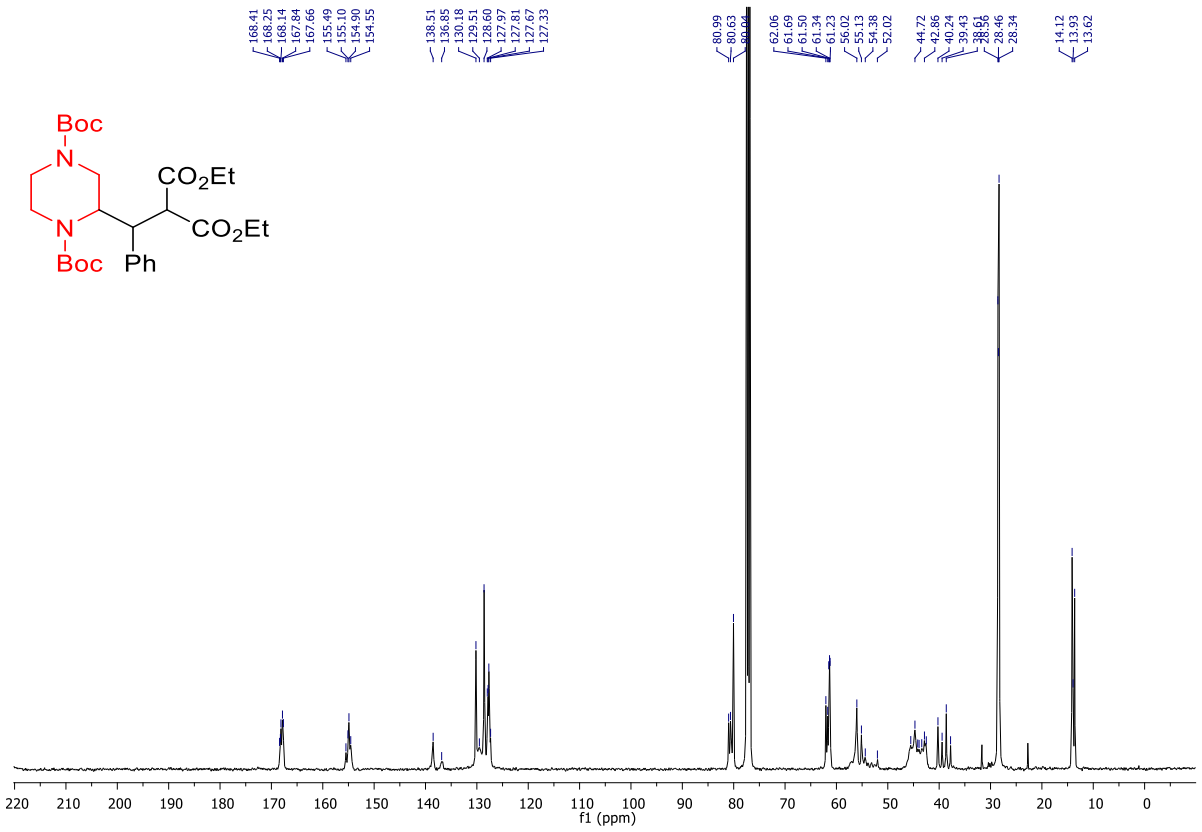

Figure 3-46: 13C NMR spectrum of product 3.16

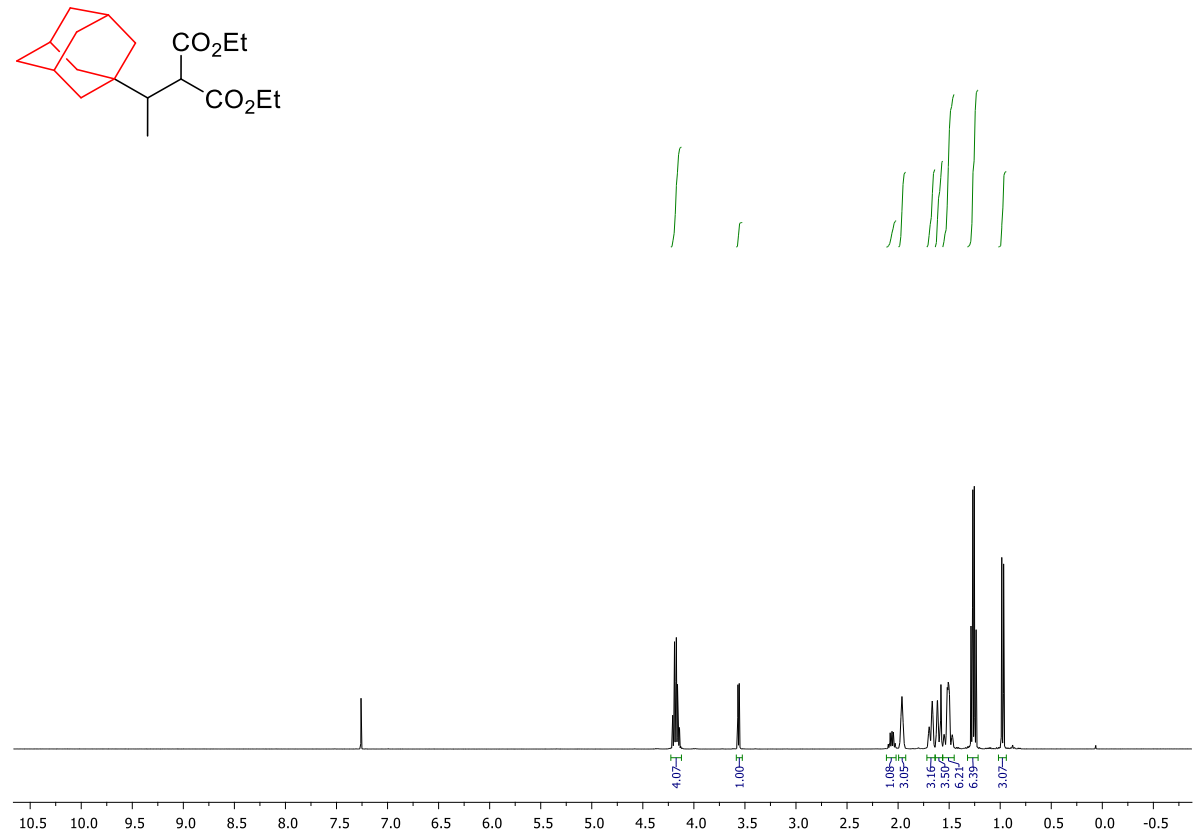

Figure 3-47: 1H NMR spectrum of product 3.17

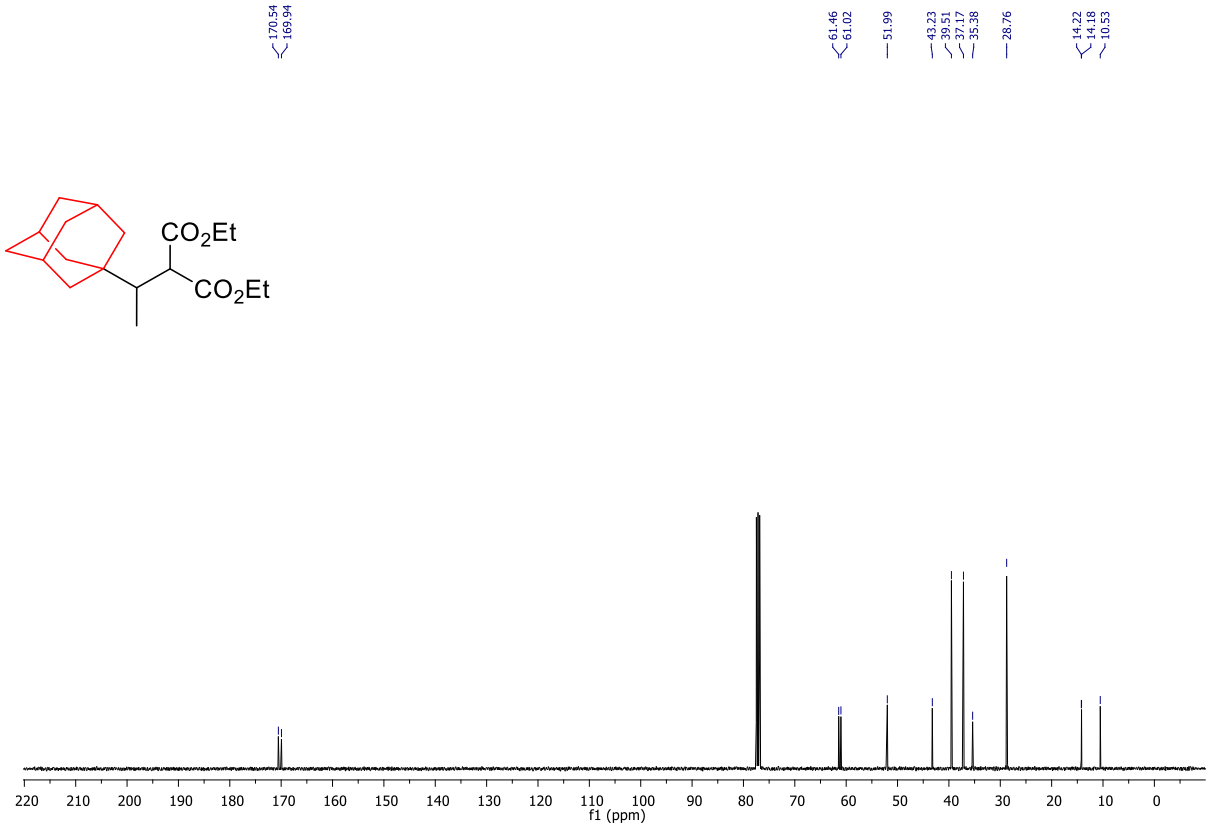

Figure 3-48: 13C NMR spectrum of product 3.17

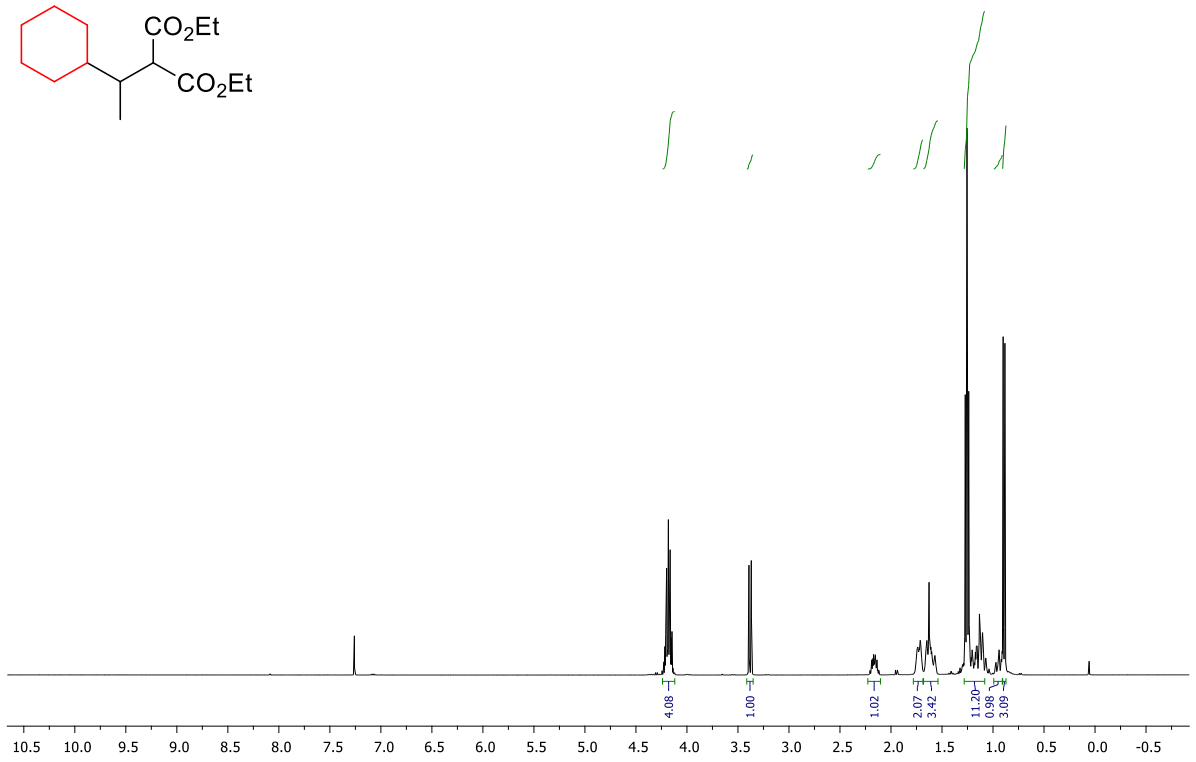

Figure 3-49: 1H NMR spectrum of product 3.18

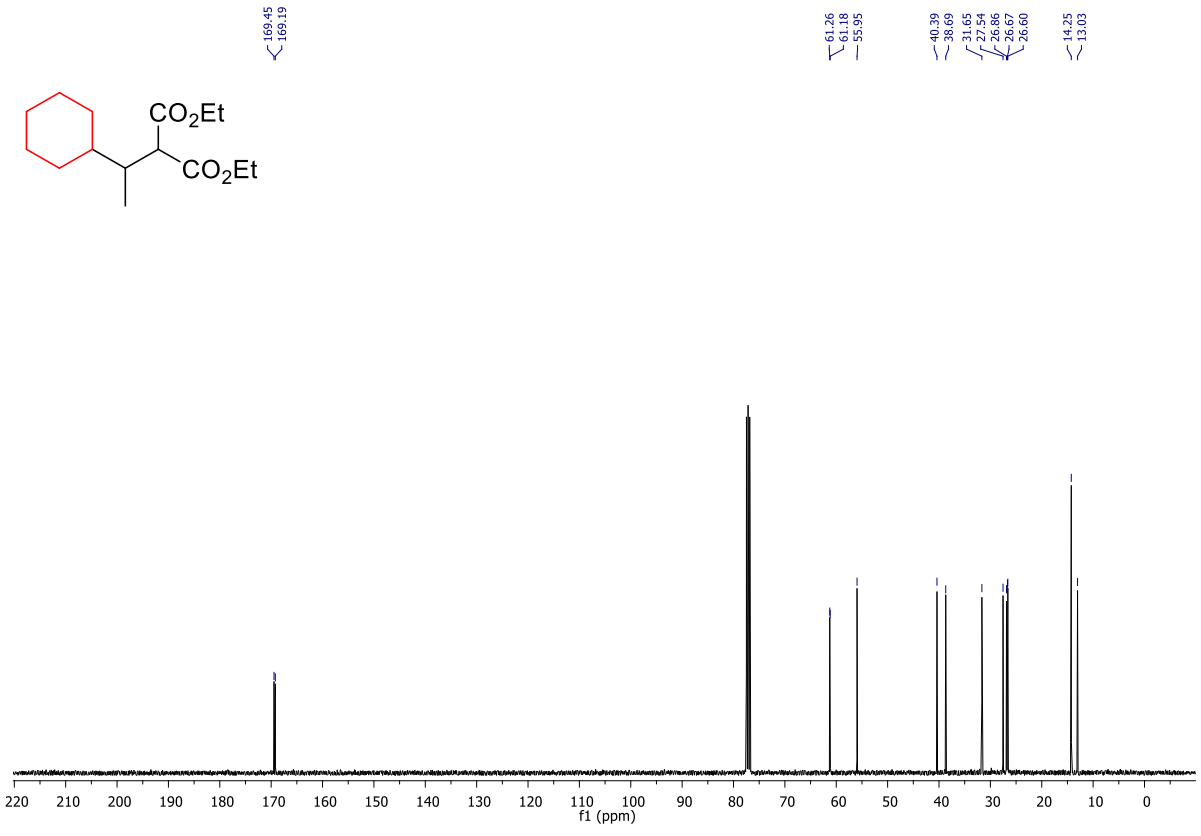

Figure 3-50: 13C NMR spectrum of product 3.18

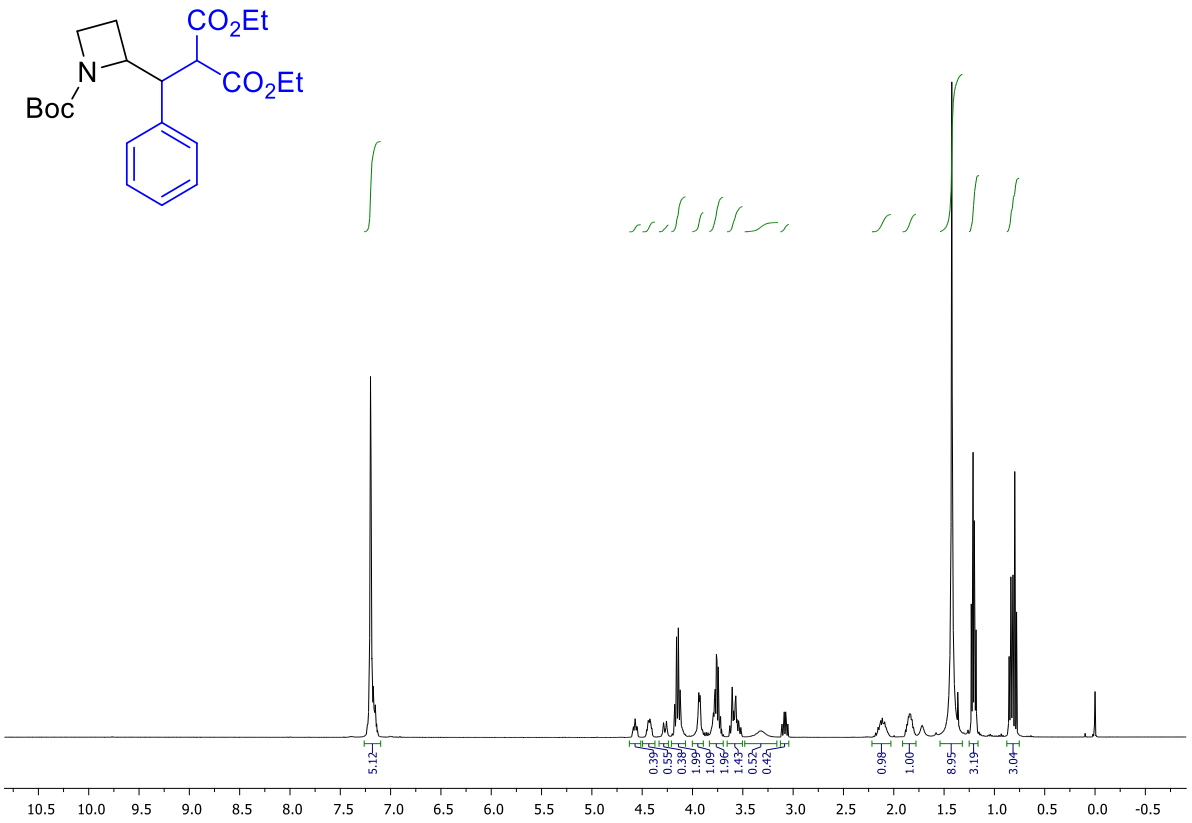

Figure 3-51: 1H NMR spectrum of product 3.23

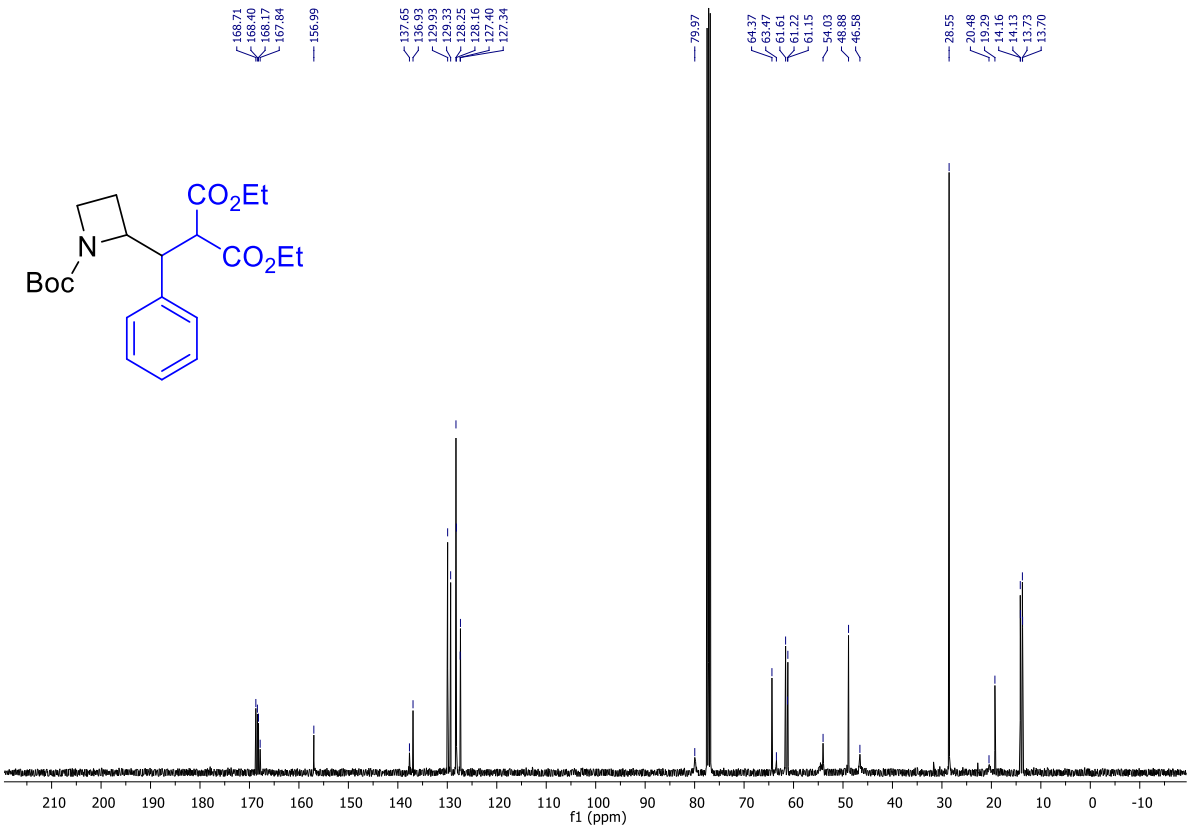

Figure 3-52: 13C NMR spectrum of product 3.23

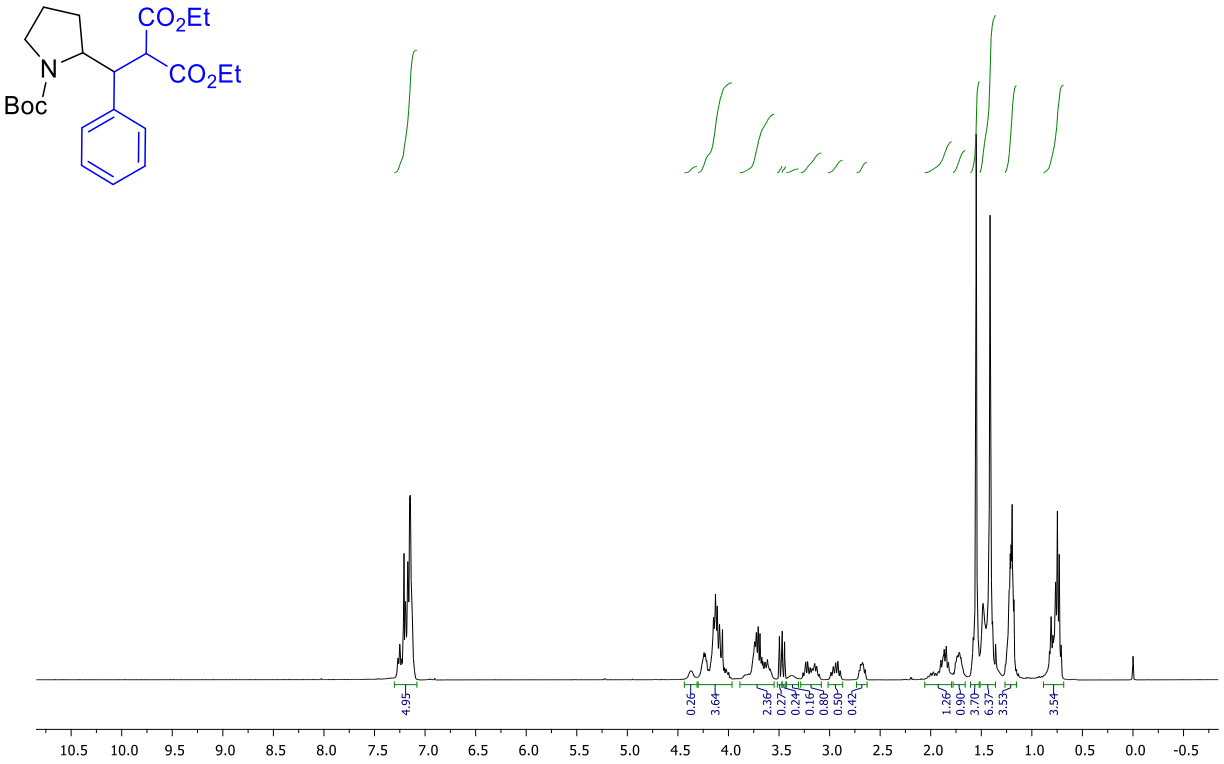

Figure 3-53: 1H NMR spectrum of product 3.24

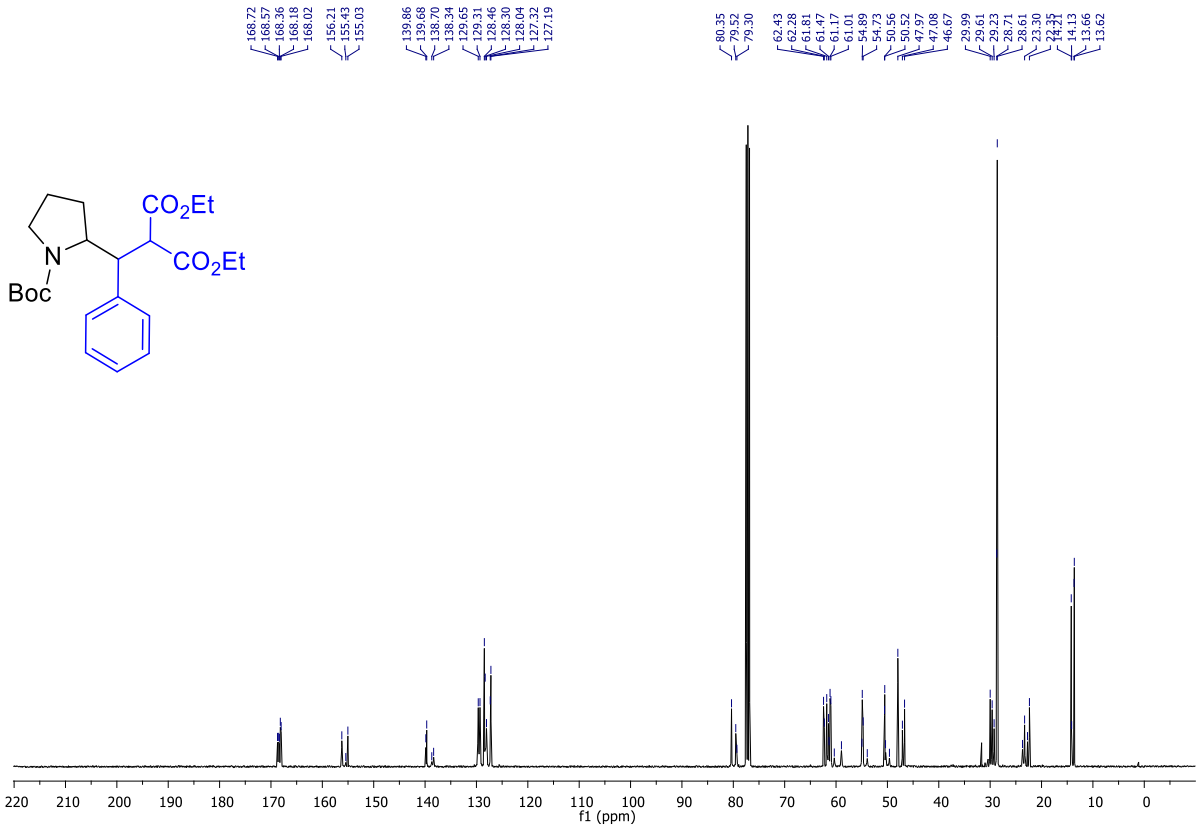

Figure 3-54: 13C NMR spectrum of product 3.24

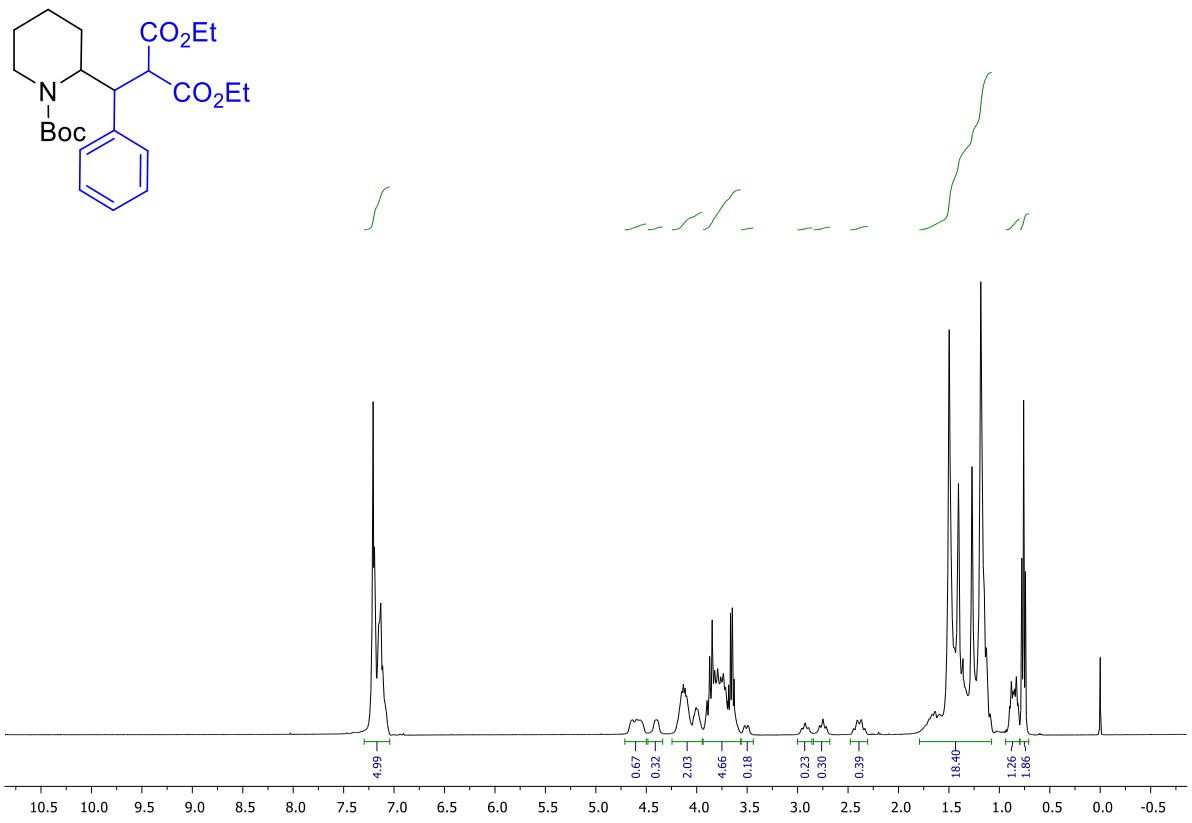

Figure 3-55: 1H NMR spectrum of product 3.25

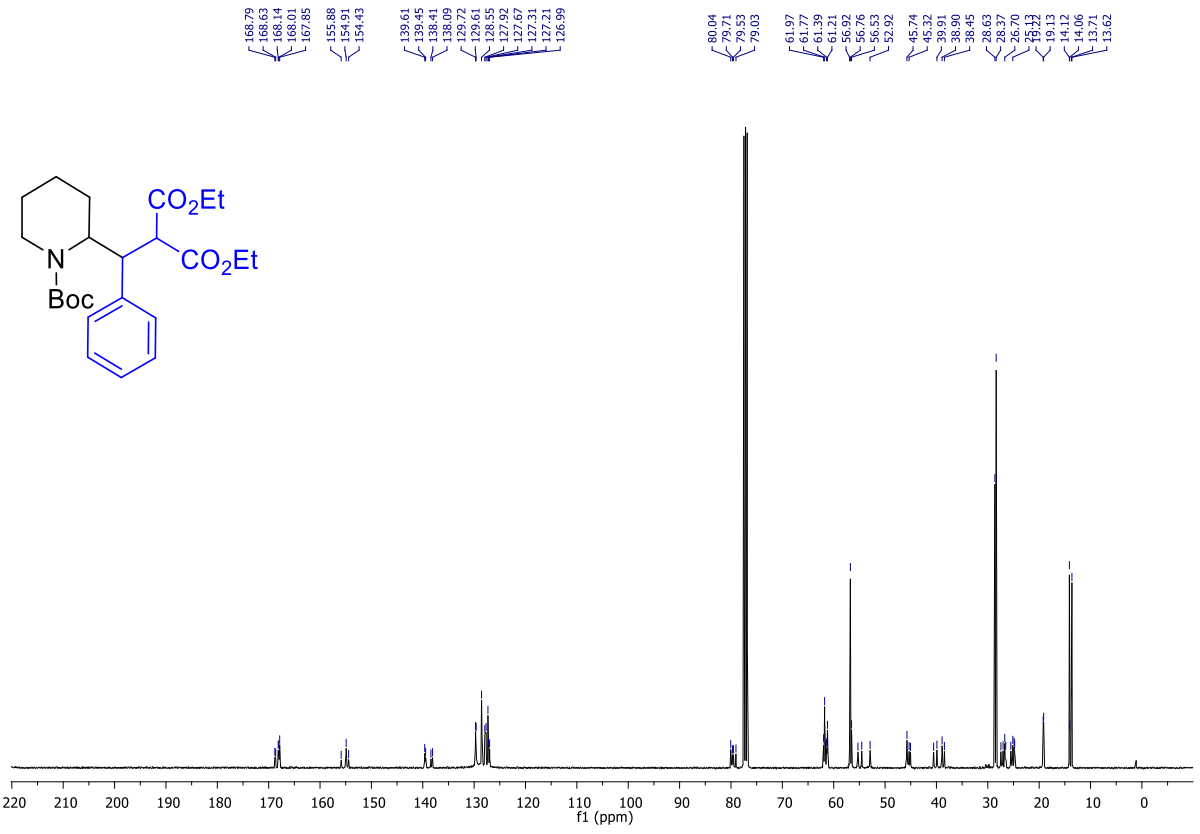

Figure 3-56: 13C NMR spectrum of product 3.25

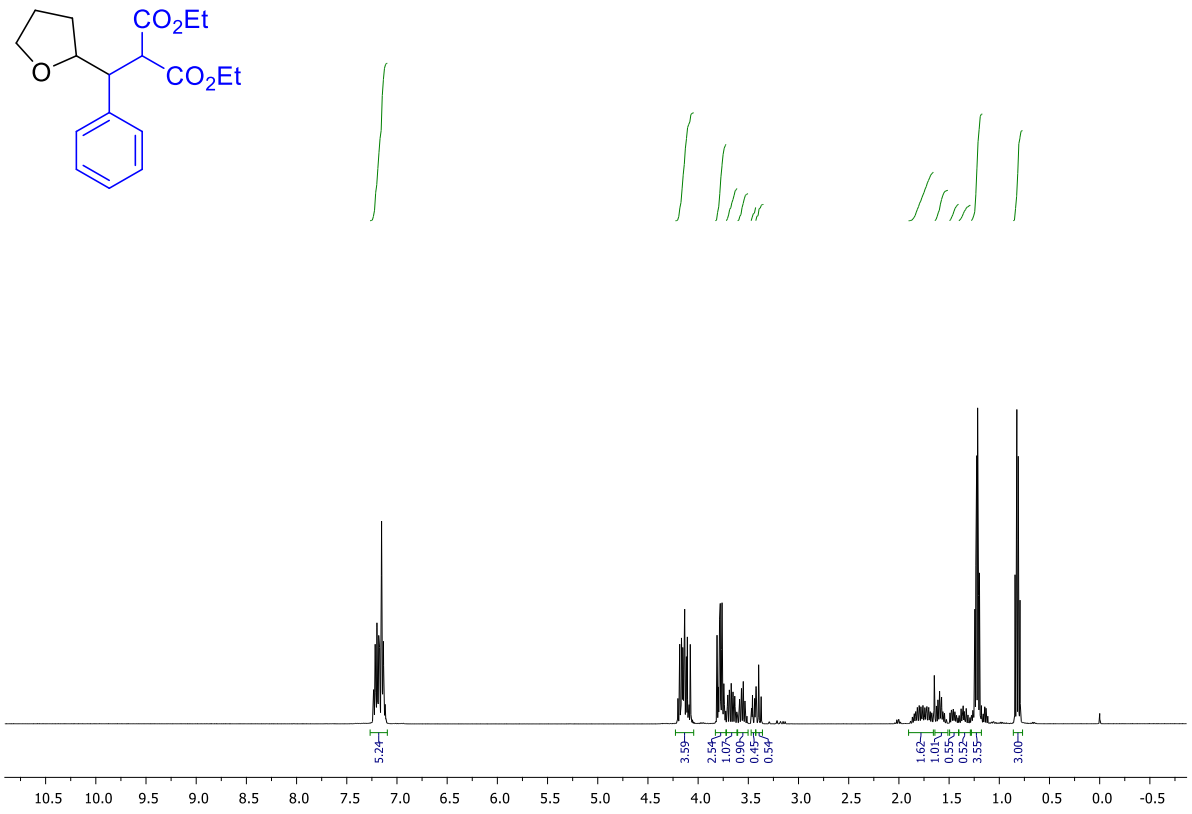

Figure 3-57: 1H NMR spectrum of product 3.26

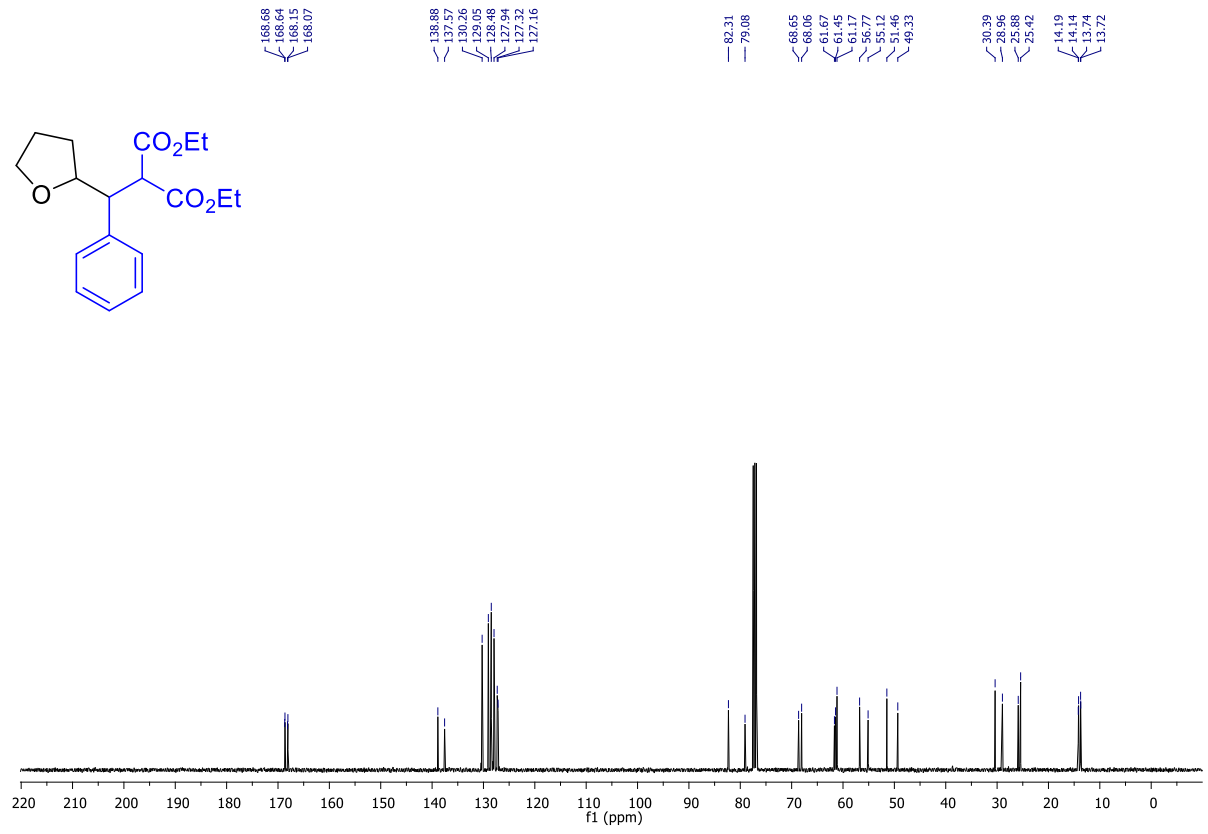

Figure 3-58: 13C NMR spectrum of product 3.26

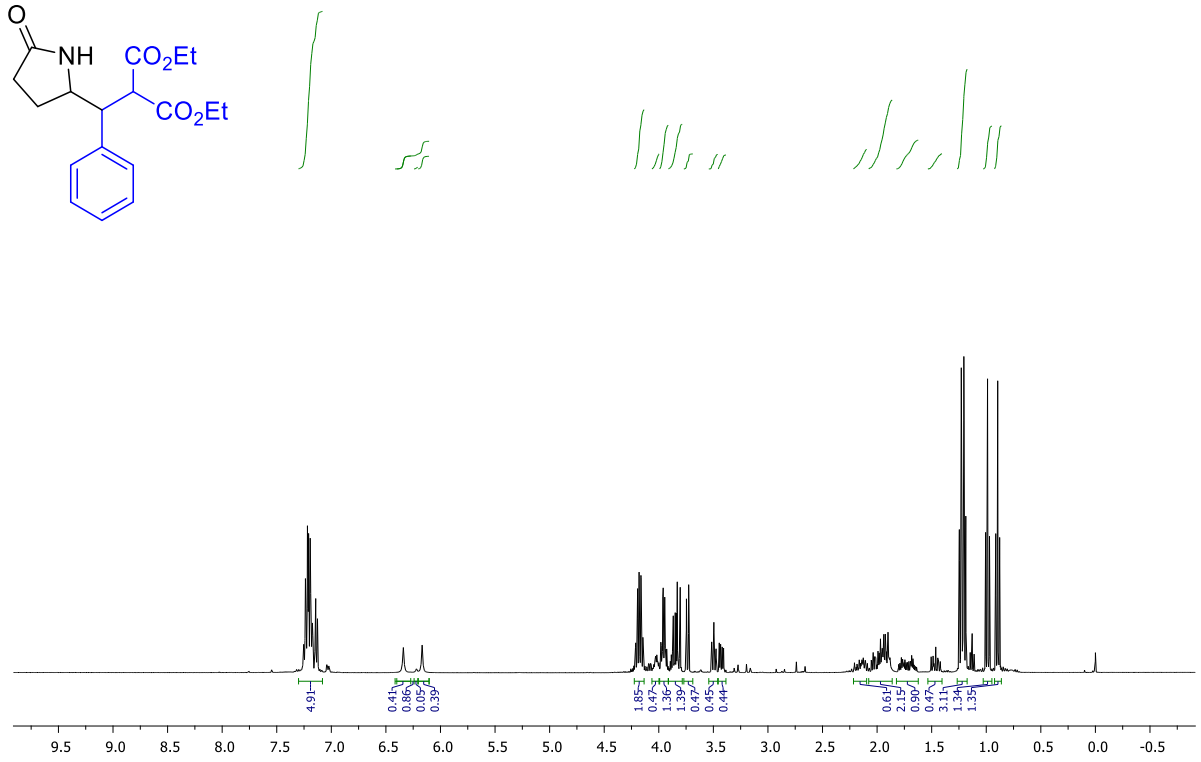

Figure 3-59: 1H NMR spectrum of product 3.27

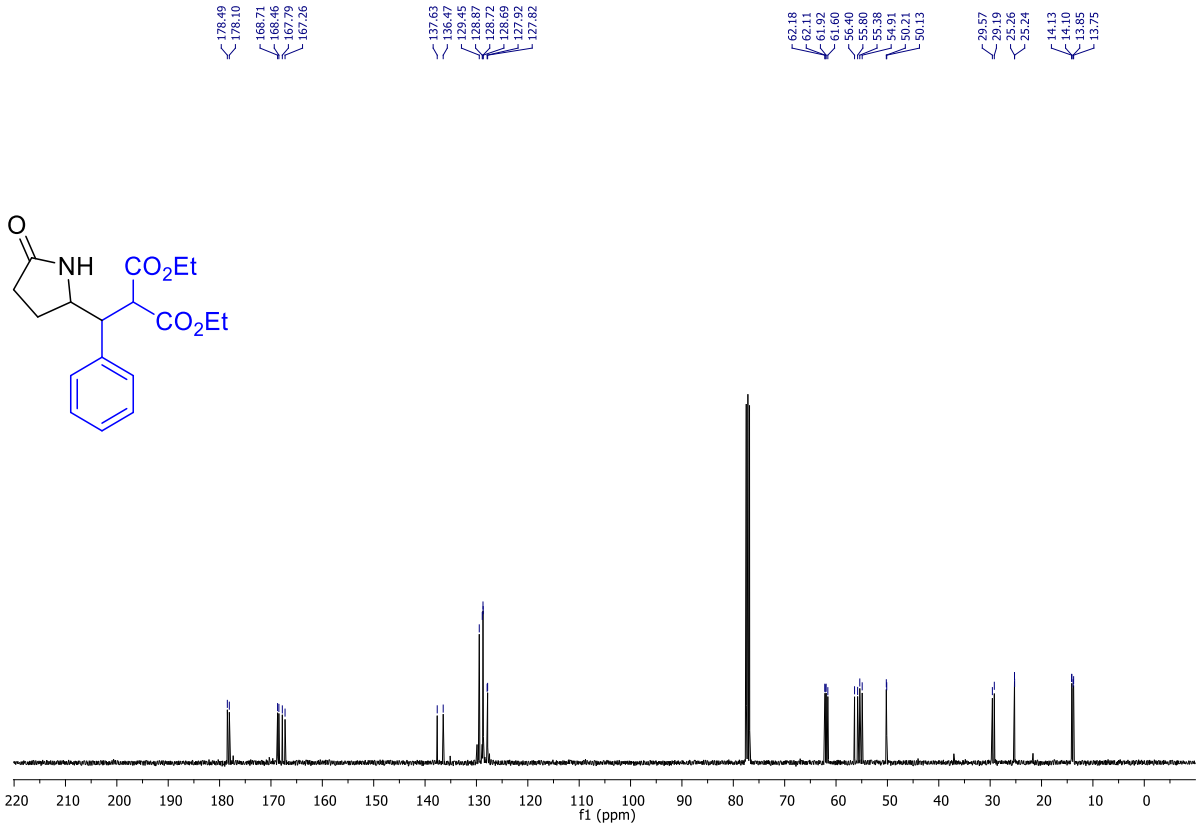

Figure 3-60: 13C NMR spectrum of product 3.27

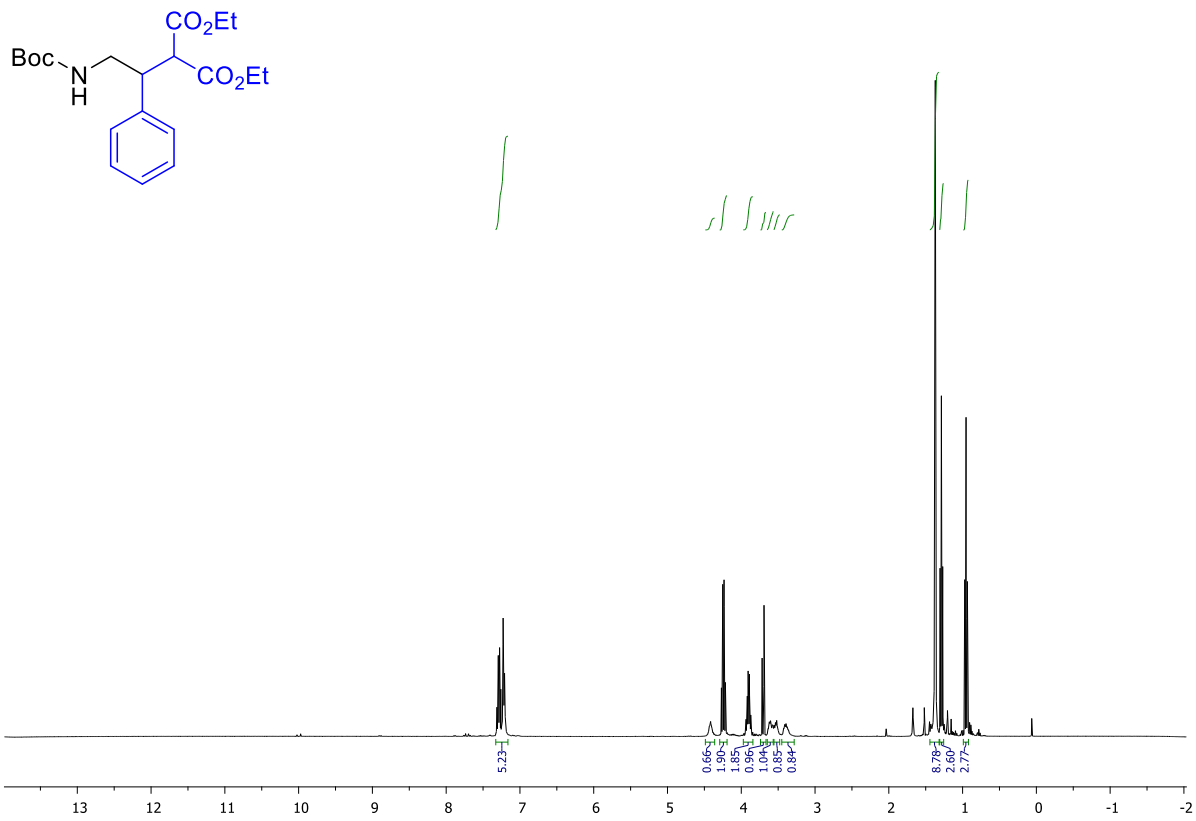

Figure 3-61: 1H NMR spectrum of product 3.28

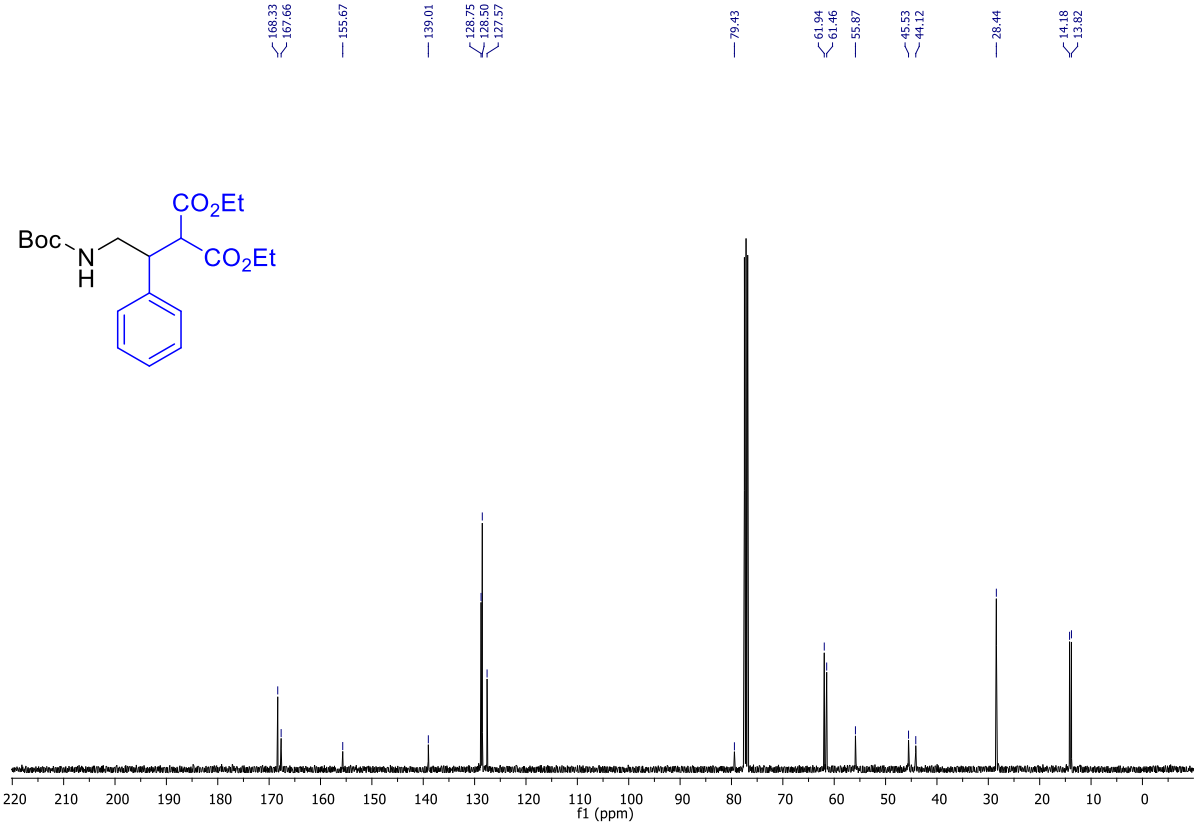

Figure 3-62: 13C NMR spectrum of product 3.28

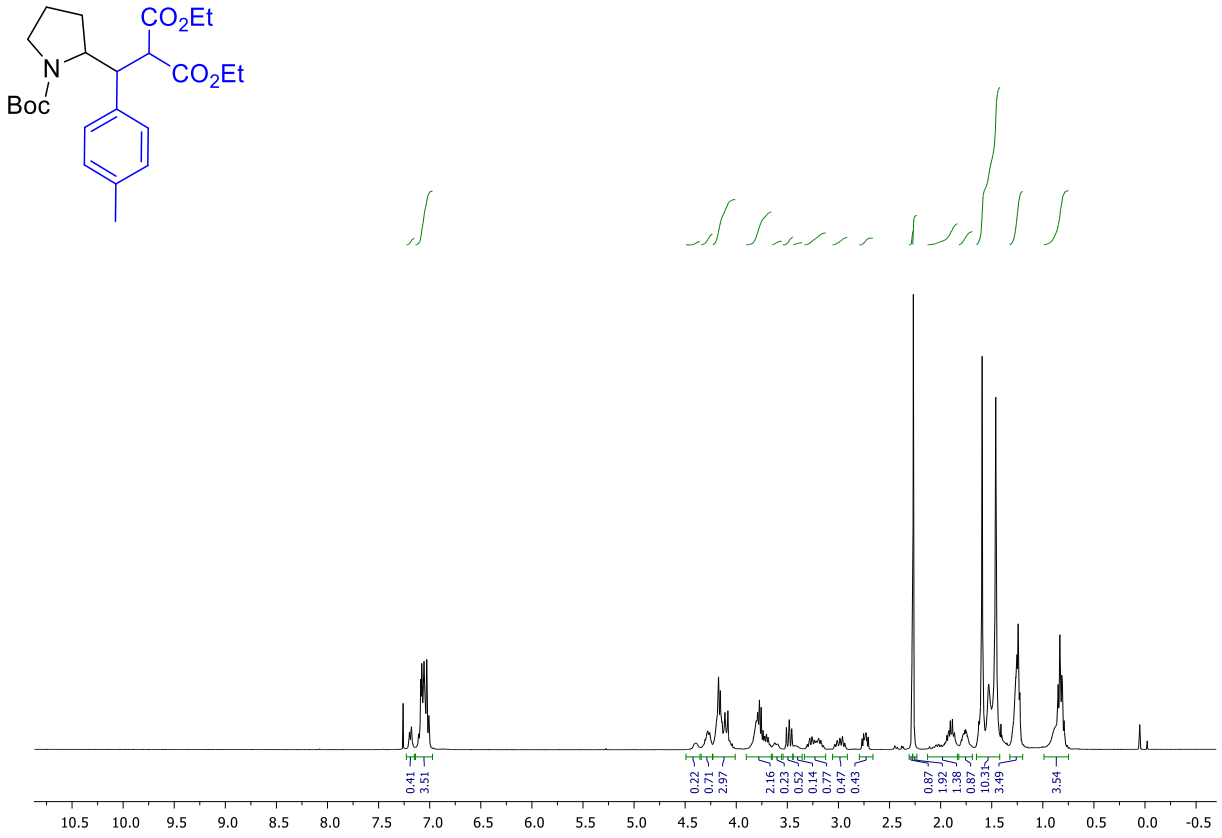

Figure 3-64: 1H NMR spectrum of product 3.29

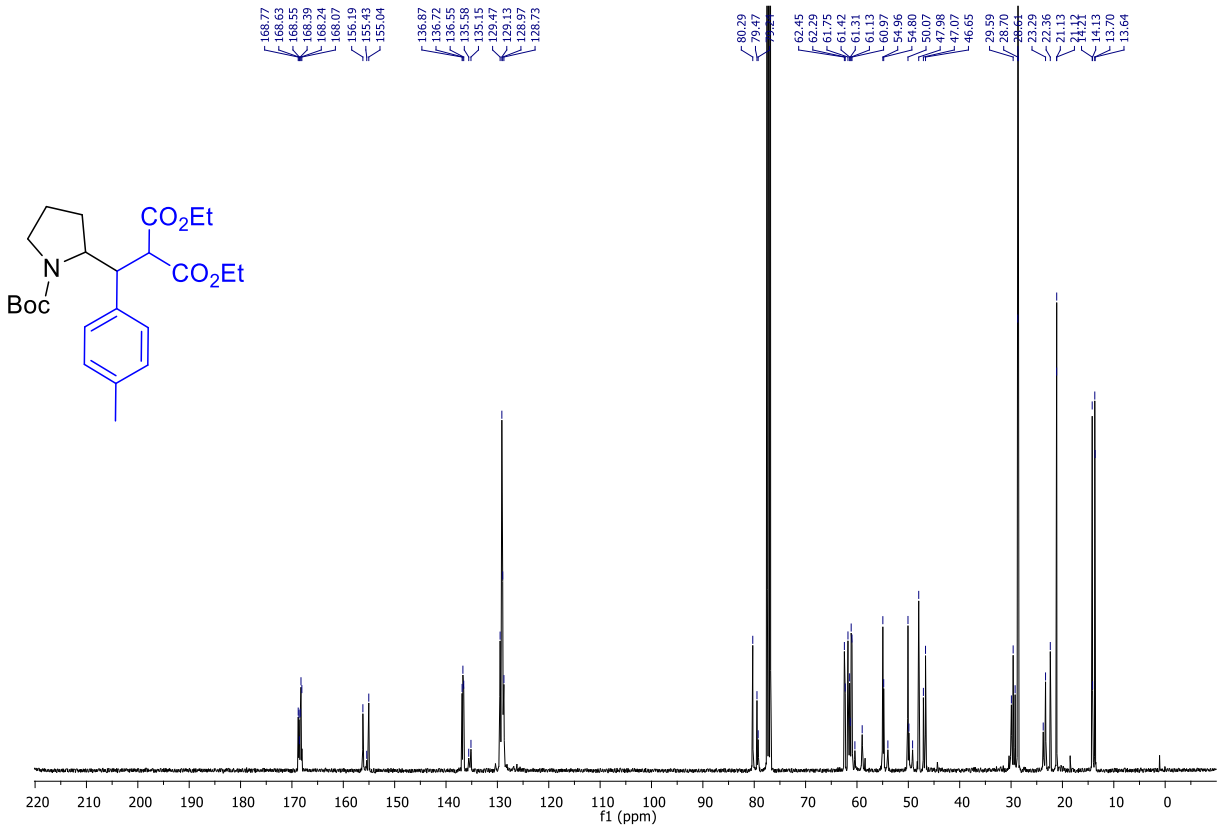

Figure 3-63: 13C NMR spectrum of product 3.29

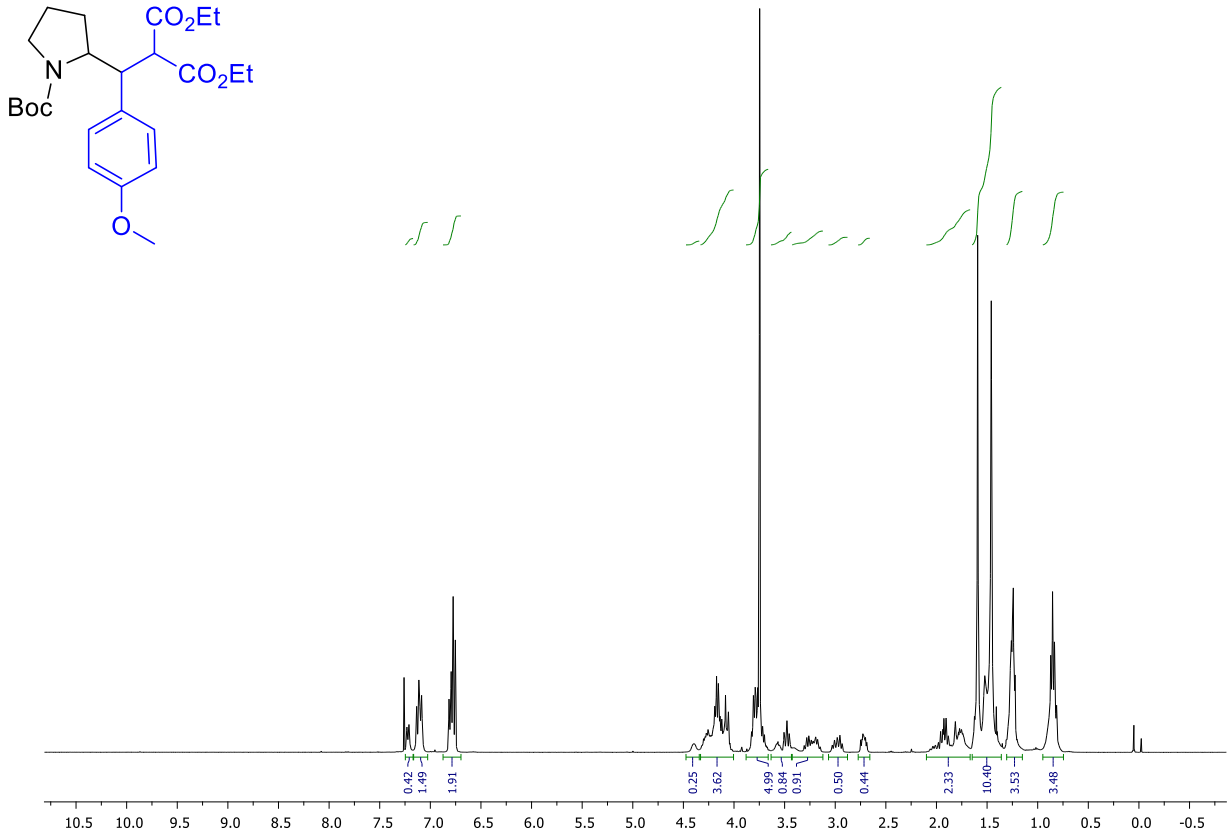

Figure 3-65: 1H NMR spectrum of product 3.30

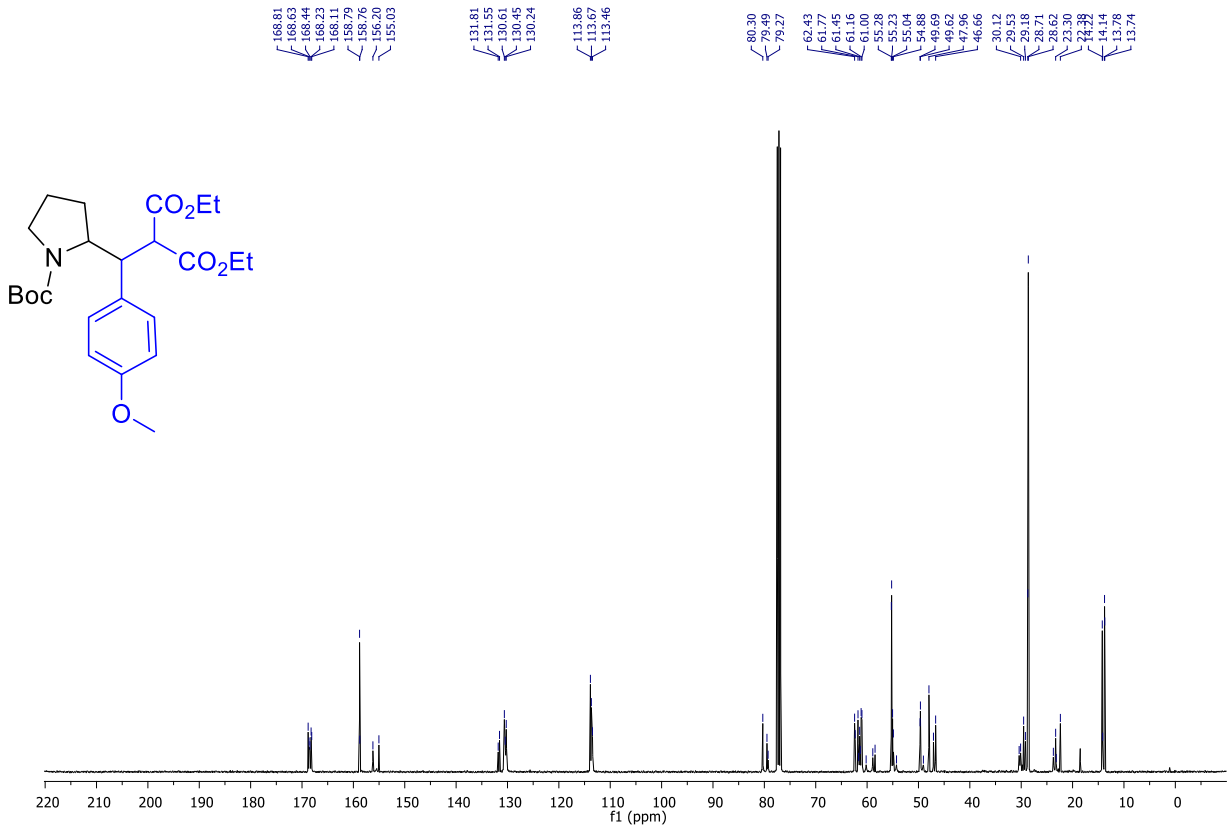

Figure 3-66: 13C NMR spectrum of product 3.30

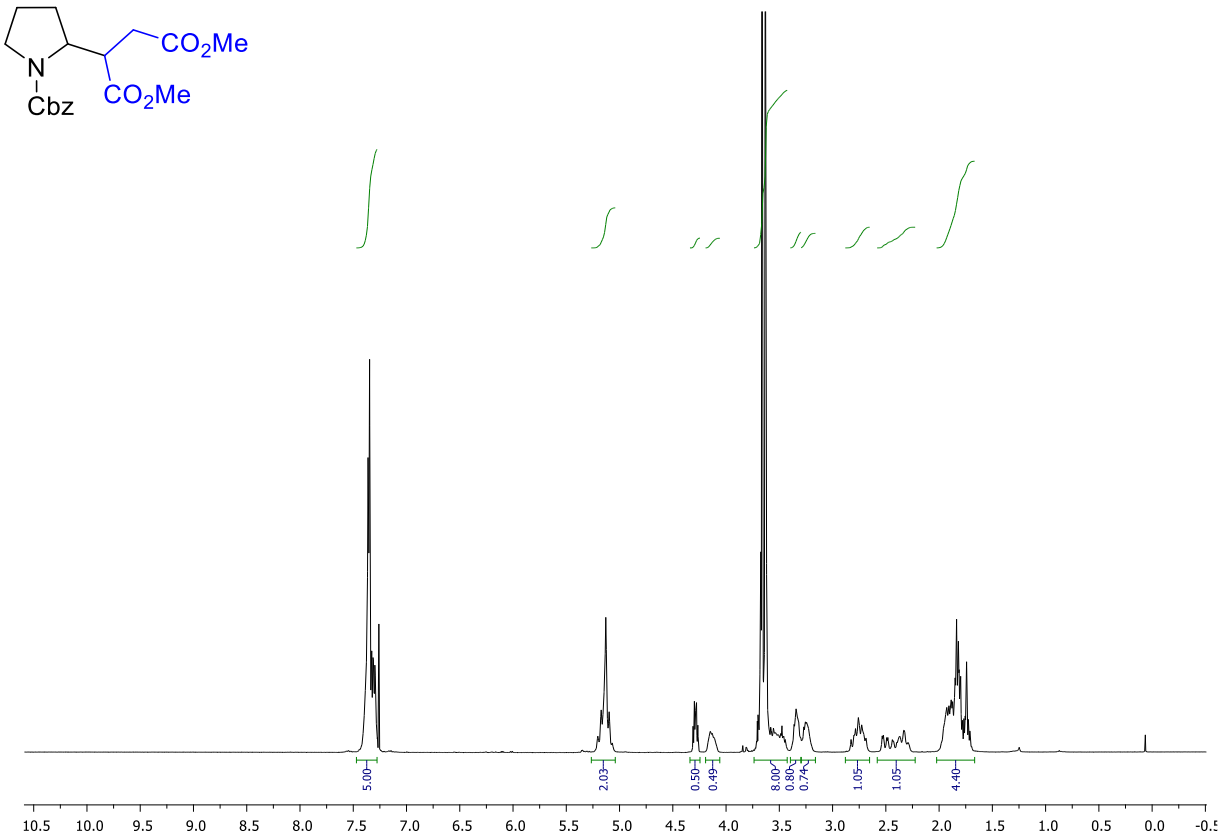

Figure 3-67: 1H NMR spectrum of product 3.31

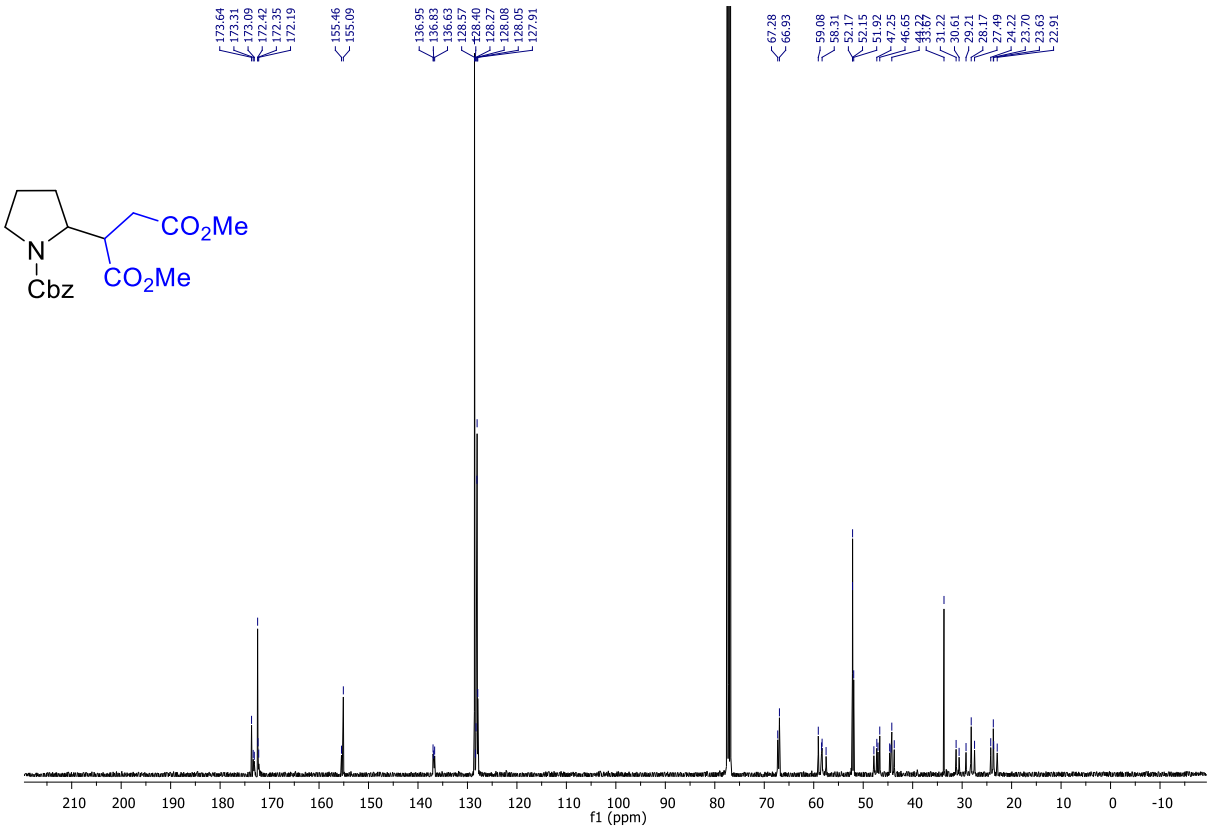

Figure 3-68: 13C NMR spectrum of product 3.31

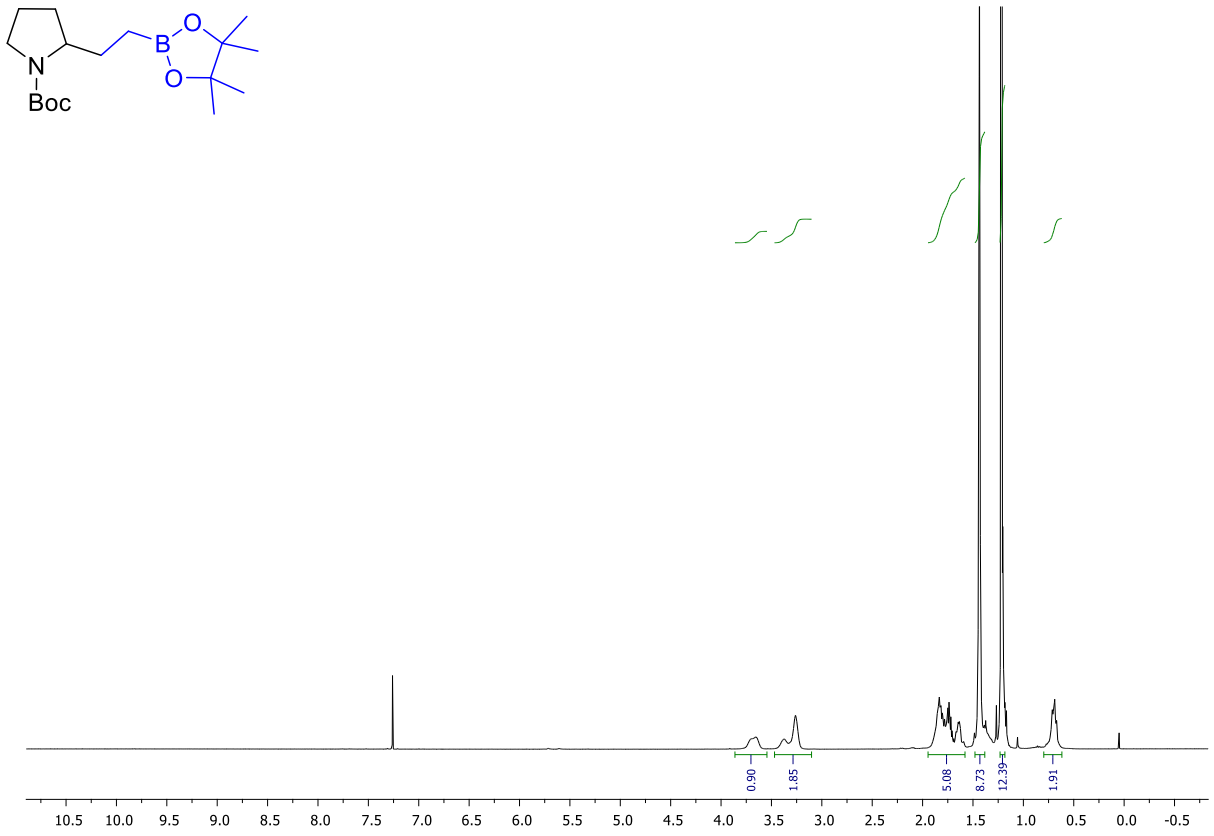

Figure 3-69: 1H NMR spectrum of product 3.32

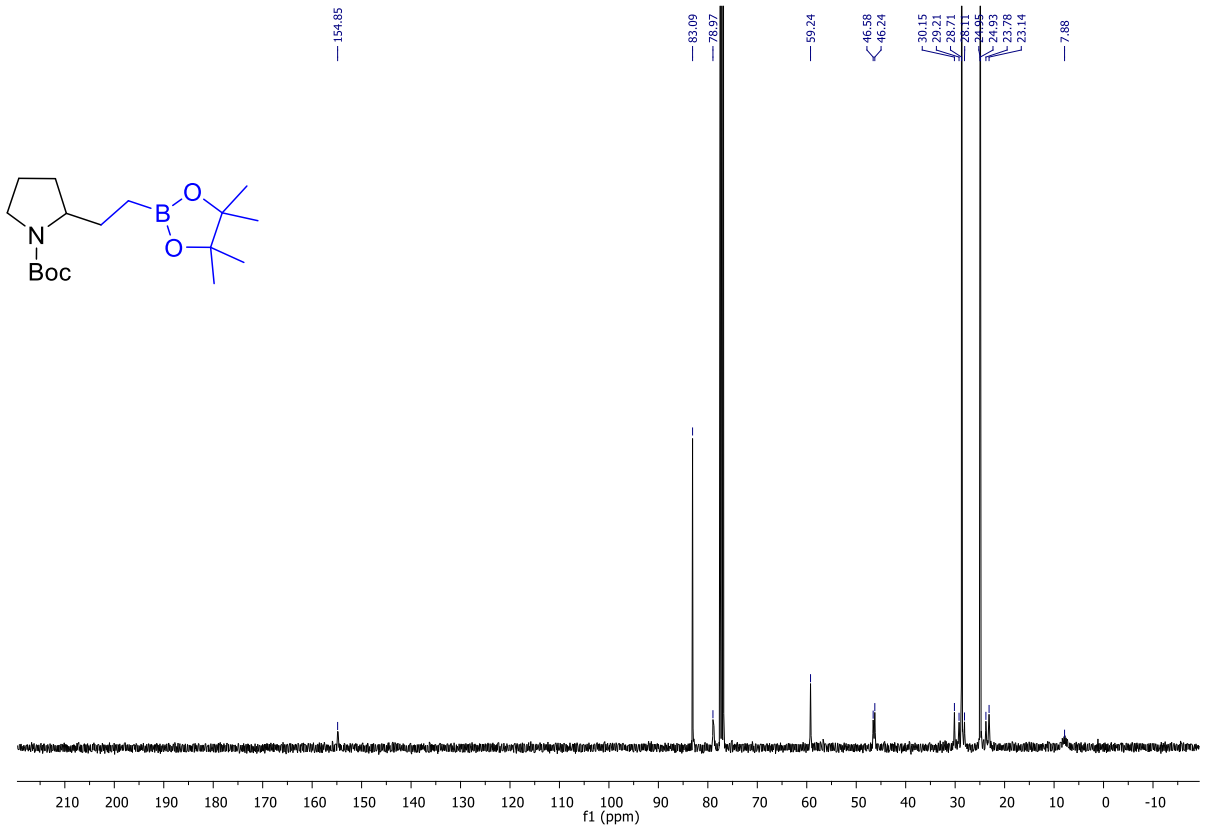

Figure 3-70: 13C NMR spectrum of product 3.32

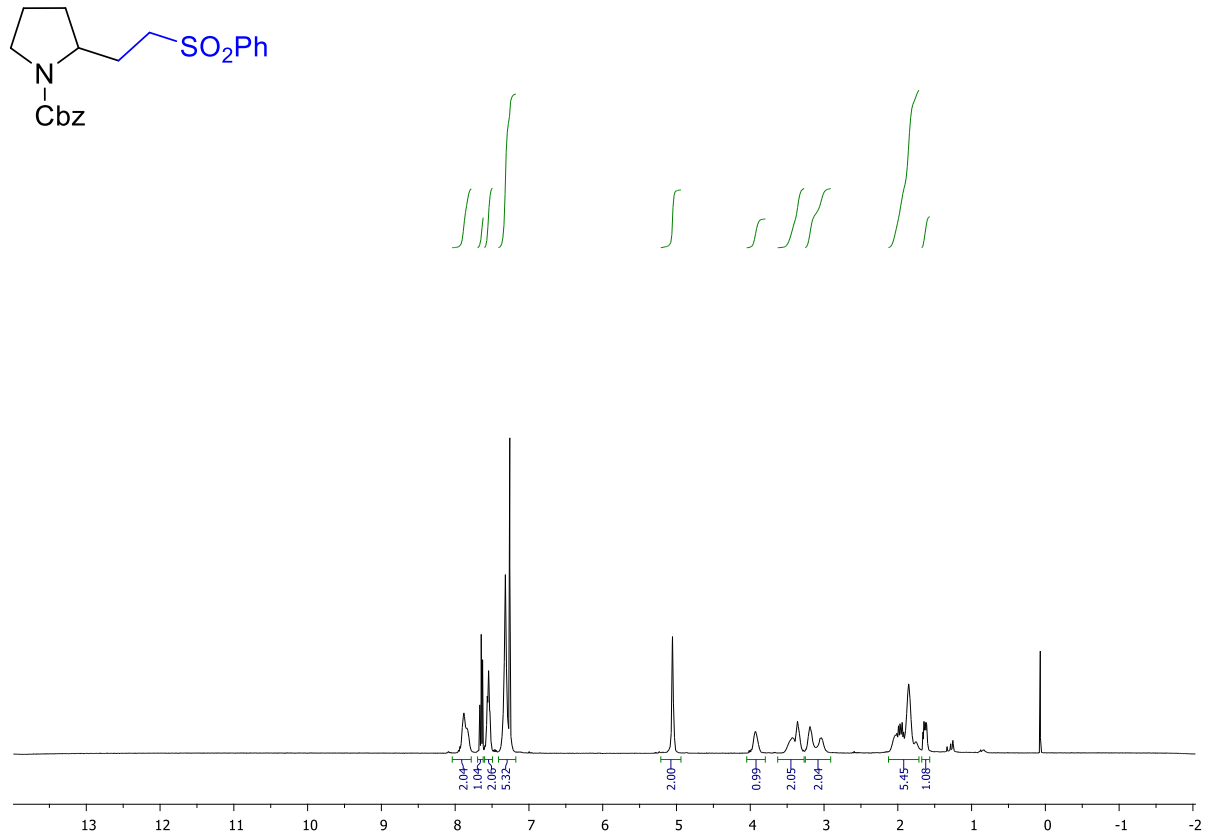

Figure 3-72: 1H NMR spectrum of product 3.33

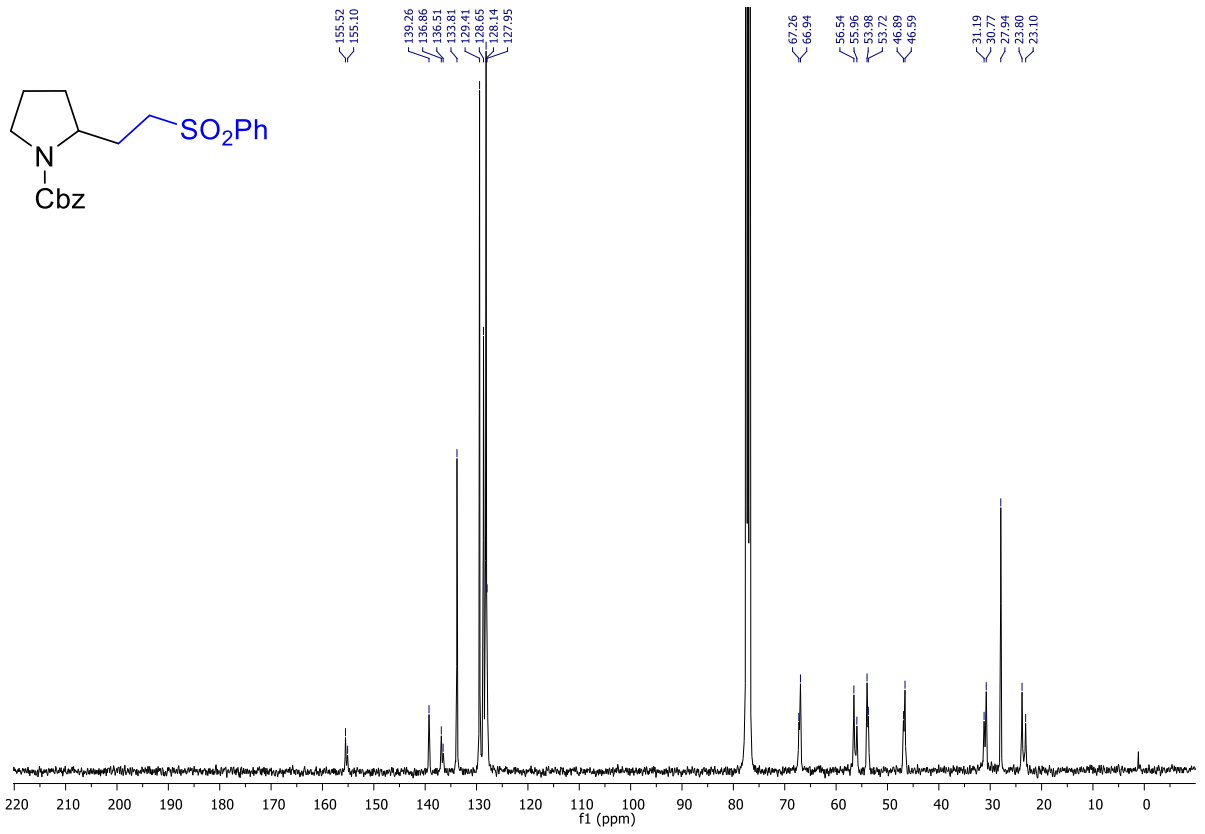

Figure 3-71: 13C NMR spectrum of product 3.33

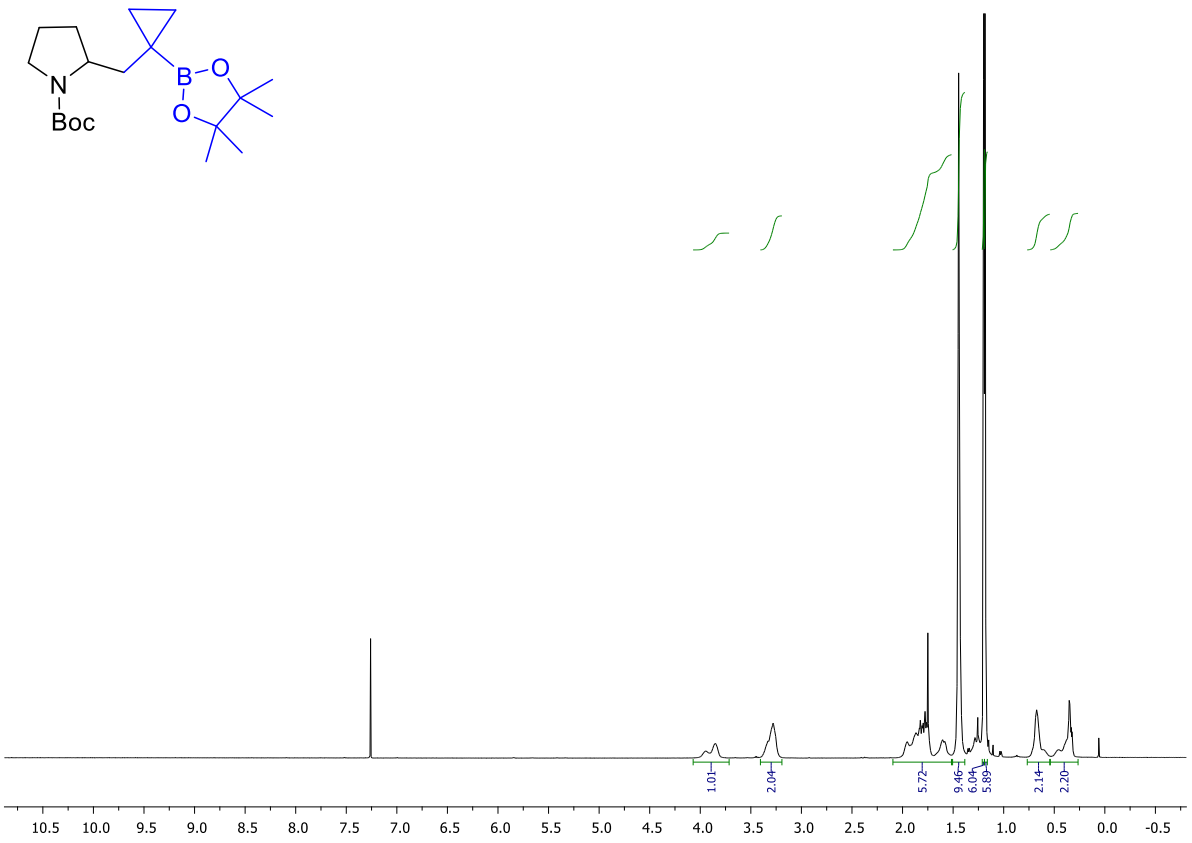

Figure 3-73: 1H NMR spectrum of product 3.34

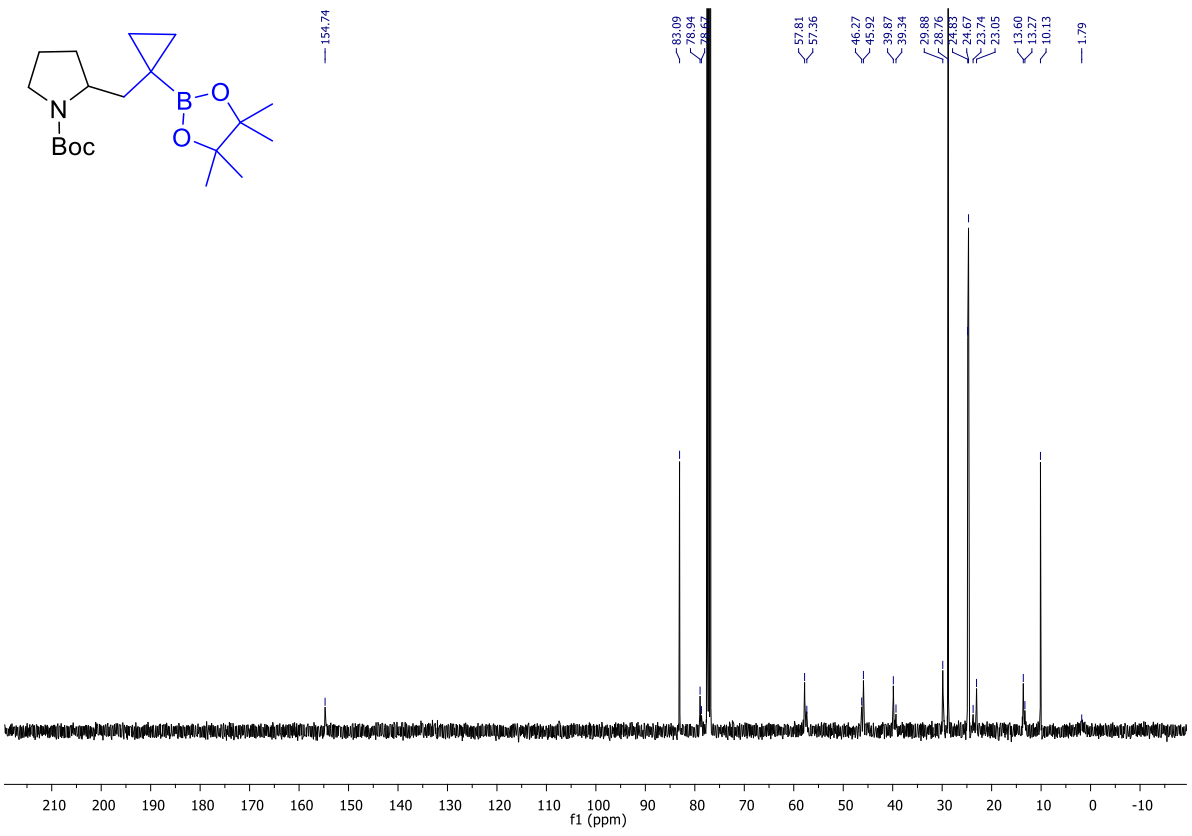

Figure 3-74: 13C NMR spectrum of product 3.34

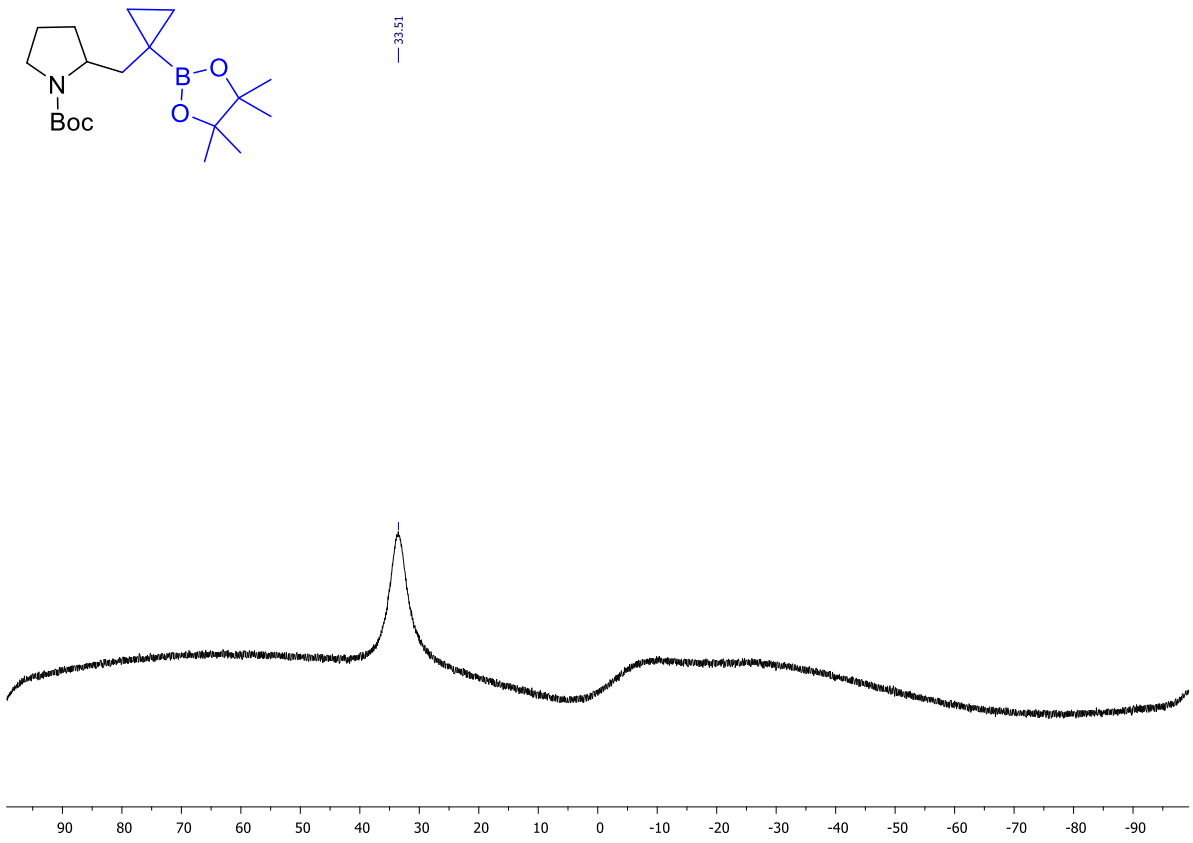

Figure 3-75: 11B NMR spectrum of product 3.34

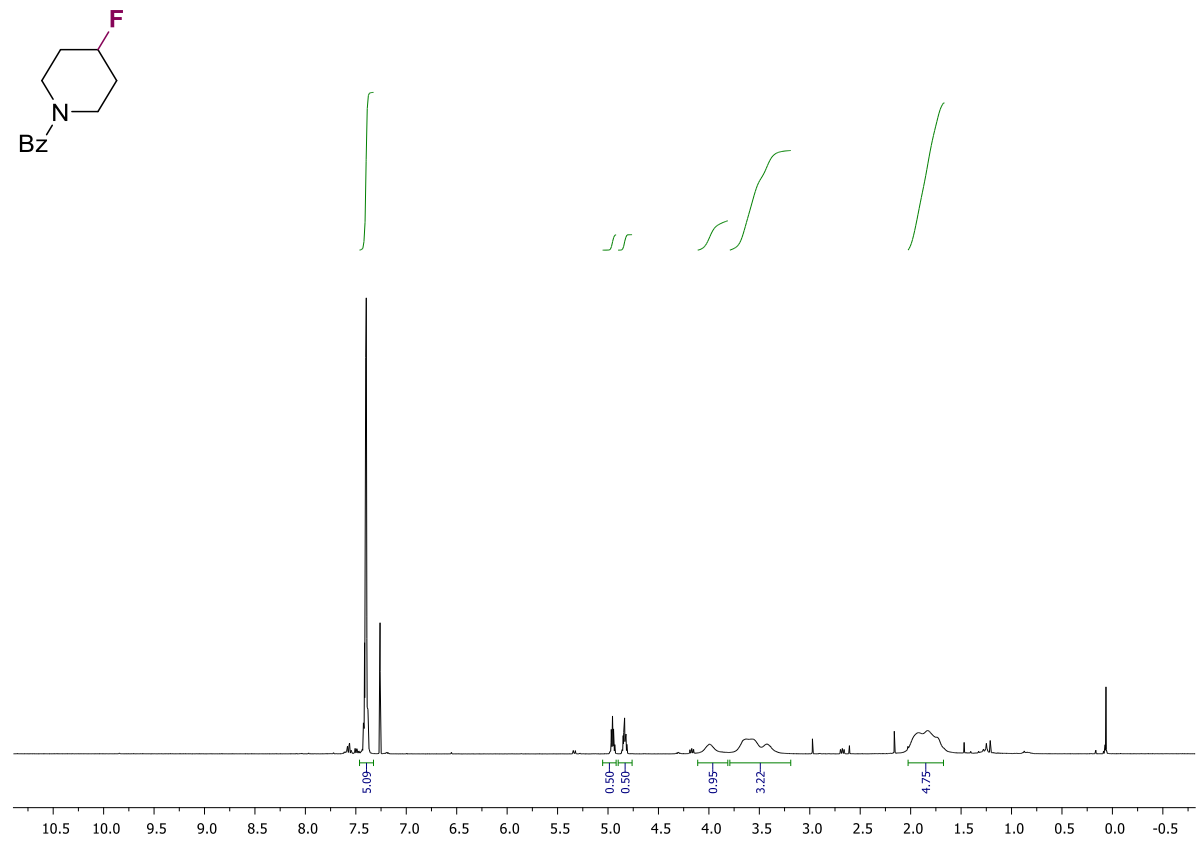

Figure 3-76: 1H NMR spectrum of product 3.43

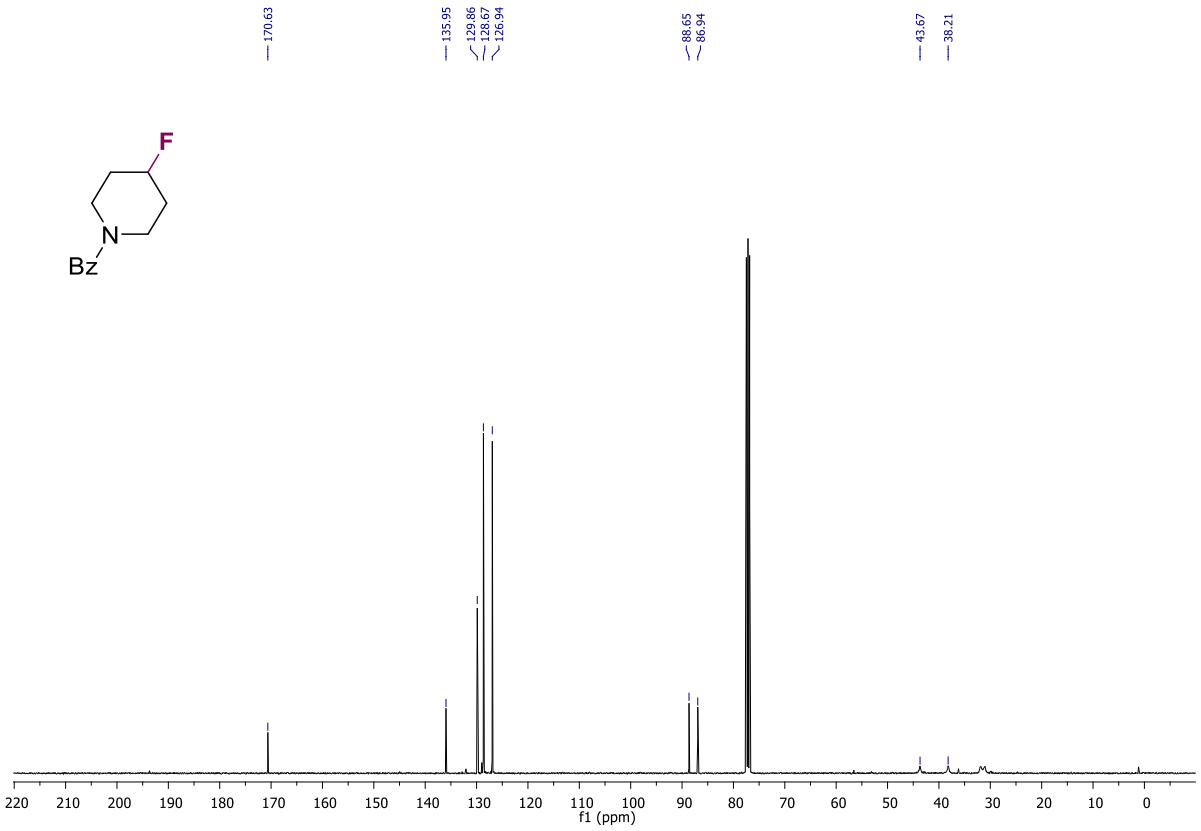

Figure 3-77: 13C NMR spectrum of product 3.43

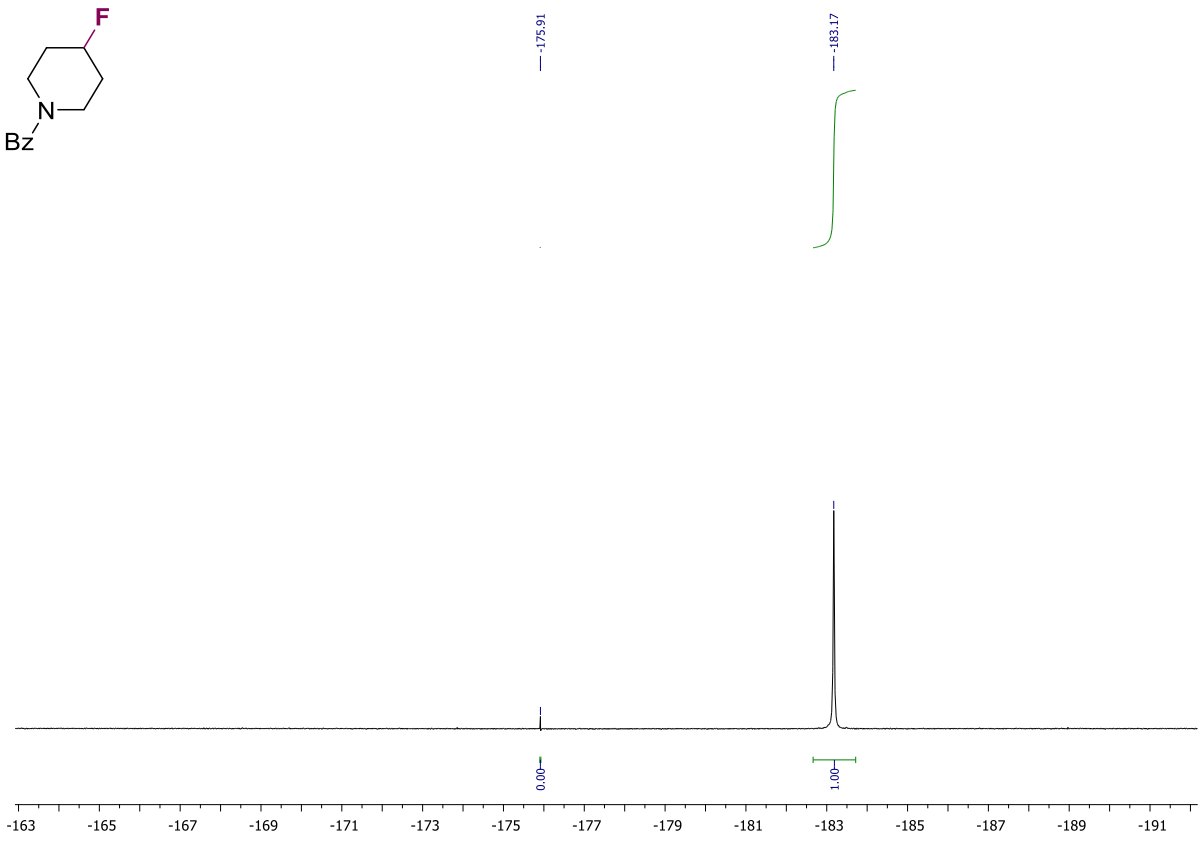

Figure 3-78: 19F NMR spectrum of product 3.43

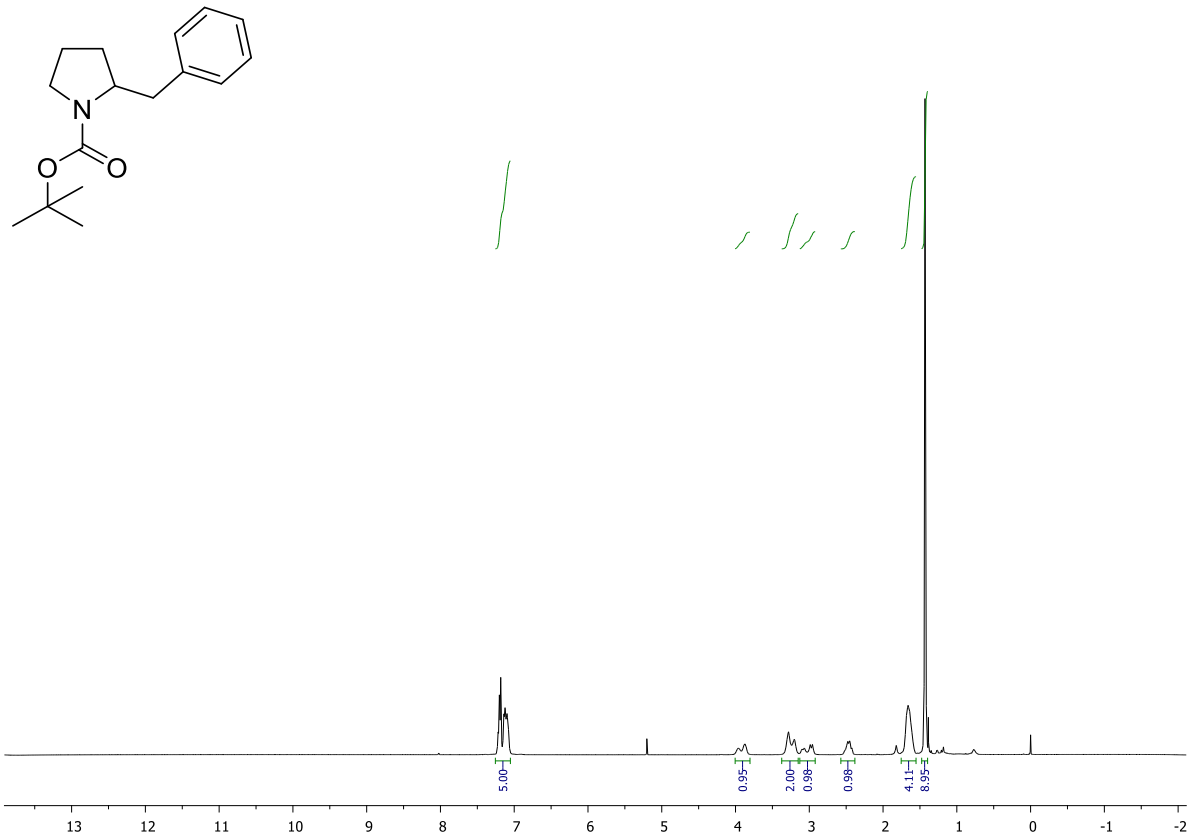

Figure 3-79: 1H NMR spectrum of product 3.45

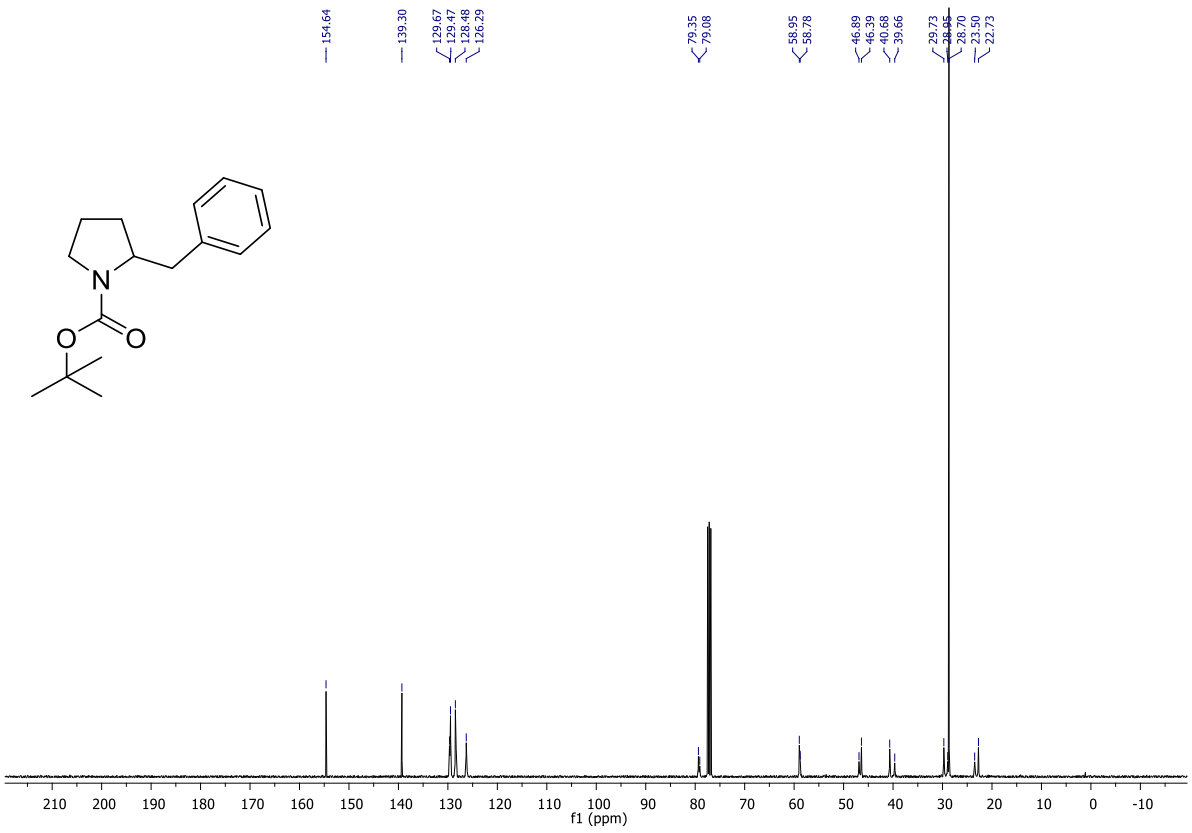

Figure 3-80: 13C NMR spectrum of product 3.45

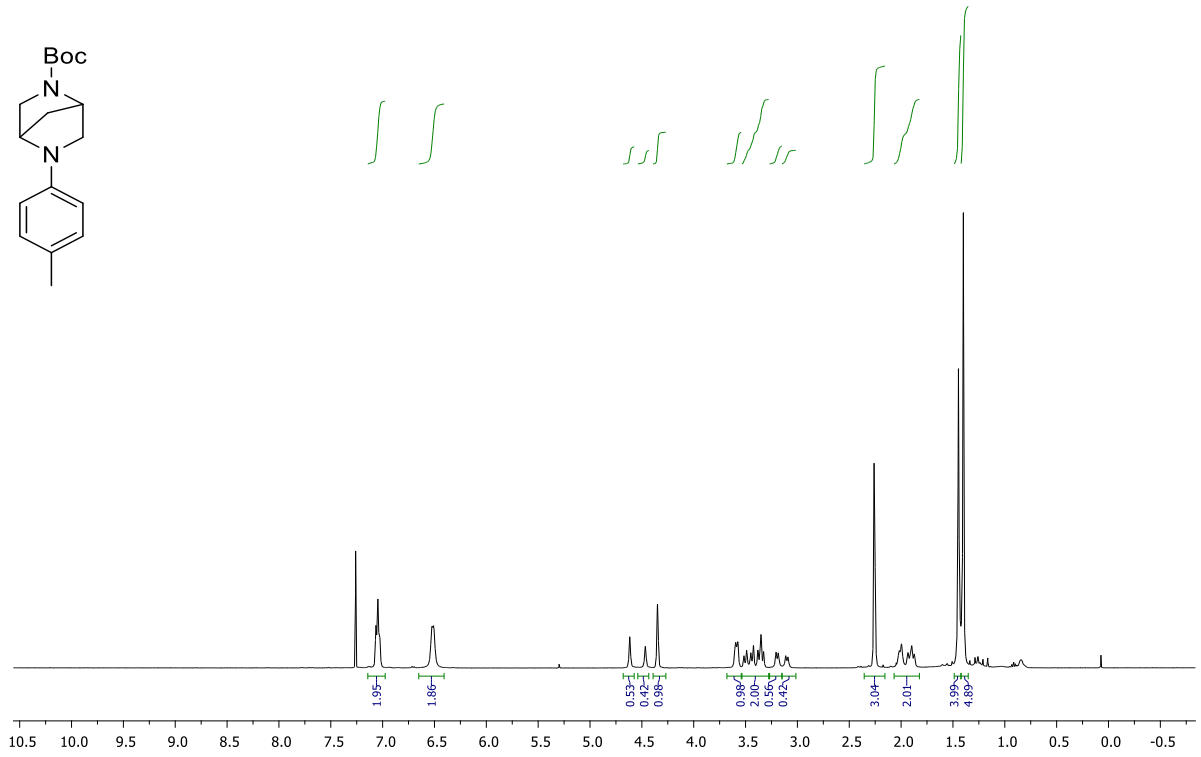

Figure 3-81: 1H NMR spectrum of product 3.48

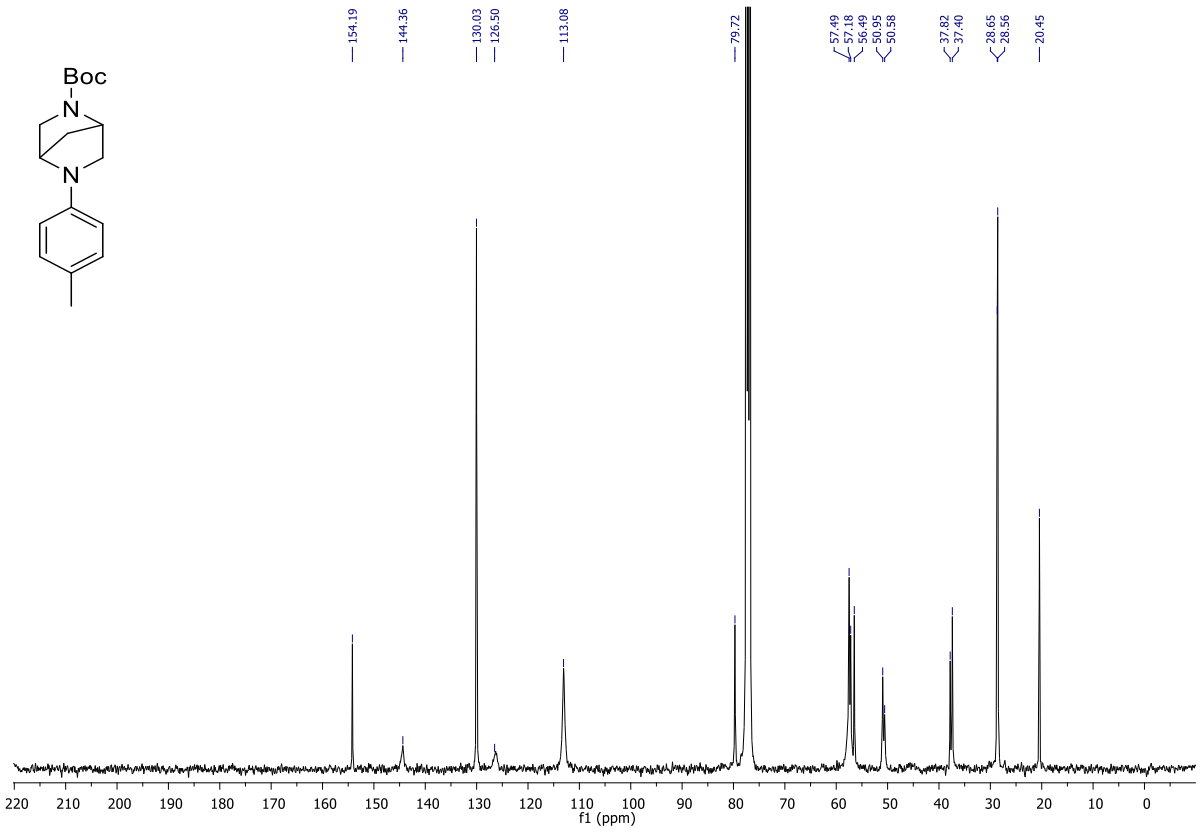

Figure 3-82: 13C NMR spectrum of product 3.48

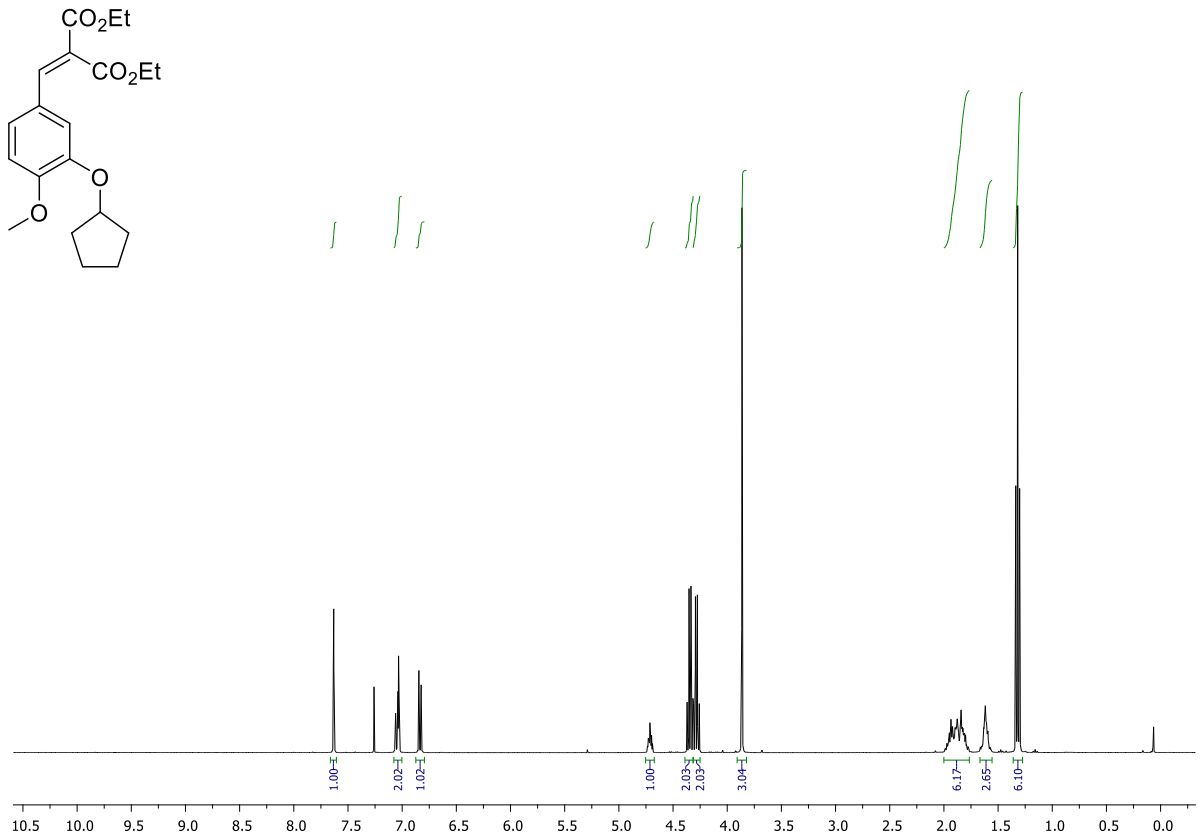

Figure 3-83: 1H NMR spectrum of product 3.51

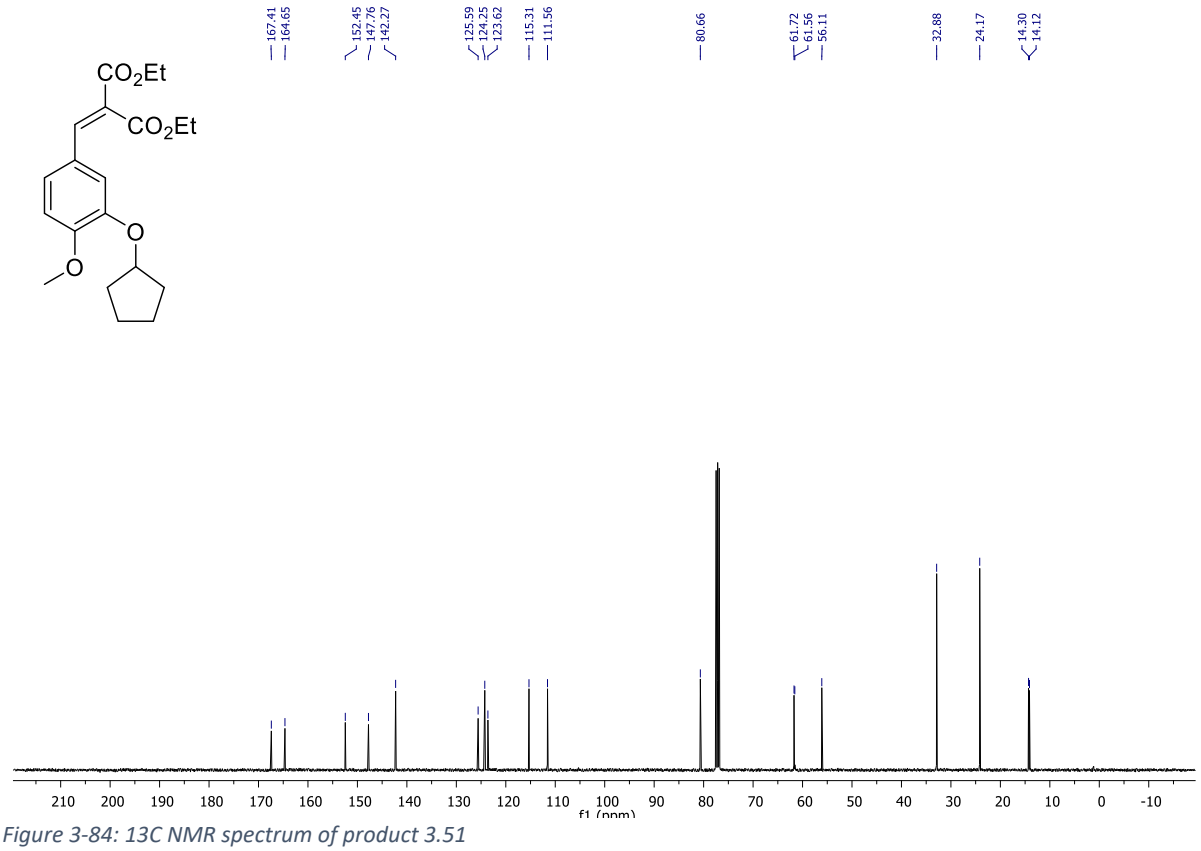

Figure 3-84: 13C NMR spectrum of product 3.51

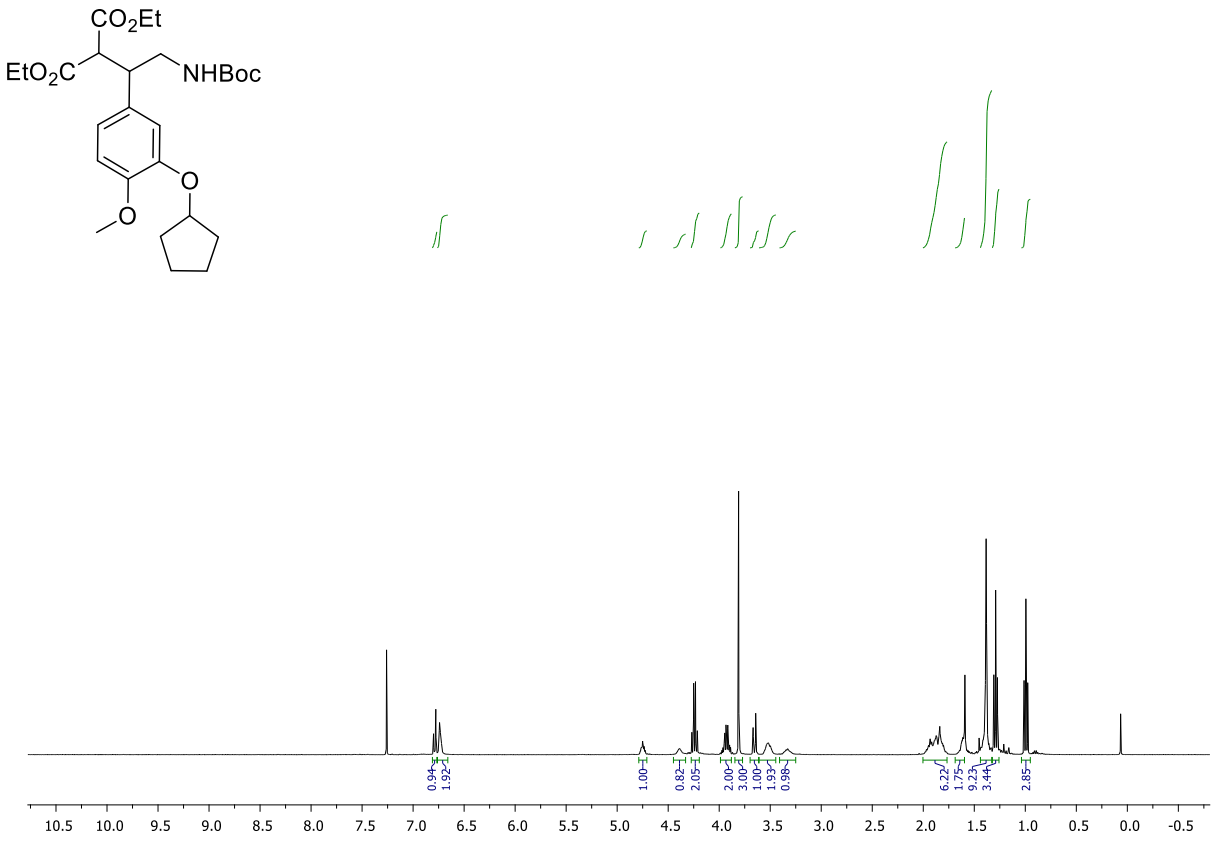

Figure 3-85: 1H NMR spectrum of product 3.52

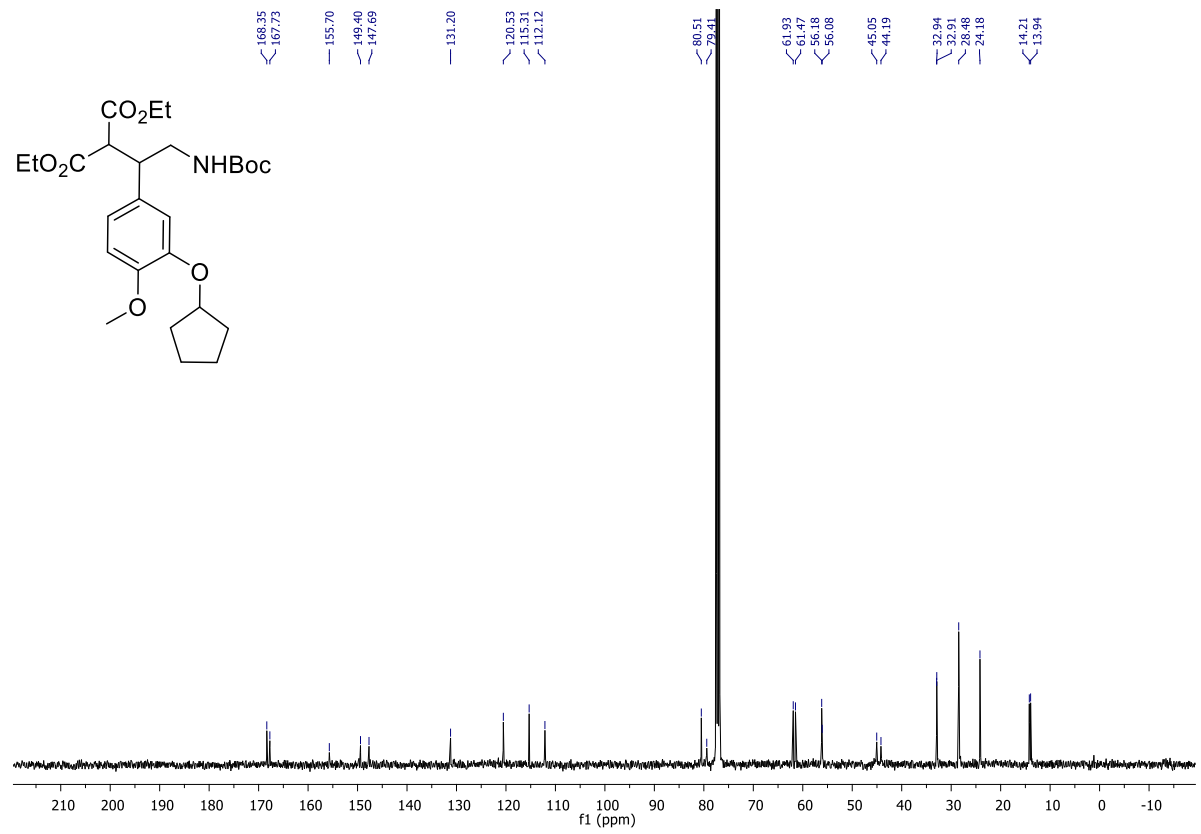

Figure 3-86: 13C NMR spectrum of product 3.52

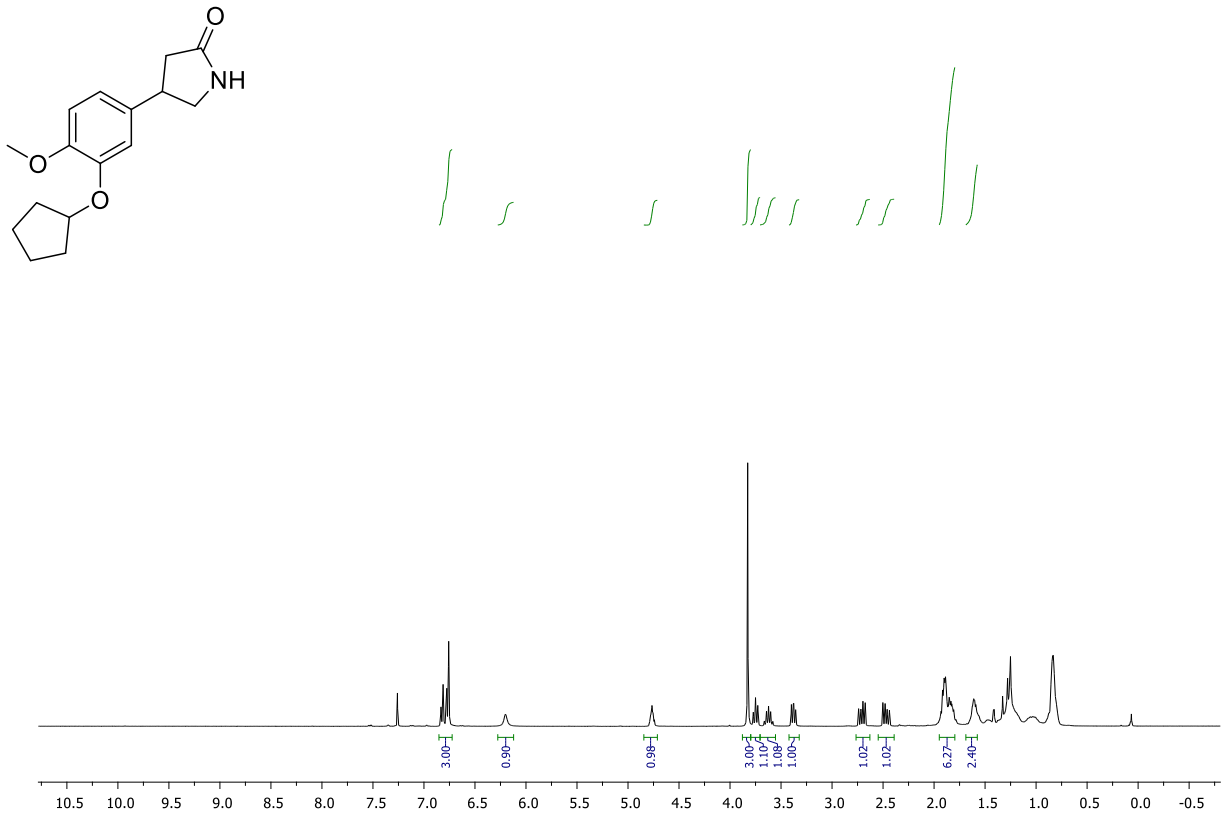

Figure 3-87: 1H NMR spectrum of product 3.54

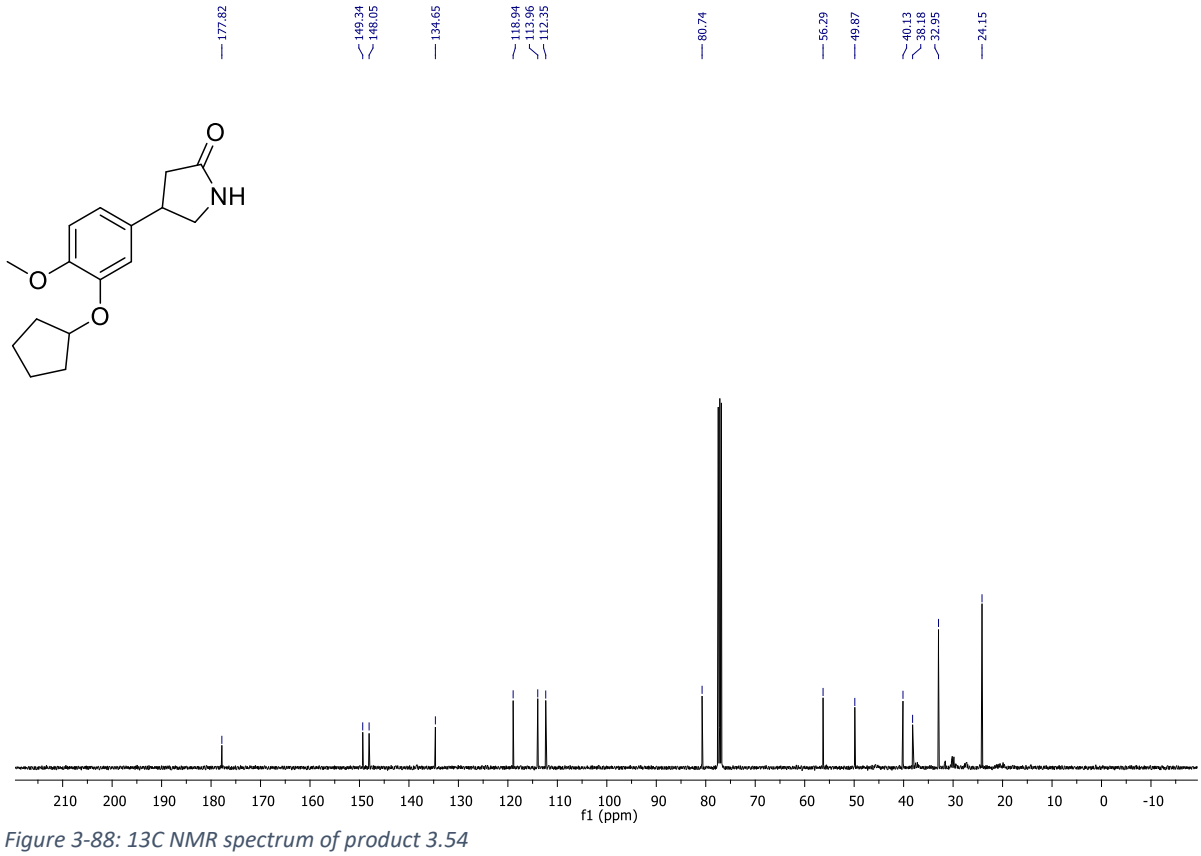

Figure 3-88: 13C NMR spectrum of product 3.54

References

1. Vijayakrishnan, S., Ward, J. W. & Cooper, A. I. Discovery of a Covalent Triazine Framework Photocatalyst for Visible-Light-Driven Chemical Synthesis using High-Throughput Screening. *ACS Catal.* **12**, 10057–10064 (2022).
2. Chu, L., Ohta, C., Zuo, Z. & MacMillan, D. W. C. Carboxylic Acids as A Traceless Activation Group for Conjugate Additions: A Three-Step Synthesis of (±)-Pregabalin. *J. Am. Chem. Soc.* **136**, 10886–10889 (2014).
3. Speckmeier, E., Fischer, T. G. & Zeitler, K. A Toolbox Approach To Construct Broadly Applicable Metal-Free Catalysts for Photoredox Chemistry: Deliberate Tuning of Redox Potentials and Importance of Halogens in Donor–Acceptor Cyanoarenes. *J. Am. Chem. Soc.* **140**, 15353–15365 (2018).
4. Ramirez, N. P. & Gonzalez-Gomez, J. C. Decarboxylative Giese-Type Reaction of Carboxylic Acids Promoted by Visible Light: A Sustainable and Photoredox-Neutral Protocol. *Eur. J. Org. Chem.* **2017**, 2154–2163 (2017).
5. Constantin, T. *et al.* Aminoalkyl radicals as halogen-atom transfer agents for activation of alkyl and aryl halides. *Science* **367**, 1021–1026 (2020).
6. Kitcatt, D. M., Nicolle, S. & Lee, A.-L. Direct decarboxylative Giese reactions. *Chem. Soc. Rev.* **51**, 1415–1453 (2022).
7. Schwarz, J. & König, B. Decarboxylative reactions with and without light – a comparison. *Green Chem.* **20**, 323–361 (2018).
8. Edwards, J. T. *et al.* Decarboxylative alkenylation. *Nature* **545**, 213–218 (2017).
9. Zhang, B. *et al.* Ni-electrocatalytic Csp3–Csp3 doubly decarboxylative coupling. *Nature* **606**, 313–318 (2022).
10. Toriyama, F. *et al.* Redox-Active Esters in Fe-Catalyzed C–C Coupling. *J. Am. Chem. Soc.* **138**, 11132–11135 (2016).
11. White, J. L. *et al.* Light-Driven Heterogeneous Reduction of Carbon Dioxide: Photocatalysts and Photoelectrodes. *Chem. Rev.* **115**, 12888–12935 (2015).
12. Navarro-Jaén, S. *et al.* Highlights and challenges in the selective reduction of carbon dioxide to methanol. *Nat. Rev. Chem.* **5**, 564–579 (2021).

13. Peng, J.-B., Geng, H.-Q. & Wu, X.-F. The Chemistry of CO: Carbonylation. *Chem* **5**, 526–552 (2019).
14. Hermann, T. Industrial production of amino acids by coryneform bacteria. *J. Biotechnol.* **104**, 155–172 (2003).
15. Wendisch, V. F., Jorge, J. M. P., Pérez-García, F. & Sgobba, E. Updates on industrial production of amino acids using Corynebacterium glutamicum. *World J. Microbiol. Biotechnol.* **32**, 32:105 (2016).
16. Murali, N., Srinivas, K. & Ahring, B. K. Biochemical Production and Separation of Carboxylic Acids for Biorefinery Applications. *Fermentation* **3**, 3:22 (2017).
17. Ren, S. *et al.* Porous, Fluorescent, Covalent Triazine-Based Frameworks Via Room-Temperature and Microwave-Assisted Synthesis. *Adv. Mater.* **24**, 2357–2361 (2012).
18. Kuhn, P., Antonietti, M. & Thomas, A. Porous, Covalent Triazine-Based Frameworks Prepared by Ionothermal Synthesis. *Angew. Chem. Int. Ed.* **47**, 3450–3453 (2008).
19. Vonlanthen, D. *et al.* Conformationally Controlled Electron Delocalization in n-Type Rods: Synthesis, Structure, and Optical, Electrochemical, and Spectroelectrochemical Properties of Dicyanocyclophanes. *Chem. Eur. J.* **17**, 7236–7250 (2011).
20. Ghosh, I. *et al.* Organic semiconductor photocatalyst can bifunctionalize arenes and heteroarenes. *Science* **365**, 360–366 (2019).
21. Prier, C. K., Rankic, D. A. & MacMillan, D. W. C. Visible Light Photoredox Catalysis with Transition Metal Complexes: Applications in Organic Synthesis. *Chem. Rev.* **113**, 5322–5363 (2013).
22. Meier, C. B. *et al.* Structure-property relationships for covalent triazine-based frameworks: The effect of spacer length on photocatalytic hydrogen evolution from water. *Polymer* **126**, 283–290 (2017).
23. Zhu, Q. & Nocera, D. G. Photocatalytic Hydromethylation and Hydroalkylation of Olefins Enabled by Titanium Dioxide Mediated Decarboxylation. *J. Am. Chem. Soc.* **142**, 17913–17918 (2020).
24. Shu, C., Mega, R. S., Andreassen, B. J., Noble, A. & Aggarwal, V. K. Synthesis of Functionalized Cyclopropanes from Carboxylic Acids by a

Radical Addition–Polar Cyclization Cascade. *Angew. Chem. Int. Ed.* **57**, 15430–15434 (2018).

25. Ventre, S., Petronijevic, F. R. & MacMillan, D. W. C. Decarboxylative Fluorination of Aliphatic Carboxylic Acids via Photoredox Catalysis. *J. Am. Chem. Soc.* **137**, 5654–5657 (2015).
26. Zuo, Z. *et al.* Merging photoredox with nickel catalysis: Coupling of α-carboxyl sp 3 -carbons with aryl halides. *Science* **345**, 437–440 (2014).
27. Johnston, C. P., Smith, R. T., Allmendinger, S. & MacMillan, D. W. C. Metallaphotoredox-catalysed sp3–sp3 cross-coupling of carboxylic acids with alkyl halides. *Nature* **536**, 322–325 (2016).
28. U. Dighe, S., Juliá, F., Luridiana, A., Douglas, J. J. & Leonori, D. A photochemical dehydrogenative strategy for aniline synthesis. *Nature* **584**, 75–81 (2020).
29. Sun, X., Chen, J. & Ritter, T. Catalytic dehydrogenative decarboxyolefination of carboxylic acids. *Nat. Chem.* **10**, 1229–1233 (2018).
30. Martinez, C. A. *et al.* Development of a Chemoenzymatic Manufacturing Process for Pregabalin. *Org. Process Res. Dev.* **12**, 392–398 (2008).
31. Kaur, R. & Pandey, S. K. Efficient synthesis of (−)-(R)- and (+)-(S)-rolipram. *Tetrahedron Lett.* **58**, 4333–4335 (2017).
32. Nagy, B. S., Llanes, P., Pericas, M. A., Kappe, C. O. & Ötvös, S. B. Enantioselective Flow Synthesis of Rolipram Enabled by a Telescoped Asymmetric Conjugate Addition–Oxidative Aldehyde Esterification Sequence Using *in Situ* -Generated Persulfuric Acid as Oxidant. *Org. Lett.* **24**, 1066–1071 (2022).
33. Pieber, B. *et al.* Semi-heterogeneous Dual Nickel/Photocatalysis using Carbon Nitrides: Esterification of Carboxylic Acids with Aryl Halides. *Angew. Chem. Int. Ed.* **58**, 9575–9580 (2019).
34. Iwata, Y., Tanaka, Y., Kubosaki, S., Morita, T. & Yoshimi, Y. A strategy for generating aryl radicals from arylborates through organic photoredox catalysis: photo-Meerwein type arylation of electron-deficient alkenes. *Chem. Commun.* **54**, 1257–1260 (2018).

35. Bhattacherjee, A. *et al.* Picosecond to millisecond tracking of a photocatalytic decarboxylation reaction provides direct mechanistic insights. *Nat. Commun.* **10**, 10:5152 (2019).
36. Skubi, K. L., Blum, T. R. & Yoon, T. P. Dual Catalysis Strategies in Photochemical Synthesis. *Chem. Rev.* **116**, 10035–10074 (2016).
37. Capaldo, L., Buzzetti, L., Merli, D., Fagnoni, M. & Ravelli, D. Smooth Photocatalyzed Benzylation of Electrophilic Olefins via Decarboxylation of Arylacetic Acids. *J. Org. Chem.* **81**, 7102–7109 (2016).
38. Couteau, C., Paparis, E., Chauvet, C. & Coiffard, L. Tris-biphenyl triazine, a new ultraviolet filter studied in terms of photoprotective efficacy. *Int. J. Pharm.* **487**, 120–123 (2015).
39. Gollwitzer, A., Dietel, T., Kretschmer, W. P. & Kempe, R. A broadly tunable synthesis of linear α-olefins. *Nat. Commun.* **8**, 1226 (2017).
40. Gholami, Z., Gholami, F., Tišler, Z. & Vakili, M. A Review on the Production of Light Olefins Using Steam Cracking of Hydrocarbons. *Energies* **14**, 14:8190 (2021).
41. Kautzky, J. A., Wang, T., Evans, R. W. & MacMillan, D. W. C. Decarboxylative Trifluoromethylation of Aliphatic Carboxylic Acids. *J. Am. Chem. Soc.* **140**, 6522–6526 (2018).
42. DeHovitz, J. S. *et al.* Static to inducibly dynamic stereocontrol: The convergent use of racemic β-substituted ketones. *Science* **369**, 1113–1118 (2020).
43. Vijeta, A., Casadevall, C., Roy, S. & Reisner, E. Visible-Light Promoted C–O Bond Formation with an Integrated Carbon Nitride–Nickel Heterogeneous Photocatalyst. *Angew. Chem. Int. Ed.* **60**, 8494–8499 (2021).
44. Chen, X. *et al.* Integrating single Ni sites into biomimetic networks of covalent organic frameworks for selective photoreduction of CO2. *Chem. Sci.* **11**, 6915–6922 (2020).
45. Seo, H., Katcher, M. H. & Jamison, T. F. Photoredox activation of carbon dioxide for amino acid synthesis in continuous flow. *Nat. Chem.* **9**, 453–456 (2017).
46. Lima, F. *et al.* Organic photocatalysis for the radical couplings of boronic acid derivatives in batch and flow. *Chem. Commun.* **54**, 5606–5609 (2018).

47. Seo, H., Liu, A. & Jamison, T. F. Direct β-Selective Hydrocarboxylation of Styrenes with CO2Enabled by Continuous Flow Photoredox Catalysis. *J. Am. Chem. Soc.* **139**, 13969–13972 (2017).
48. Rosso, C. *et al.* An oscillatory plug flow photoreactor facilitates semi-heterogeneous dual nickel/carbon nitride photocatalytic C–N couplings. *React. Chem. Eng.* **5**, 597–604 (2020).
49. Noble, A., Mega, R. S., Pflästerer, D., Myers, E. L. & Aggarwal, V. K. Visible-Light-Mediated Decarboxylative Radical Additions to Vinyl Boronic Esters: Rapid Access to γ-Amino Boronic Esters. *Angew. Chem. Int. Ed.* **57**, 2155–2159 (2018).
50. Aggarwal, V. K., Bae, I., Lee, H.-Y., Richardson, J. & Williams, D. T. Sulfur-Ylide-Mediated Synthesis of Functionalized and Trisubstituted Epoxides with High Enantioselectivity; Application to the Synthesis of CDP-840. *Angew. Chem. Int. Ed.* **42**, 3274–3278 (2003).
51. Warrelow, G. J.; Boyd E. C.; Alexander, R. P. Tri-Substituted Phenyl Derivatives As Phosphodiesterase Inhibitors, WO 94/14742, 1994
52. Chen, M. & Dong, G. Direct Catalytic Desaturation of Lactams Enabled by Soft Enolization. *J. Am. Chem. Soc.* **139**, 7757–7760 (2017).

Chapter 4

Towards Autonomous Optimization of Photocatalytic Reactions

Author Contributions

This project is a collaborative effort between multiple researchers, and the work of others has been included for context.

Dr. Tianwei Dai programmed the KUKA mobile robot, the Automation Portal, and filmed demonstrations of some of the workflow.

Mr. Rob Clowes designed the programs on ChemSpeed platform and assisted with hardware construction for the workflow. Ms. Nicola Rankin assisted with 3D printing.

Mr. Richard Lyons, and Mr. Ian Coates synthesized trial polymers that the thesis author tested for photochemical dehydrogenative arylation in Figure **4-16** and Figure **4-17** respectively. Their synthesis and characterization have not been included in this chapter and these polymers were deselected for further use.

Brackets and side mounts for linear actuators onto the ChemSpeed platform were fabricated by the University of Liverpool chemistry workshop.

Introduction

Inspired by the work by the Leonori group[1] and building upon our previous work on mobile robotic workflows and the results of **Chapter 3,** we started to explore further possibilities for polymer catalysed photochemical synthesis. From Chapter 3, we found that CTF-2 was an active photocatalyst for dehydrogenative arylation. Unfortunately, however, attempts to probe the substrate scope revealed that yields were modest for varying the amine partner, and were significantly lowered compared to those reported with the iridium photocatalyst – or failed to produce product in several cases (Scheme **4-1**).

While the workflow constructed in previous chapters was successful in identifying successful photocatalysts, a major time limiting step was the optimization step. We recognized the capabilities of our high throughput platforms in combination with our KUKA mobile robots could address this, and we began work on designing and implementing a workflow for autonomous optimization. Here, instead of a human researcher, a KUKA mobile robot would prepare reactions, transfer vials, irradiate, and analyse autonomously – using the results to determine the next set of conditions to try.

Our motivation for optimizing this reaction was motivated primarily by the reported by the Leonori group that ammonia could be directly used for aniline synthesis. Currently, industrial production of aniline is widely produced through 2 energy intensive routes, ammonolysis of phenol, or reduction of nitrobenzene.[2,3] Nitrobenzene is typically produced industrially through reaction of benzene with nitric acid, and sulphuric acid, producing large quantities of hazardous waste, and potentially explosive trinitro by-products. As an alternative, dehydrogenative arylation of cyclohexanone with ammonia could provide a less hazardous route and could mitigate acid waste.

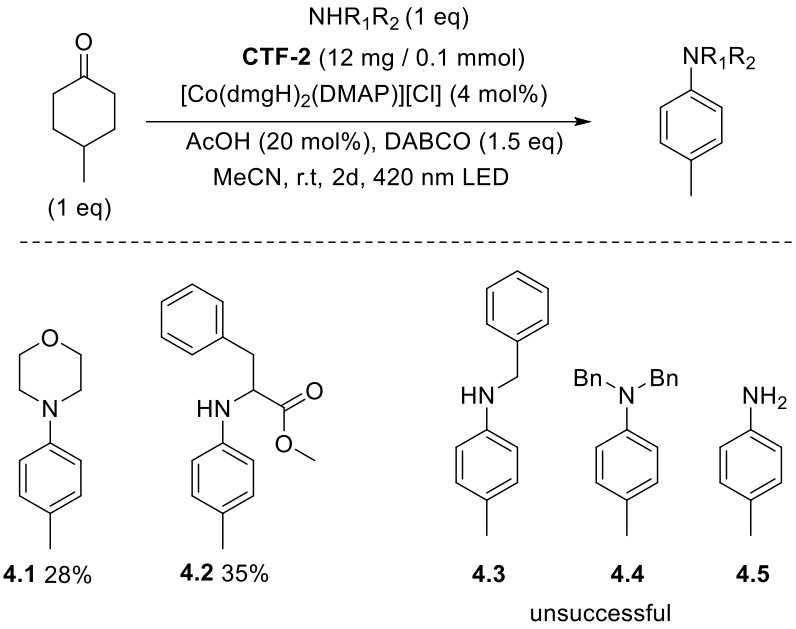

Scheme 4-1: Attempted substrate scope expansion of CTF-2 catalysed dehydrogenative arylation.

Rather than building bespoke hardware, we envisioned a strategy of adapting existing laboratory equipment to the workflow by retrofitting equipment to be used by the arm of the mobile robot (Figure **4-1**). While our group has previously reported on utilizing KUKA mobile robots for hydrogen evolution,[4] several parts of this workflow was unable to be directly transferred to this workflow. A primary issue was the dispensing of non-benign chemicals and solvents in a safe manner, while also maintaining an inert atmosphere suitable for photocatalysis. To achieve this, we decided to adapt our existing ChemSpeed platforms for use with KUKA mobile robots. ChemSpeed platforms which contain solid and liquid dispensing capabilities have been extensively used by our group but are designed exclusively for human operation.

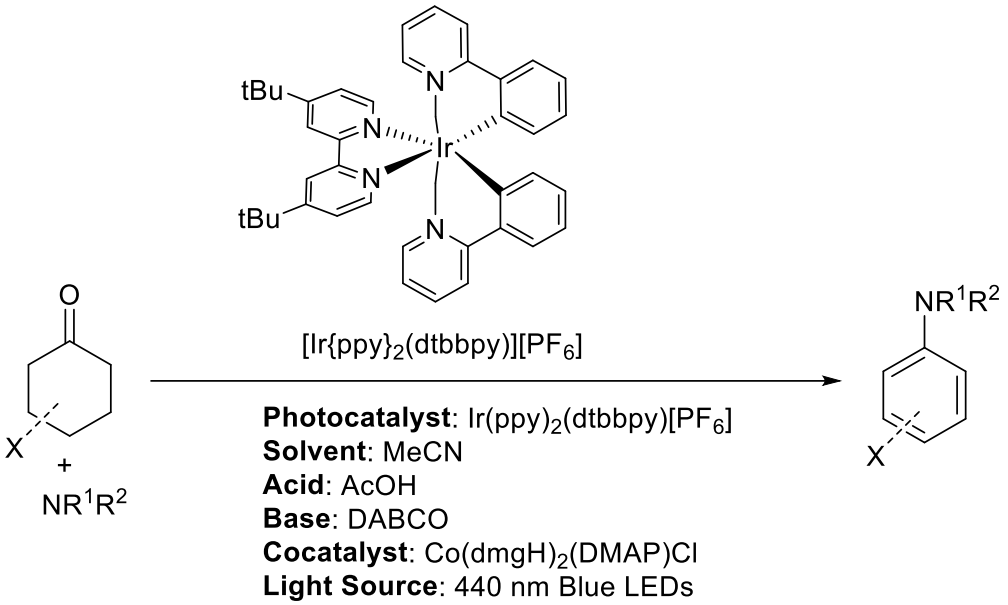

Scheme 4-2: Photochemical dehydrogenative aniline synthesis and parameters to optimize.

We also chose LC-MS as our main point of analysis for the reaction rather than GC-MS. While GC-MS has some significant advantages, such as minimal sample preparation, and little to no method development needed, it limits the amount of chemistry available for analysis, and LC-MS would be far more flexible. Rather than be bespoke solution for optimizing dehydrogenative arylation, we wanted a system that could be flexible, and readily adaptable to diverse types of chemistry.

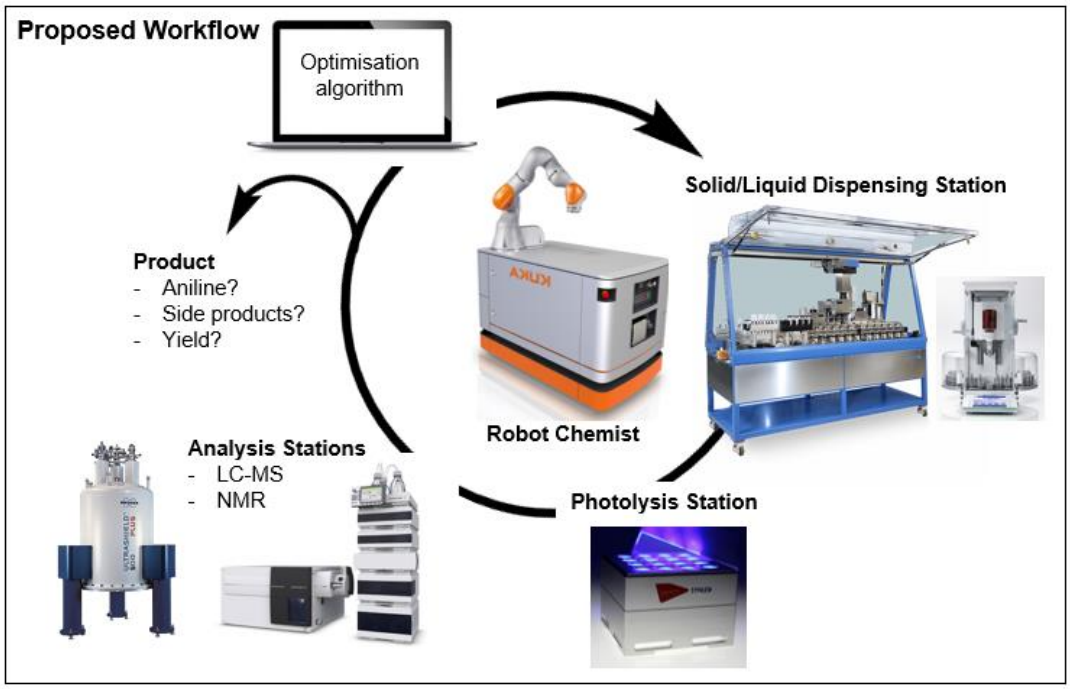

Figure 4-1: Proposed workflow for closed-loop reaction optimization.

Results and Discussion

ChemSpeed Integration

The main obstacle in integrating the ChemSpeed (ISynth) platform was operation of the hood door of the ChemSpeed platform that is designed for human manipulation. (Figure **4-2**). The hood is heavy and has in-built hydraulic supports as a safety system that was not trivial to replace. Our approach was to modify and retrofit the hood door using linear actuators to open and close the door of the ChemSpeed. Due to safety and cost concerns, we tested our solution on an older Formax platform with the same kind of door-opening mechanism as the ISynth that was due for decommission. Metal brackets to support the weight of the actuators on the side of the door (Figure **4-3**), and fittings to drill to the side of the door to enable the actuators to push and pull the door were constructed by the Department of Chemistry Workshop. Using a Raspberry Pi, we were able to control the actuators software control in combination with a relay and were able to open and close the door remotely.

Figure 4-2: Unmodified ChemSpeed ISynth platform (above), Hinge mechanism and hydraulic supports (lower).

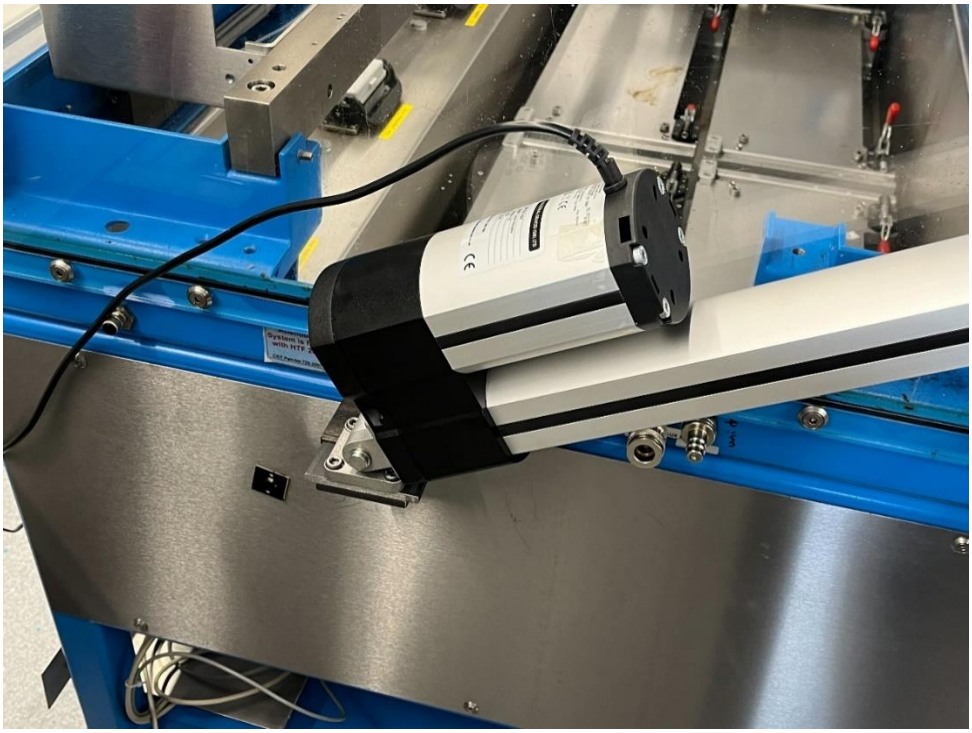

Figure 4-3: Metal fittings for mounting linear actuators to side of Formax housing (upper); Brackets for attaching end of actuators to side of Formax hood (lower)

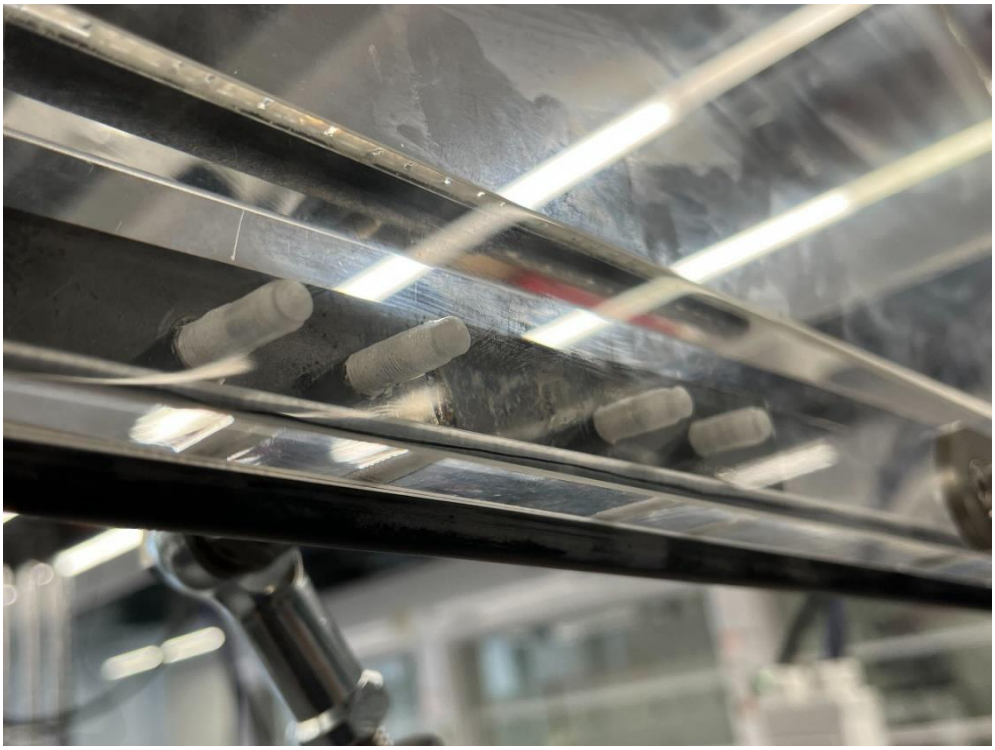

Figure 4-4: Drilled holes on inside of hood door (upper); side view of fully extended linear actuators (lower).

Upon successfully controlling the actuators, another issue was safety. The actuator system has no way of detecting whether a human or mobile robot is working inside the ChemSpeed, and no force detection, leading to potential crush injury to humans, or damage to the KUKA platforms. To mitigate this, we devised an arrangement of a pair of light curtains, which would cut power to the actuators in the case of anything crossing their infrared beams, prohibiting someone from being trapped, or a mobile robot from being damaged if a close command was sent by accident.

Figure 4-5: Extruded aluminium framework for supporting light curtains.

Using extruded aluminium framework attached to the side of the housing (Figure **4-5**), the light curtains were suspended on either side of the ChemSpeed, and connected to the light curtains, and cut power anytime something crossed the beams, allowing for safe operation of the automatic doors. We tested door-opening system on the Formax housing for robustness over many operations (~50 repetitions) and observed no cracking on the frame of the door, no disconnection of the actuators from the mounting brackets, and no desynchronization of the two actuators. Satisfied with the safety of the system, we then proceeded to install both the light curtains and the actuators on our ISynth platform (Figure **4-6**). Boards to both support the extruded aluminium framework, and to provide visibility to users and avoid trip hazards were installed.

Figure 4-6: Fully constructed actuator and light curtain system installed on ISynth platform.

The layout of the ISynth required some modifications to accommodate the KUKA platform, as adequate space is required for the grippers to grasp the vials and the LC-MS racks. The generalized layout in shown in (Figure **4-7)**. Red indicates a zone for stock solutions, yellow indicates the LC-MS vial reformatting zone, while orange represents the crimp sealing rack where the various reactions are prepared for photoirradiation following dispensing and sealing under nitrogen.

The blue zone represents the placement of a calibration cube as a fixed reference position for the KUKA mobile robot to accurately pick up and place the vials and racks after they have been placed in the ISynth. A benefit of our flexible approach is that the chemistry available to be tested on the ISynth is very broad. If the substrates can be dispensed as stock solution or dispensed as a powder (using the built-in solid dispensing module) it is likely to be dispensed into the reaction vials. As is a common obstacle with these platforms, a significant quantity of material is required and is unsuitable for handling small quantities of irreplaceable chemicals.

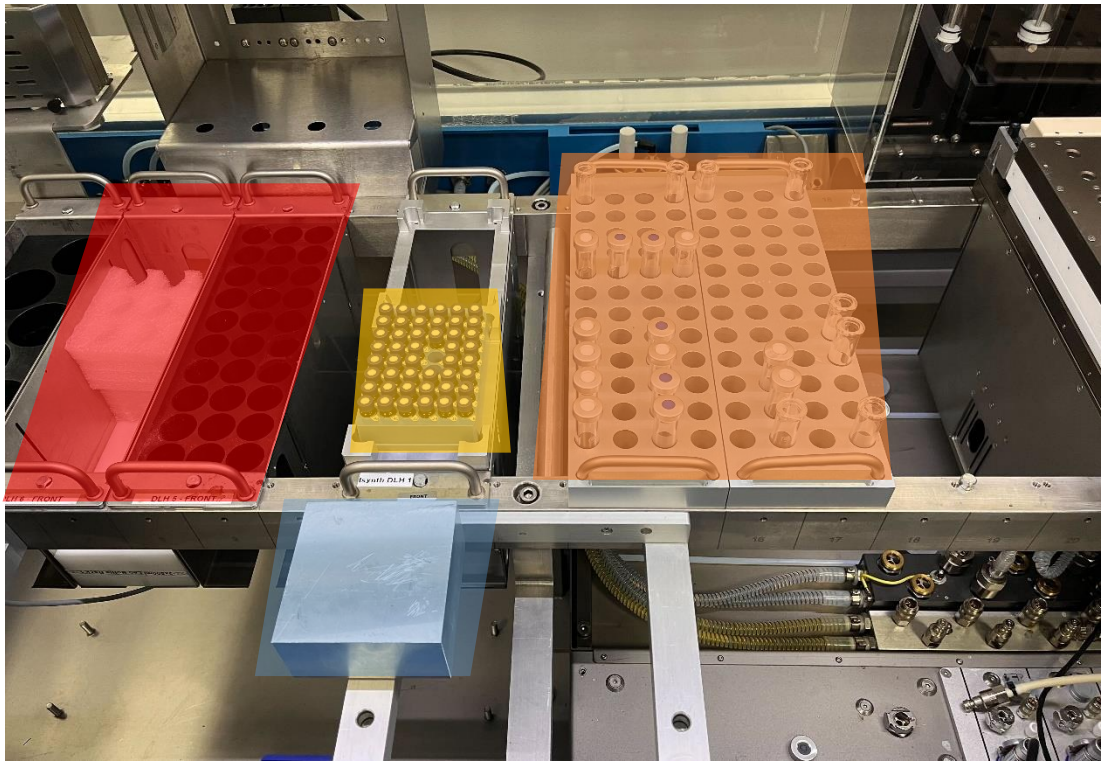

Figure 4-7: Deck layout for KUKA compatible reaction optimization.

LC-MS Integration

Our main analysis method for photocatalytic performance was LC-MS, which we proceeded to integrate into our workflow using the KUKA mobile robot. We used a LC-MS instrument from Waters, that contained a modification designed for the placement of racks with a general robotic arm. The modification (Automation Portal) was supplied by Waters and was used as-is with no further modifications. Using the Waters Automation Portal, we used our mobile robot platform to load racks of LC-MS vials into the tray, which would then be loaded into the autosampler of the instrument (Figure **4-8**).

Figure 4-8: Automation Portal (side view) for insertion of LC-MS racks.

Once the lack is loaded into the autosampler, the next stage is remote sampling. Using premade **.csv** queue files, we could input files in this format in batches of 32 samples at a time (along with several blank injections) by importing to an AutoLynx Queue folder.

A challenge we had to solve however was how to extract data from the LC-MS, which is designed for manual operation, and not closed loop automation. The produced data files were produced in proprietary file formats that could only be read by the software accompanying the LC-MS and were not extractable to a format to inform our planned optimizer. Consequently, we had to devise methods for automatically extracting the quantity of product formation, and to write the data in a format which could be fed to our optimizer. Using an **.xml** parser, we were able parse through the generated **.xml**, and output them into a suitable format (Figure **4-9**).

```
import xml.etree.ElementTree as ET
import csv


tree = ET.parse('QueueTest4.xml')
root = tree.getroot()

f= open('Test.csv', 'w')
writer = csv.writer(f)



for SAMPLE in root.iter('SAMPLE'):
    sampleid = SAMPLE.get('id')
    samplename = SAMPLE.get('name')
    for PEAK in SAMPLE.iter('PEAK'):
        samplearea = PEAK.get('area')
        sampleconc = PEAK.get('analconc')
        print(sampleid, samplename, samplearea, sampleconc)
        csvwriter = [sampleid, samplename, samplearea, sampleconc]
        writer.writerow(csvwriter)
```

Figure 4-9: Exemplar python script for extraction of data from obtained LC-MS chromatograms.

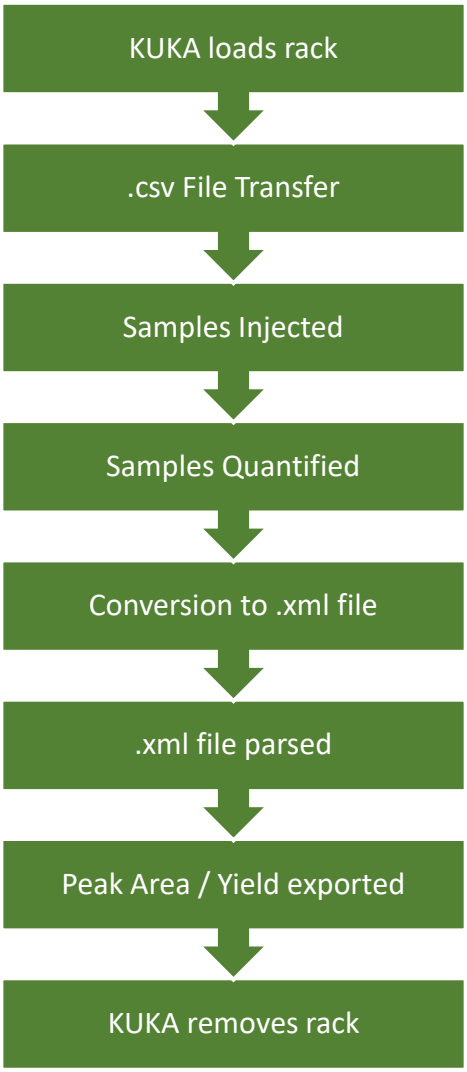

Figure 4-10: Process for automatic LC-MS data acquisition, quantification, and data extraction.

This approach does have some disadvantages. For each compound to be optimized, a separate LC-MS method must be created (along with calibration curves). In addition, peak detection is largely dependent on retention times in the chromatogram. If specific reaction conditions result in formation of a by-product near the desired peak, this might be counted as product formation, and the optimizer might suggest conditions that promote this. Compounds must absorb under UV irradiation order to quantify, and substrates not easily ionizable with electrospray ionization (ESI) will not be able to be cross verified using MS measurements.

Workflow Assembly

With the hardware components of the workflow integrated, we then tested the basic vial manipulation and movement of the KUKA in a test workflow (minus any dispensing of chemicals) (Figure **4-11**).

Figure 4-11: KUKA starting position (Upper); KUKA opening door of ISynth (middle); KUKA placing vials onto SynLED photoreactor (lower).

Figure 4-12: Returning of irradiated samples to ISynth and reformat to LC-MS (upper); Insertion of reformatted samples to LC-MS (lower).

The KUKA mobile robot successfully moved from a home position, opened, and closed the door of the ISynth, picked up vials, and transported them the photoreactors. It then moved those vials back to the ISynth for reformatting to LC-MS, and then transported the rack to the LC-MS for analysis (Figure **4-12**). In this case, only vials containing water were transported, and no programs on the ChemSpeed were executed.

Photocatalyst Screening

Screening polymers synthesized in **Chapter 2**, we found that POX-SO2 was remarkably more active for the dehydrogenative arylation reaction using the SynLED photoreactors than CTF-2 (Figure **4-13**). We observed that other phenoxazine based polymers were inefficient, and we hypothesized that the inclusion of the sulphone moiety was beneficial for catalysis. Sulphone based polymers are known to be active for hydrogen evolution,[5–7] and analogues have been incorporated into COFs for the same purpose,[8] and we wondered if this moiety would be active for dehydrogenative arylation. Anthraquinone polymers proved to generally have poor performance, while g-C_3N_4 was highly ineffective giving only 5% LC-MS yield.

Based on this, we screened a variety of sulphone based linear conjugated polymers (Figure **4-14**, Figure **4-15**), and closely related derivatives that have shown some activity in hydrogen evolution. As we hypothesized, several of these polymers proved to be active for photocatalytic dehydrogenative arylation, yielding significantly superior performance to CTF-2. PS-ODec, and FS-TEG slightly outperformed POX-SO_2, however we opted to maintain POX-SO_2 for further investigation as our main catalyst in the workflow, as it was easier to synthesize, and we were concerned with the solubility of PS-ODec in certain solvent combinations, which could complicate LC-MS analysis further. POX-SO_2 meanwhile is insoluble in tested solvents.

Curiously, we observed that incorporating fluorine into the polymers increased the yield in both sulphone and benzodithiophene polymers, but in both cases, polymers containing 2 fluorine atoms on the phenyl monomer, led to lower yields compared to the mono and tetrafluorinated polymers.

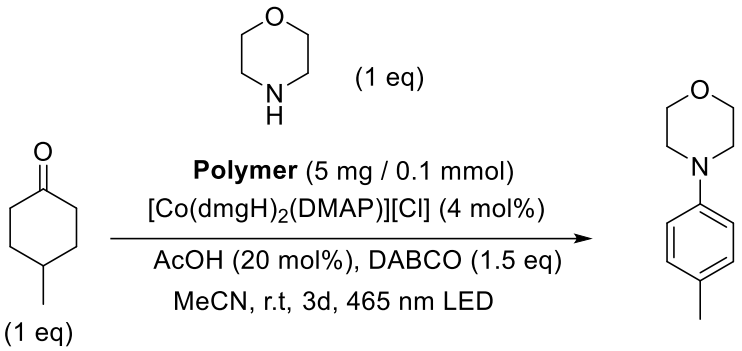

Scheme 4-3: HT screening of polymers for photocatalytic dehydrogenation.

Polymer	LC-MS Yield / %
CTF-2	13
TAA	6
EY-TrE	7
NMeA-Ph	7
POX-Ph	4
POX-SO_2	40
POX-BTZ	Trace
POX-BPy	5
NMeA-TrE	16
Cz	Trace
RB-TrE	9
TXO-HCP	3
AQO-Ph	5
AQO-TrE	5
AQO-BPy	4
AQO-Phen	7
AQO-SO_2	5
AQO-TAZ	6
XBCN117	24
XBCN118	28
XBCN120	31
gC_3N_4	5
FP-F4-Oct	4
FP-F2-Oct	0

FP-Oct	0
FPy-Oct	9
FPy-Oct-N-Oxide	15
FBT-F2-Oct	35
FS-Dec	41
FS-Dodec	16
FS-TEG	43
FS-Py-Ph	23
FF-PyPh-Oct	23
FF-PyPh-TEG	3
PS-ODec	42
CPDTS-Dec	13
FP-F-Oct	9
P7	15
P10	25
SO_2-PhF	33
SO_2-Ph2pF	17
SO_2-Ph2oF	24
SO_2-Ph4F	34
SO_2-BDTP	29
BDTP-Ph	20
BDTP-PhF	41
BDTP-Ph2pF	35
BDTP-Ph2oF	40
BDTP-Ph4F	44
BDTP-SO_2	30
BDTP-BDTP	32

Figure 4-13: Screening results for dehydrogenative arylation of morpholine and 4-methyl cyclohexanone

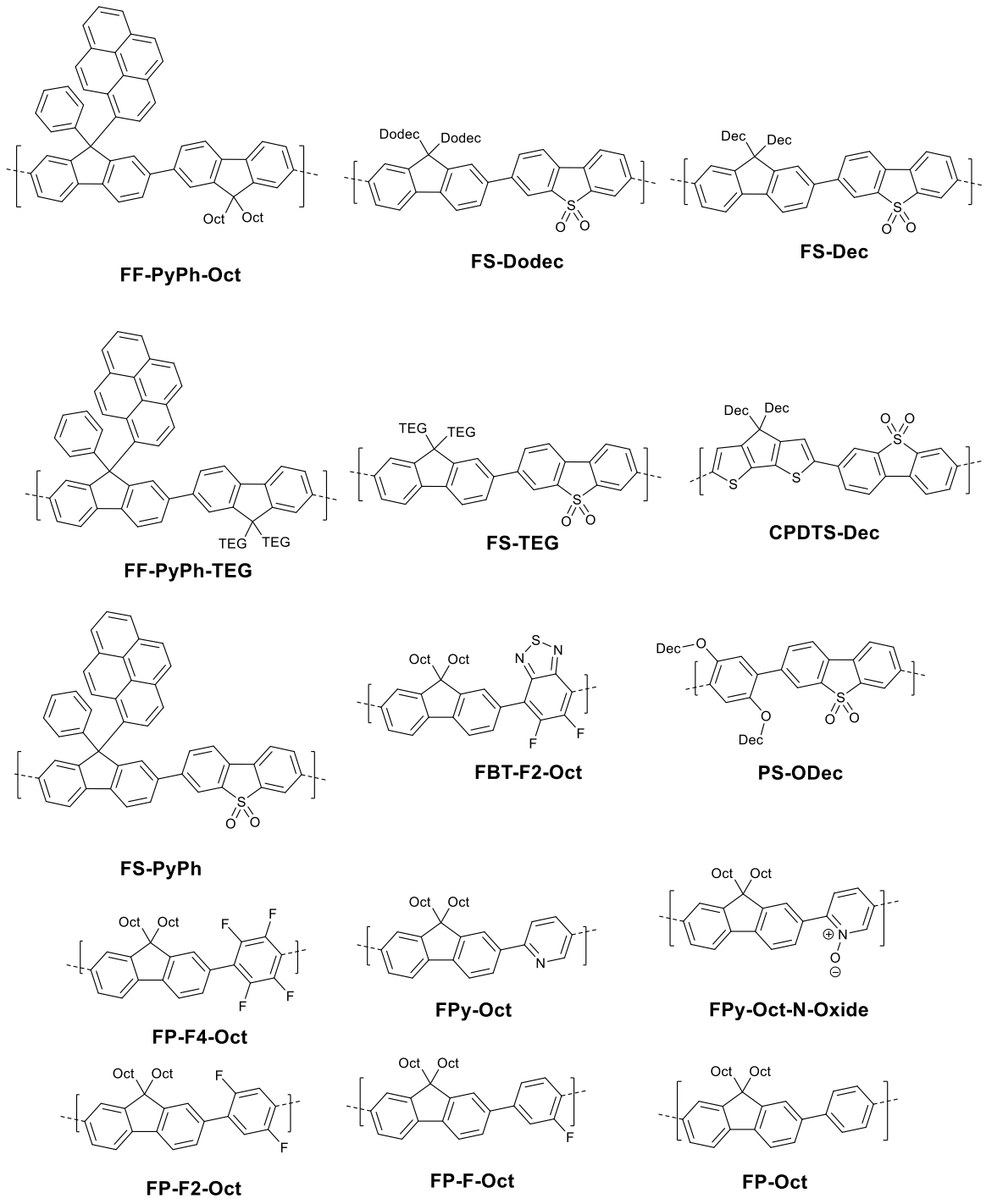

Figure 4-14: Sulphone and fluorenone based polymers screened for dehydrogenative arylation. Polymers in figure were synthesized by Mr. Richard Lyons.

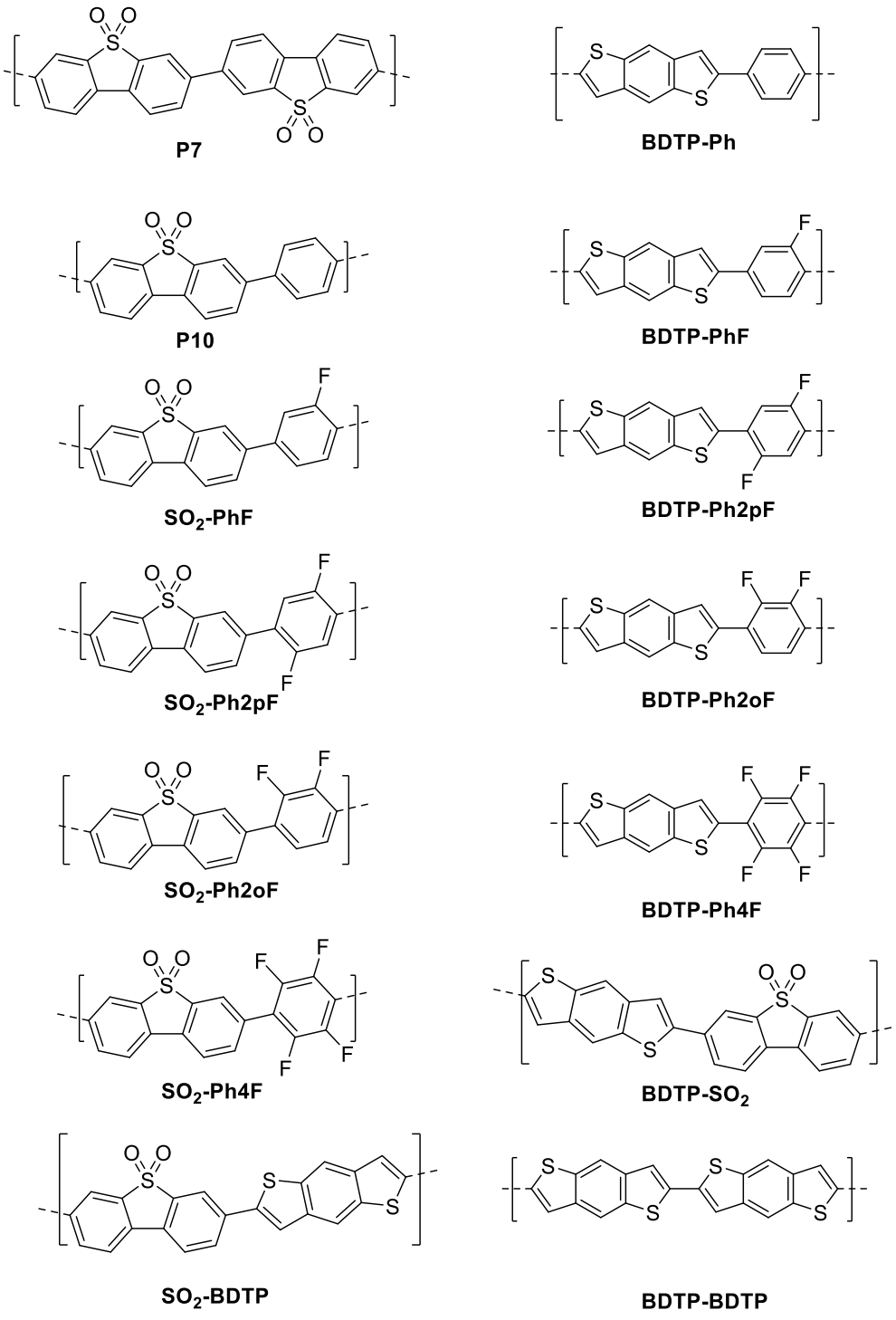

Figure 4-15: Sulphone and benzodithiophene polymers screened for dehydrogenative arylation. Polymers in figure were synthesized by Mr. Ian Coates.

Based on the general success of sulphone containing containing polymers, we also plan to test sulphone-based FS-COF - a crystalline, highly dispersible, and porous photocatalyst that is highly active for hydrogen evolution for this reaction.[9] Our group demonstrated that this material showed significantly enhanced performance compared to an amorphous analogue, and we wonder if similar gains might be realized here.

Conclusions

We have successfully designed, constructed, and integrated the hardware components for this reaction optimization workflow. The modular nature in comparison to fully integrated solutions means that, in principle, various analysis or preparation modules can be fitted in, rather than a ground-up redesign of the entire system. For example, bench-top NMR modules could be integrated for additional analysis, dedicated solid dispensing stations, or the activation of heating from our stirrer plates. A longer-term goal of this project is to apply it to multi-step synthesis, where each step of a synthetic route (such as to an API) is optimized by our mobile robot.

We soon plan to refine and integrate the software components, such as automatically running executable programs on the ChemSpeed, and general reliability. Ideally, the KUKA platform can run for days (potentially even weeks) without human intervention. While the throughput is currently modest, (32 samples can be irradiated at a time) it is more than sufficient at this stage. We are currently investigating how to improve this throughput by incorporating well plates, although there are practical barriers, such as transport of the plates while maintaining an inert environment.

POX-SO_2 was also discovered to be significantly more active photocatalyst than our previously utilized CTF-2. We discovered that several polymers containing

the sulphone moiety were active towards dehydrogenative arylation. While the polymer is synthesized using Suzuki coupling, POX-SO_2 can be reasonably synthesized on scale – however we are still searching for alternatives, such as FS-COF, that might offer superior performance for photocatalytic dehydrogenation. We hope to soon discover conditions where polymers can offer a mild alternative to industrial aniline synthesis.

Troubleshooting

Some major problems we had largely relied on reliability of the capping and parsing the data from the LC-MS reliably. While the issues will likely be unique from workflow to workflow, some general troubleshooting steps we can offer are listed below:

1. The crimping module for the ChemSpeed should be calibrated as accurately as possible, with multiple reproducibility studies performed as needed. This was often one the biggest failure points in the entire series of experiments and could often stop runs completely if the calibration was slightly off, resulting in crushed caps and potential exposure to of chemicals outside of the Chemspeed ventilation.
2. Loading of the racks onto the LC-MS automation portal needs to be very accurate – to sub millimetre accuracy – otherwise it is possible for the hollow interior of the autosampler racks to fall on top of the hinge mechanism, and cause jams.
3. Data extraction LC-MS traces, should ideally have some level of error-correction during the peak area extraction stage, to handle unexpected results. For instance, if we are looking for Peak A, and the software does not find Peak A (and consequently no peak element in the XML file) – say in the case of an improperly reformatted sample, the XML parser should be able to handle this by outputting a value of 0 for example. Maximum and minimum peak areas can also be set as a sort of sample quality control to account for abnormally high or low peak area values of products or standards.

Experimental

CTF-2 catalysed dehydrogenative arylation: General Procedure A

Amine coupling partner (0.4 mmol), [Co(dmgH)$_2$(DMAP)][Cl] (7.2 mg, 4mol%), AcOH (5µL, 0.2 eq), DABCO (68 mg, 0.6 mmol, 1.5 eq), CTF-2 (48 mg), 4-methyl cyclohexanone (49µL, 0.4 mmol), and acetonitrile (2 mL) are combined under nitrogen, sparged, and irradiated for 3 days under 427 nm irradiation with Kessil lamps. The mixture was repeatedly diluted with diethyl ether (8 mL x 3), shaken thoroughly, the polymer allowed to settle to the bottom, and the supernatant removed. The combined ether layers were concentrated under vacuum and purified by column chromatography in ether/hexane gradient.

4-(p-tolyl)morpholine (4.1)

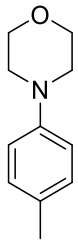

Performed using General Procedure A to yield the product as a white solid (19.6 mg, 28% yield). Spectroscopic data was consistent with authentic sample and literature values. [1]

ethyl p-tolylphenylalaninate (4.2)

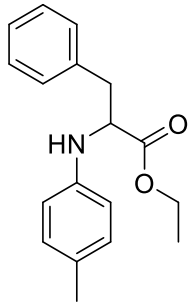

Performed using General Procedure A to yield the product as a white solid (39.8 mg, 35% yield). Data was consistent with literature values.[1]

^{1}H NMR (400 MHz, $CDCl_3$) δ 7.30 – 7.05 (m, 5H), 6.90 (d, *J* = 8.1 Hz, 2H), 6.50 – 6.39 (m, 2H), 4.23 (t, *J* = 6.4 Hz, 1H), 4.09 – 3.97 (m, 2H), 3.03 (d, *J* = 6.4 Hz, 2H), 2.15 (s, 3H), 1.08 (t, *J* = 7.1 Hz, 3H).

^{13}C NMR (101 MHz, $CDCl_3$) δ 173.45, 144.25, 136.64, 129.95, 129.45, 128.58, 127.78, 127.04, 113.96, 61.14, 58.30, 38.88, 20.53, 14.24.

High-throughput screening of polymers for dehydrogenative arylation:

Morpholine, 4-methyl cyclohexanone, DABCO, acetic acid and acetonitrile were combined and sparged with nitrogen and placed in the ISynth platform. $[Co(dmgH)_2(DMAP)][Cl]$ was dissolved in DMSO, and similarly prepared as above. Vials were charged with polymer (5 mg) and were placed inside a ChemSpeed platform, and the ChemSpeed was purged with nitrogen (2 hrs). Stock solutions of the substrates and additives, followed by the coboloxime catalyst were dispensed to each vial under nitrogen (0.1 mmol scale reaction per vial) and were crimp sealed. The vials were then manually transferred to SynLED photoreactor stations and irradiated for 3 days.

The vials were then transferred manually back to the ChemSpeed, and the vials were diluted ethyl acetate (8 mL), and an aliquot of each vial was transferred to a LC-MS vial. The samples were then analysed by LC-MS (30% MeCN in H_2O,

0.1% formic acid) and quantified using a pre-made calibration curve with authentic p-tolyl morpholine using TargetLynx/QuanLynx software.

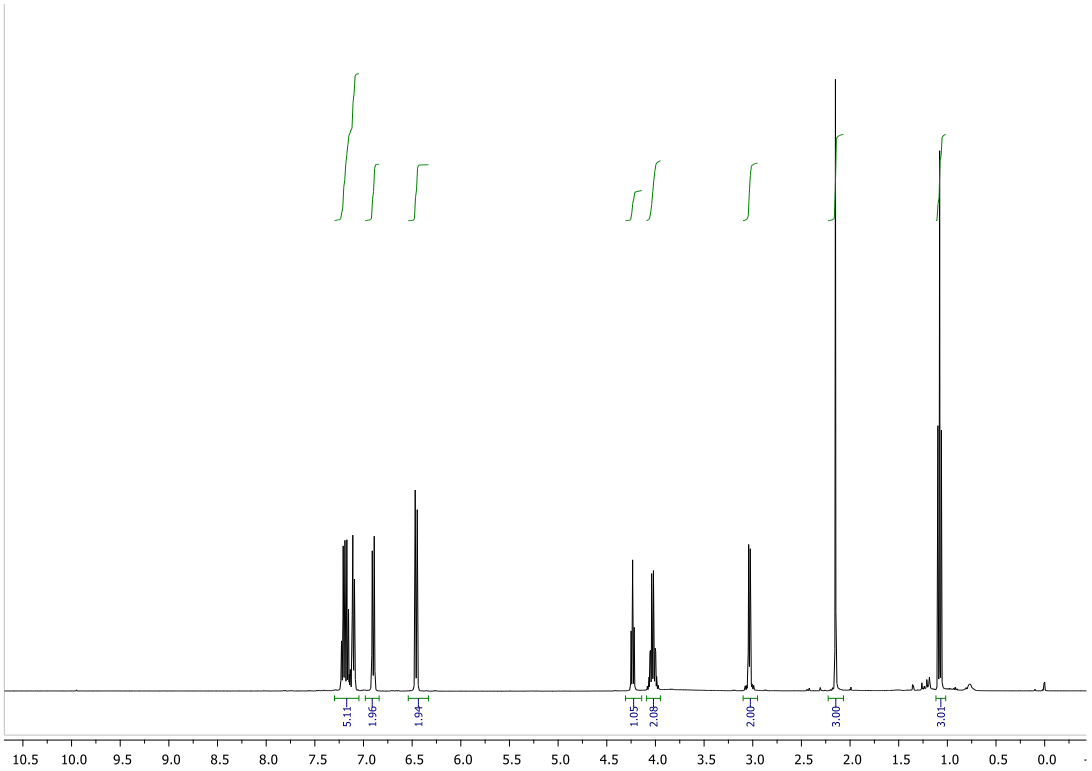

Figure 4-16: 1H NMR spectrum of product 4.2

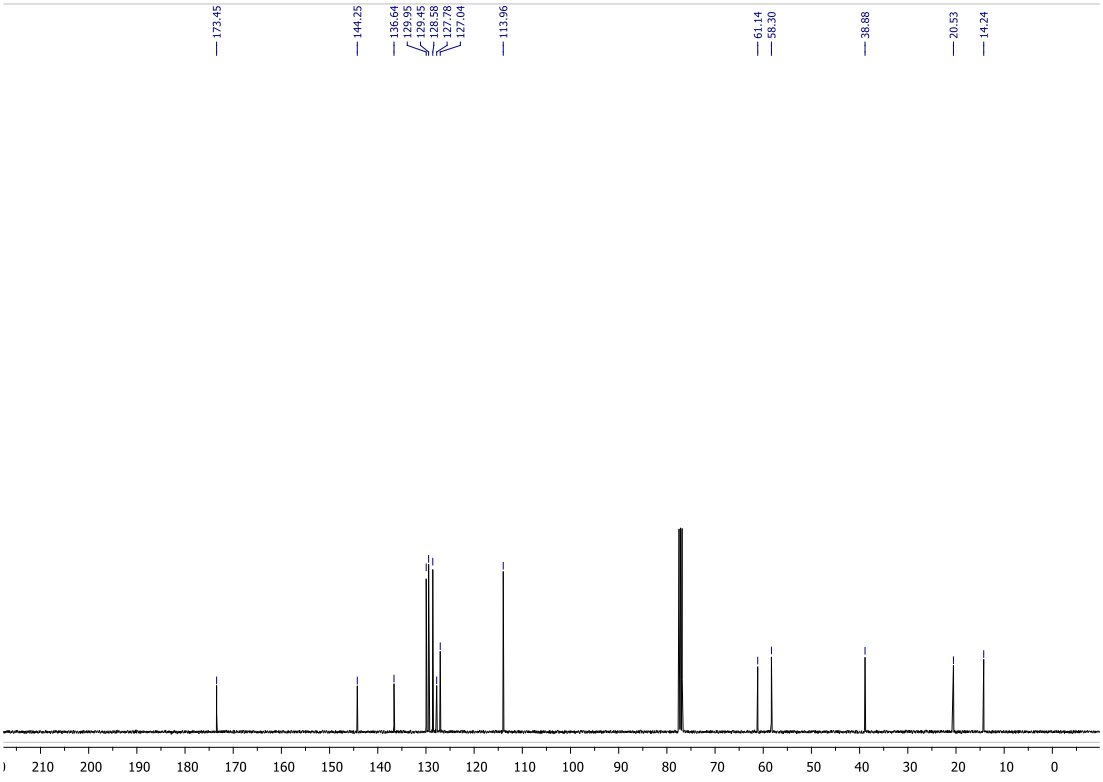

Figure 4-17: 13C NMR spectrum of product 4.2

References

1. U. Dighe, S., Juliá, F., Luridiana, A., Douglas, J. J. & Leonori, D. A photochemical dehydrogenative strategy for aniline synthesis. *Nature* **584**, 75–81 (2020).
2. Morisse, C. G. A. *et al.* Toward High Selectivity Aniline Synthesis Catalysis at Elevated Temperatures. *Ind. Eng. Chem. Res.* **60**, 17917–17927 (2021).
3. Driessen, R. T. *et al.* Industrial Process Design for the Production of Aniline by Direct Amination. *Chem. Eng. Technol.* **40**, 838–846 (2017).
4. Burger, B. *et al.* A mobile robotic chemist. *Nature* **583**, 237–241 (2020).
5. Sprick, R. S. *et al.* Visible-Light-Driven Hydrogen Evolution Using Planarized Conjugated Polymer Photocatalysts. *Angew. Chem. Int. Ed.* **55**, 1792–1796 (2016).
6. Ye, H. *et al.* Bandgap engineering of novel peryleno[1,12- *bcd*]thiophene sulfone-based conjugated co-polymers for significantly enhanced hydrogen evolution without co-catalyst. *J. Mater. Chem. A* **8**, 20062–20071 (2020).
7. Sprick, R. S. *et al.* Photocatalytic Hydrogen Evolution from Water Using Fluorene and Dibenzothiophene Sulfone-Conjugated Microporous and Linear Polymers. *Chem. Mater.* **31**, 305–313 (2019).
8. Wang, X. *et al.* Sulfone-containing covalent organic frameworks for photocatalytic hydrogen evolution from water. *Nat. Chem.* **10**, 1180–1189 (2018).

Chapter 5

Conclusions and Future Work

To summarize, in **Chapter 2** and **Chapter 3** we used a high-throughput discovery workflow aided by robotic platforms for the discovery of novel photocatalysts. By testing trial polymer candidates against a library of known reactions, we rapidly screened for hits using GC-MS to identify novel organic photoredox catalysts. From this workflow, we discovered a covalent triazine framework (CTF-2) as a catalyst that could photochemically induce decarboxylation and could be used for a variety of reactions including fluorination,[1] conjugate addition,[2] dehydrogenative arylation,[3] along with metallaphotoredox arylation[4] and alkylation[5] – but was not successful in a decarboxylative olefination reaction[6].

We also investigated the stability and recyclability of the polymer and found that it could be recycled for at least 4 cycles after and was stable after nearly 200 hours of irradiation. Initial studies into the decarboxylative reaction mechanism indicates that it appears to follow a single electron transfer mechanism[7] rather than an energy transfer process[8]. Unfortunately, the performance of CTF-2 still falls short of organometallic iridium complexes, however to the best of our knowledge this is the first time that decarboxylative alkylation, arylation, and dehydrogenative arylation have been performed with a single heterogeneous organic polymer.

For future work, we are currently investigating the combination of enzymes and organic polymers in heterogeneous photo-biocatalysis for highly enantioselective organic synthesis[9]. Other goals for us are also working towards integrating these new catalysts into photo flow reactors[10,11] to work towards larger scale synthesis[12]. We are also working on attempting to gain further insights into the electrochemical properties of CTF-2, and other insoluble polymers, which we have previously been unable to do. Beyond CTF-2, being able to reliably obtain redox potentials for insoluble, poorly dispersible polymers would be of general benefit to us.

In **Chapter 4** we also described our work towards closed-loop automation workflows for robotic reaction optimization. We are working towards enhancing the robustness of our workflow to minimize the failure rates, and plan to work towards multi-day unsupervised experiments. We also have plans to potentially integrate additional modules into our workflow, such as microwave reactors, and benchtop NMR. Aside from our optimization of photochemical dehydrogenative arylation for aniline synthesis, we are also exploring the photochemical degradation of persistent organic pollutants, such as perfluorooctanoic acid[13] using organic polymers.

Other ideas include sequential optimization of a multi-step synthesis, where several steps towards a target molecule are optimized autonomously[14]. In the long term, we also plan on incorporating our workflow for human-in-the-loop optimization problems, where humans and optimization algorithms work together[15] to perform experiments. Currently, the optimizer contains no chemical knowledge, and treats each parameter independently[16]. For chemical systems with many variables, the full factorial of combinations can reach 10^9 or orders of magnitude greater, which becomes impractical to explore efficiently. Here, humans may be able to impart prior chemical knowledge, and restrict the search space. The combination of optimization algorithms and humans working together could accelerate the rate of improvement, compared to either working alone[17].

Overall, the grand plan of this project is to build a general, robust, platform for organic synthesis using mobile robots. In essence, if we can dispense something safely on a ChemSpeed platform, our KUKA mobile robots should be able to do chemistry with it.

References

1. Ventre, S., Petronijevic, F. R. & MacMillan, D. W. C. Decarboxylative Fluorination of Aliphatic Carboxylic Acids via Photoredox Catalysis. *J. Am. Chem. Soc.* **137**, 5654–5657 (2015).
2. Chu, L., Ohta, C., Zuo, Z. & MacMillan, D. W. C. Carboxylic Acids as A Traceless Activation Group for Conjugate Additions: A Three-Step Synthesis of (±)-Pregabalin. *J. Am. Chem. Soc.* **136**, 10886–10889 (2014).
3. U. Dighe, S., Juliá, F., Luridiana, A., Douglas, J. J. & Leonori, D. A photochemical dehydrogenative strategy for aniline synthesis. *Nature* **584**, 75–81 (2020).
4. Zuo, Z. *et al.* Merging photoredox with nickel catalysis: Coupling of α-carboxyl sp 3 -carbons with aryl halides. *Science* **345**, 437–440 (2014).
5. Johnston, C. P., Smith, R. T., Allmendinger, S. & MacMillan, D. W. C. Metallaphotoredox-catalysed sp3–sp3 cross-coupling of carboxylic acids with alkyl halides. *Nature* **536**, 322–325 (2016).
6. Sun, X., Chen, J. & Ritter, T. Catalytic dehydrogenative decarboxyolefination of carboxylic acids. *Nat. Chem.* **10**, 1229–1233 (2018).
7. Ramirez, N. P. & Gonzalez-Gomez, J. C. Decarboxylative Giese-Type Reaction of Carboxylic Acids Promoted by Visible Light: A Sustainable and Photoredox-Neutral Protocol. *Eur. J. Org. Chem.* **2017**, 2154–2163 (2017).
8. Pieber, B. *et al.* Semi-heterogeneous Dual Nickel/Photocatalysis using Carbon Nitrides: Esterification of Carboxylic Acids with Aryl Halides. *Angew. Chem. Int. Ed.* **58**, 9575–9580 (2019).
9. DeHovitz, J. S. *et al.* Static to inducibly dynamic stereocontrol: The convergent use of racemic β-substituted ketones. *Science* **369**, 1113–1118 (2020).
10. Rosso, C. *et al.* An oscillatory plug flow photoreactor facilitates semi-heterogeneous dual nickel/carbon nitride photocatalytic C–N couplings. *React. Chem. Eng.* **5**, 597–604 (2020).
11. Tobin, J. M. *et al.* Polymer-Supported Photosensitizers for Oxidative Organic Transformations in Flow and under Visible Light Irradiation. *ACS Catal.* **7**, 4602–4612 (2017).

12. Harper, K. C. *et al.* Commercial-Scale Visible Light Trifluoromethylation of 2-Chlorothiophenol Using CF_3I Gas. *Org. Process Res. Dev.* **26**, 404–412 (2022).
13. Gomez-Ruiz, B. *et al.* Photocatalytic degradation and mineralization of perfluorooctanoic acid (PFOA) using a composite TiO2−rGO catalyst. *J. Hazard. Mater.* **344**, 950–957 (2018).
14. Cortés-Borda, D. *et al.* An Autonomous Self-Optimizing Flow Reactor for the Synthesis of Natural Product Carpanone. *J. Org. Chem.* **83**, 14286–14299 (2018).
15. Gopfert, J. P., Kuhl, U., Hindemith, L., Wersing, H. & Hammer, B. Intuitiveness in Active Teaching. *IEEE Trans. Hum.-Mach. Syst.* **52**, 458–467 (2022).
16. Burger, B. *et al.* A mobile robotic chemist. *Nature* **583**, 237–241 (2020).
17. Duros, V. *et al.* Intuition-Enabled Machine Learning Beats the Competition When Joint Human-Robot Teams Perform Inorganic Chemical Experiments. *J. Chem. Inf. Model.* **59**, 2664–2671 (2019).